

# **Multifunctional Catalysis for Sequential Reactions**

James Andrew McManus

Submitted in accordance with the requirements for the degree of  
Doctor of Philosophy

The University of Leeds

School of Chemistry

April 2017

The candidate confirms that the work submitted is his own and that appropriate credit has been given where reference has been made to the work of others.

This copy has been supplied on the understanding that it is copyright material and that no quotation from the thesis may be published without proper acknowledgement.

© 2017 The University of Leeds and James Andrew McManus

The right of James Andrew McManus to be identified as Author of this work has been asserted by him in accordance with the Copyright, Designs and Patents Act 1988.

## Acknowledgements

Firstly, I would like to thank Prof. John Blacker selecting me for such an interesting and varied project. His supervision, guidance and positive reinforcement throughout has been invaluable. Not every PhD student has the opportunity to pick up the skills I have gained during my research, as well as being exposed to such a wide variety of research from chemists and chemical engineers that have been a part of the Blacker group and the iPRD.

I would also like to thank Dr Bao Nguyen for his assistance in NMR spectroscopy, molecular modelling and guidance during the project. Also, for giving me a space in his lab to work in.

For my first year, in the basement, I would like to thank Drs Katie Jolley, Jess Breen and Will Reynolds for running the lab and being approachable for any problems. Next, a thank you to Phil, Lisa, Chris, Yuhan, Nick, Maria, Pete, Jing and Mindaugas for making the office and lab a lively and fun workplace. I would also like to thank Dr Mary Bayana for her invaluable help with the analytical equipment during the rest of my project.

For my two years in Bao's lab, I would like to thank Grant, Rachel, Lewis, Ryan, Ben and Tom for welcoming me into their office and making it a great place to work. Also, thank you for being available to visit the pub from time to time.

I would like to thank Simon Barret for his constant maintenance of the NMR spectrometers and the running of special experiments.

I would like to thank Dr Chris Pask for all my x-ray crystallography data and his x-ray knowledge, and Dr Mike Chapman for assistance in crystal growing and advice.

I would like to thank my parents and my brother for supporting me and always being there. I would especially like to thank my loving wife Becca for her positive reinforcement throughout my project and putting up with all the late nights and weekends that were spent on my research, particularly towards the end of the project.

## Abstract

1,2-Diols and 1,2-ketoalcohols are important functional groups that can require multiple steps to synthesise, which increases yield losses, waste and often uses stoichiometric reagents and toxic/expensive catalysts. The ability to transform simple substrates into more complex products in one-pot with two or more catalysed steps is desirable, especially if a single catalyst can carry out both reactions.

A multifunctional catalyst system was designed to transform primary alcohols into 1,2-diols through three sequential catalysed transformations; transfer dehydrogenation, benzoin condensation, and transfer hydrogenation. Two families of novel ligands and iridium(III) complexes bearing either thiazole or triazole rings were synthesised towards creating a multifunctional catalyst and characterised using mass spectrometry, NMR spectroscopy and x-ray crystallography. During the synthesis of the ligands, the alkylation of thiazole compounds and the DIBAL-H reduction of a thiazole ester were developed.

The organo-organometallic complexes were tested for the transfer dehydrogenation of benzyl alcohol and the reaction was investigated to show that the equilibrium between the forward and reverse reaction, and not catalyst deactivation, was the cause of limited conversion. The hydrogen acceptor was varied and acetone was found to be the most effective when used as a dilute solvent with strictly inert reaction conditions, reaching up to 78% conversion. Four of the novel complexes gave comparable conversions to the control catalyst; however, the benzoin condensation reaction was not successful.

The transfer hydrogenation of benzaldehyde was tested and found give quantitative conversions with the majority of novel complexes. A substrate scope identified that the more electron rich substrates were more easily oxidised. With a secondary alcohol, the transfer dehydrogenations occurred at a faster rate compared to the primary alcohol, reaching quantitative conversion.

# Table of Contents

1. Introduction .....	5
1.1. Multicatalysis .....	5
1.2. Advantages .....	6
1.3. Disadvantages.....	7
1.4. Tandem taxonomy.....	7
1.5. Cooperative Catalysis.....	8
1.6. Sequential Catalysis.....	10
1.7. Relay Catalysis.....	12
1.8. Multifunctional Catalysis .....	15
1.9. Hydrogen Transfer Reactions.....	24
1.10. Organocatalysis.....	35
1.11. Summary .....	44
1.12. Aims and Objectives.....	45
2. Synthesis of Novel Thiazole and Triazole Iridium(III) Complexes .....	47
2.1. Introduction.....	47
2.2. Control Catalysts .....	54
2.3. Synthesis of Thiazole and Thiazolium Iridium(III) Complexes .....	57
2.4. Triazole Ligands .....	90
2.5. Summary .....	104
3. Catalyst Testing .....	106
3.1. Introduction.....	106
3.2. Control Reactions .....	106
3.3. Transfer Dehydrogenation of Benzyl Alcohol .....	112
3.4. Transfer Dehydrogenation of Benzyl Alcohol Derivatives.....	142
3.5. Summary .....	148
4. Conclusions and Future Work.....	150

5. Experimental.....	153
5.1. General Experimental.....	153
5.2. Control Compounds .....	154
5.3. Thiazole Compounds.....	159
5.4. Triazole Compounds .....	185
5.5. Catalyst Testing Experiments.....	197
5.6. Transfer Dehydrogenation Experiments .....	201
5.7. Transfer Hydrogenation of Benzoin 129 with Benzyl Alcohol 39 .....	218
5.8. Control Test for Side Reactions using an IR Probe .....	219
5.9. Benzoin Condensation with Benzaldehyde 67 .....	220
5.10. Transfer Hydrogenation.....	220
5.11. Reactions using a Carousel Reactor .....	221
5.12. Scope .....	224
5.13. Transfer Dehydrogenation of ( <i>R</i> )- and ( <i>S</i> )-1-Phenylethanol 51 with Complex C.13.....	225
5.14. Transfer Dehydrogenation of Benzyl Alcohol 39: Catalyst Loading Tests .....	225
5.15. Transfer Dehydrogenation of 1-Phenylethanol 51: Catalyst Loading Tests .....	227
5.16. Analytical Data for Catalysis Products.....	228
5.17. GC Calibration Data .....	232
6. References .....	234
7. Appendix.....	241

## Abbreviations

ACP	Acyl carrier protein
AT	Acetyl transferase
Bn	Benzyl
CE	Condensing enzyme
CoA	Coenzyme A
COSY	COrelated SpectroscopY
Cp*	Pentamethylcyclopentadiene
CsDPEN	<i>N</i> -Camphorsulphonyl-1,2-diphenylethylenediamine
Cy	Cyclohexyl
DBU	1,8-Diazabicycloundec-7-ene
DIAD	Diisopropyl azodicarboxylate
DIBALH	Diisobutylaluminium hydride
DPEN	1,2-diphenylethylenediamine
DPEphos	Bis-[(2-diphenylphosphino)phenyl]ether
dppf	1,1'-Bis(diphenylphosphino)ferrocene
ee	Enantiomeric excess
FAS	Fatty acid synthase
HMBC	Heteronuclear Multiple Bond Connectivity
HMQC	Heteronuclear Multiple Quantum Coherence
HOMO	Highest occupied molecular orbital
KR	Ketoacyl reductase
LABA	Long acting $\beta_2$ -agonist
Mes	Mesityl
MT	Malonyl Transferase
NHC	<i>N</i> -Heterocyclic carbene
NMR	Nuclear magnetic resonance
NOESY	Nuclear Overhauser Effect SpectroscopY
PKU	Phenylketonuria
TE	Thioesterase
TEAF	Triethylamine/formic acid (2:5)
TES	Triethylsilyl
TMS	Trimethylsilyl

TON	Turn-over number
TPP	Thiamine pyrophosphate
TRIBAL	Triisobutylaluminium
Ts	<i>p</i> -Toluenesulfonyl
TsDPEN	<i>N-p</i> -Tosyl-1,2-diphenylethylenediamine



# 1. Introduction

This chapter introduces the topics of multicatalysis, organometallic catalysts for hydrogen transfer reactions and organo catalysts for the benzoin condensation and related reactions. Examples of the research reported in these areas are reviewed.

## 1.1. Multicatalysis

Multicatalysis has been a growing area for the use in organic synthesis over the last two decades (Figure 1). Combining multiple catalysts in a one-pot process to carry out sequential reactions is a desirable method of reaching complex targets and improving reaction efficiency.<sup>1</sup>

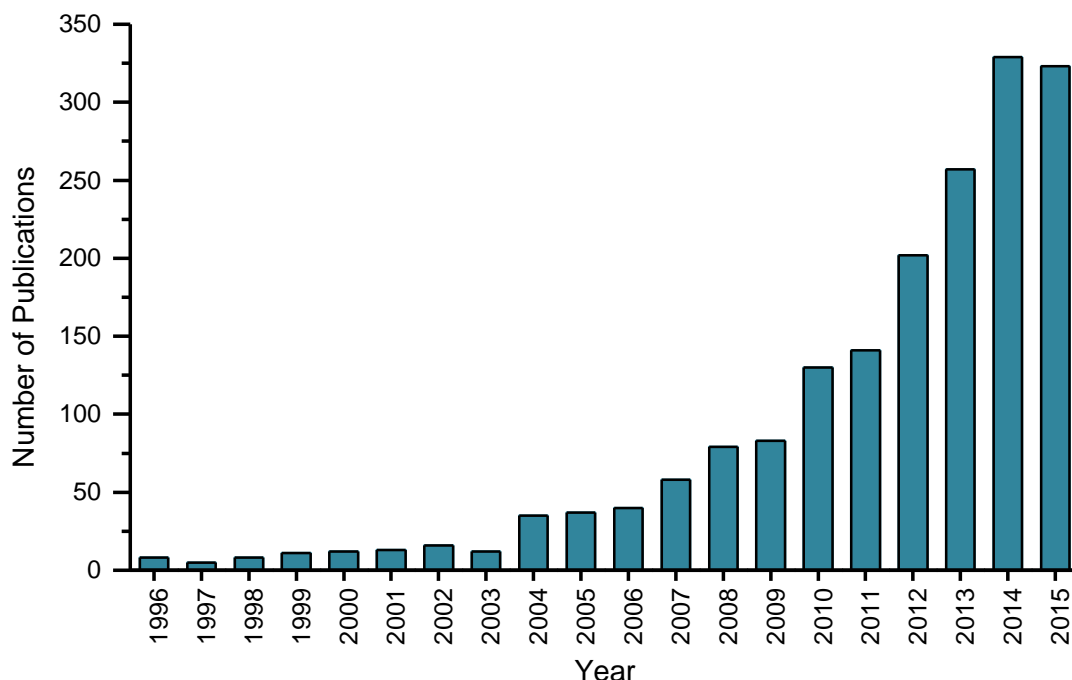


**Figure 1** The number of publications from 1996 to 2015 as identified by Web of Science™ to include in the topics either: “multicatalysis”, “multifunctional catalysis”, “tandem catalysis”, “domino catalysis”, “relay catalysis”, “sequential catalysis”, and “cooperative catalysis”.

Multicatalysis is defined as two or more catalysed reactions that have distinct catalytic cycles, which are carried out on a single substrate in the same reaction vessel (Figure 2). Catalysts or reagents can be added during the reaction in order to activate or control the sequence of reactions.

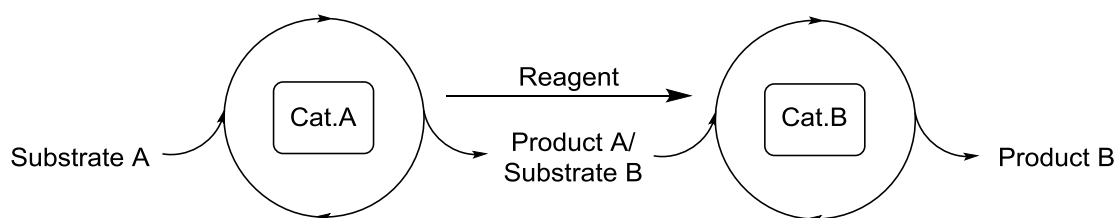
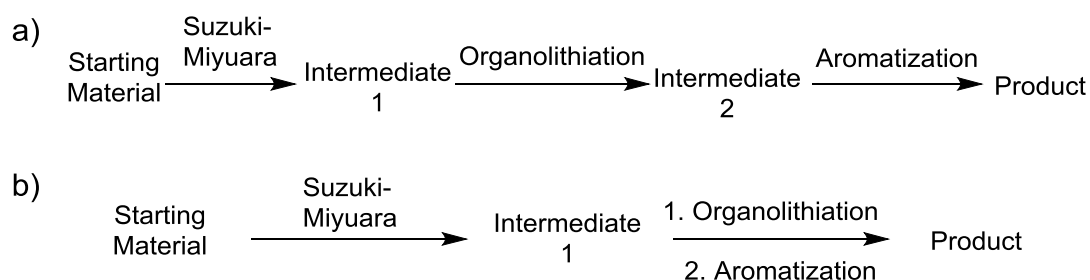


**Figure 2** Multicatalysis with two catalysts in one-pot, where the product of the first reaction is the substrate for the second reaction.

Multicatalysis has enormous potential, as many metal/metal, organo/organo, metal/organo, enzyme/metal and enzyme/enzyme catalysts can theoretically be combined; provided the desired reaction sequence is feasible.

## 1.2. Advantages

The work-up and isolation of products throughout a synthesis are often the most expensive, time consuming and wasteful stages of an experiment. By combining two or more catalytic reactions in one-pot, with only a single work-up stage, syntheses can be made more efficient and reduce yield losses. Desai, senior chemist at The Dow Chemical Company at the time of publication, has estimated the scale of the costings for a palladium catalysed Suzuki-Miyuara coupling, organolithiation and aromatisation route, as compared to telescoping the last two reactions (Scheme 1).<sup>2</sup> For a tonne scale process, the total costs for producing one kilogram of product for the original route and the telescoped route is \$31,000 and \$14,700 respectively; a cost reduction of 53%. In addition, the batch cycle time was reduced by 61 hours.



**Scheme 1** a) Original three stage route with the isolation of two intermediates, and b) the improved two stage route with a single intermediate.

By utilizing selective catalysts in one-pot, intermediates can be further reacted upon without the need for protecting groups. Where the intermediates are

reactive species, yield losses due to degradation or side reactions can be reduced, as the lifetime of the intermediates will be shortened.

As the reactions occur in one-pot with the same solvent, the process is less wasteful. In addition, as the reactions will be at the same temperature, heating or cooling the reactor is more economical. However, the catalysts must be active under the same conditions for this to apply.

### **1.3. Disadvantages**

By combining multiple catalysts in one-pot, there is a larger probability that side products will be produced if the catalysts are less than perfectly selective; a problem which requires careful planning of the reaction sequence and investigation of catalytic intermediates to overcome. Biological synthesis has evolved to have selective catalysts; which produce key intermediates without side reaction or deactivation. Catalyst deactivation is more prevalent; therefore, previous mechanistic knowledge of the individual catalysts is beneficial when designing a novel multicatalysis process.

Optimization of multicatalysis can be difficult, as it is rare that all the catalysts will share optimal conditions. In addition, any reagents used in the reactions must be tolerated by all the catalysts as well as any intermediates formed. This can be improved with compartmentalised catalysts in micelles or membranes to allow reactions to occur in different solvents.<sup>3</sup> The substrate scope of the reactions can be narrow, as the substrates (and their successive intermediates) must be compatible with the catalysts in the desired order. In multicatalysis two or more catalyst species are present, therefore the opportunity for catalyst recovery and recycling is greatly reduced for mixed species; which would require subsequent separation and purification before reuse. This can be overcome with multifunctional catalysts that tether two or more catalysts together as a single species.

### **1.4. Tandem taxonomy**

In the literature, many terms are used to describe the different multicatalytic processes and have unfortunately become interchangeable. Fogg and Santos attempted to clarify the different types of multicatalysis, with a more recent review by Patil expanding the definitions further.<sup>4, 5</sup> Multicatalysis can be

subdivided into three main groups; cooperative catalysis, relay catalysis, and sequential catalysis (Figure 3).

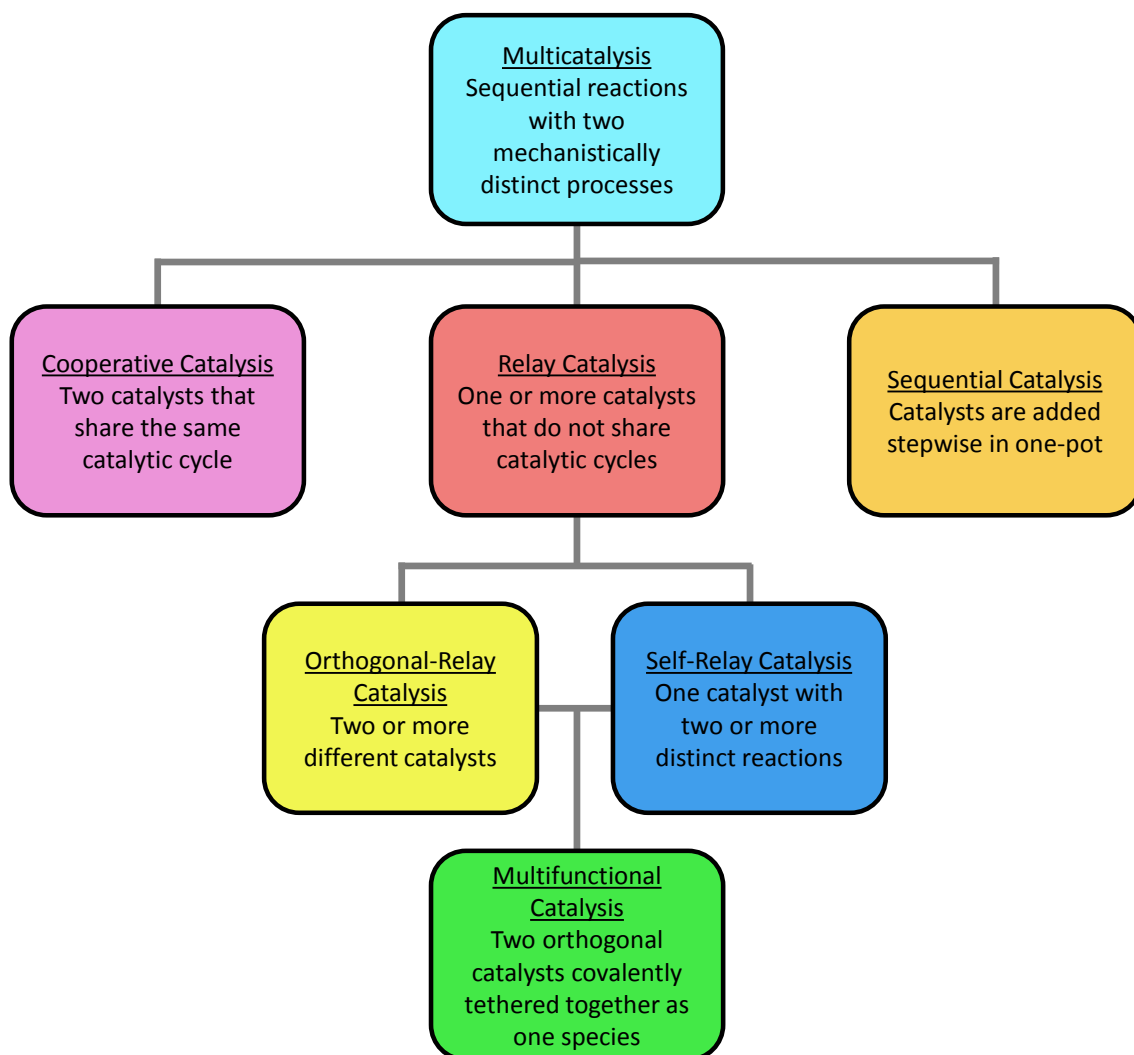


**Figure 3** The definitions of the different multicatalytic processes.

## 1.5. Cooperative Catalysis

In cooperative catalysis, two catalysts, either separate or tethered, work together within the same catalytic cycle in order to catalyse a transformation (Figure 4).<sup>6, 7</sup>

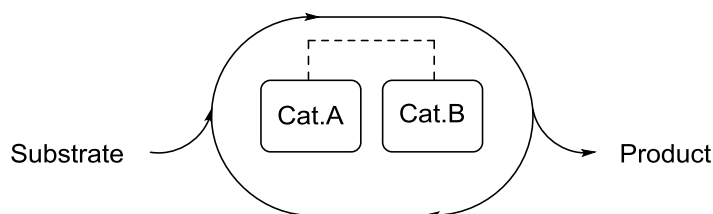
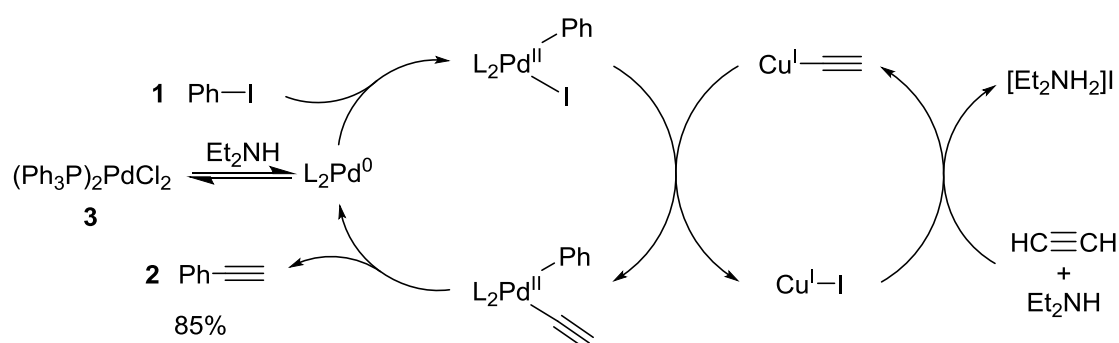


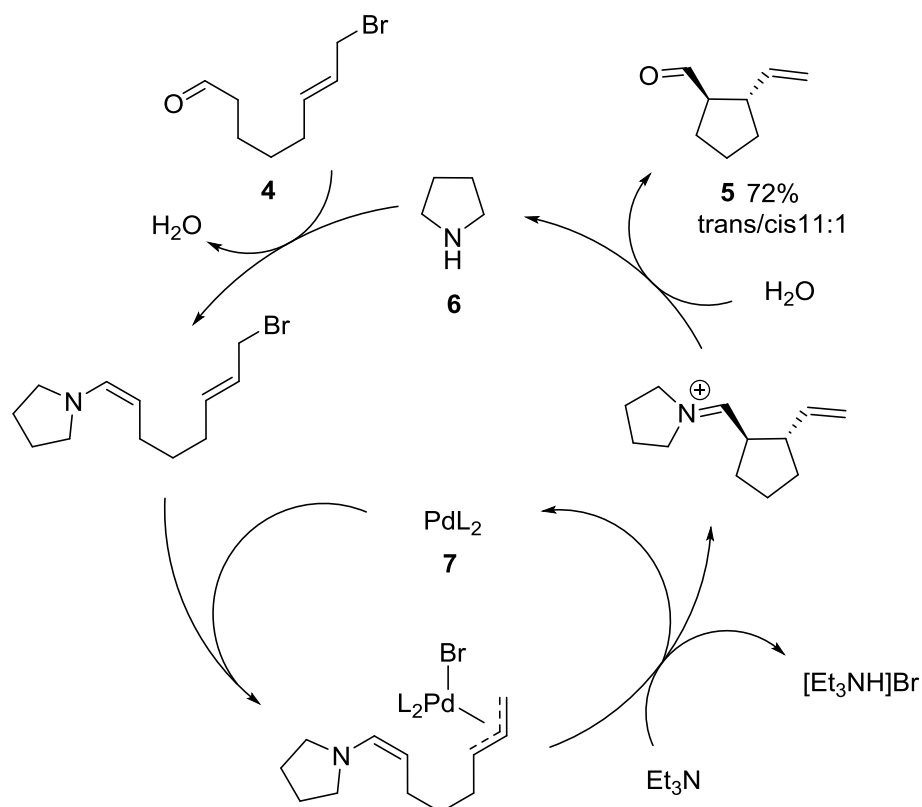
**Figure 4** Cooperative multicatalysis whereby catalysts A and B work together in the same catalytic cycle to carry out a transformation.

One of the most famous examples of metal/metal cooperative multicatalysis is the Sonogashira coupling reaction, catalysed by a palladium catalyst **3** and a copper salt (Scheme 2).<sup>8</sup>



**Scheme 2** The Sonogashira coupling reaction; **1** (10 mmol), **2** (excess), **3** (0.5 mol%), CuI (1.0 mol%), Et<sub>2</sub>NH (0.2 M), rt, N<sub>2</sub>, 6 h.

Cooperative catalysis is useful to activate multiple functional groups in order to achieve transformations faster or allow previously inactive catalysts to function. Examples include imidazole,<sup>9</sup> lanthanide,<sup>10, 11</sup> cinchona/silver,<sup>12</sup> samarium/ mercaptan,<sup>13</sup> palladium/copper,<sup>14</sup> and ruthenium/palladium cooperative catalytic systems.<sup>15</sup> Saicic used a proline organocatalyst with a palladium organometallic catalyst to generate 5- and 6-membered cycloalkanes via cooperative multicatalysis (Scheme 3).<sup>16</sup>



**Scheme 3** A pyrrolidine/palladium cooperative multicatalysis process to generate a 5-membered ring with the Tsuji-Trost reaction: **4** (0.16 mmol), Pd(PPh<sub>3</sub>)<sub>4</sub> (5.0 mol%), **6** (40 mol%), Et<sub>3</sub>N (1.0 eq), THF (0.3 M), rt, inert atmosphere, 30 min.

## 1.6. Sequential Catalysis

Sequential catalysis is a one-pot reaction with only a single catalyst present at the start of the reaction. The first reaction is carried out and when the end-point is reached, the second catalyst is added to the reaction. Further catalysts can be added to continue the sequence (Figure 5).

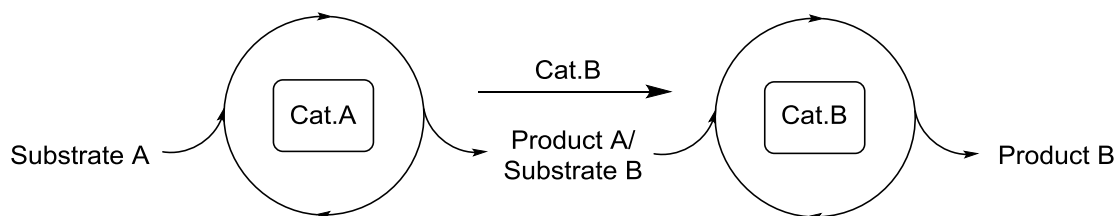
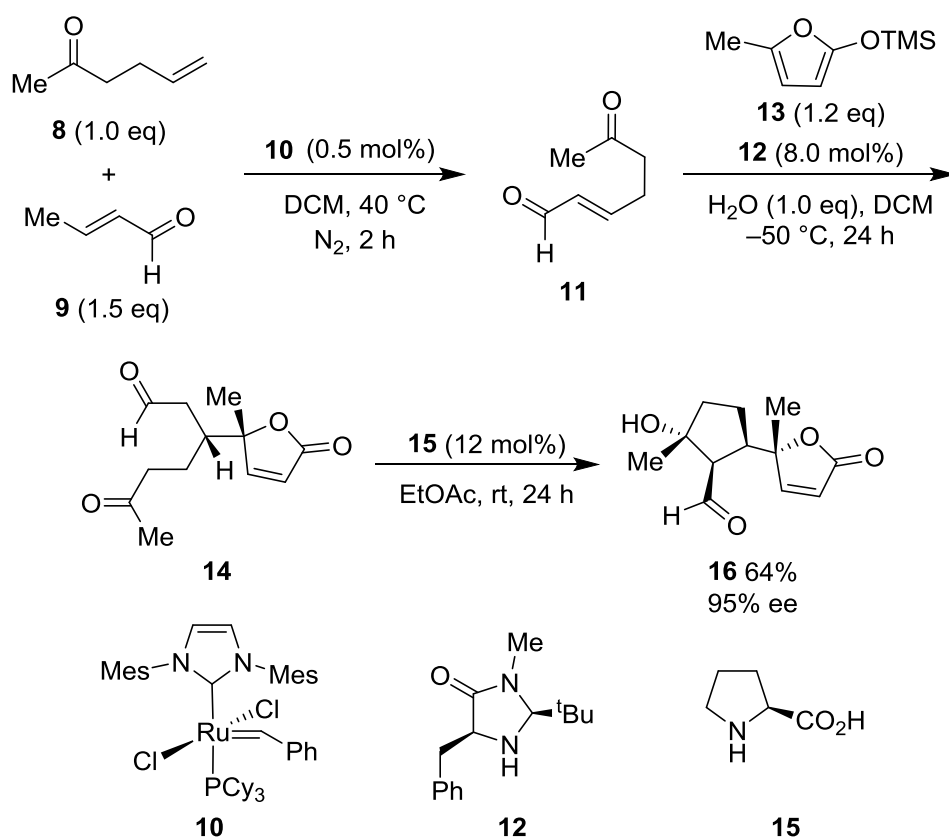


**Figure 5** Sequential multicatalysis, whereby the second catalyst is added to the reaction after the first catalysed transformation is complete.

This type of multicatalysis is useful if the initial substrate can react with the subsequent catalysts, as undesired reactions can be avoided. However,

reaction monitoring must be put in place to identify the end-points; which can increase process time and cost. In addition, large-scale addition of a solid catalyst to a working reactor has practical limitations. Examples include a ruthenium/ytterbium,<sup>17</sup> and a palladium/Brønsted acid/thiourea sequential multicatalysis process.<sup>18</sup> MacMillan has utilized sequential multicatalysis to carry out a metathesis/Mukaiyama-Michael addition/intramolecular aldol triple cascade, making five carbon-carbon bonds and four stereocentres in one-pot (Scheme 3).<sup>19</sup>



**Scheme 4** A sequential multicatalysis metathesis/Mukaiyama-Michael/aldol reaction.

## 1.7. Relay Catalysis

Relay catalysis consists of one or more catalysts, present from the start of the reaction, with two or more distinct catalytic cycles. There are two types of relay catalysis: self-relay and orthogonal-relay.

### 1.7.1. Self-relay

In a self-relay multicatalysis process, only one catalyst is present in the reaction, which carries out different transformations on the initial substrate and the intermediate produced (Figure 6).

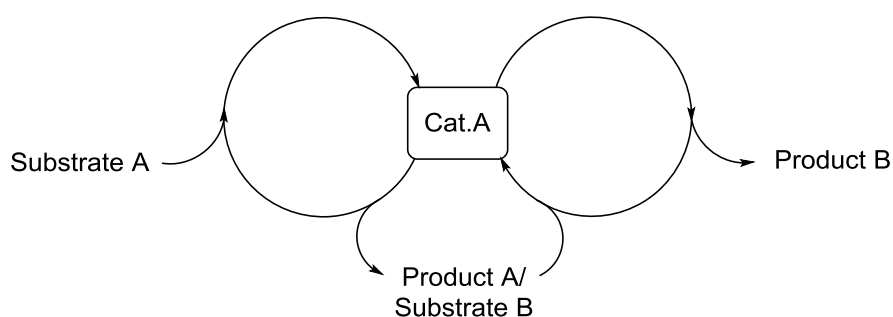
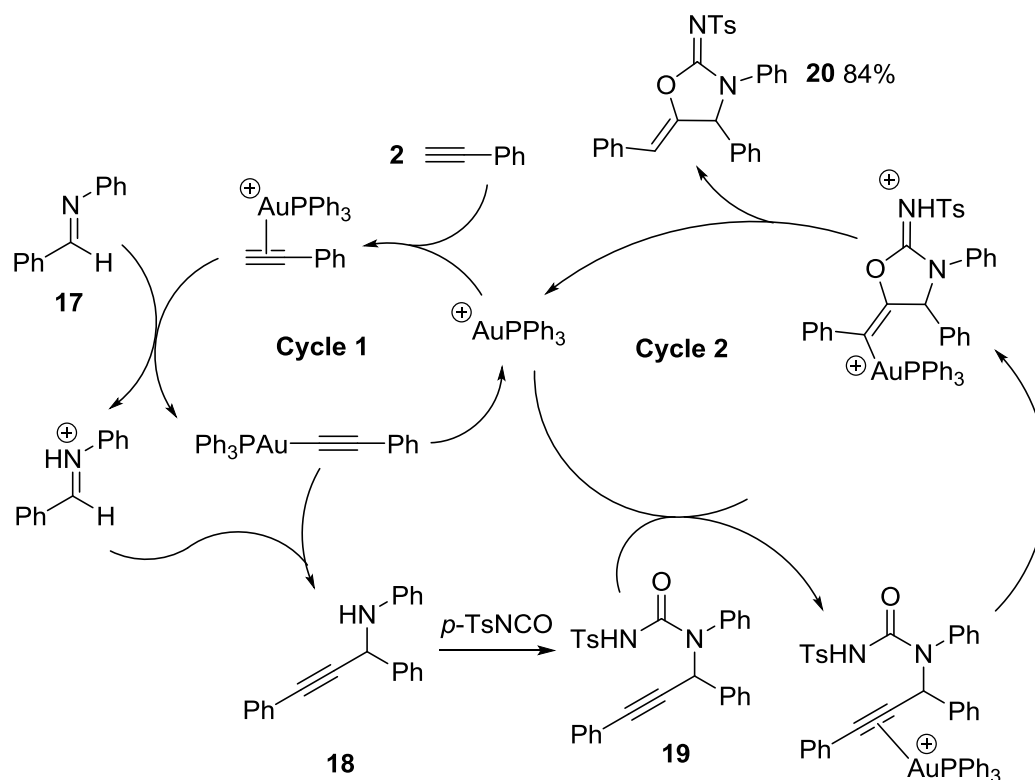


**Figure 6** Self-relay multicatalysis, whereby a single catalyst carries out two different sequential transformations, with two distinct catalytic cycles.

Examples include: ruthenium catalysed C-H activation/Michael addition,<sup>20</sup> copper catalysed  $S_NAr$ /denitrogenation/cyclisation,<sup>21</sup> ruthenium catalysed metathesis/hydrogenation/hydrogen transfer,<sup>22</sup> and gold catalysed addition/Petasis-Ferrier rearrangement using self-relay catalysis.<sup>23</sup> Toste and Campbell utilized self-relay multicatalysis for an alkynylation/cyclization reaction sequence, with a gold triphenylphosphine catalyst (Scheme 5).<sup>24</sup>





**Scheme 5** Self-relay multicyclic catalysis of an alkylation/cyclization cascade for cyclic carbamimidates: imine (0.50 mmol), alkyne (0.60 mmol),  $p\text{-TsHNCO}$  (0.60 mmol),  $\text{Ph}_3\text{PAuCl}$  (5.0 mol%),  $\text{AgNTf}_2$  (5.0 mol%),  $\text{CHCl}_3$  (0.2 M), 35 °C, 20 h.

Problems can occur with substrates inserting into the wrong catalytic cycle and the reaction conditions must be balanced in order not to favour one catalytic transformation over the other.

### 1.7.2. Orthogonal-relay

In an orthogonal-relay catalysis process, two or more different catalysts are present in the reaction, which selectively react with a substrate in distinct catalytic cycles (Figure 7).

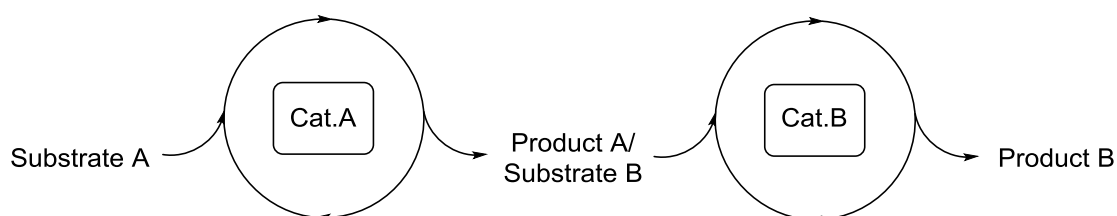
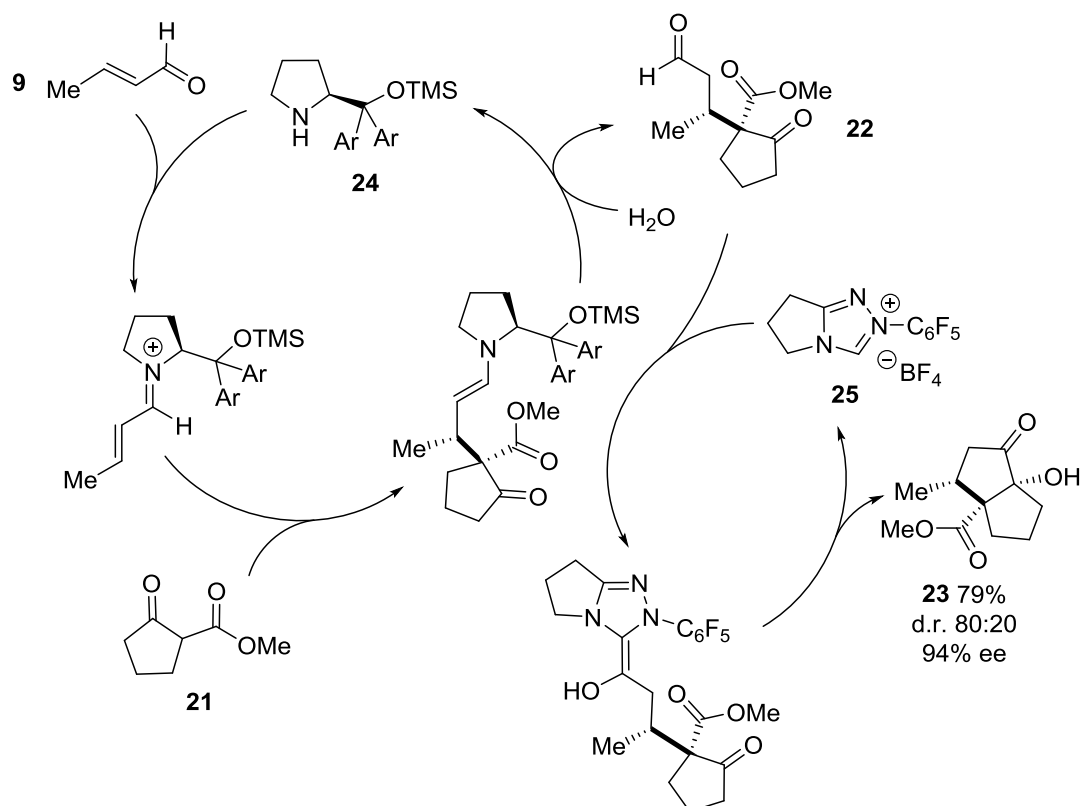


**Figure 7** Orthogonal-relay catalysis, whereby two different catalysts carry out sequential transformations with distinct catalytic cycles and both catalysts are present from the start.

Rovis has combined a chiral proline catalyst **24** and an NHC catalyst **25**, to achieve a Michael addition/intramolecular crossed-benzoin orthogonal-relay system (Scheme 6).<sup>25</sup>



**Scheme 6** Proline and NHC catalyzed Michael addition/crossed benzoin reaction in one-pot; proline (Ar = 3,5-(CF<sub>3</sub>)<sub>2</sub>-C<sub>6</sub>H<sub>3</sub>, 20 mol%), NHC (10 mol%), NaOAc (10 mol%), CHCl<sub>3</sub>, 22 °C, 14 h.

Examples include: a rhodium/palladium catalyzed allylation/*N*-allylation sequence,<sup>26</sup> an NHC/cinchonine catalyzed oxidation/oxa-Michael addition sequence,<sup>27</sup> a cobalt/ruthenium catalyzed hydration/dehydrogenation sequence,<sup>28</sup> and a ruthenium/proline catalyzed oxidation/Michael addition/aldol reaction sequence.<sup>29</sup>

## 1.8. Multifunctional Catalysis

In order to differentiate between multicatalysis and multifunctional catalysis (Figure 3), the following definition for multifunctional catalysis is described: a combination of auto-relay and orthogonal-relay catalysis, whereby a single molecular catalyst has two or more catalytic sites that have orthogonal chemical reactivities and are tethered together by a covalent bond or through a bridging ligand which is strongly bound to a metal centre (Figure 8).<sup>30</sup>

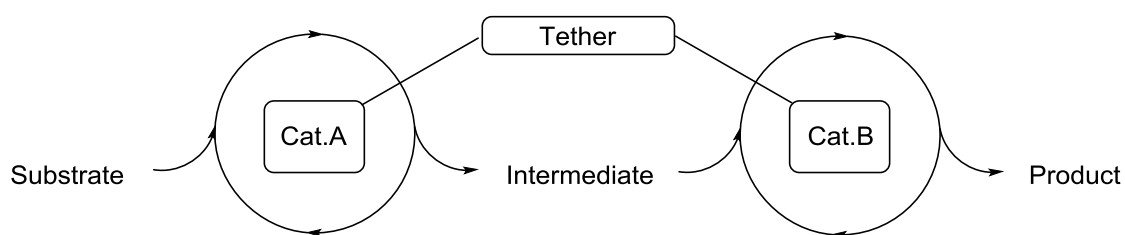


**Figure 8** A multifunctional catalyst, combining catalyst A with catalyst B via a covalent tether, which can carry out sequential reactions.

Nature is by far the best example of combined catalysis, as many enzymes in the body work together to produce complex molecules within cellular systems. Enzymatic reactions do not require work-up or isolation, are very atom efficient and have mild reaction conditions. An example of an enzyme which carries out multiple reactions is Fatty Acid Synthase (FAS) (Figure 9).

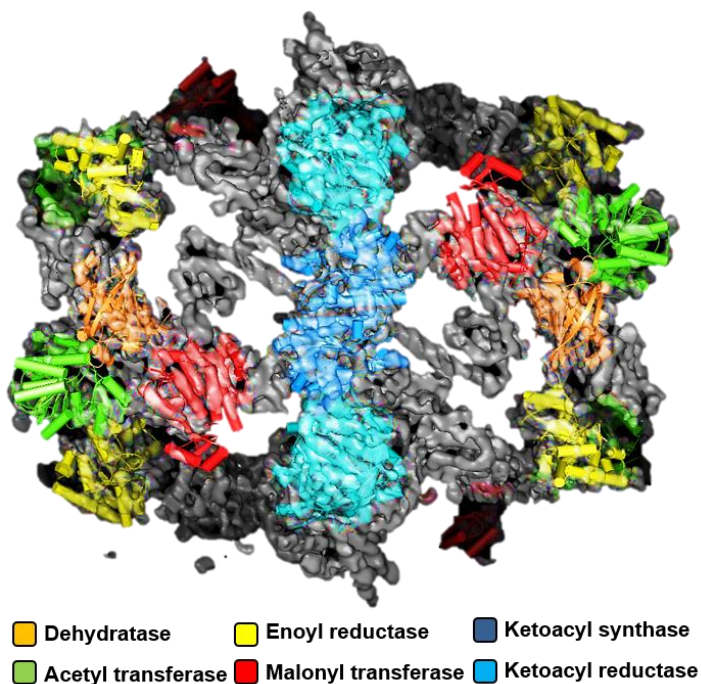


**Figure 9** The X-ray crystal structure of fungal FAS with enzymatic sites identified.<sup>31</sup>

FAS is a dimer complex, which makes the enzyme more stable and allows intermediates to be transferred more easily from one site to the next by reducing the diffusion distance between catalysts. In addition, it is harder for intermediates to leave the enzyme complex and therefore minimises side reactions on route to palmitate **26** (Figure 10).<sup>32</sup>

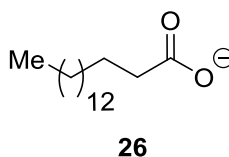
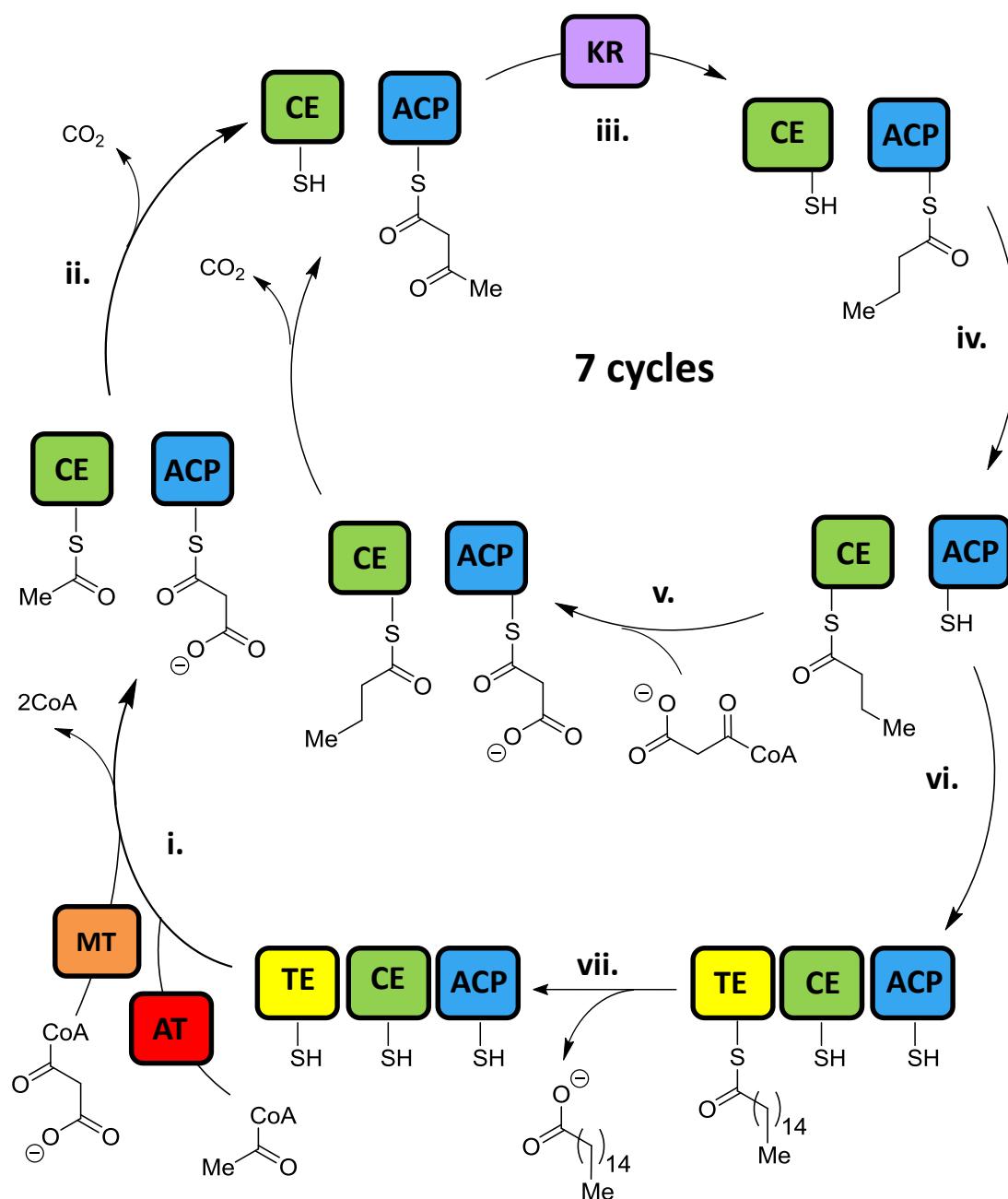


**Figure 10** Palmitate

FAS is a multifunctional enzyme used to make fatty acids in eukaryote cells. The three active domains on the enzyme are made up of several catalytic sites which are present on the polypeptide chain, which are required in sequence (Scheme 7).



**Scheme 7** The catalytic cycle of FAS; i) Acetyl CoA and malonyl CoA bind to the acetyl transferase (AT) and malonyl transferase (MT). The acetyl group is transferred to the condensing enzyme (CE) and the malonyl group is transferred to the acyl carrier protein (ACP). ii) Addition of the acetyl group to the malonyl group occurs with loss of CO<sub>2</sub>. iii) The acetoacetyl group is reduced by the ketoacyl reductase (KR). iv) The butyryl group is translocated from ACP to CE. v) Another malonyl group binds to ACP and the cycle is repeated six times until palmitoyl-CE is formed. vi) Palmitoyl is translocated to thioesterase (TE). vii) Palmitoyl is hydrolysed by TE to **26** and released.<sup>32</sup>

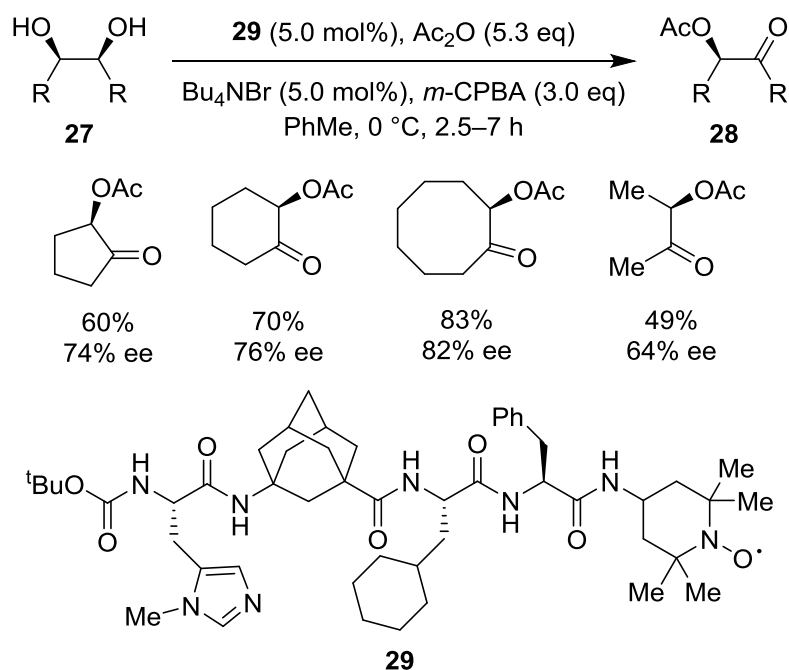
The disadvantages to multifunctional catalysis are:

- The catalysts must be synthesised in advance; other multicatalysis processes simply combine catalysts in one-pot.
- The catalysts must both be active under the same reaction conditions.
- The substrate scope can be smaller than with the individual catalysts.

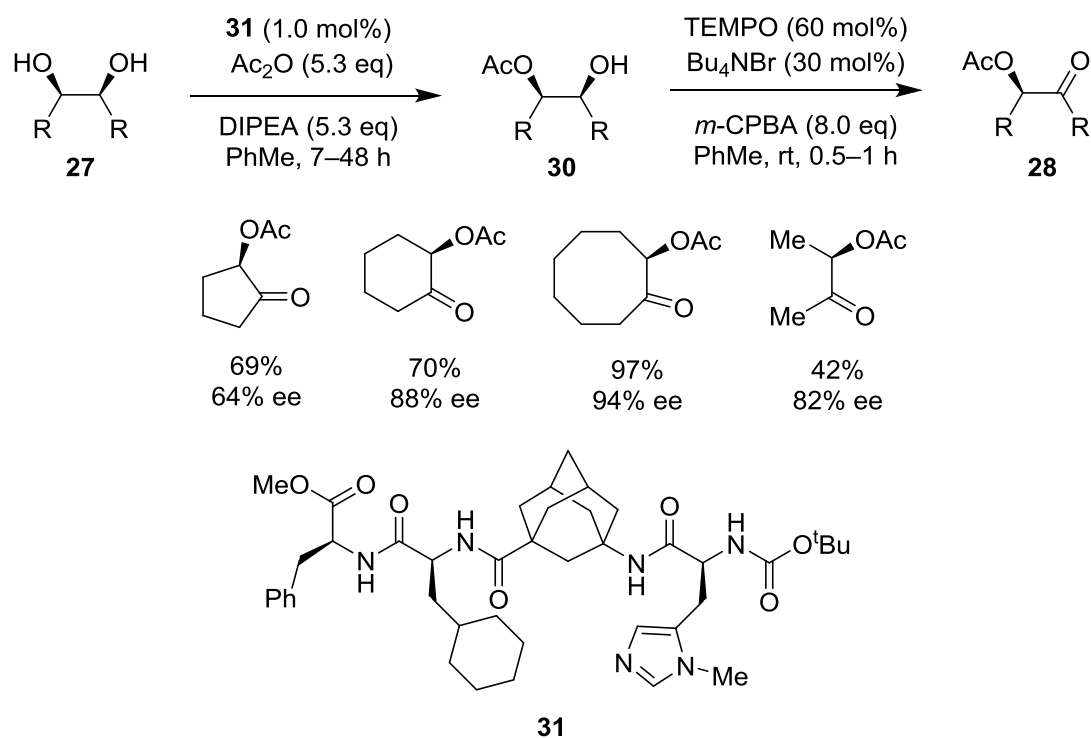
The advantages to multifunctional catalysis are:

- The catalysts can be easily recovered and recycled compared to mixed catalysts in one-pot.
- The rate of the reaction can be increased, as the catalytic sites are in very close proximity to each other reducing the diffusion distance between catalysts.
- Multifunctional catalysts often display a synergistic effect in contrast to the individual catalysts in one-pot.
- Asymmetric transformations can also be enhanced with asymmetric catalysts as the close proximity of the catalysts helps to induce chirality of the substrates.<sup>30</sup>

Schreiner demonstrated that lower catalyst and reagent loadings are a common benefit of multifunctional catalysis, with their organo-multifunctional oligopeptide/TEMPO catalyst **29** (Scheme 8).<sup>33</sup> Compared to the analogous orthogonal-relay process (Scheme 9), the catalyst and reagent loadings were reduced by 92% and 63% respectively.<sup>34</sup>



**Scheme 8** An organo-multifunctional catalyst to carry out catalytic desymmetrization and oxidation sequential reactions of 1,2-diols.



**Scheme 9** An orthogonal-relay multicatalysis process with separate TEMPO and oligopeptide catalysts to carry out catalytic desymmetrization and oxidation sequential reactions of 1,2-diols.

Peris has developed a series of organometallic multifunctional catalysts, which combined two different transition metals with a range of NHC bridging ligands (Figure 11). Peris displayed how difficult the design of multifunctional catalyst can be, by comparing bimetallic catalysts for the tandem cyclisation/alkylation reaction sequence towards alkylated indoles (Table 1).<sup>35</sup>

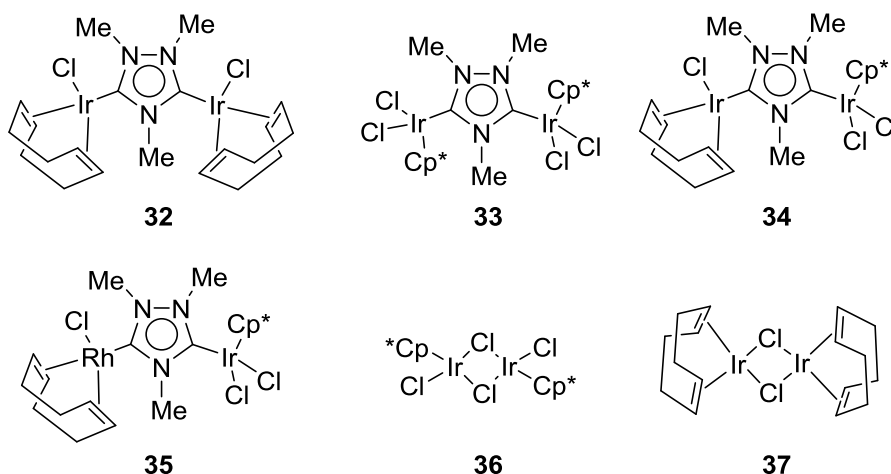
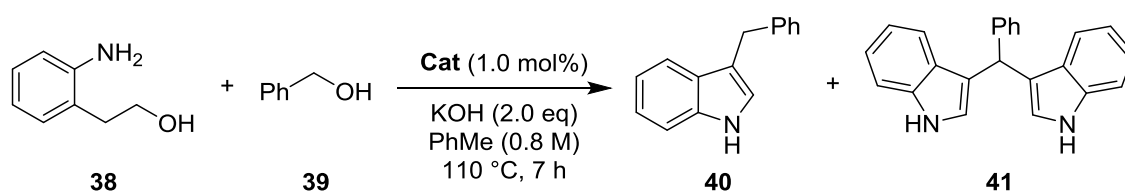


**Figure 11** Bimetallic complexes with mixtures of iridium(I)/iridium(III) and rhodium(I).

The iridium(I)/iridium(III) bimetallic catalyst **34** gave the best activity and selectivity towards the *bis*-indole **41** (entry 3, Table 1). Catalyst **35** (entry 4, Table 1) gave poor activity and no selectivity, suggesting that the Rh<sup>I</sup>(cod) fragment is responsible. However, the comparisons between the Ir<sup>III</sup>Cp\* fragment in catalysts **33**, **34** and **35** (entries 2-4, Table 1) show contrasting results. Therefore, designing multifunctional catalysts requires mechanistic knowledge before producing an efficient catalyst system.



**Table 1** 1,2-Aminophenylethyl alcohol cyclisation/alkylation with **39** catalysed by bimetallic multifunctional catalysts.



Entry	Catalyst	<b>40</b> (%) <sup>a</sup>	<b>41</b> (%) <sup>a</sup>
1	<b>32</b>	22	73
2	<b>33</b>	11	73
3	<b>34</b>	10	86
4	<b>35</b>	15 <sup>b</sup>	15 <sup>b</sup>
5	<b>36</b>	38	57
6	<b>37</b>	17	41

<sup>a</sup> Conversions determined using <sup>1</sup>H NMR; <sup>b</sup> Reaction time 20 h.

The hetero-bimetallic complexes **35** and **42–46** were compared to the corresponding mixture of homo-bimetallic complexes (Figure 12).<sup>35–38</sup> The combination of palladium and iridium complexes enhances the reactivity of the catalysts for a dehalogenation/hydrogenation reaction sequence; the multifunctional hetero-bimetallic catalysts, with the exception of **42**, (entries 2–5, Table 2) outperform a one-to-one mixture of the homo-bimetallic catalysts (entry 6, Table 2).

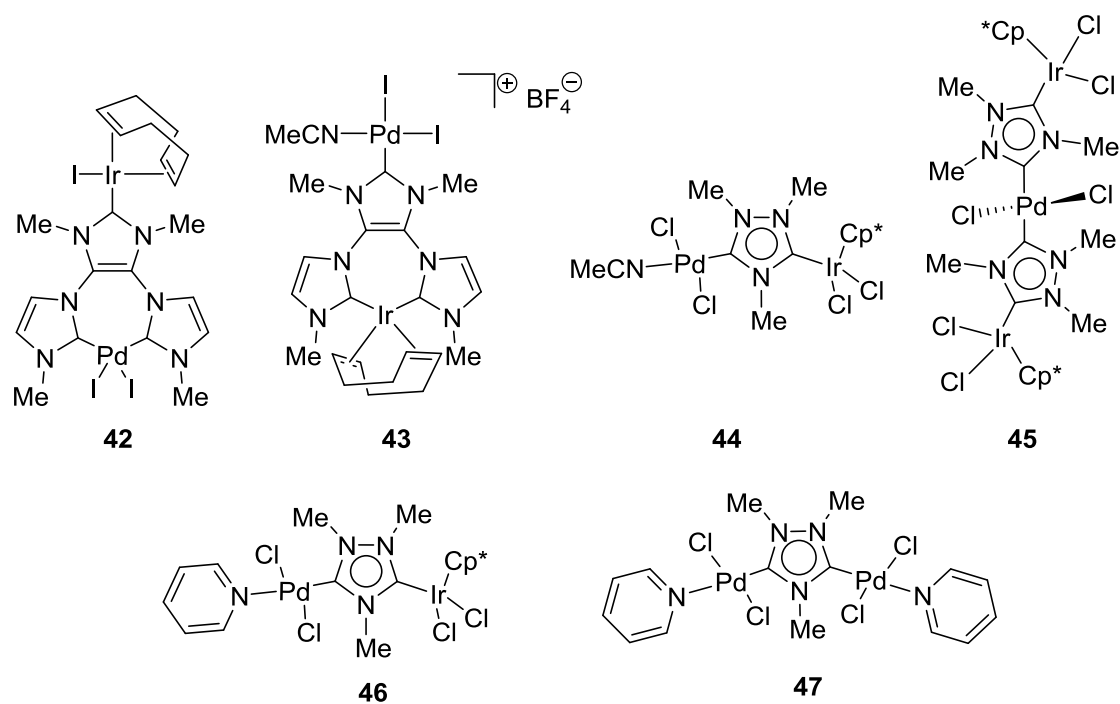
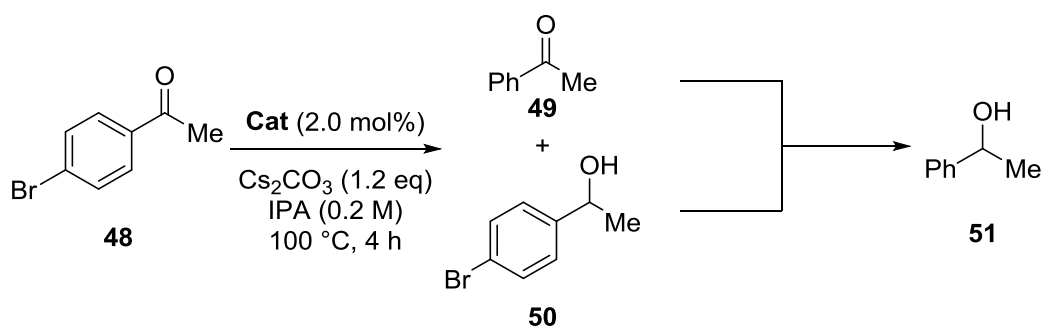


**Figure 12** Hetero- and homo- bimetallic complexes reported by Peris for use in tandem catalysis.

**Table 2** Sequential dehalogenation/hydrogenation reactions catalysed by bimetallic complexes.

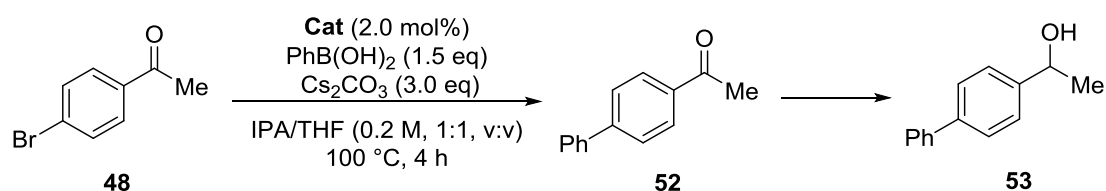


Entry	Catalyst	49 (%) <sup>a</sup>	50 (%) <sup>a</sup>	51 (%) <sup>a</sup>
1	42	70	9	21
2	43	1	0	99
3	44	22	0	75
4	45	0	0	95
5	46	0	0	99
6	33 + 47	72	0	25

<sup>a</sup> Yields determined using GC.

A Suzuki-Miyaura/hydrogenation reaction sequence has also been carried out with the multifunctional catalysts; both hetero-bimetallic catalysts convert the starting material to product, however the yields are low (entries 1 and 2, Table 3), and a one-to-one mixture of the homo-bimetallic catalysts only produced a 5% yield (entry 3, Table 3). The yield with catalyst **46** was increased to 88% by extending the reaction time to 7 hours (entry 4, Table 3).

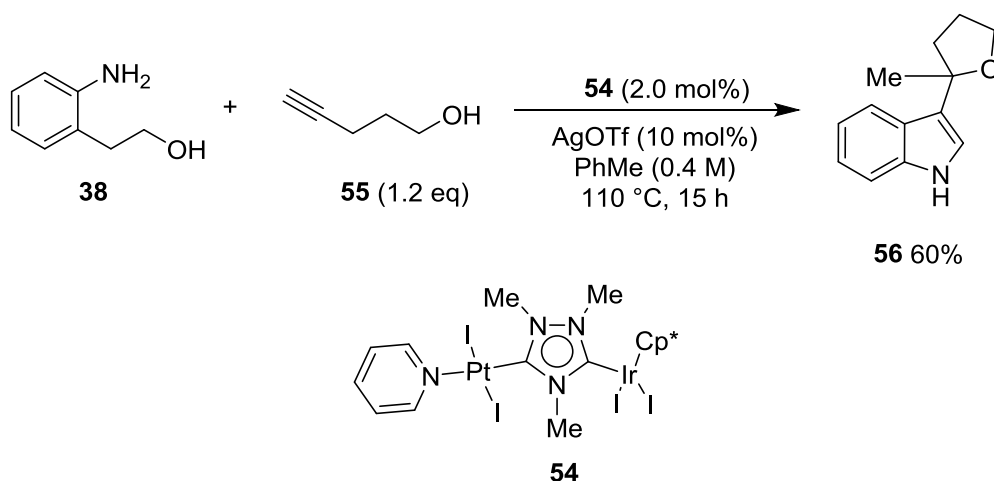
**Table 3** Sequential Suzuki-Miyaura/hydrogenation reactions catalysed by bimetallic complexes.



Entry	Catalyst	<b>49</b> (%) <sup>a</sup>	<b>50</b> (%) <sup>a</sup>	<b>51</b> (%) <sup>a</sup>	<b>52</b> (%) <sup>a</sup>	<b>53</b> (%) <sup>a</sup>
1	<b>43</b>	10	0	5	52	31
2	<b>46</b>	0	0	0	58	28
3	<b>33</b> + <b>47</b>	0	0	0	55	5
4	<b>46</b>	0	0	0	2 <sup>b</sup>	88 <sup>b</sup>

<sup>a</sup> Yields determined using GC; <sup>b</sup> Reaction time 7 hours.

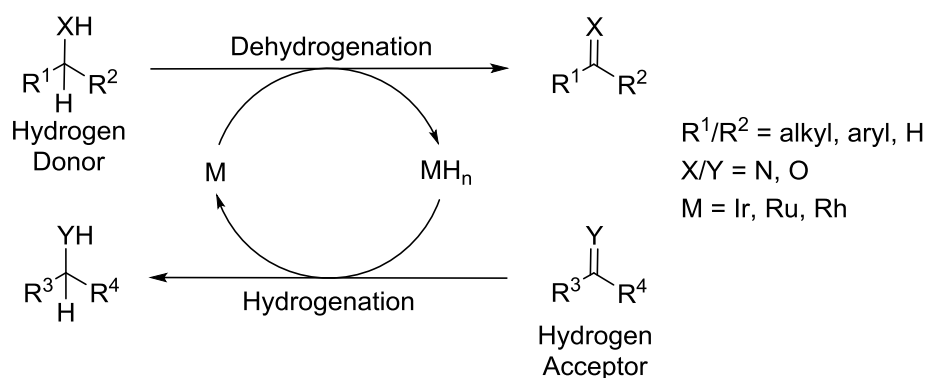
The palladium(II)/iridium(III) multifunctional catalyst **46** has catalysed a Suzuki-Miyaura/ $\alpha$ -alkylation reaction sequence and a nitroarene reduction/alcohol oxidation/coupling reaction sequence.<sup>39</sup> An iridium(III)/platinum(II) multifunctional catalyst **54** has been utilized and shown to be more active than the mixed homo-bimetallic analogous reaction (Scheme 10).<sup>40</sup> To date, there have been no reports of an organometallic/organo multifunctional catalyst system.



**Scheme 10** 1,2-Aminophenyl ethyl alcohol cyclisation/hydroalkoxylation/indole addition reaction sequence catalysed by a platinum(II)/iridium(III) multifunctional catalyst; alkyne addition after 12 hours, yield determined using GC.

## 1.9. Hydrogen Transfer Reactions

Transition metal catalysts have been intensively researched for carbonyl/imine/alkene reduction and alcohol/amine dehydrogenation through hydrogen transfer reactions. Hydrogen transfer is the abstraction of hydrogen from a hydrogen donor and subsequent addition of hydrogen to a hydrogen acceptor and vice versa (Scheme 11).<sup>41</sup>



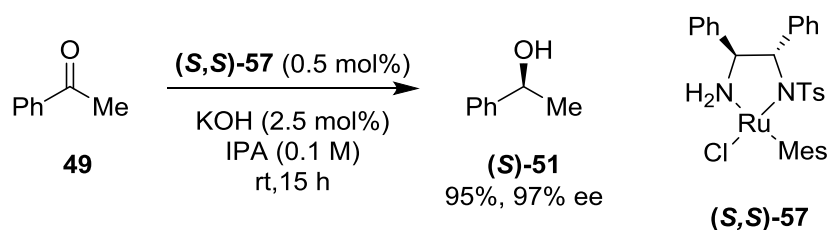
**Scheme 11** Dehydrogenation of the hydrogen donor and hydrogenation of the hydrogen acceptor.

Hydrogenation using a metal catalyst with gaseous hydrogen as the hydrogen source requires high pressures, high temperatures, flammable gases and expensive reactor set-ups. Although hydrogen gas is the most atom

economical method for hydrogenation reactions, using organic molecules as the hydrogen source is more efficient and greatly reduces the risk and cost of the reactions.<sup>42</sup> In 1975, the first generation hydrogen transfer catalysts, such as  $[\text{RuCl}_2(\text{PPh}_3)_3]$ , gave low activity and required high temperatures (180 °C), with long reaction times.<sup>43</sup> In 1991, the reactivity of  $[\text{RuCl}_2(\text{PPh}_3)_3]$  was increased ten-thousand-fold with the addition of base, forming the highly reactive dihydro-ruthenium(II) species  $[\text{H}_2\text{Ru}(\text{PPh}_3)_3]$ , allowing the reaction to proceed at lower temperatures.<sup>44</sup>

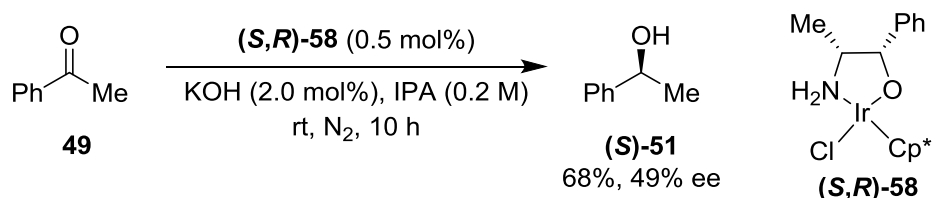
### 1.9.1. Transfer Hydrogenation

The most common hydrogen donor system used for transfer hydrogenation reactions is *iso*-propanol, for the reduction of carbonyls and alkenes.<sup>45</sup> The reverse hydrogen transfer reaction is a disadvantage, as it reduces the yield. However, acetone is the by-product of the reaction, which is highly volatile and can be easily removed to drive the equilibrium to the desired product. Transfer hydrogenation with a chiral catalyst, with either a chiral ligand or complex, can induce chirality into the products selectively. An efficient asymmetric catalyst is highly desirable, as many pharmaceutical molecules require specific chirality for selective activity with enzymes and biological receptor sites. Noyori showed that acetophenone **49** can be asymmetrically reduced with a chiral ruthenium(II) catalyst **57** to (*S*)-phenylethanol **51** (Scheme 12).<sup>46</sup>

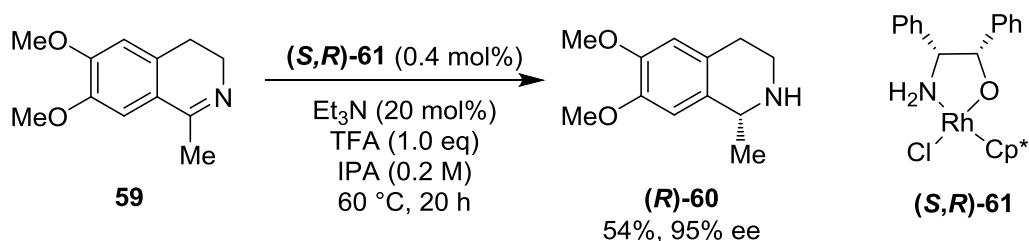


**Scheme 12** Asymmetric reduction of acetophenone with a ruthenium(II) catalyst **57**.

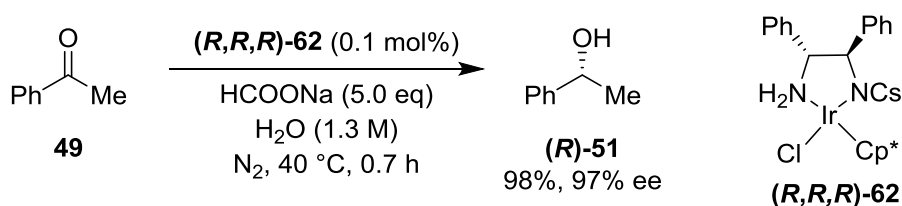
Blacker has invented iridium(III) and rhodium(III) catalysts for the transfer hydrogenation of ketones (Scheme 13) and imines asymmetrically (Scheme 14).<sup>47</sup> In addition, asymmetric transfer hydrogenation of ketones in neat water, using CsDPEN iridium(III) catalysts was achieved (Scheme 15).<sup>48</sup> Both enantiomers are accessible with the opposite ligand enantiomer.



**Scheme 13** Asymmetric transfer hydrogenation of ketone **49** to alcohol **51** with high enantioselectivity using an iridium(III) catalyst **58**; yield determined using GC.

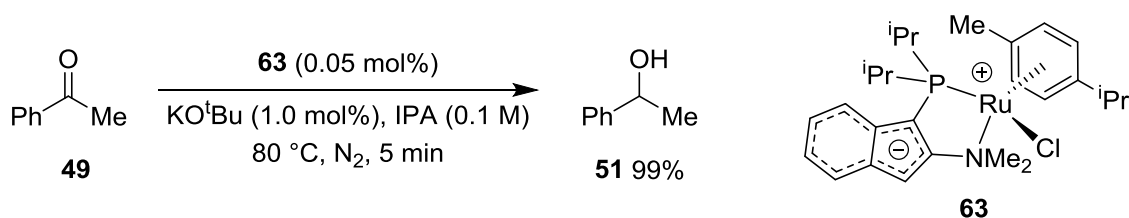


**Scheme 14** An asymmetric transfer hydrogenation of imine **59** to amine **60** with high enantioselectivity using a rhodium(III) catalyst **61**; yield determined using GC.



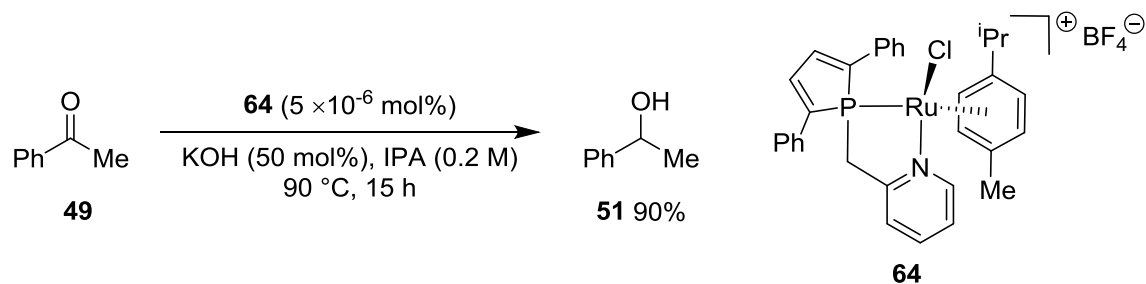
**Scheme 15** Ketone transfer hydrogenation in neat water with an iridium(III) catalyst **62**. Cs = camphor sulfonyl.

Stradiotto achieved ketone transfer hydrogenation with zwitterionic ruthenium(II) catalyst **63** at very low catalyst loadings (0.05 mol%) with short reaction times (5 min), but without asymmetric induction.<sup>49</sup>



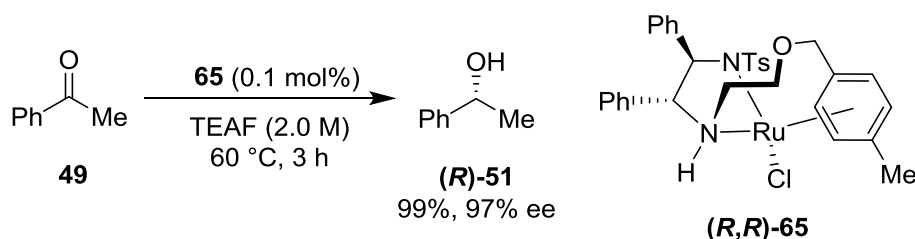
**Scheme 16** Ketone transfer hydrogenation with a zwitterionic ruthenium(II) catalyst.

Mathey and Le Floch achieved ketone reduction (Scheme 17) with an extremely low catalyst loading ( $5 \times 10^{-6}$  mol%).<sup>50</sup>



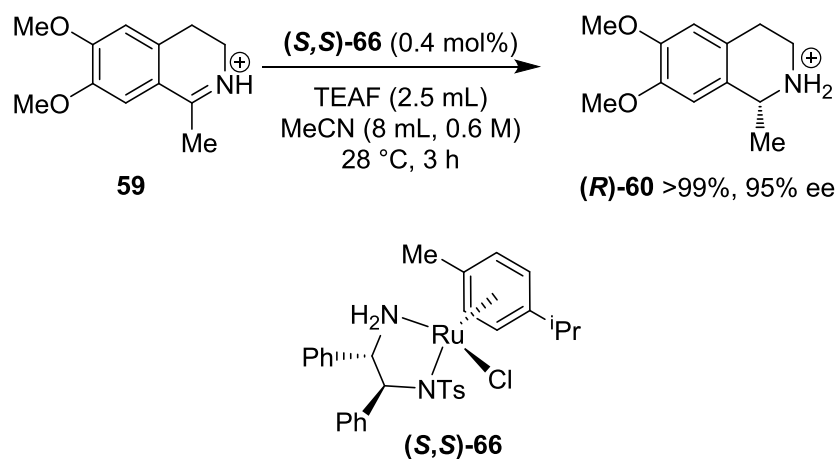
**Scheme 17** Ketone transfer hydrogenation with a phosphole ruthenium(II) complex at  $5 \times 10^{-6}$  mol% catalyst loading.

A hydrogen donor system where the reverse reaction cannot occur can be achieved using a TEAF solution (2:5 triethylamine/formic acid), whereby formic acid is the source of hydrogen, producing gaseous carbon dioxide which makes the reaction essentially irreversible. However, the reaction scope is limited by the acidic nature of the conditions, which may degrade certain catalysts, substrates and/or reagents. Ikariya has utilized this system for the asymmetric reduction of ketones with an arene tethered catalyst **65** (Scheme 18).<sup>51</sup>



**Scheme 18** Asymmetric reduction of a carbonyl with formic acid using a ruthenium(II) catalyst **65**.

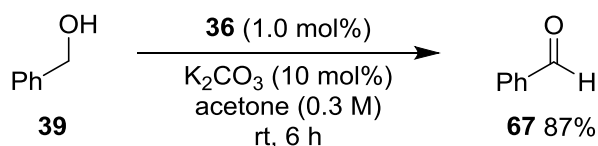
Imines, which are protonated prior to reduction, can be also be reduced to amines asymmetrically with the TEAF system (Scheme 19).<sup>52</sup>



**Scheme 19** Asymmetric reduction of a secondary imine with TEAF using a ruthenium(II) catalyst **66**.

### 1.9.2. Transfer Dehydrogenation

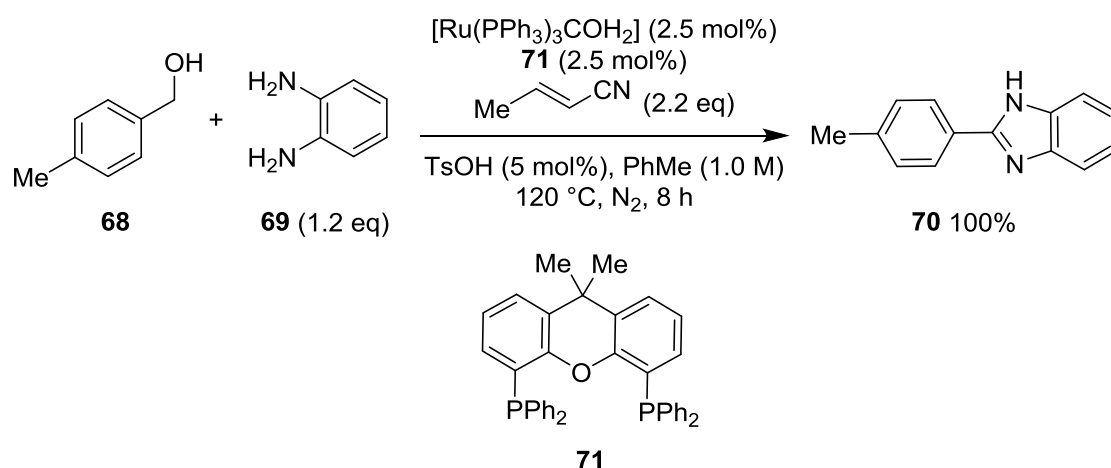
A transfer dehydrogenation reaction is the abstraction of hydrogen from a substrate by the metal catalyst and its subsequent transfer to a hydrogen acceptor.<sup>53</sup> Acetone is a commonly used hydrogen acceptor which produces *iso*-propanol as a by-product. As with transfer hydrogenation reactions, the reverse reaction with *iso*-propanol can result in lower product yields. Fujita and Yamaguchi carried out the transfer dehydrogenation of primary alcohols with acetone as the hydrogen acceptor (Scheme 20).<sup>54</sup>



**Scheme 20** The transfer dehydrogenation of **39** with acetone as the hydrogen acceptor using iridium(III) chloride dimer **36**; yield determined using GC.

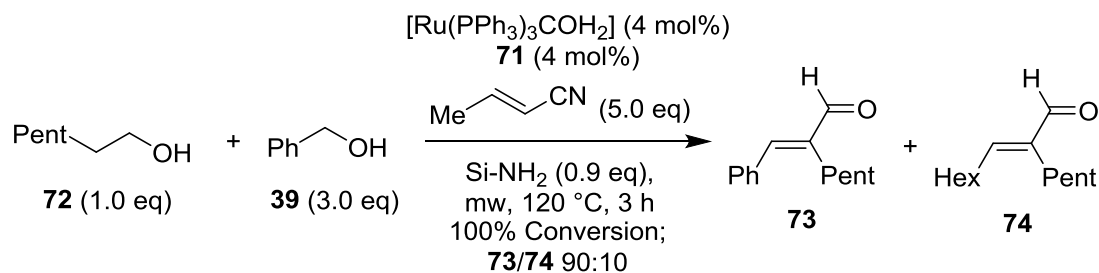
Blacker, Marsden and Williams have prepared benzimidazoles by unlocking the reactivity of alcohols through transfer dehydrogenation with a ruthenium(II)/xantphos **71** catalyst. Crotonitrile was used as the hydrogen acceptor (Scheme 21).<sup>55</sup>





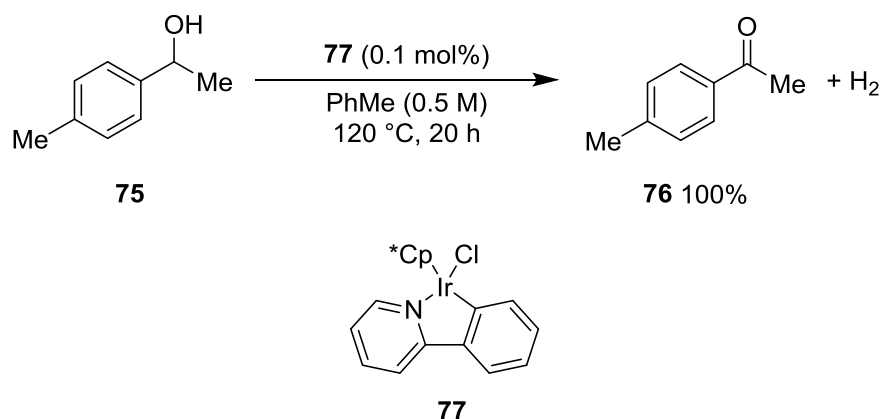
**Scheme 21** Synthesis of a substituted benzimidazole from the dehydrogenation of a primary alcohol; yield determined using GC.

Williams has combined the ruthenium(II) complex  $[\text{Ru}(\text{PPh}_3)_3\text{COH}_2]$  and biphosphine ligand **71** in combination with a silica supported amine catalyst to carry out a transfer dehydrogenation reaction followed by a cross coupling of primary alcohols (Scheme 22).<sup>56</sup>



**Scheme 22** Synthesis of substituted  $\alpha,\beta$ -unsaturated aldehydes.

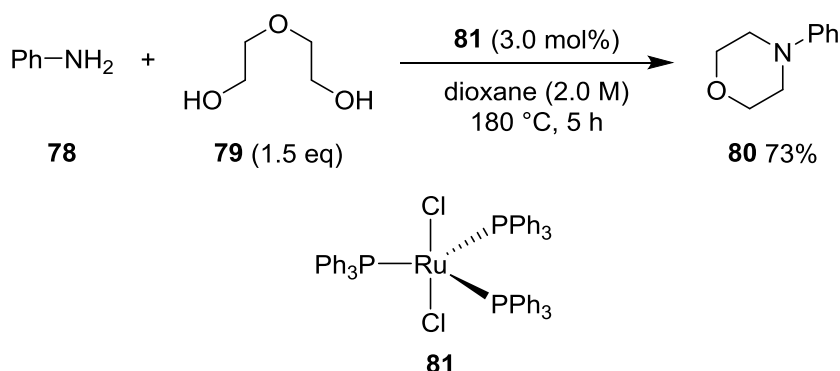
Transfer dehydrogenation of the alcohol substrate is necessary to generate electrophiles in order to achieve the cross-coupling. An excess of crotonitrile, the hydrogen acceptor, is required for the reaction, otherwise the reaction does not occur. Fujita and Yamaguchi carried out the acceptorless dehydrogenation of secondary alcohols, with the aim of improving atom economy, releasing hydrogen gas from the reaction (Scheme 23).<sup>57</sup>



**Scheme 23** An acceptorless secondary alcohol dehydrogenation using an iridium(III) catalyst; yield determined using GC.

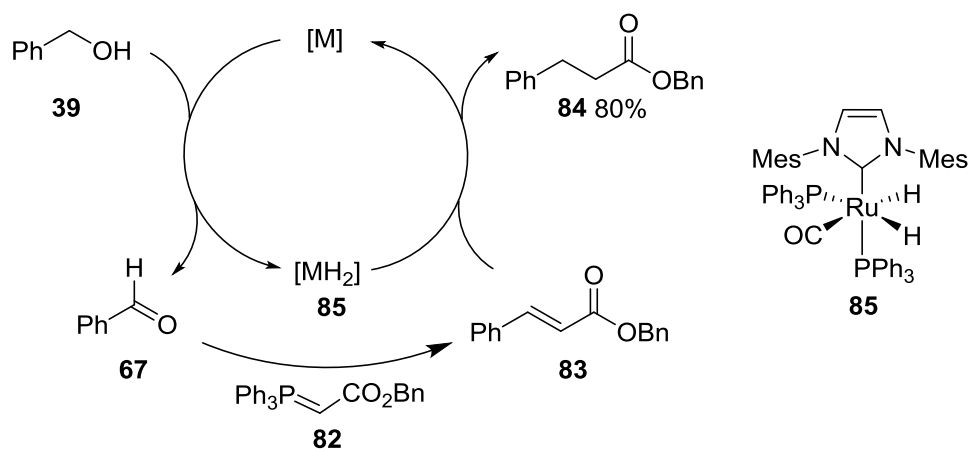
### 1.9.3. Hydrogen Borrowing

After a dehydrogenation reaction, the metal catalyst stores the abstracted hydrogen until a suitable hydrogen acceptor is available. However, the stored hydrogen can be returned to the substrate following an intermediate transformation. The catalyst effectively ‘borrows’ the hydrogen using hydrogen transfers.<sup>58</sup> By dehydrogenating an alcohol substrate, unlocking a more reactive carbonyl functional group, intermediate transformations can be more easily performed.<sup>59</sup> As both the hydrogen donor and the hydrogen acceptor are incorporated into the product, the reactions have excellent atom economy. Watanabe performed the catalysed *N*-alkylation of amines using a rhodium catalyst (Scheme 24).<sup>60</sup>

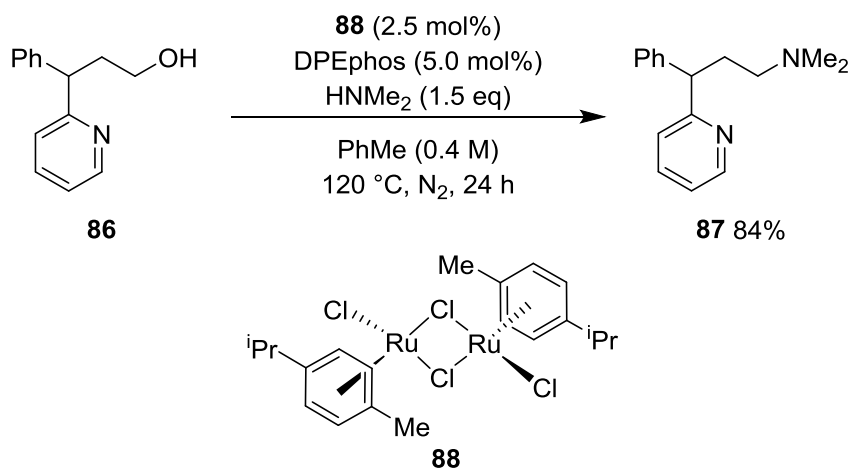


**Scheme 24** Substituted morpholine synthesis using hydrogen borrowing with intermediate imine formations.

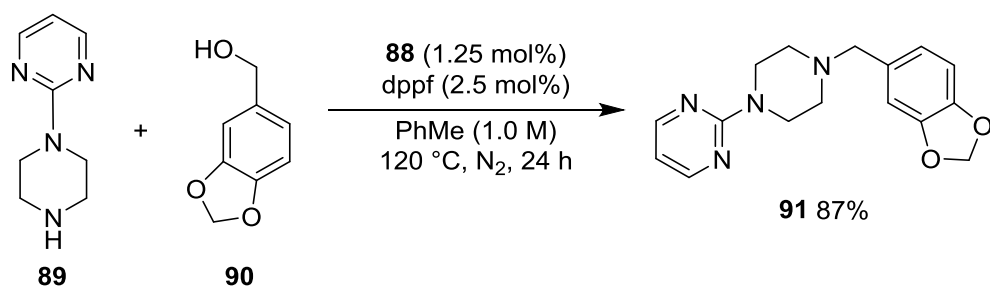
Williams has utilized the hydrogen borrowing methodology for an indirect Wittig reaction (Scheme 25),<sup>61</sup> and as a substitute for alkyl halides in the synthesis of Pheniramine **86** (Scheme 26) and Piribedil **90** (Scheme 27).<sup>62</sup>



**Scheme 25** Hydrogen borrowing and intermediate Wittig reaction to produce an alkane from an alcohol; **84** (1.0 mol%), **81** (1.1 eq),  $\text{CH}_2\text{CHSiMe}_3$  (2.0 mol%), PhMe (1.0 M), 80 °C, 24 h.

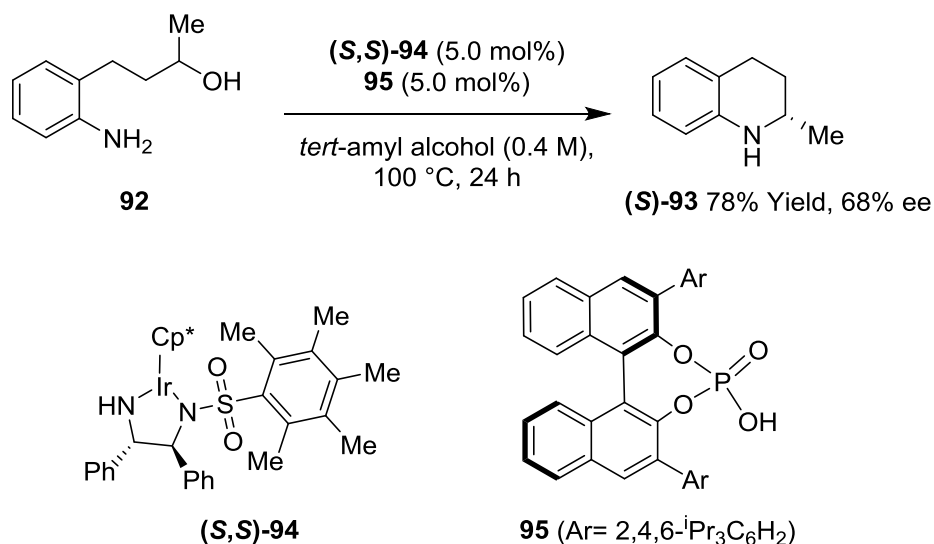


**Scheme 26** Synthesis of antihistamine drug Pheniramine **87**, using hydrogen borrowing with an intermediate imine formation.

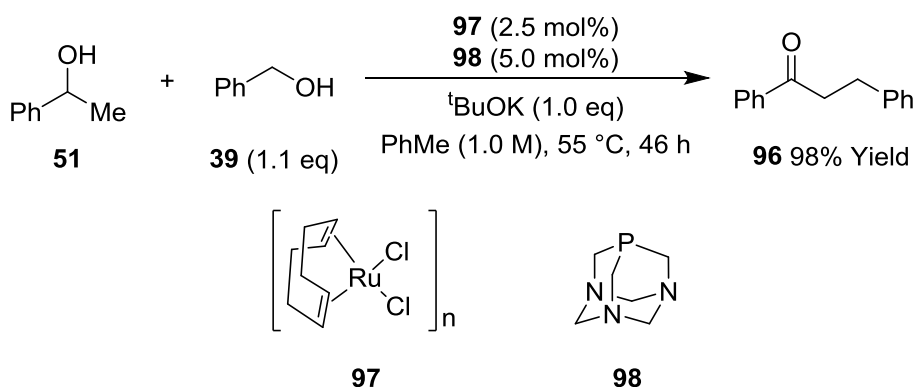


**Scheme 27** Synthesis of dopamine agonist drug Piribedil **91**, using hydrogen borrowing with an intermediate imine formation.

Zhao prepared a quinoline asymmetrically with a hydrogen borrowing method involving an intramolecular cyclisation step (Scheme 28).<sup>63</sup> Taddei has coupled primary and secondary alcohols with a ruthenium(II) catalyst through an intermediate aldol elimination (Scheme 29).<sup>64</sup>

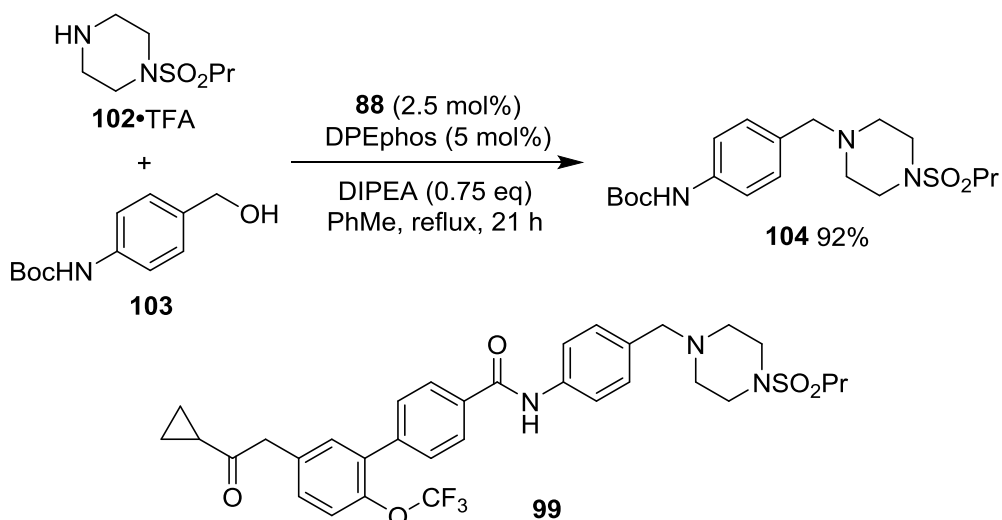


**Scheme 28** An asymmetric quinolone synthesis, using hydrogen borrowing with an intermediate intramolecular imine formation step.

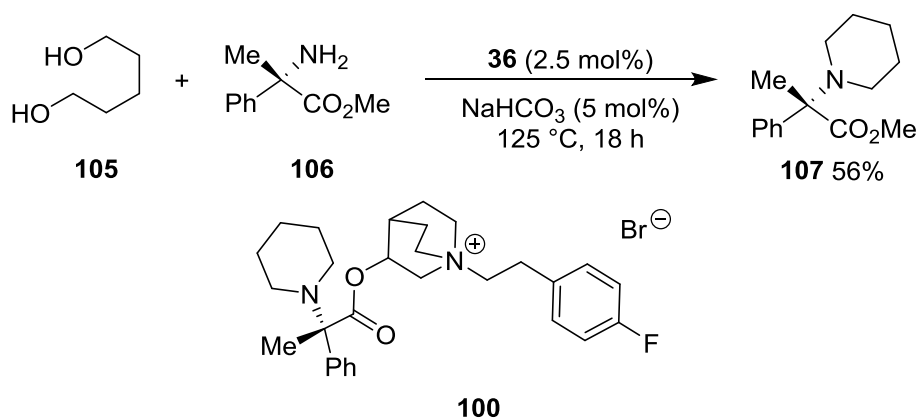


**Scheme 29** Cross-aldol elimination reaction between reduced primary and secondary alcohols with a final alkene transfer hydrogenation; yield determined using GC.

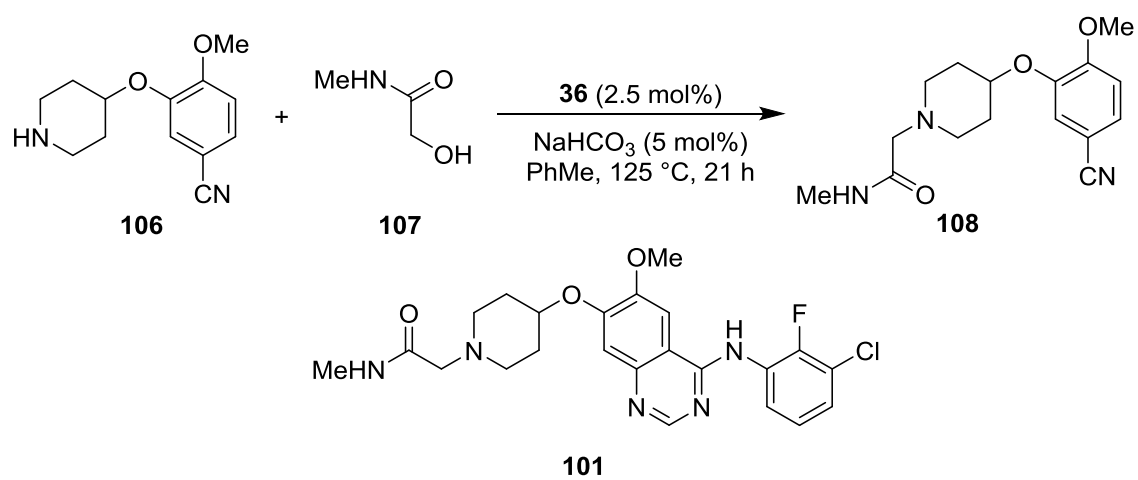
Leonard, Blacker and Marsden reported the use of hydrogen borrowing methodologies with iridium(III) and ruthenium(II) catalysts to improve the synthesis of pharmaceutically relevant intermediates towards anithepatitis drug **99** (Scheme 30), muscarinic antagonist **100** (Scheme 31) and antiproliferative drug **101** (Scheme 32).<sup>65</sup> The routes previously used alkyl halides or  $\alpha$ -halo-carbonyls to achieve the desired intermediates, which are more hazardous and inefficient reagents. However, the use of hydrogen borrowing requires high temperatures, large catalyst loadings and often aromatic solvents; which may not transfer to large scale projects easily.



**Scheme 30** Improved route to intermediate **104** for the synthesis of anithepatitis drug **99**.



**Scheme 31** Improved route to intermediate **107** for the synthesis of muscarinic antagonist **100**.



**Scheme 32** Improved route to intermediate **108** for the synthesis of antiproliferative drug **101**.

## 1.10. Organocatalysis

Many metal catalysts are strictly regulated in order to ensure that any metal contaminants in pharmaceutical drug products remain below toxic levels (Table 4).<sup>66</sup>

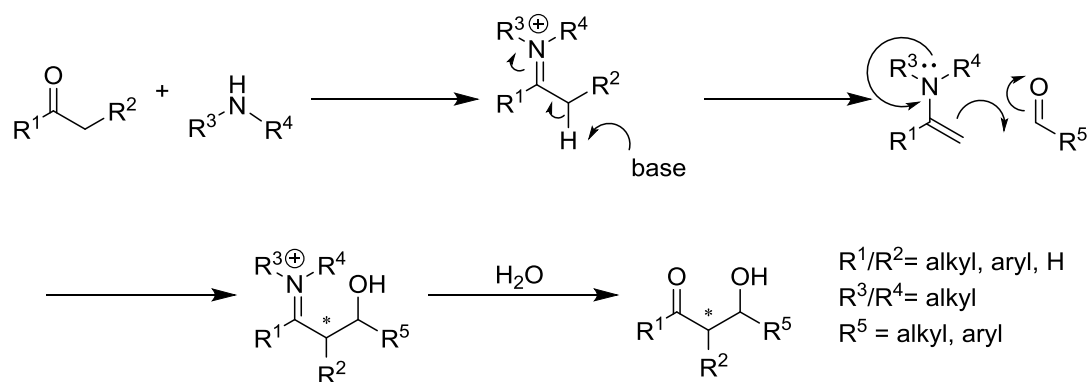
**Table 4** The concentration limits for human exposure to metal residues in pharmaceutical drug products.<sup>66</sup>

Classification	Concentration (ppm) <sup>a</sup>	
	Oral Exposure	Parenteral Exposure
Class 1A: Pt, Pd	10	1
Class 1B: Ir, Rh, Ru, Os	10	1
Class 1C: Mo, Ni, Cr, V	25	2.5
Class 2: Cu, Mn	250	25
Class 3: Fe, Zn	1300	130

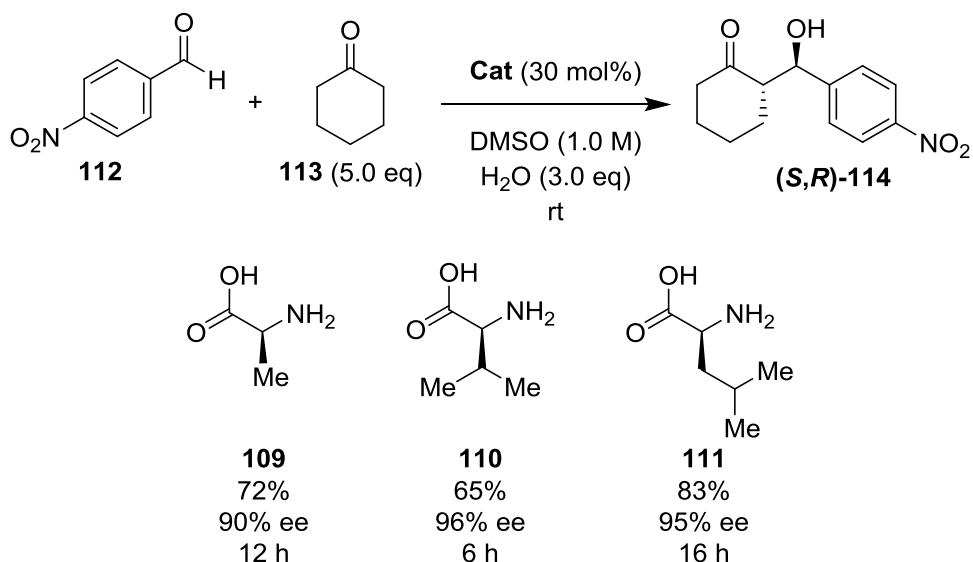
<sup>a</sup>The concentration limits are based on the permitted daily exposure ( $\mu\text{g}/\text{day}$ ) divided by the daily dose ( $\text{g}/\text{day}$ ) for an assumed daily dose of 10 grams of the drug product.

In order to remove impurities, extra scavenging and purification steps are added to syntheses; increasing plant time and costs at scale. An advantage for using organocatalysts is that the issue of metal contamination is avoided. However, the turnover numbers (TON) for these catalysts are low, so high catalyst loadings (10–30 mol%) are normally required for these reactions (cf. iridium/ruthenium catalysts; see 1.9.1). On the other hand, organocatalysts can be inexpensive compared to precious metal catalysts, which still makes them attractive. Primary and secondary amines are used as catalysts for a range of reactions, many of which use chiral amines to induce high enantioselectivity in the products. Stork showed that an amine can be used to catalyse the aldol reaction, where the amine forms an enamine, which raises the HOMO of the nucleophile making it more susceptible to electrophilic attack

(Scheme 33).<sup>67</sup> Hayashi reported using chiral amines, such as amino acids *L*-alanine **109**, *L*-valine **110** and *L*-leucine **111**, to give enantiomeric products (Scheme 34).<sup>68</sup> Lu used amine catalysts for the Mannich reaction (Scheme 35).<sup>69</sup>

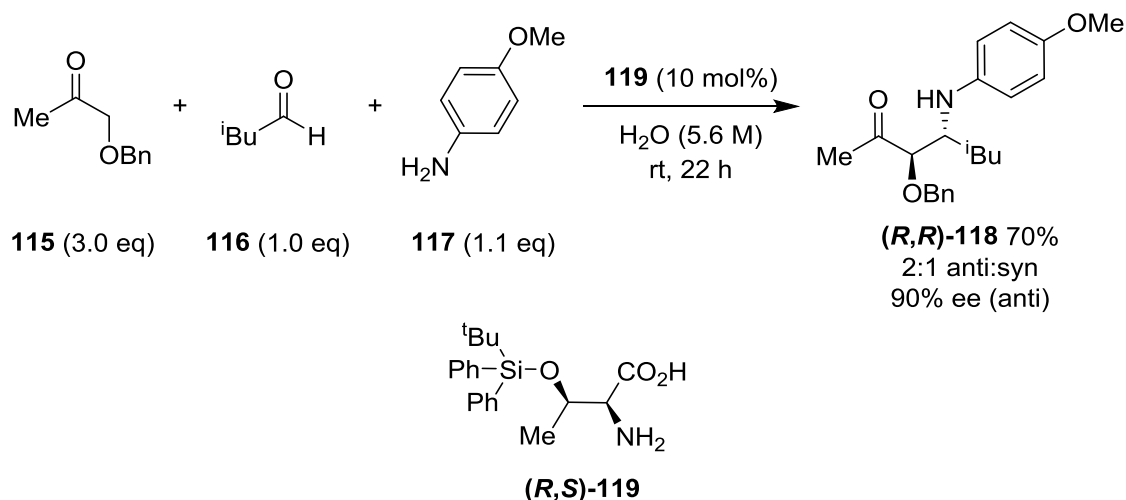


**Scheme 33** Reaction mechanism for amine catalysed aldol reaction.



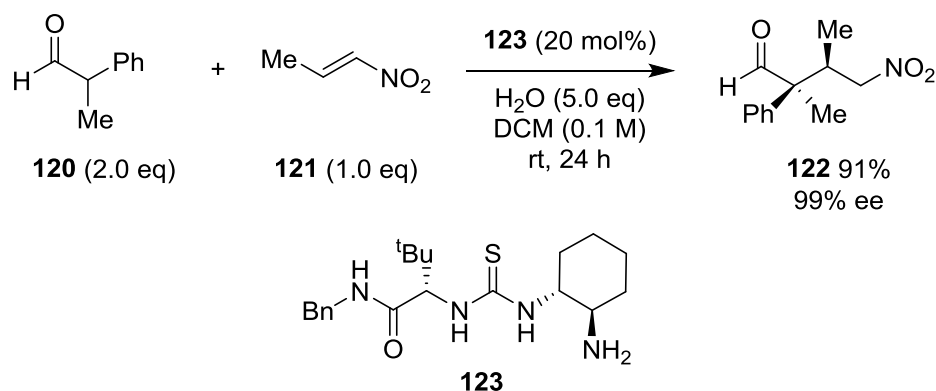
**Scheme 34** The aldol reaction of cyclohexanone **113** and *p*-nitrobenzaldehyde **112** catalysed by *L*-alanine **109**, *L*-valine **110** and *L*-leucine **111**.





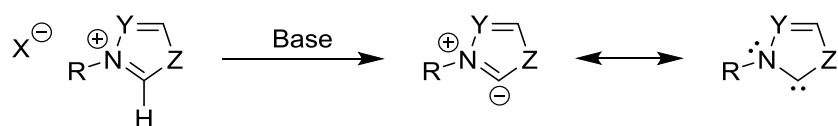
**Scheme 35** Aminoacid catalysed Mannich reaction.

Jacobsen reported an amine catalyst for Michael addition reactions to nitroalkenes (Scheme 36).<sup>70</sup>



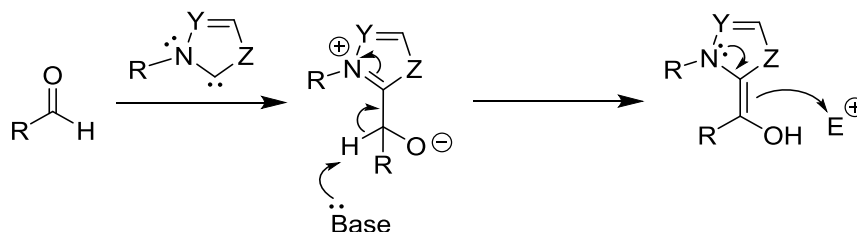
**Scheme 36** Amine catalysed Michael addition reaction.

*N*-Heterocyclic carbenes (NHCs) are a useful class of compounds, mainly used as ligands for organometallic reactions. However, the electronic and steric stability of these carbenes means they are excellent as organocatalysts, as they have dual modes of action; good electron acceptors and good electron donors.<sup>71, 72</sup> NHCs are easily generated with a base (Scheme 37).



**Scheme 37** Activation of an NHC with a base; Y = CH, N; Z = NR, S; X = halide,  $\text{BF}_4^-$ ,  $\text{PF}_6^-$ ; R = alkyl, aryl.

The electronic and steric properties of NHCs can easily be tuned by altering the substituents on the heteroatoms and on the backbone of the ring. For organocatalysis, the nucleophilic strength of NHCs makes them useful catalysts for electrophilic addition to aldehyde groups. The electron withdrawing ability of NHCs can decrease the  $pK_a$  of the 'aldehyde' proton, reversing the reactivity of the group and allowing umpolung reactions with electrophiles (Scheme 38).



**Scheme 38** Formation of an enamine type intermediate for attack onto electrophiles during NHC catalysis.

The  $pK_a$  of the C-2 position is important in catalysis, as deprotonation is essential for generating a carbene for an active catalyst (Figure 13). The more acidic the C-2 position, the milder the base required for the reactions. O'Donoghue and Smith have reported on the  $pK_a$  values of triazolium, imidazolium and thiazolium salts (Figure 13).<sup>73</sup>

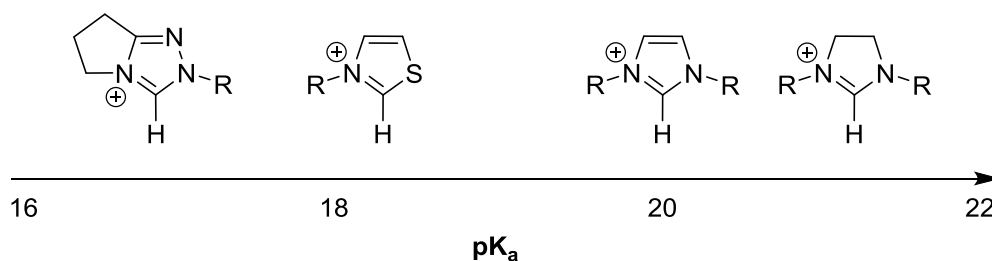


**Figure 13** The approximate  $pK_a$ s of the different types of NHC catalysts.

### 1.10.1. Thiazolium Catalysts

Thiamine pyrophosphate (TPP) **124** (Figure 14) is the catalytic cofactor used by the pyruvate dehydrogenase enzyme, which carries out the oxidative decarboxylation of pyruvate **125** (Scheme 39).

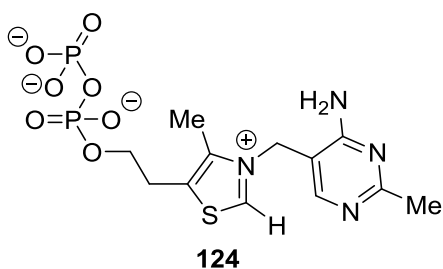
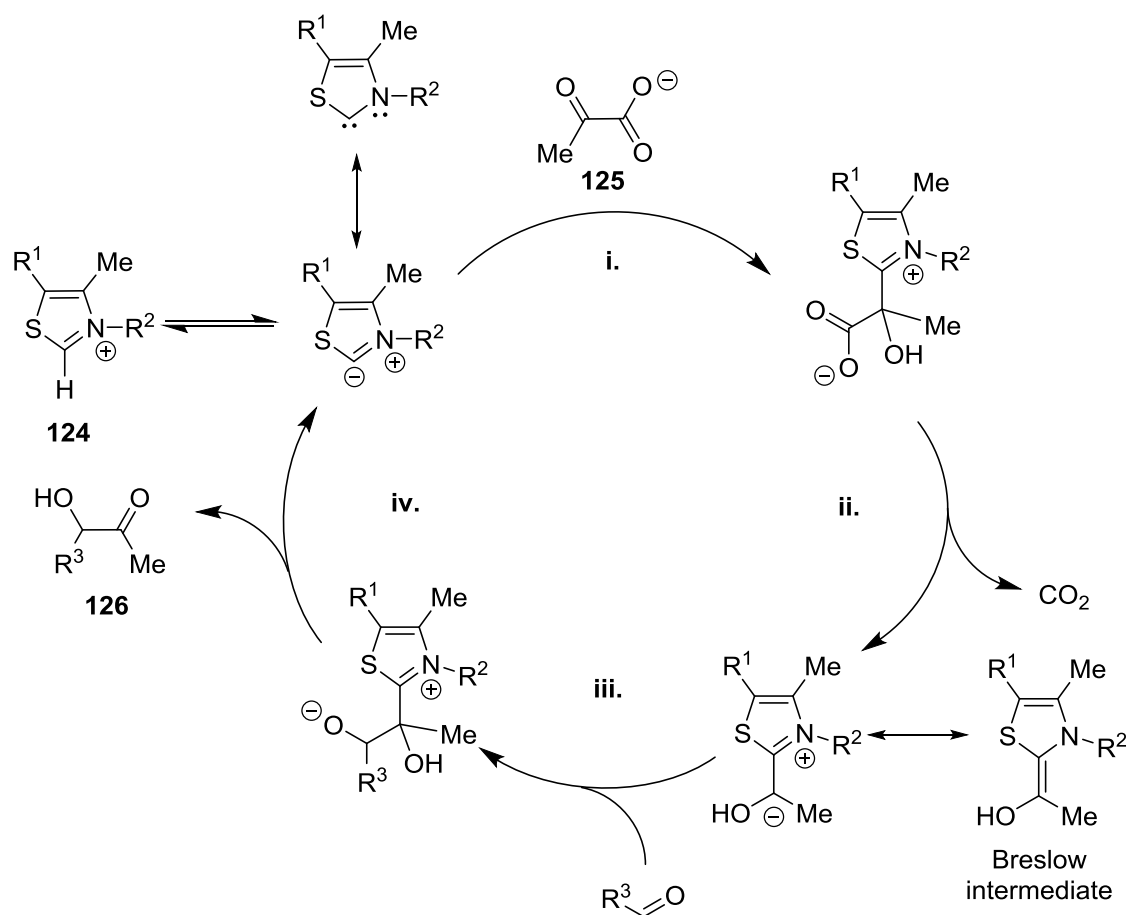


**Figure 14** Thiamine pyrophosphate (TPP) 113.

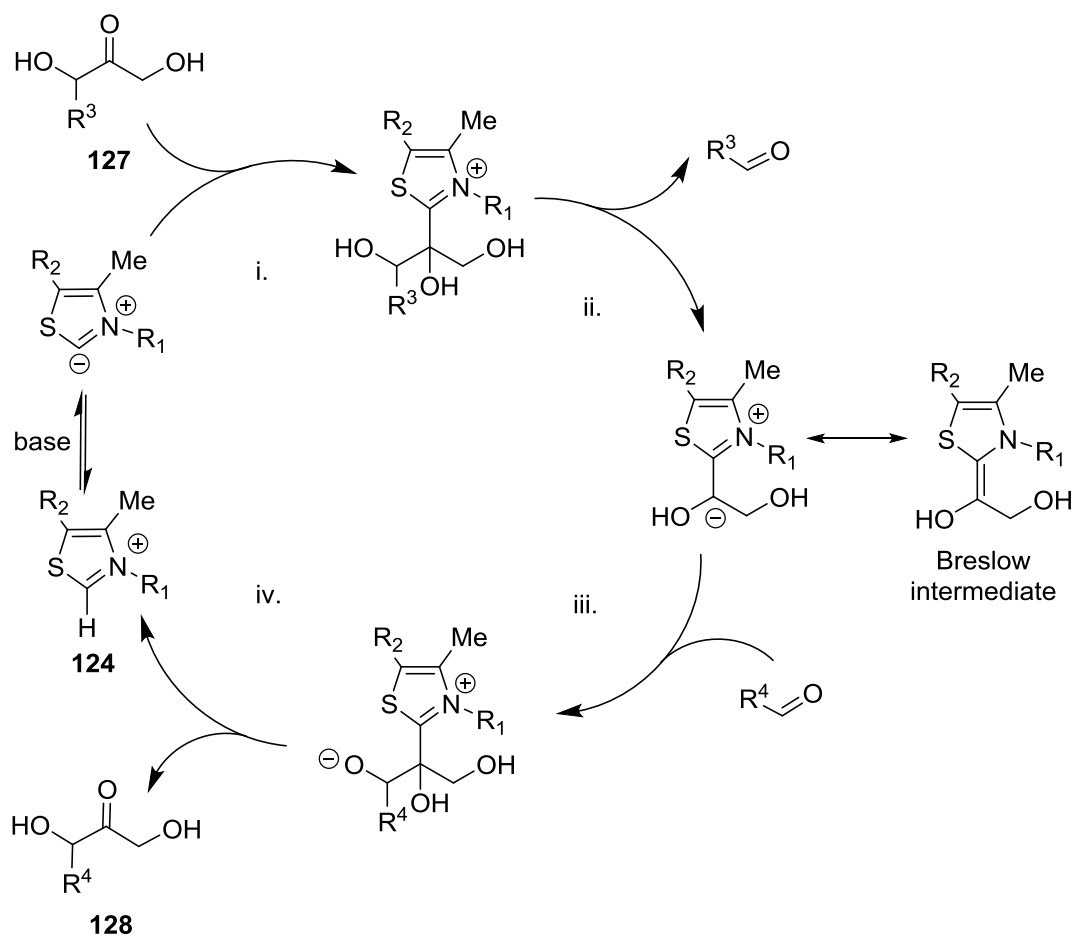
A key feature of the thiamine structure is a more acidic proton ( $pK_a = 17.7$ ) between the nitrogen and the sulfur of the thiazolium ring.<sup>74</sup> Deprotonation generates a nucleophilic anion, which can then attack pyruvate **125**.



**Scheme 39** The catalytic cycle for the decarboxylation of pyruvate **125** using TTP **124**, producing an  $\alpha$ -hydroxyketone **126**; i) substrate binding; ii) decarboxylation; iii) benzoin condensation; iv) product release.

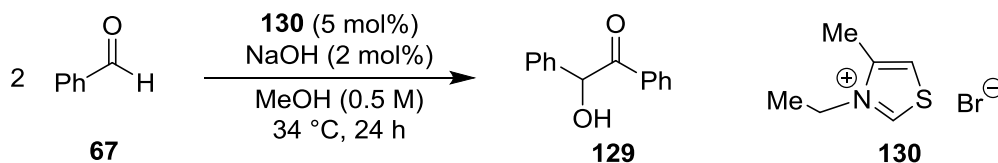
After decarboxylation, an activated intermediate is generated, due to the positive charge on the *N*-atom acting as an electron sink, which promotes a negative charge on the carbonyl carbon. The acetyl group is then transferred to a lipoamide molecule, generating an acetyl lipoamide, which goes on to make acetyl CoA. In place of a lipoamide, addition of an aldehyde would generate an  $\alpha$ -hydroxyketone.

TPP is a cofactor for the transketolase enzyme (Scheme 40), which is the terminal catalyst in the fatty acid synthase complex. The thiazolium anion attacks the ketose substrate **127** and a retro-benzoin condensation reaction occurs, resulting in the loss of an aldehyde group. The activated glycoaldehyde Breslow intermediate carries out a benzoin condensation reaction with a suitable aldehyde to generate a new ketose product **128**, which is then released.

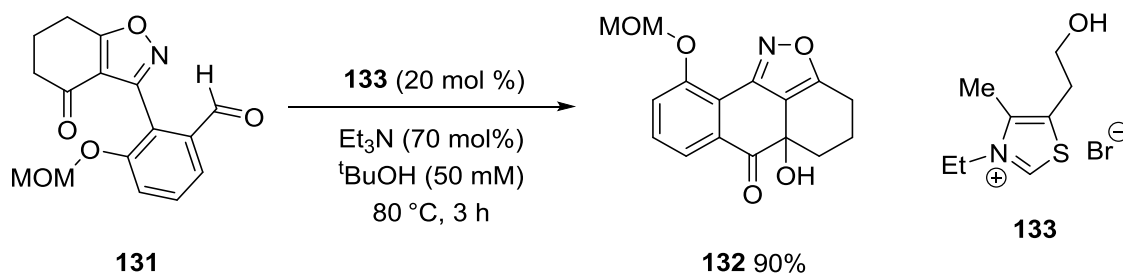


**Scheme 40** Transketolase enzymatic cycle; i) substrate binding; ii) retro-benzoin condensation; iii) benzoin condensation; iv) product release.

The Buck reaction uses potassium cyanide (25 mol%) to catalyse the benzoin condensation *in vitro*.<sup>75</sup> Ugai showed that the benzoin condensation can also be catalysed by thiazolium catalysts.<sup>76</sup> Breslow achieved the benzoin condensation of benzaldehyde with a simple thiazolium catalyst whilst developing the mechanistic understanding of the reaction (Scheme 41).<sup>77</sup> Bode has used a thiazolium catalyst for an intramolecular benzoin condensation (Scheme 42).<sup>78</sup>



**Scheme 41** The benzoin condensation of **67** with a simple thiazolium catalyst **130**; the yield was only qualitatively determined.



**Scheme 42** An intramolecular benzoin condensation catalysed by a thiazolium catalyst **133**.

### 1.10.2. Triazolium Catalysts

O'Donoghue has investigated the acidity of the heterocyclic C-H of triazolium compounds (Figure 15), which are more acidic than analogous thiazolium and imidazolium heterocycles (Figure 13).<sup>73</sup>

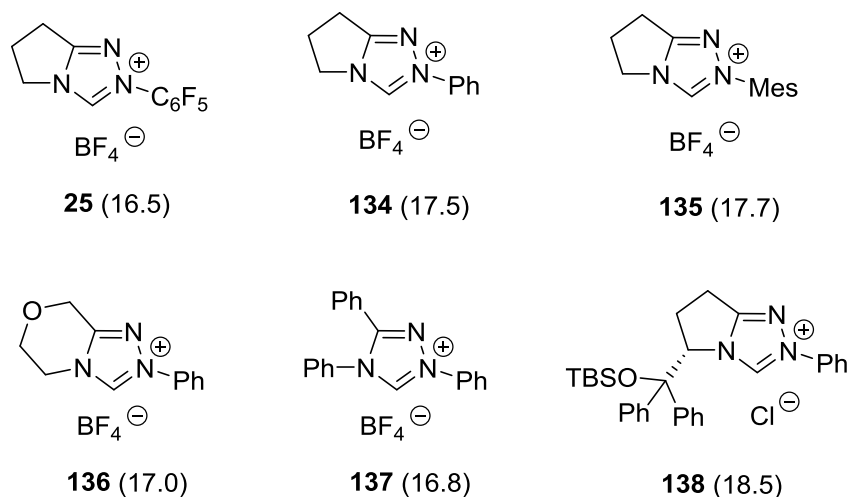
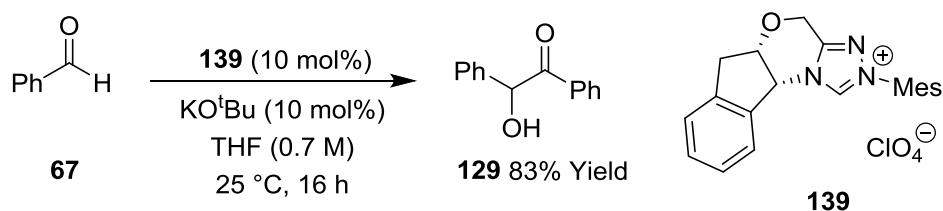


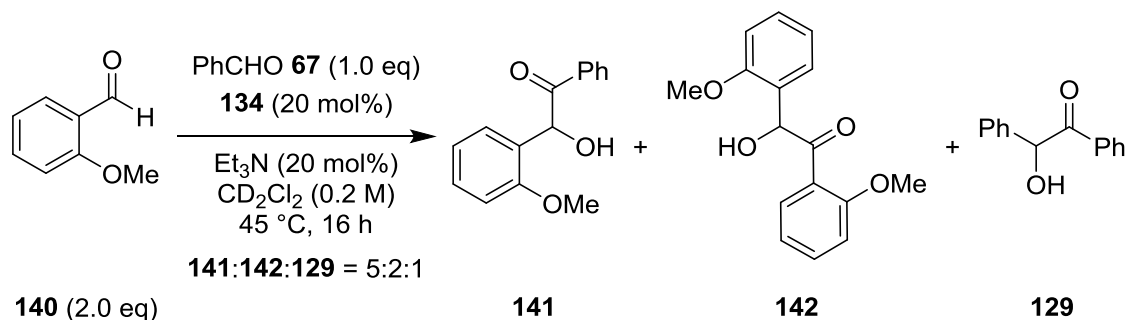
**Figure 15** The  $\text{pK}_a$ s (in parentheses) for a range of triazolium heterocycles; determined from the rate constants for deuterium exchange, in deuterium oxide at 25 °C, and measured using  $^1\text{H}$  NMR.

The structural variations of the triazolium catalysts help to account for the trend in the  $\text{pK}_a$  values. A more electron withdrawing *N*-aryl substituent reduces the  $\text{pK}_a$  of the triazolium catalyst (**25**<**134**<**135**). Incorporation of an oxygen atom in the aliphatic ring also reduces the  $\text{pK}_a$  (**134**<**136**), whereas a silyl side chain causes an increase in  $\text{pK}_a$  (**137**<**138**). Bode carried out a homo-benzoin condensation with a triazolium catalyst (Scheme 43).<sup>79</sup>



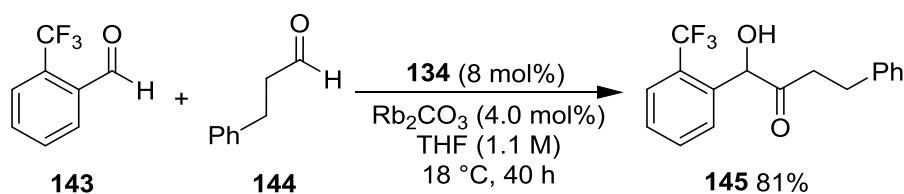
**Scheme 43** Triazolium catalysed homo-benzoin condensation.

O'Donoghue has carried out a cross-benzoin reaction which has produced three products (Scheme 44).<sup>80</sup>

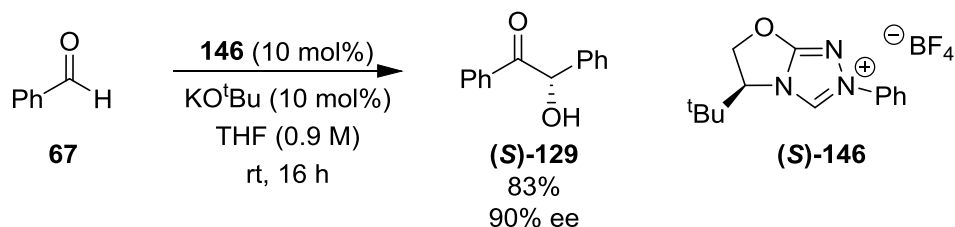


**Scheme 44** A triazolium catalysed cross-benzoin condensation, producing a mixture of cross- and homo- coupled aldehydes; product ratio determined using  $^1\text{H}$  NMR spectroscopy.

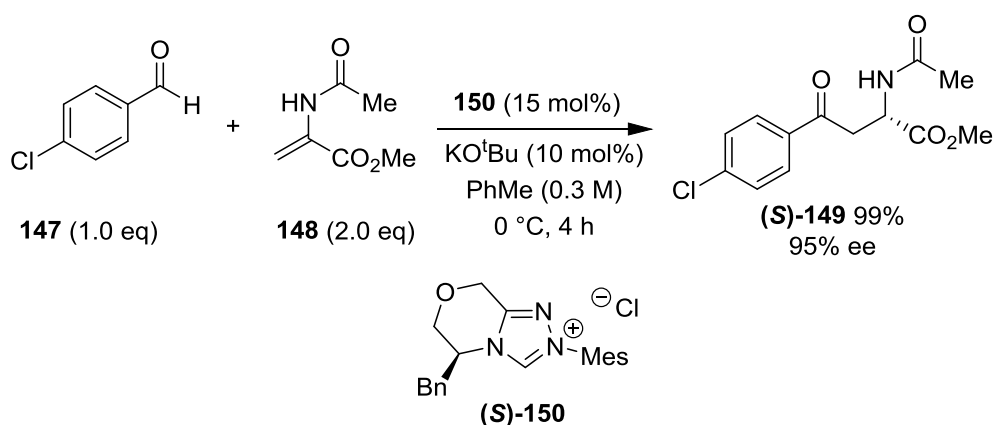
Zeitler and Connon showed that a cross-benzoin condensation can be catalysed by a triazolium catalyst (Scheme 45).<sup>81</sup> Enders has used chiral triazoliums for asymmetric homo-benzoin condensations (Scheme 46).<sup>82</sup> The Stetter reaction is another useful reaction between aldehydes and  $\alpha,\beta$ -unsaturated carbonyls that can be catalysed by triazolium catalysts (Scheme 47).<sup>83</sup>



**Scheme 45** The triazolium catalysed cross-benzoin condensation.



**Scheme 46** Triazolium catalysed asymmetric benzoin condensation.



**Scheme 47** Triazolium catalysed Stetter reaction.

### 1.11. Summary

The research reviewed in this chapter has covered multicatalysis, with a particular emphasis on multifunctional catalysis, organometallic catalysts for hydrogen transfer reactions and organocatalysed benzoin condensation reactions. The work shows potential for a multifunctional catalyst combining an NHC organocatalyst with an organometallic hydrogen transfer catalyst to achieve sequential reactions.

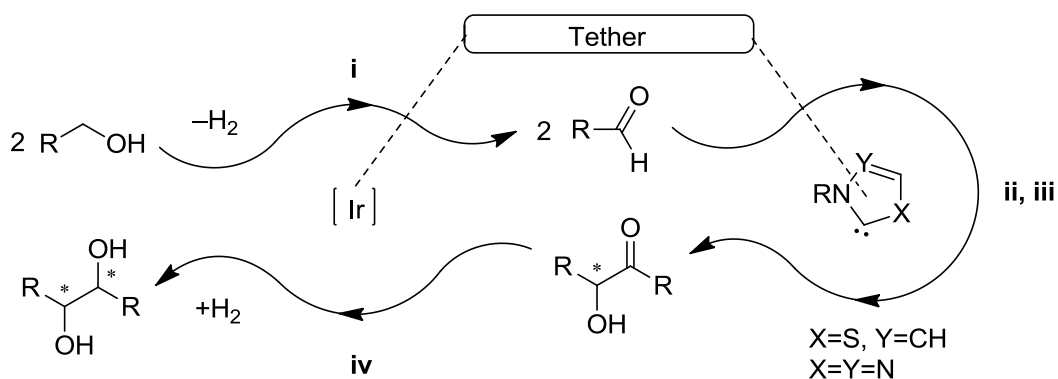


## 1.12. Aims and Objectives

The aim of this project was to design and synthesise novel ligands and iridium(III) complexes that combine organo and organometallic catalysts, and use these complexes to carry out multifunction catalysis for sequential reactions.

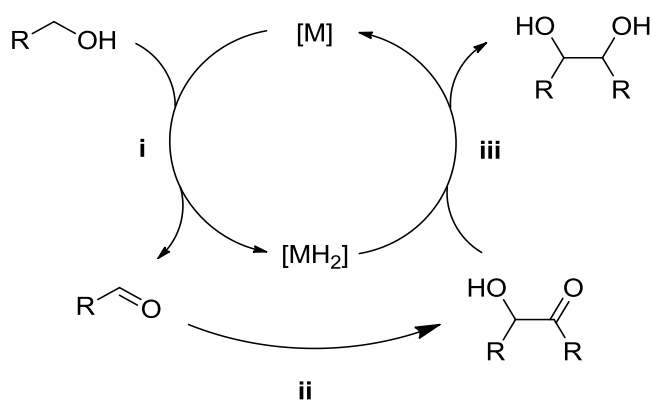
The proposed multicatalytic cycle involves two hydrogen transfer reactions, that can be catalysed using an iridium(III) organometallic catalyst (see Chapter 1.9), and a benzoin condensation, that can be catalysed using a thiazolium or triazolium organocatalyst (see Chapter 1.10). The proposed pathway is as follows (Scheme 48):

- The catalytic cycle begins with the transfer dehydrogenation of two primary alcohols by the organometallic catalyst.
- The thiazolylidene catalyst attacks one of the resulting aldehydes.
- The second aldehyde is attacked by the Breslow intermediate to form the  $\alpha$ -hydroxyketone from the benzoin condensation.
- Transfer hydrogenation of the  $\alpha$ -hydroxyketone produces the 1,2-diol.



**Scheme 48** Proposed multicatalytic cycle; i) transfer dehydrogenation, ii) Breslow intermediate formation, iii) benzoin condensation, iv) transfer hydrogenation.

With this reaction sequence, it could also be possible to exploit hydrogen borrowing methodology; eliminating the need for hydrogen acceptors/donors (Scheme 49) (see Chapter 1.9.3).<sup>61</sup>



**Scheme 49** Proposed catalytic cycle with hydrogen borrowing methodology; i) transfer dehydrogenation, ii) benzoin condensation, iii) transfer hydrogenation.

With a successful system, the rates of catalysis will be compared against the rates for the separate catalysts and the scope of the reaction will be investigated. With different alcohols or amines, cross-benzoin products could be achieved. NHC organocatalysts are active catalysts for a wide range of reactions, therefore the reaction scope can be expanded; such as decarboxylation reactions of carboxylic acids and the Stetter reaction between  $\alpha,\beta$ -unsaturated carbonyls and aldehydes.

## 2. Synthesis of Novel Thiazole and Triazole Iridium(III) Complexes

### 2.1. Introduction

The review of mult catalysis in Chapter 1 covered the use of organometallic catalysts, organocatalysts and combinations of the two within the same reaction creating a positive synergistic effect. There is an absence in the literature for the use of a multifunctional catalyst combining an organometallic catalyst and an organocatalyst in a single species. In this chapter, the design ideas behind the development of an organo/organometallic multifunctional catalyst and the synthetic routes to the complexes that fit the design objectives will be discussed.

#### 2.1.1. Functional Groups Targeted for Sequential Reactions

Pharmaceutical molecules that contain a 1,2-diol, 1,2-ketoalcohol, 1,2-aminoalcohol or a 1,2-ketoamine groups (Figure 16) can have synthetic routes that are long, use stoichiometric toxic reagents or expensive catalysts. A route to Formoterol, a long acting  $\beta_2$ -agonist (LABA), involves the synthesis of an  $\alpha$ -haloketone, an asymmetric borohydride reduction, and two hydrogenations over precious metal catalysts (Scheme 50).<sup>84, 85</sup> Another example of 1,2-diol formation from two alcohols involves a Wittig reaction and subsequent dihydroxylation with osmium tetroxide (Scheme 51).<sup>86, 87</sup>

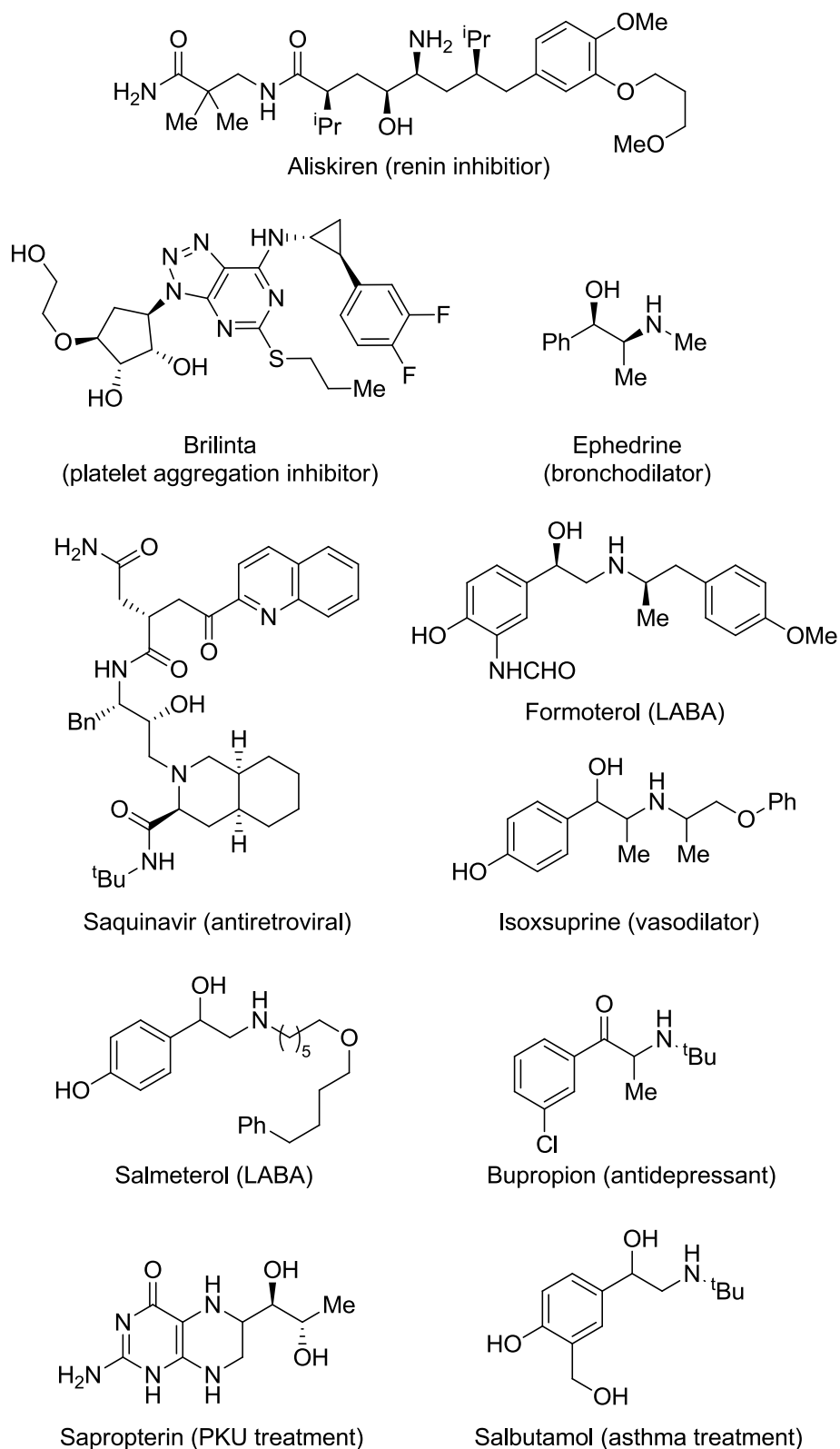
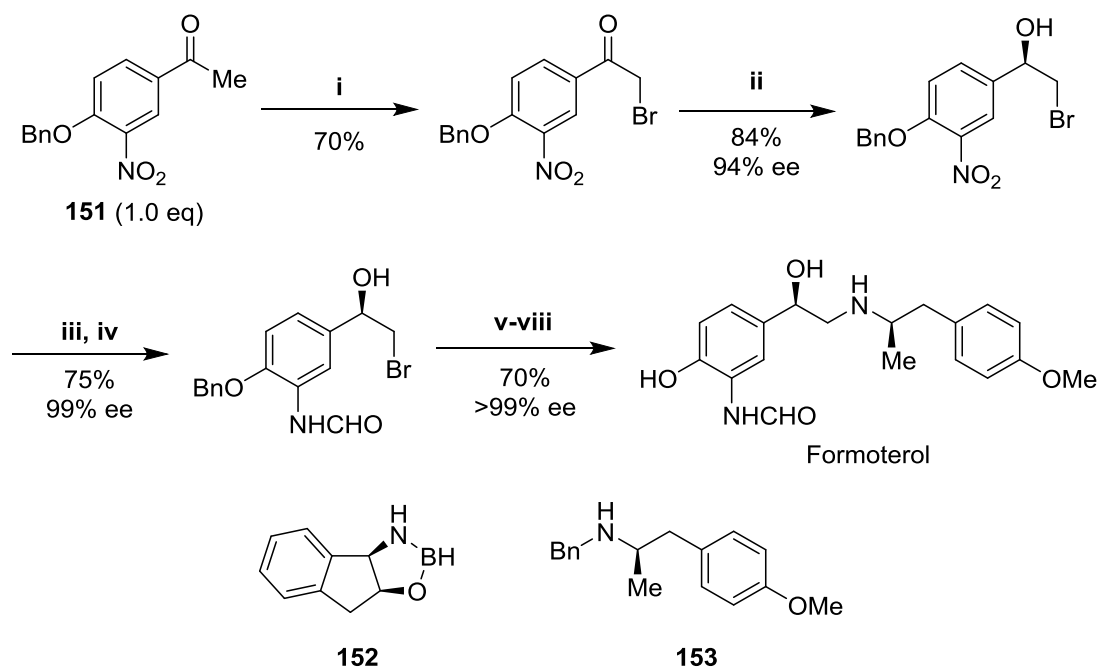
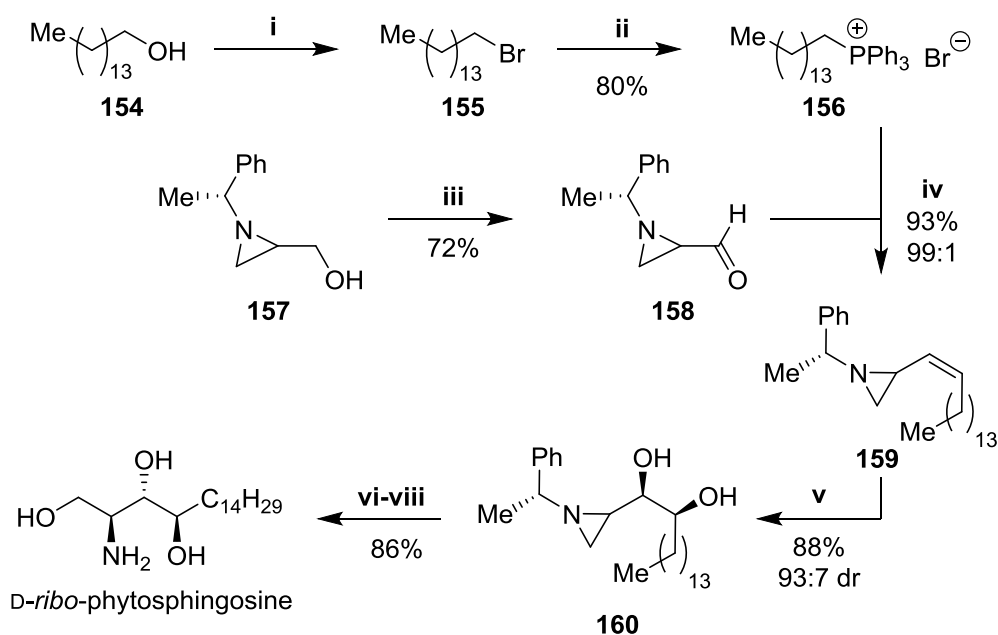


**Figure 16** Pharmaceuticals containing a 1,2-diol, 1,2-aminoalcohol or 1,2-ketoamine group.



**Scheme 50** A 100 g scale synthetic route to long acting  $\beta_2$ -agonist Formoterol. Conditions: i)  $\text{Br}_2$  (1.0 eq),  $(\text{PhCO}_2)_2$  (1 mol%),  $\text{CHCl}_3$  (0.4 M), rt. ii) **152** (5 mol%),  $\text{BH}_3 \cdot \text{Me}_2\text{S}$  (0.7 eq), THF (0.3 M), 25 °C, 3 h. iii)  $\text{PtO}_2$  (2 mol%),  $\text{H}_2$ , 45 psi, THF/Toluene (1:1, 0.7 M), 8 h. iv)  $\text{HCO}_2\text{H}$  (2.0 eq),  $\text{Ac}_2\text{O}$  (1.5 eq), 15 °C, 0.3 h. v) **153** (0.95 eq),  $\text{K}_2\text{CO}_3$  (2.5 eq), THF/MeOH (1:1, 0.3 M), 25 °C, 2 h. vi) neat, 120 °C, 24 h. vii) Pd/C (10% Pd),  $\text{H}_2$ , 45 psi, EtOH (0.5 M), 3 h. viii) fumaric acid (0.5 eq), reflux, 2 h.

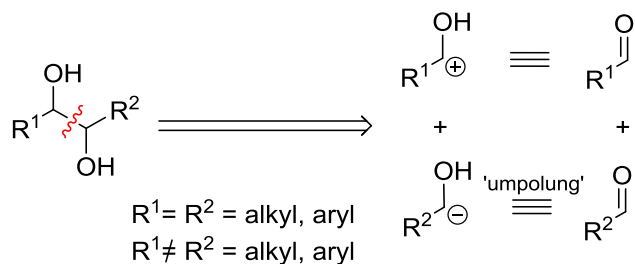
Both of these routes to 1,2-aminoalcohols are long, which increases yield losses between steps and overall reaction times, and use stoichiometric reagents which form large amounts of by-product; such as phosphine, boron and osmium waste.



**Scheme 51** A synthetic route to *D-ribo*-phytosphingosine. Conditions; i)  $\text{H}_2\text{SO}_4$ ,  $\text{HBr}$ . ii)  $\text{PPh}_3$  (1.1 eq),  $\text{MeCN}$  (0.3 M), reflux, 30 h. iii)  $\text{DMSO}$  (2.5 eq), oxalylchloride (1.2 eq),  $\text{Et}_3\text{N}$  (4.0 eq),  $\text{DCM}$  (0.3 M),  $-78^\circ\text{C}$ , 2 h. iv)  $\text{LiHMDS}$  (1 M in  $\text{THF}$ ),  $\text{THF}$  (0.3 M), rt, 2 h. v)  $\text{OsO}_4$  (5 wt% in  $\text{H}_2\text{O}$ , 0.1 eq),  $\text{NMO}$  (3.0 eq),  $\text{acetone}/\text{H}_2\text{O}$  (9:1, 0.1 M),  $0^\circ\text{C}$ , 4 h. vi)  $\text{AcOH}$  (5.0 eq),  $\text{DCM}$  (0.3 M). vii)  $\text{KOH}$  (3.0 eq),  $\text{EtOH}$  (0.3 M), rt, 8 h. viii)  $\text{Pd}(\text{OH})_2$  (20 wt%),  $\text{H}_2$ , 100 psi,  $\text{EtOH}$  (0.3 M), rt.

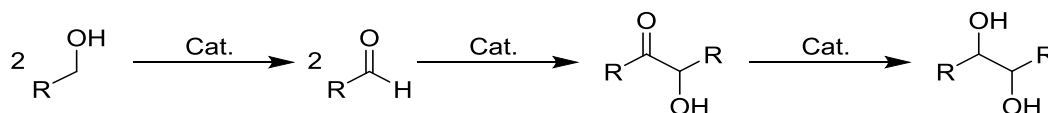
### 2.1.2. Design of the Multifunctional Catalyst

To design a multifunctional catalyst, the reaction sequence has to be selected, so that the catalysts can be chosen for each step and then both catalysts can be connected together to form a single species. The simplest retrosynthetic disconnection of a 1,2-diol is the carbon-carbon bond, to give two aldehydes as synthetic equivalents (Scheme 52).



**Scheme 52** Retrosynthetic analysis of a 1,2-diol.

The chosen reaction sequence was the dehydrogenation of primary alcohols and the sequential benzoin condensation of the aldehyde intermediates to produce an  $\alpha$ -hydroxyketone, which can undergo a further hydrogen transfer reaction to generate a 1,2-diol. The overall transformation is a carbon-carbon bond formed between two identical or different primary alcohols in a multicyclic one-pot reaction (Scheme 53).



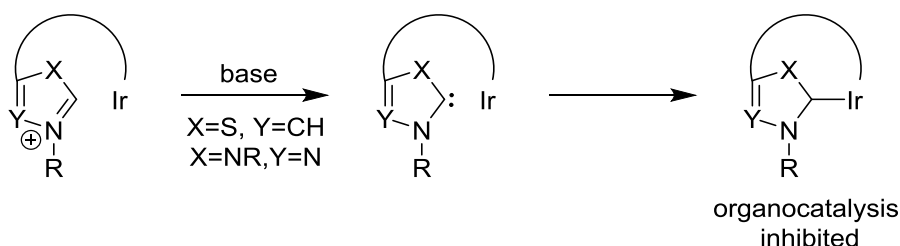
**Scheme 53** Outline of the reaction sequence, with each step catalysed by the same multifunctional catalyst.

Aldehydes are good electrophiles and can easily form unwanted impurities during reactions. By generating the aldehydes *in situ*, impurity formation can be avoided; these occur during the work-up, isolation and purification stages of a synthesis. Thiazolium salts will catalyse the benzoin/acyloin condensation of two aldehydes to make 1,2-diols, or similarly an aldimine and aldehyde can be condensed to form 1,2-aminoalcohol.<sup>77,78</sup> Enders has reported the use of organocatalysis to produce 1,2-ketoamines.<sup>88</sup> Since the multifunctional catalyst has two active sites tethered in close proximity to each other, the diffusion distance between both sites is shorter; therefore the reactive aldehyde intermediates might be converted at a faster rate, limiting the number of unwanted side reactions.

With the reaction sequence decided upon, the next step was to design the multifunctional catalyst. Three main factors have guided the design of the multifunctional complexes that are discussed in this chapter; tether length, organocatalyst acidity, and ligand coordination properties.

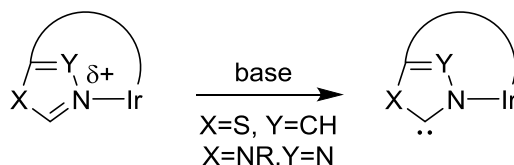
1. To make a multifunctional catalyst, both catalysts must be covalently tethered together, or have a strong coordination to a metal. The length and geometry of the tether will affect the rate of reaction and the ability of the two catalysts to interfere with each other's catalytic cycle. Ideally, a short covalent tether would minimise the diffusion distance between catalytic sites and lead to improved kinetics. Since NHCs form strong carbene-metal

$\sigma$ -bonds, if the tether were too flexible the carbene generated on the organocatalyst might prefer to coordinate to the metal centre and block both activities. Therefore, the organocatalyst should be prevented from binding to the metal centre by constraining the geometry (Scheme 54).



**Scheme 54** Inhibition of the organocatalyst via strong carbene-metal bond.

A long, rigid tether would hold the carbene away from the metal, however this might encourage dimerization. The heterocycle might employ a donor atom to coordinate to the metal and geometrically prevent carbene-coordination (Scheme 55).



**Scheme 55** The locked position of the organocatalyst, preventing carbene-metal bond formation.

- In order for the multifunctional catalyst to work, both catalysts must be able to exist in their activated states. To activate the organocatalyst, the thiazole ring must first be deprotonated to generate the active carbene species. This requires the  $\text{pK}_a$  of the thiazole to be low enough to enable the use of a weak base. Thiazoles are weak acids ( $\text{pK}_a \sim 28$ ), however *N*-alkylated thiazolium species create an electron sink on the *N*-atom of the ring making the C-2 position acidic ( $\text{pK}_a \sim 17\text{--}19$ ). It was thought that coordinating the heterocycle to the metal centre via the *N*-donor atom would create a pseudo-thiazolium, or triazolium species, which should have an increased C-2 proton acidity (Figure 17).





**Figure 17** Proposed design of the organocatalyst to increase the acidity of the ring;  
a) pseudo-thiazolium, and b) pseudo-triazolium.

There are only a few examples of complexes that have thiazoles<sup>89-92</sup> (Figure 18) or triazoles<sup>93-95</sup> (Figure 19) coordinated to iridium, ruthenium or rhodium metal centres via the heteroatom donors.

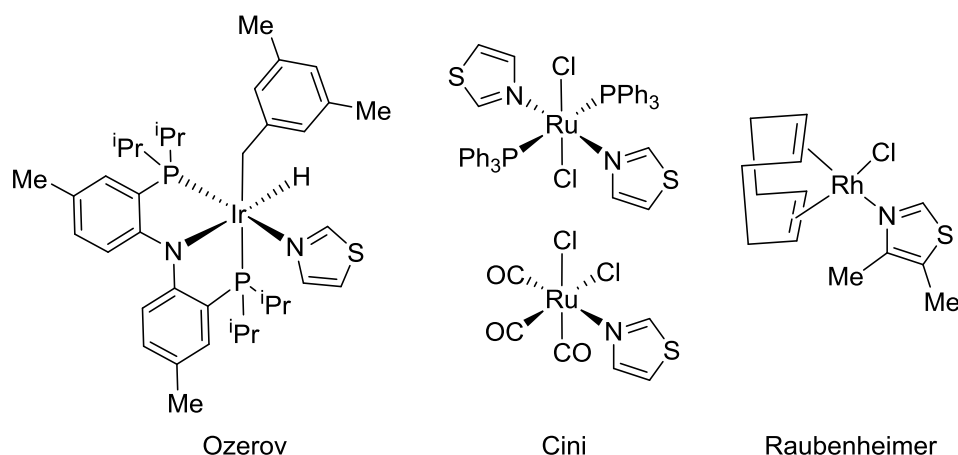


**Figure 18** Examples of iridium(III)<sup>89</sup>, ruthenium(II)<sup>90, 91</sup> and rhodium(I)<sup>92</sup> complexes that have 1,3-thiazole ligands coordinated to the metal via a *N*-donor.

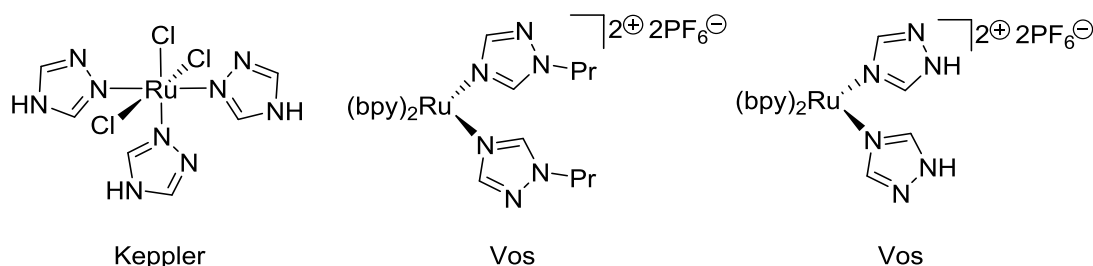


**Figure 19** Examples of ruthenium(III)<sup>93</sup> and ruthenium(II)<sup>94, 95</sup> complexes that have a 1,2,4-triazole ligand coordinated to the metal via a *N*-donor.

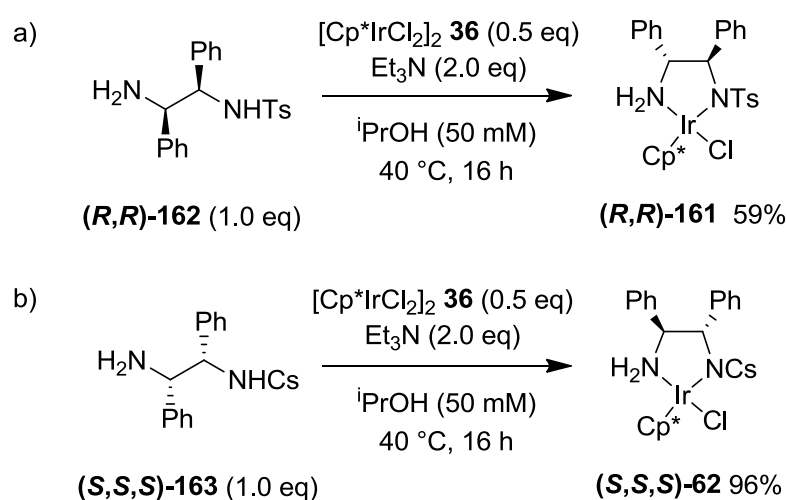
- In order for the iridium to be active, the number of labile and vacant sites on the metal centre of the organometallic catalyst could affect the rate of the hydrogen transfer reactions. If the complex was coordinatively and electronically saturated as an 18-electron species, a hemi-labile ligand would have to disassociate to allow the 16-electron species to accept

hydrogen from the substrate. Conversely, increasing the number of donor sites on the ligand will increase the chelate effect to the metal and improve the structural robustness of the multifunctional catalyst. Tridentate, bidentate and monodentate ligands have also been designed and synthesised in this chapter.

## 2.2. Control Catalysts

### 2.2.1. TsDPEN and CsDPEN Iridium(III) Complexes

For comparison of catalytic activity, TsDPEN and CsDPEN iridium(III) complexes (*R,R*)-**161** and (*S,S,S*)-**62** were prepared with iridium(III) chloride dimer **36** (Scheme 56), as both are known in the literature for hydrogen transfer reactions with alcohols and aldehydes/ketones (see Chapter 1.9).<sup>47</sup>

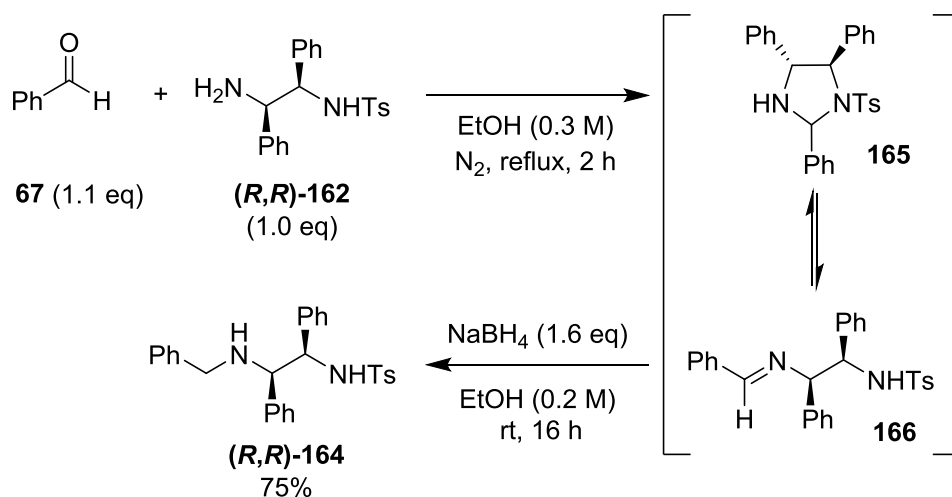


**Scheme 56** The preparation of known iridium(III) complexes; a) (*R,R*)-**161**, and b) (*S,S,S*)-**62**.<sup>47</sup>

### 2.2.2. Benzyl Tethered TsDPEN Iridium(III) Complex

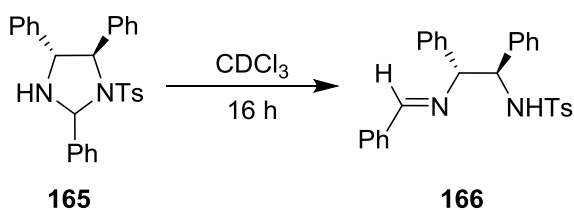
To use as a control study, to compare to the catalysis of a thiazole-tethered ligand, a non-coordinating benzene-tethered ligand was prepared following a literature procedure.<sup>96</sup> Transforming the primary amine, which has been shown to be important in the bifunctional outer-sphere mechanism of the hydrogen transfer reaction (see Chapter 1.9), into a secondary amine could affect the

hydrogen transfer reactions. In addition, the presence of the benzene ring could influence the steric interactions of the reaction. The control ligand **164** was prepared via the reductive amination of benzaldehyde **67** with (*R,R*)-TsDPEN **162** (Scheme 57).



**Scheme 57** Synthesis of *N*-benzyl control ligand (*R,R*)-**164**.

The intermediate was formed as a mixture of the imine and cyclic aminal **165**, which was shown using <sup>1</sup>H NMR to fully convert to the imine **166** over time (Scheme 58).



**Scheme 58** Conversion of cyclic aminal **165** to the imine **166**.

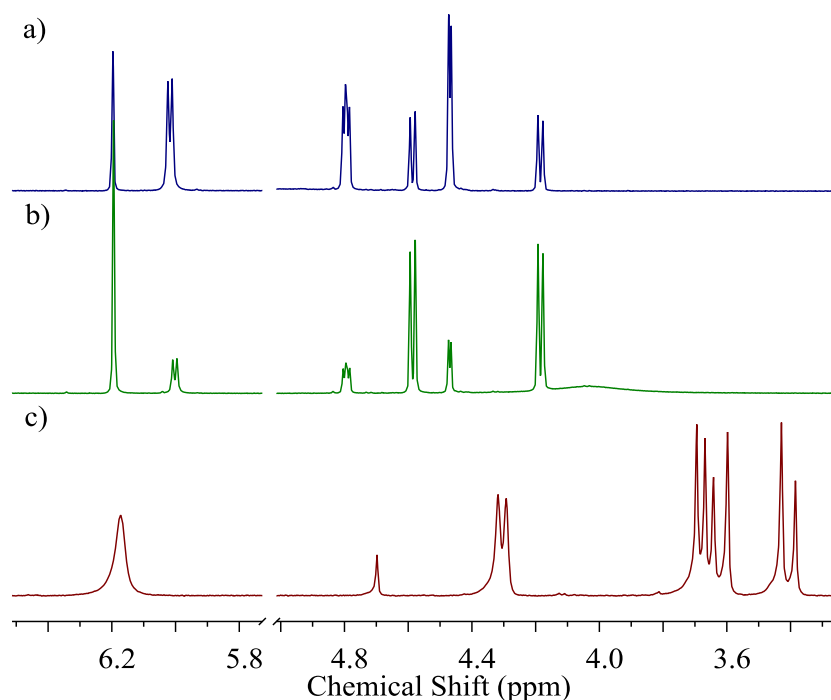


**Figure 20** Stacked  $^1\text{H}$  NMR spectra showing the conversion of intermediates over time; a) 1.5:1 mixture of aminal **165** and imine **166**, b) 3.2:1 mixture of imine **166** and aminal **165**, c) amine ligand **164**.

In 2008, Wills prepared benzyl TsDPEN ligand **164**,<sup>97</sup> and in 2009 prepared a ruthenium(II) complex **167** from the ligand for the asymmetric transfer hydrogenation of acetophenone **49** (Figure 21).<sup>98</sup> The analogous iridium(III) complex **168** was prepared from the iridium(III) chloride dimer **36** (Scheme 59).

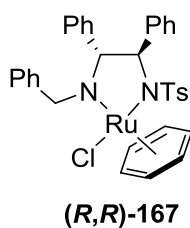
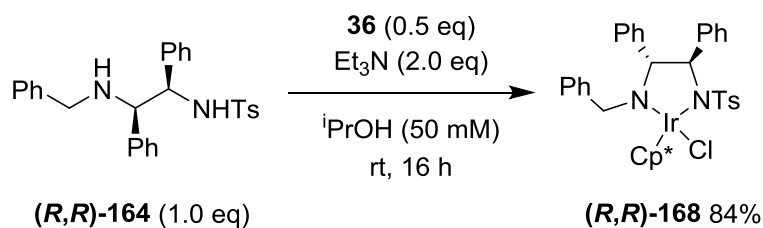


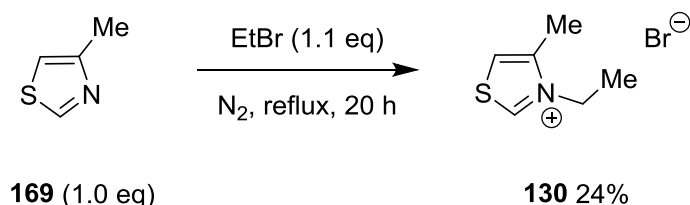
**Figure 21** Wills' ruthenium(II) complex **167** with ligand **164**.



**Scheme 59** Preparation of benzyl tethered TsDPEN iridium(III) catalyst **168**.

### 2.2.3. Thiazolium Control Catalyst

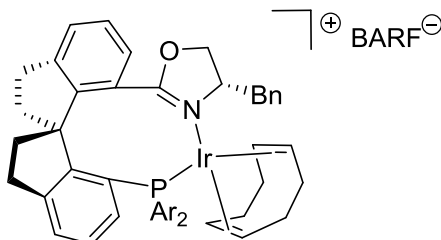
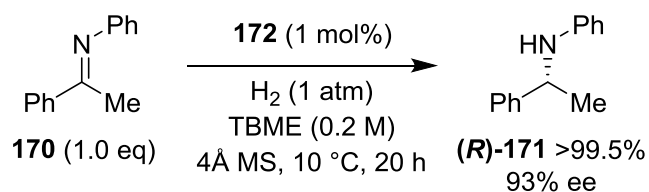
A simple thiazolium compound was synthesised to use as a control catalyst for the benzoin condensation reaction and investigate the reaction conditions of the organocatalysis, from the neat reaction of 4-methyl-1,3-thiazole **169** and bromoethane (Scheme 60).



**Scheme 60** Synthesis of 4-methyl-3-ethylthiazolium bromide **130**.

### 2.3. Synthesis of Thiazole and Thiazolium Iridium(III) Complexes

The synthesis of novel thiazole and thiazolium complexes is discussed in this section. The synthetic routes to the ligands designed were based on simple reactions in order to arrive at new ligands in a small number of steps. There are many catalyst systems reported in the literature that give high conversions and selectivities; however, if the synthesis of the ligand or catalyst is long and complicated the overall efficiency of the catalyst is reduced. Zhou reported an asymmetric catalyst **172** for the hydrogenation of ketimines in very high conversions and enantioselectivities (Scheme 61); however, the synthesis of the ligand required 13 steps and a resolution.<sup>99</sup>



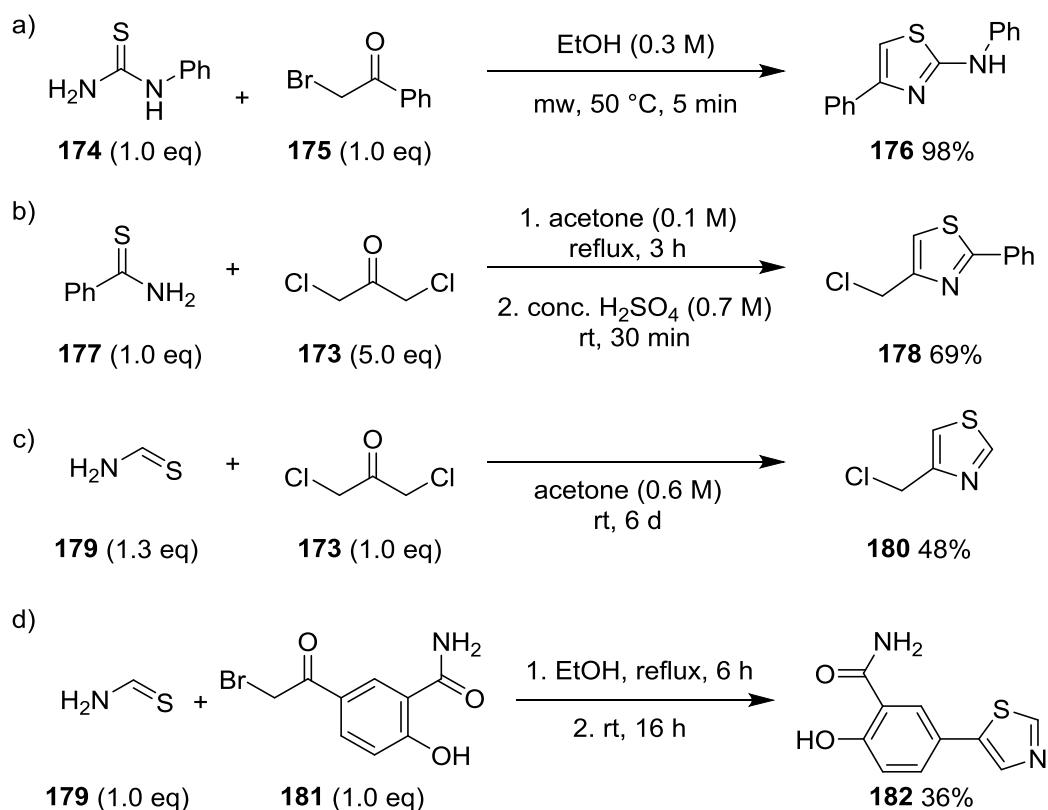
**172**

Ar = 3,5-diMe-C<sub>6</sub>H<sub>3</sub>

BARF = Tetrakis[3,5-bis(trifluoromethyl)phenyl]borate

**Scheme 61** The hydrogenation of ketimine **170** with Zhou's expensive catalyst **172** with high conversion and enantioselectivity.

The preparation of 1,3-thiazoles synthesised from  $\alpha$ -haloketones and thioformamides or thioalkylamides have been reported in the literature (Scheme 62).<sup>100-103</sup> However, the use of  $\alpha$ -haloketones (especially dichloroacetone **173**) is often undesirable due to the high toxicity of these compounds. Using thioalkylamides is safer than thioformamides, however the C-2 position of the thiazole ring would be substituted, which would prevent carbene formation and organocatalysis.



**Scheme 62** Examples of the reported synthetic routes to thiazole rings.

A thiazole ring with an aldehyde substituent in the 4-position would create a single methylene unit tether from a simple reductive amination reaction with an existing amine ligand, such as TsDPEN **162**. The 5-membered ring iridicyclic would prevent carbene-metal bond formation (Figure 22).

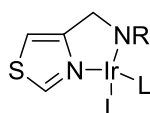


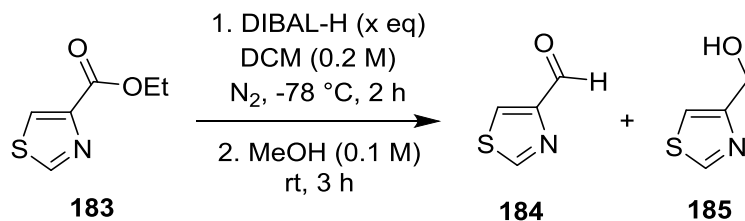
**Figure 22** A 5-membered iridicyclic highlighting the prevention of thiazolyldiene coordinating to the metal centre.

### 2.3.1. Synthesis of 1,3-Thiazole-4-carboxaldehyde **184**

As the most reactive position is the C-2 position, beginning a synthesis with a thiazole ring can be difficult. Therefore, commercially available thiazoles that are substituted on the 4- or 5-position, with the 2-position unsubstituted, formed the basis of the preparation of the thiazole ligands. Ethyl-4-thiazolecarboxylate **183** was converted to 4-thiazolecarboxaldehyde **184** through an ester reduction with DIBAL-H. With a standard acidic work-up, the

major product in the reaction was the alcohol **185**, as a result of over-reduction. Jamison investigated the reduction of esters to aldehydes in continuous flow using 1.5 equivalents of DIBAL-H and a methanol quench,<sup>104</sup> however using the same conditions in batch the over-reduction was still observed (entry 1, Table 5).

**Table 5** The selectivity of the reduction of ethyl-4-thiazolecarboxylate **183** to the product aldehyde **184** by varying the number of equivalents of DIBAL-H.

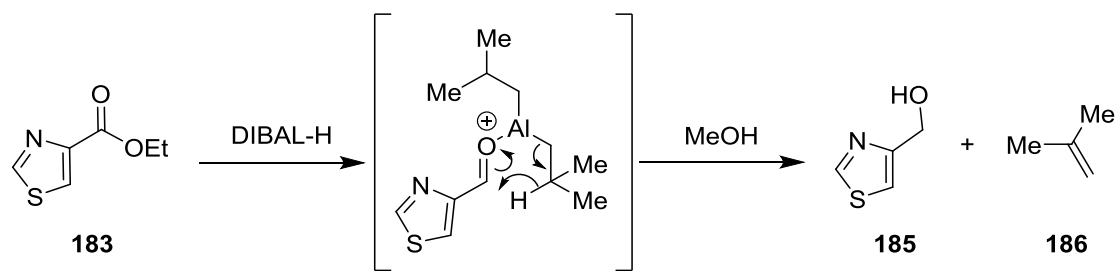


Entry	DIBALH (x eq)	Product Distribution (%) <sup>a</sup>		
		Ester	Aldehyde	Alcohol
1	1.50	0	17	83
2	0.95	0	25	75
3	0.33	93	7	0
4	0.50	14	86	0
5	0.75	0	100	0

<sup>a</sup> Distribution calculated from the integration of signals in the <sup>1</sup>H NMR spectra.

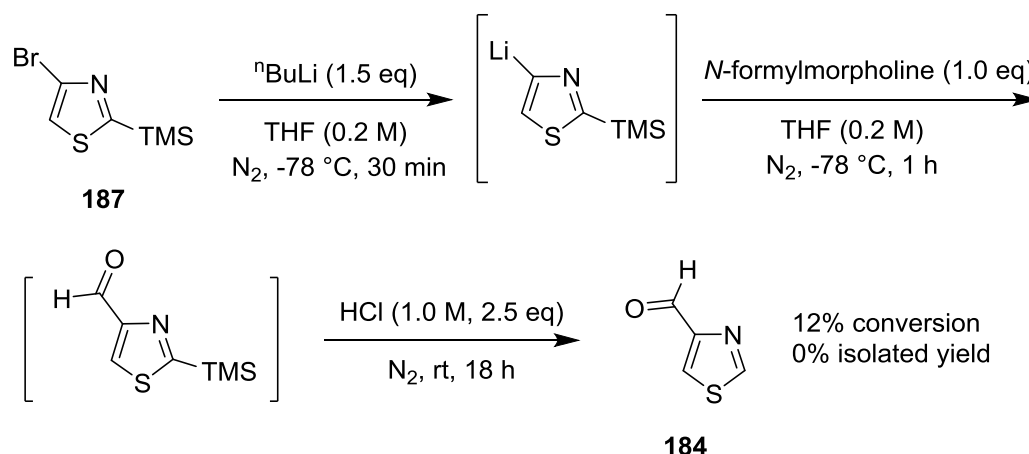
This suggests that there is an 83% excess of available hydrides for the reaction. As only a 50% excess is used in the reaction, it is proposed that DIBAL-H was transferring multiple hydrides (Scheme 63); one hydride from the Al-H bond and up to two hydrides from the methine C-H bonds of the *iso*-butyl groups, generating *iso*-butene **186**. In a similar example, Makio and Fujita demonstrate the reduction of imines with a TRIBAL reagent and observe *iso*-butene **186** during the reaction.<sup>105</sup> With 0.75 equivalents of DIBAL-H (entry 3, Table 5) only the aldehyde **184** is formed and with an isolated yield of 92%.





**Scheme 63** Mechanism of further hydride transfer over-reducing the ester **183** to the alcohol **185** and producing *iso*-butene **186**.

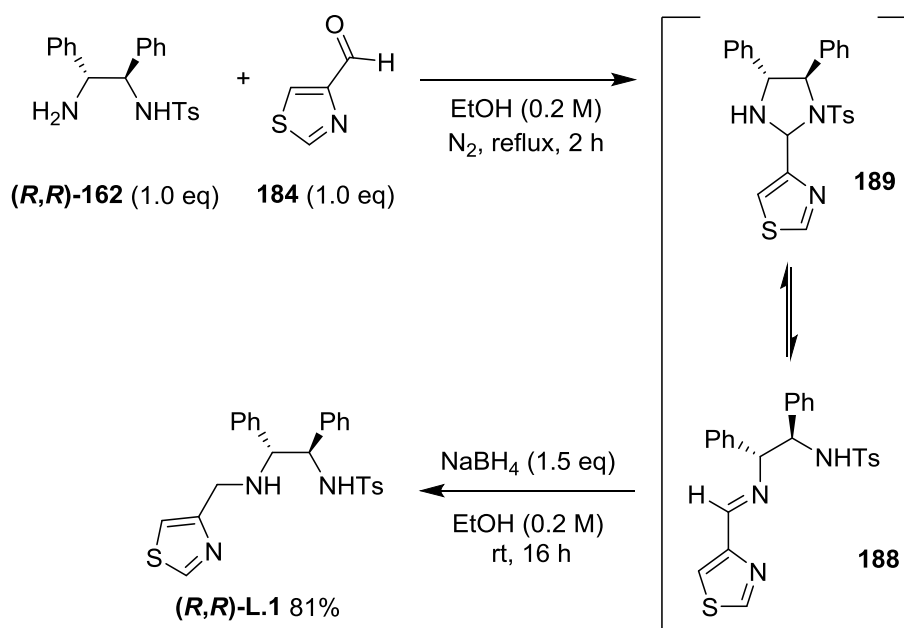
In 1987, Dondoni reported a route to **184** from inexpensive starting material 4-bromo-2-(trimethylsilyl)-thiazole **187** (Scheme 64).<sup>106</sup> After carrying out the reaction following Dondoni's procedure, a low yield of the desired aldehyde was achieved (12% using <sup>1</sup>H NMR) and this route was disregarded after two attempts.



**Scheme 64** The formylation of thiazole and subsequent TMS deprotection to aldehyde **184**.

### 2.3.2. Thiazole Tethered TsDPEN Iridium(III) Complex C.1

The thiazole-tethered TsDPEN ligand **L.1** was prepared from (*R,R*)-**162** and **184** via reductive amination reaction using sodium borohydride. As with the control ligand **164**, the intermediate from the condensation reaction is a mixture of the imine **188** and the cyclic aminal **189**, which fully converts over time to **188** (identified using <sup>1</sup>H NMR, Figure 23). The imine **188** was then reduced to the desired ligand **L.1** with sodium borohydride (Scheme 65).



**Scheme 65** Synthesis of thiazole-TsDPEN ligand **L.1**.

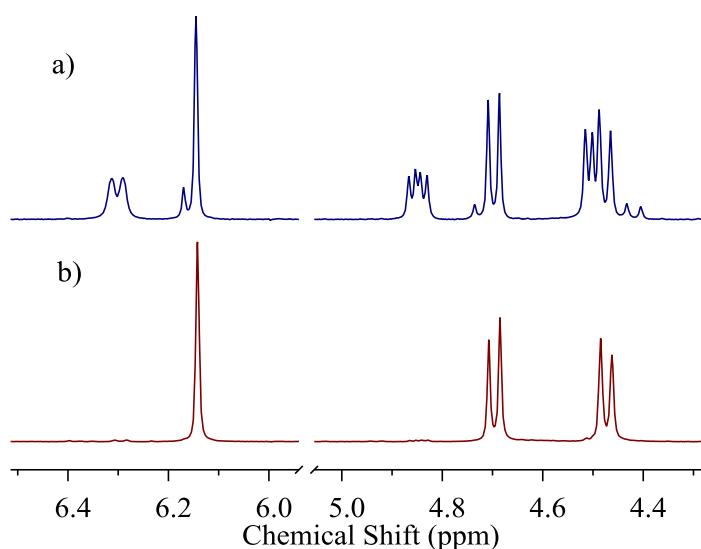
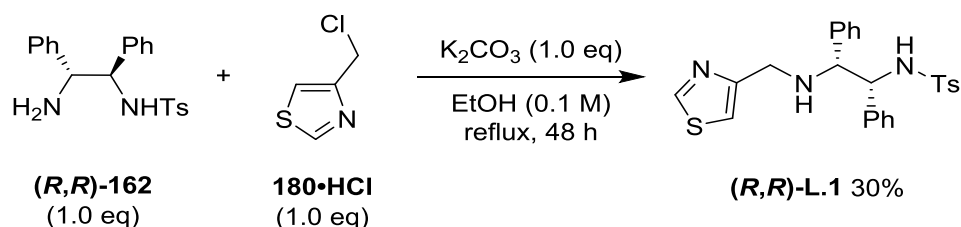


**Figure 23** Stacked  $^1\text{H}$  NMR spectra showing the conversion of intermediates; a) mixture of cyclic aminal **189** and imine **188** ( $t=0$  h), and b) imine **188** ( $t=16$  h).

In addition to the reductive amination route, **L.1** was prepared with 4-(chloromethyl)-1,3-thiazole hydrochloride **180** (Scheme 66). The yield of the  $\text{S}_{\text{N}}2$  reaction was lower than expected. This could be due to the solubility of the thiazolium salt in the reaction; however, an experiment with the salt separated into an organic layer before addition into a similar reaction also gave a low yield. The structure of ligand **L.1** was determined by x-ray crystallography (Figure 24).



**Scheme 66** The synthesis of thiazole ligand **L.1** from thiazole hydrochloride **180**.

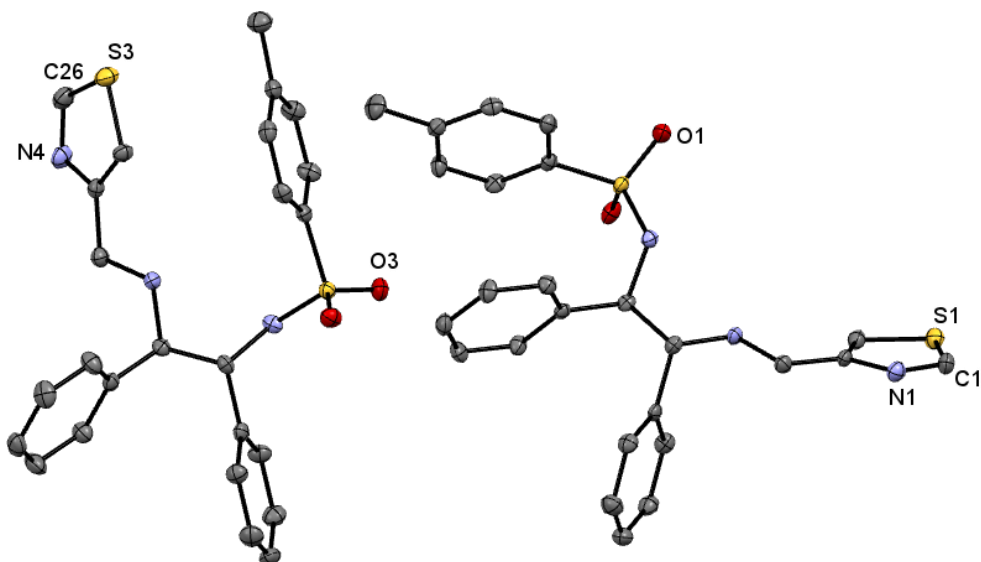
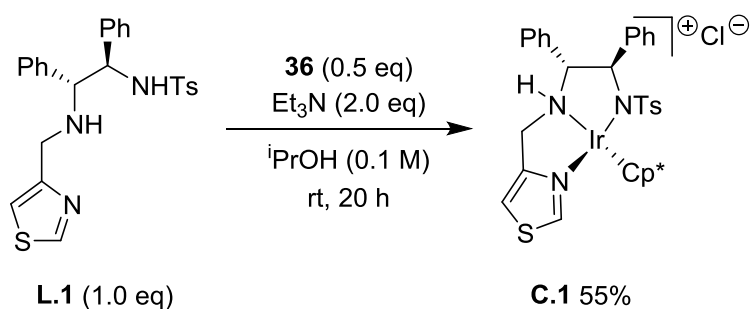


**Figure 24** The x-ray crystal structure of thiazole tethered TsDPEN ligand **L.1** with non-hydrogen atoms displayed as displacement ellipsoids, which are set at the 50% probability level. Hydrogen atoms have been removed for clarity. There are two molecules in the asymmetric unit cell, which differ in the direction of the tosyl group.

With the novel thiazole ligand in hand, an iridium(III) complex **C.1** was synthesised (Scheme 67). The target complex **C.1** was prepared via ligand substitution of thiazole **L.1** with **36**; which was achieved by Blacker with **36** and analogous ligands.<sup>47</sup>



**Scheme 67** Preparation of target catalyst **C.1**.

The complex **C.1** was identified using mass spectrometry; however,  $^1\text{H}$  NMR indicated two different species, **C.1.1** and **C.1.2**, were present in a ratio of 3:1 (Figure 25).

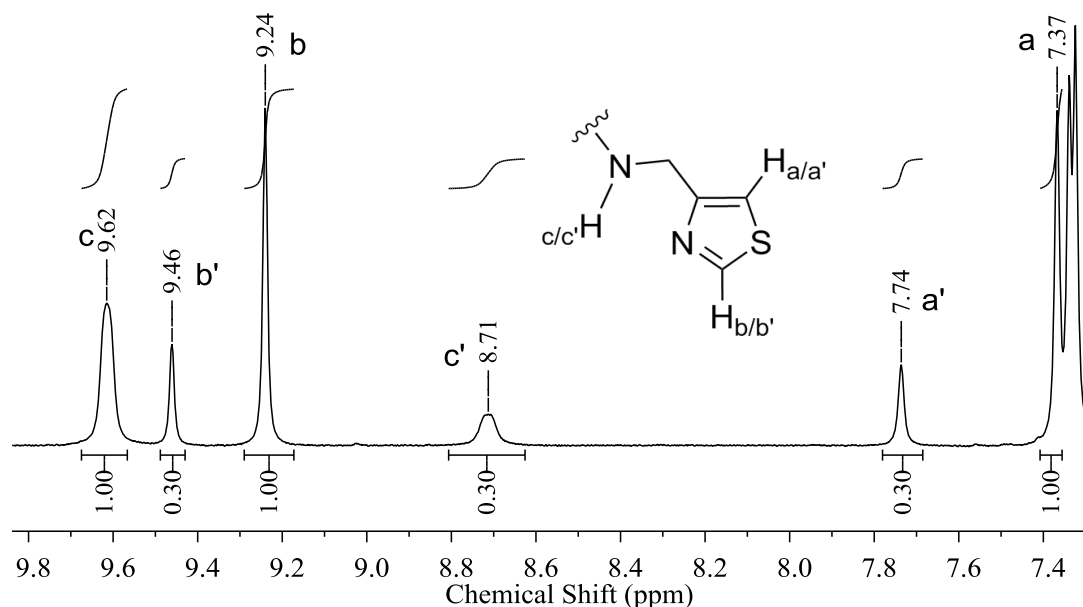


**Figure 25**  $^1\text{H}$  NMR spectrum of **C.1**, showing two distinct sets of signals for **C.1.1** and **C.1.2** in a ratio of 3:1 respectively.

The reason behind the mixture of complexes could be that there are two diastereomeric complexes, as the 4-coordinate metal centre could be acting as a stereocentre. An optically impure batch of (*R,R*)-**162** would result in diastereomers being produced in the reaction, therefore the specific rotation of the batch was measured and agrees with literature values ( $[\alpha]_{\text{D}}^{25} = -35^\circ$ ).<sup>107</sup> Another possibility is that the complex exists as two rotamers, with the tridentate ligand coordinating to the metal centre in two conformations. The energy of each of the rotamers will define the ratio in which they are present in the sample; there may also be conversion between them. However, as the ligand is tridentate, the chelating effect would make interconversion less likely. Molecular modelling of the two rotamers using DFT B3LYP/LANL2DZ suggests a ratio of complex **C.1.1** to complex **C.1.2** as 9:1 from the relative energies ( $\Delta E = 2.75 \text{ kcal mol}^{-1}$ ) (Figure 26).

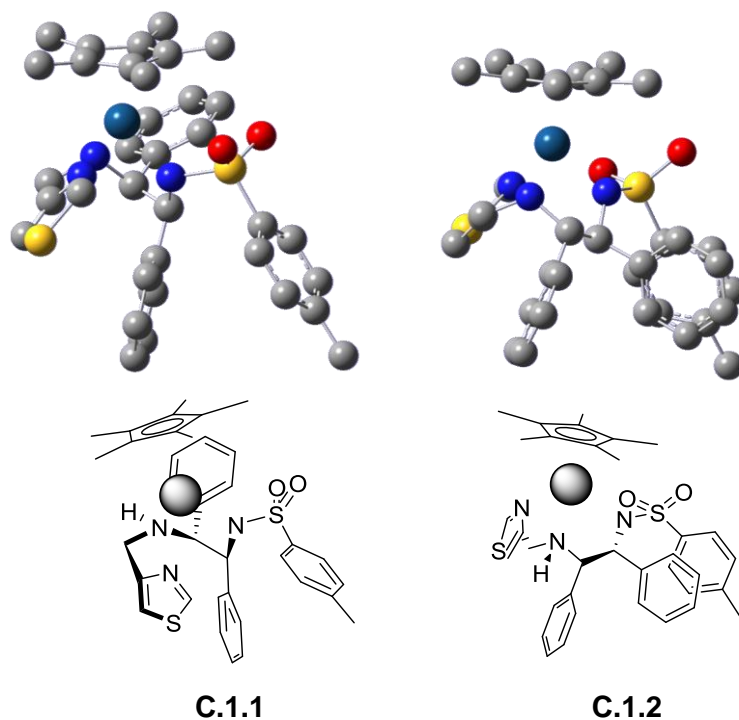
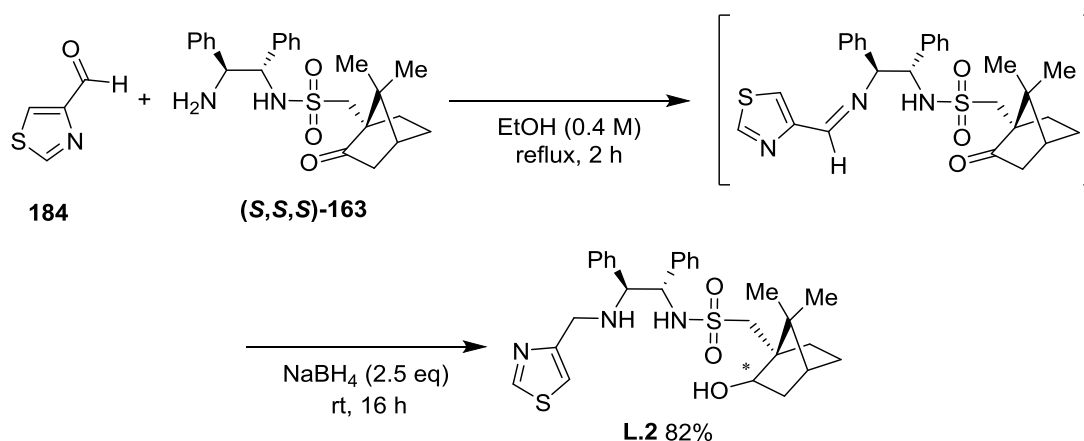


**Figure 26** Molecular modelling of the two rotamers of the iridium(III) catalyst **C.1.1** and **C.1.2** with a calculated ratio of 9:1 respectively using DFT B3LYP/LANL2DZ.

### 2.3.3. Thiazole Tethered Iridium(III) Complex **C.2**

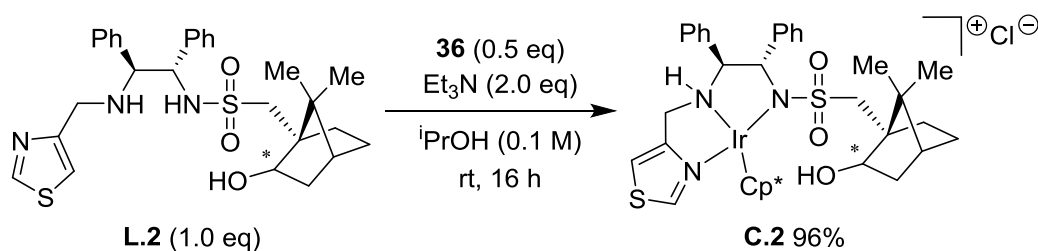
The attempted preparation of thiazole tethered CsDPEN ligand **L.2** was carried out in the same way as for the thiazole-tethered ligand **L.1** (Scheme 68).



**Scheme 68** Synthesis of thiazole tethered ligand **L.2**.

After the reduction of the imine intermediate, the ketone of the camphor group was found to have been reduced during the reaction. This was identified by

the absence of the characteristic signal (215 ppm) correlating to the highly strained ketone in the  $^{13}\text{C}$   $\{^1\text{H}\}$  NMR spectrum. The benzoin reaction could occur at the ketone,<sup>108</sup> however the distance between the thiazole catalyst and the camphor group should prevent this. The reduction of the ketone group could produce two isomers; however, the *iso*-borneol will be the major product with the alcohol in the equatorial position, as this is the kinetic product of the irreversible reaction with axial attack from sodium borohydride opposite to the bulky *gem*-dimethyl group.<sup>109</sup> The iridium(III) complex could theoretically reduce the ketone group via a transfer hydrogenation reaction, which has been discussed by Blacker to improve the enantioselectivity of transfer hydrogenation reactions; the camphor sulfonyl group is asymmetrically reduced increasing the chirality in the DPEN ligand.<sup>110</sup> However, the  $^1\text{H}$  NMR spectra indicate that only the *iso*-borneol complex is formed. Catalyst **C.2** was synthesised from the iridium(III) chloride dimer **36** (Scheme 69).



**Scheme 69** Preparation of catalyst **C.2**.

The  $^1\text{H}$  NMR spectrum for this catalyst indicates only one species is present. As the three dimensional shape of ligand **L.2** occupies a larger volume than the flat tosyl sidechain of **L.1**, the formation of one rotamer may be more selective over the other. In addition, the  $^1\text{H}$  NMR spectrum shows the alcohol is not deprotonated nor has it an O-donor to the metal centre. As with **C.1**, the amine group of **C.2** is protonated. This was confirmed using narrow-band decoupling with  $^1\text{H}$  NMR spectroscopy, irradiating the broad signal at 9.6 ppm making the proton decouple with its neighbouring protons, causing the double doublets at 4.6 ppm and 4.2 ppm, corresponding to the methane and methylene groups either side of the amine group, to become doublets (Figure 27).

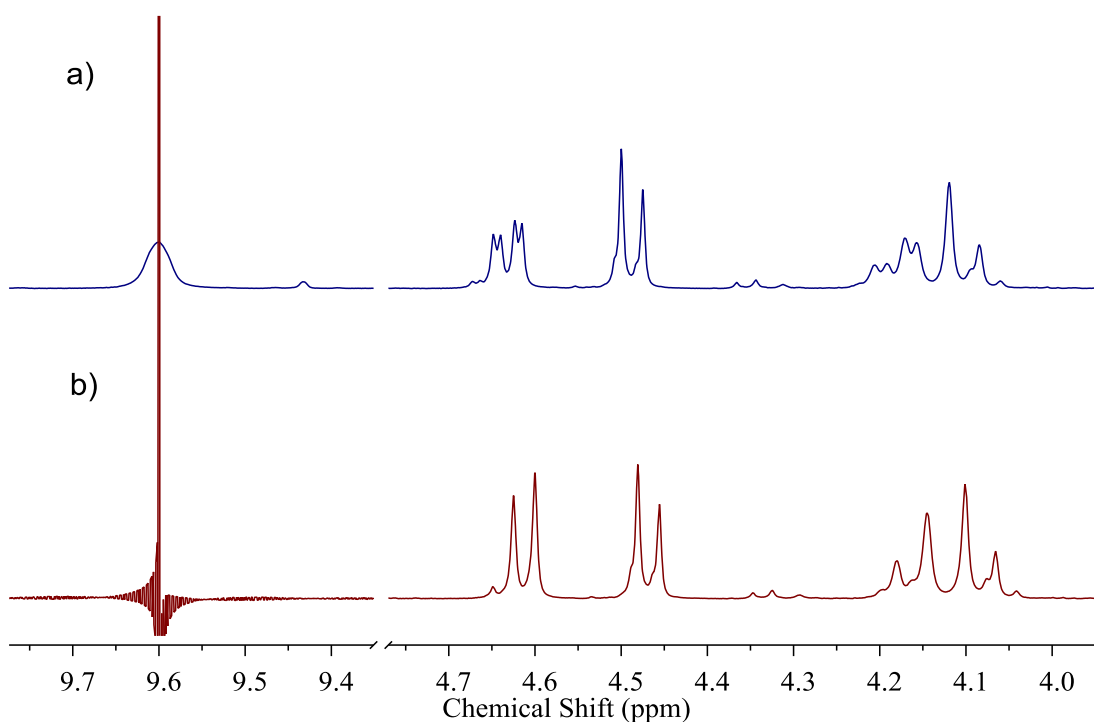
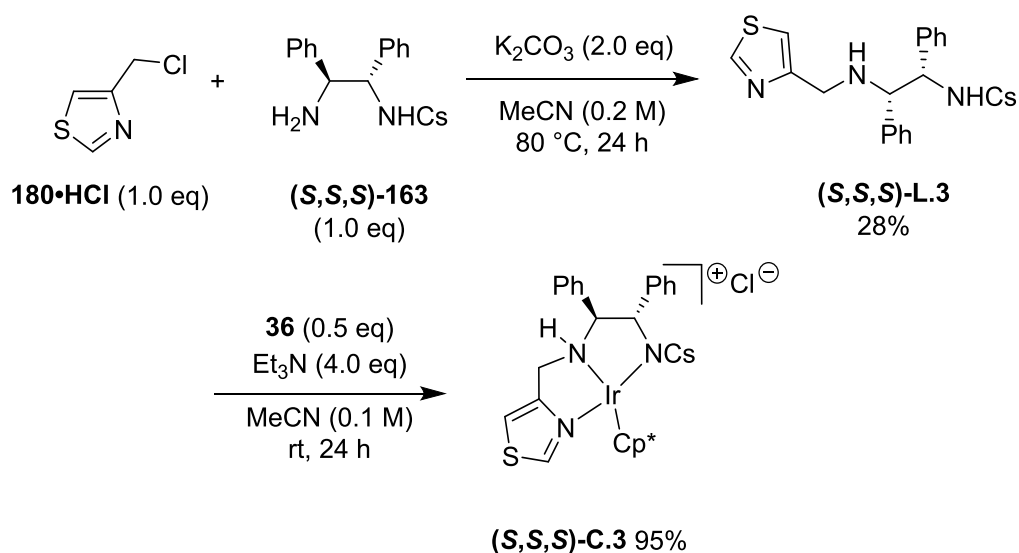


**Figure 27** a)  $^1\text{H}$  NMR spectrum of **C.2**, and b) narrowband decoupled spectrum of **C.2** after proton signal at 9.6 ppm is irradiated.

#### 2.3.4. Thiazole Tethered CsDPEN Iridium(III) Complex **C.3**

A second route to synthesise a thiazole tethered CsDPEN ligand from (*S,S,S*)-**163** was attempted with **180•HCl**; avoiding the use of a reducing agent and therefore retaining the camphor ketone group (Scheme 70). The yield of the ligand **L.3** was poor, as seen previously (2.3.2). The ligand was complexed to iridium(III) chloride dimer **36** to produce the novel complex **C.3** (Scheme 70). The ketone group of the camphor sidechain was shown to be intact, due to the characteristic signal (at 215 ppm) in the  $^{13}\text{C}$   $\{^1\text{H}\}$  NMR; which suggests that a transfer hydrogenation reaction is not occurring during the synthesis of complex **C.2** (see Chapter 2.3.3). The molecular structure was determined using x-ray crystallography (Figure 28). Both complexes display a distorted octahedral geometry about the metal centre.



**Scheme 70** The synthesis of novel ligand **L.3** and complex **C.3**.

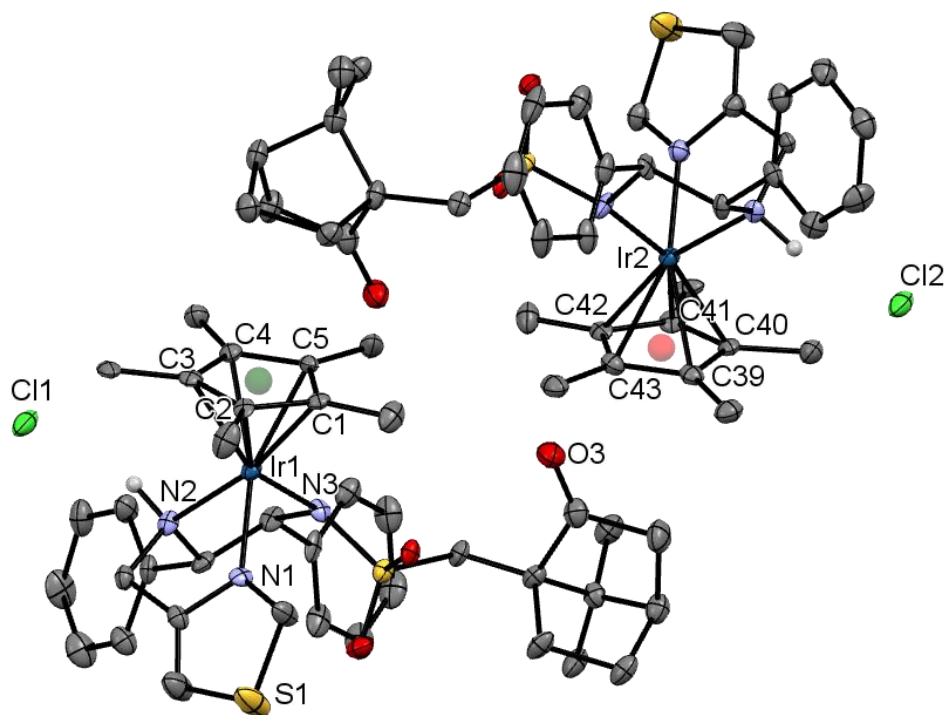


**Figure 28** The x-ray crystal structure of diastereomers **(R<sub>r</sub>)-C.3** (Ir1) and **(S<sub>r</sub>)-C.3** (Ir2) with non-hydrogen atoms displayed as displacement ellipsoids, which are set at the 50% probability level. Hydrogen atoms have been removed for clarity. Both structures appear in the asymmetric unit. The centroid of the C(1)–C(5) ring is highlighted (green).



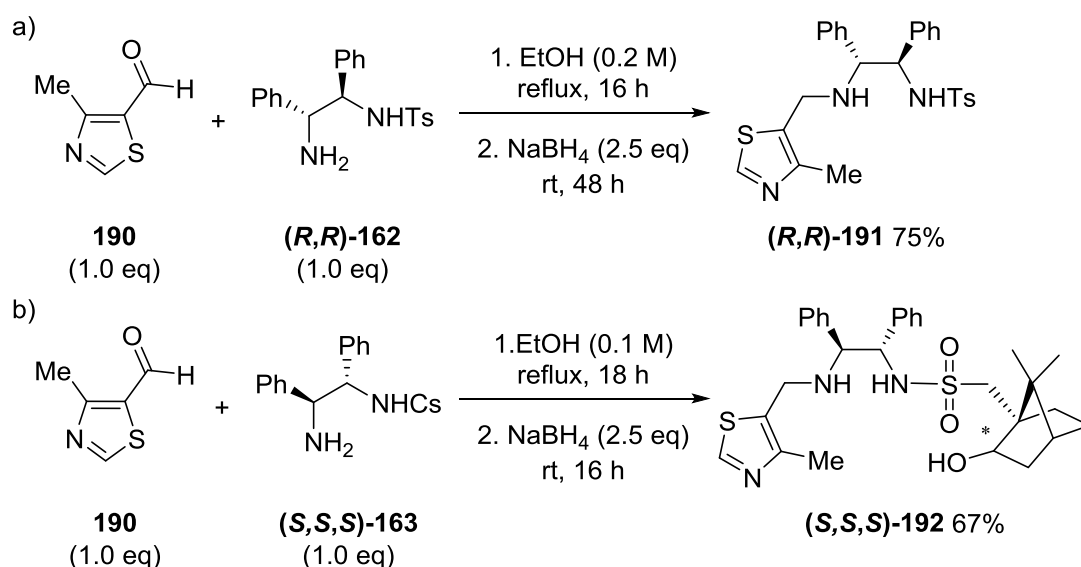
**Table 6** The bond lengths (Å) and angles (°) of the coordinating atoms of complex **C.3**; Cp\*(1) and Cp\*(2) correspond to the centroids of rings C(1)–C(5) and C(39)–C(43) respectively (Figure 28).

Ir(1)-N(1)	2.081(10)	N(1)-Ir(1)-N(2)	76.4(4)
Ir(1)-N(2)	2.157(10)	N(1)-Ir(1)-N(3)	91.8(4)
Ir(1)-N(3)	2.118(11)	N(2)-Ir(1)-N(3)	79.9(4)
Ir(1)-Cp*(1)	1.787	N(1)-Ir(1)-Cp*(1)	131.4
		N(2)-Ir(1)-Cp*(1)	133.7
		N(3)-Ir(1)-Cp*(1)	125.8
Ir(2)-N(4)	2.063(10)	N(4)-Ir(2)-N(5)	78.9(4)
Ir(2)-N(5)	2.154(10)	N(4)-Ir(2)-N(6)	84.2(4)
Ir(2)-N(6)	2.118(11)	N(5)-Ir(2)-N(6)	78.2(4)
Ir(2)-Cp*(2)	1.786	N(4)-Ir(2)-Cp*(2)	130.8
		N(5)-Ir(2)-Cp*(2)	133.0
		N(6)-Ir(2)-Cp*(2)	131.2

The crystal structure shows the complex has presented as diastereomers, due to the iridium acting as a chiral centre. Comparison of the N-Ir bond lengths (Table 6) indicates that the coordinated thiazole *N*-donor is the strongest of the three iridium bonds; this could be an indication that the metal centre is withdrawing more electron density from the thiazole ring, increasing the acidity of the *C*-2 proton. Aside from shorter N-Ir bond lengths (~0.3 Å), the measurements are of a similar order to that of the iridium(III) chloride dimer **36**.<sup>111</sup>

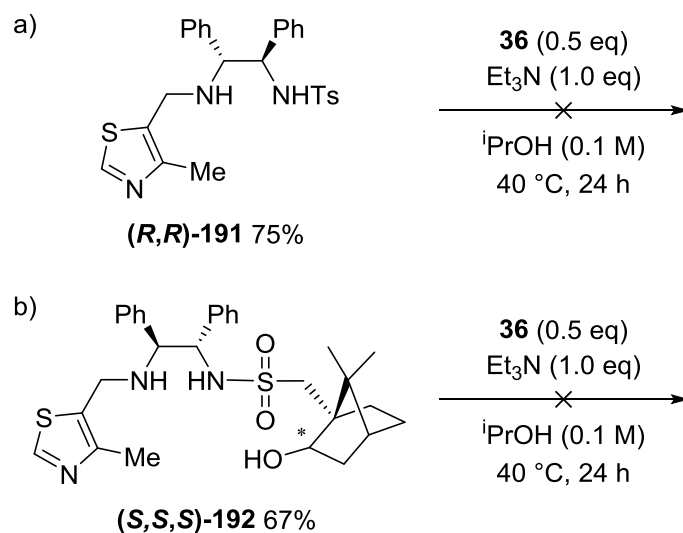
### 2.3.5. 4-Methyl-Thiazole Tethered Ligands

Another set of thiazole compounds were made with 5-formyl-4-methyl-1,3-thiazole **190**, so that the tether is in the 5-position; which does not allow tridentate coordination to the metal via the thiazole *N*-atom. Compounds **191** and **192** were synthesised with (*R,R*)-**162** and (*S,S,S*)-**163** respectively (Scheme 71).



**Scheme 71** The synthesis of 4-methylthiazole compounds **191** and **192**.

The preparation of the iridium(III) complexes with 4-methylthiazole compounds **191** and **192** was unsuccessful (Scheme 72); there was neither  $^1\text{H}$  NMR or mass spectroscopic evidence for either complex.

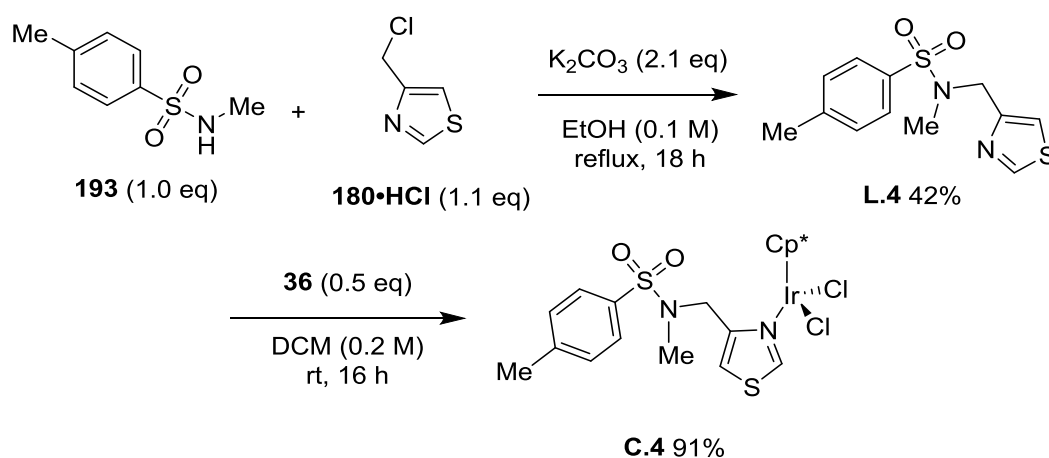


**Scheme 72** Unsuccessful coordination of thiazole compounds **191** and **192** to iridium(III) chloride dimer **36**.

This was an interesting result, as formation of the complexes was being prevented by either the thiazole ring not being able to coordinate to the metal centre, or by the small alteration to the steric interactions of the ring; a single methyl group in the 4-position. This reinforced the initial design idea that coordinating the ring to the metal would improve the ligand coordination.

### 2.3.6. Thiazole Tethered Iridium(III) Complex C.4

A novel complex **C.4** was designed with only one donor site on the ligand to identify whether the thiazole is bound strongly to the metal centre; as indicated by the short bond length in the crystal structure of **C.3** (Figure 28). Ligand **L.4** was made by the S<sub>N</sub>2 reaction of *N*-methylsulfonamide **193** and thiazole hydrochloride **180**. The thiazole ligand **L.4** was coordinated to iridium(III) **36** to give complex **C.4** (Scheme 73).



**Scheme 73** The preparation of ligand **L.4**, via S<sub>N</sub>2 reaction from sulfonamide **193** and thiazole **180·HCl**, and monodentate thiazole iridium(III) complex **C.4**.

The molecular structure of complex **C.4** was determined using x-ray crystallography; which shows that the ligand **L.4** is bound in a monodentate fashion through the *N*-atom of the thiazole (Figure 29). The complex displays a distorted octahedral geometry about the metal centre.

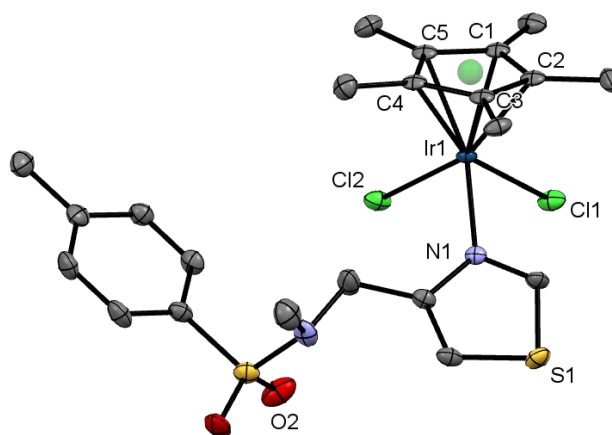


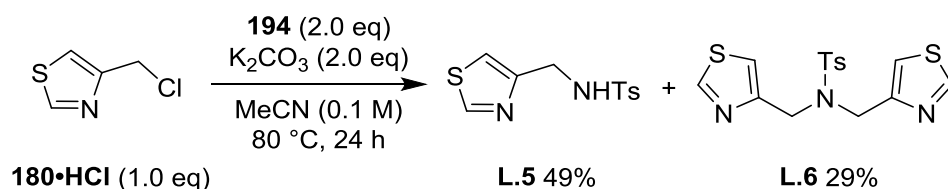
**Figure 29** The x-ray crystal structure of complex **C.4**, with non-hydrogen atoms displayed as displacement ellipsoids, which are set at the 50% probability level. Hydrogen atoms have been removed for clarity. The centroid of the C(1)–C(5) ring is highlighted (green).

**Table 7** The bond lengths (Å) and angles (°) of the coordinating atoms of complex **C.4**; Cp\*(1) corresponds to the centroid of ring C(1)-C(5) (green, Figure 29).

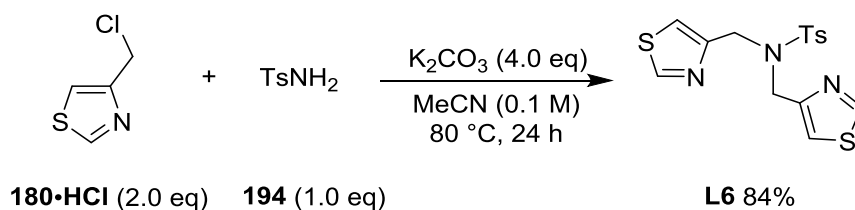
Ir(1)-Cl(1)	2.415(15)	Cl(1)-Ir(1)-Cl(2)	88.07(6)
Ir(1)-Cl(2)	2.409(15)	Cl(1)-Ir(1)-N(1)	90.73(13)
Ir(1)-N(1)	2.142(5)	Cl(2)-Ir(1)-N(1)	85.25(13)
Ir(1)-Cp*(1)	1.767	N(1)-Ir(1)-Cp*(1)	129.31
		Cl(1)-Ir(1)-Cp*(1)	126.58
		Cl(2)-Ir(1)-Cp*(1)	123.72

### 2.3.7. Thiazole Tethered Iridium(III) Complexes **C.5** and **C.6**

Two novel ligands were synthesised using *p*-toluenesulfonamide **194** and **180•HCl**. Both bidentate ligands **L.5** and **L.6** were synthesised in the same reaction and separated using column chromatography (Scheme 74). The yield of the *bis*-thiazole ligand **L.6** was improved by increasing the equivalents of the thiazole starting material (Scheme 75).

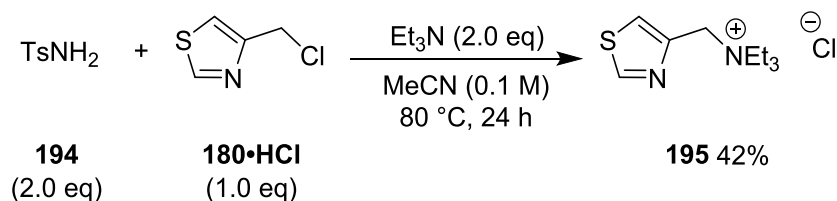


**Scheme 74** Synthesis of *mono*- and *bis*-thiazole ligands **L.5** and **L.6**.

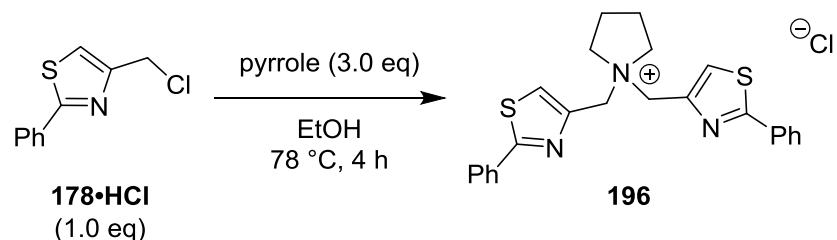


**Scheme 75** Improved synthesis of *bis*-thiazole **L.6**.

Initially, the synthesis was attempted with triethylamine as the base in the reaction. With *p*-toluenesulfonamide there was no conversion to the desired product, and only the triethyl[(1,3-thiazol-4-yl)methyl]azanium chloride salt **195**, which was analysed using  $^1\text{H}$  NMR and mass spectroscopy, was isolated (Scheme 76). In 1967, Lundina and Postovskii synthesised an analogous quaternary ammonium salt **196** via a similar route (Scheme 77).<sup>112</sup>



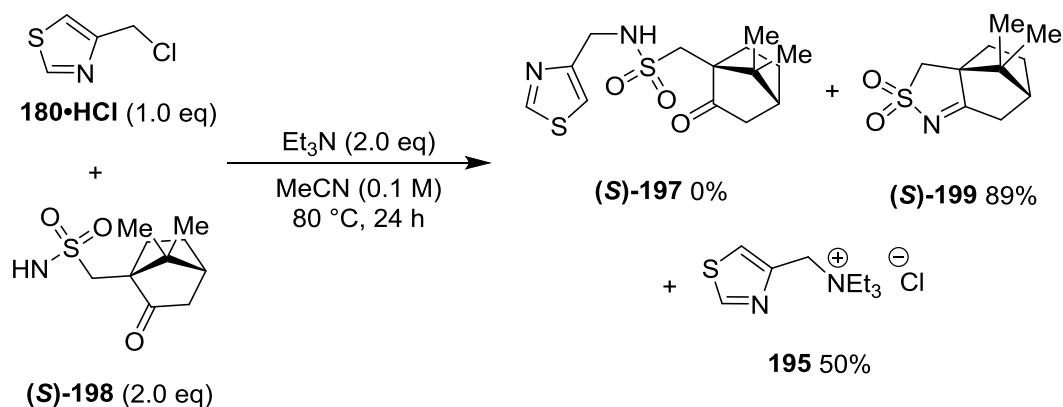
**Scheme 76** The undesired synthesis of ammonium salt **195**.



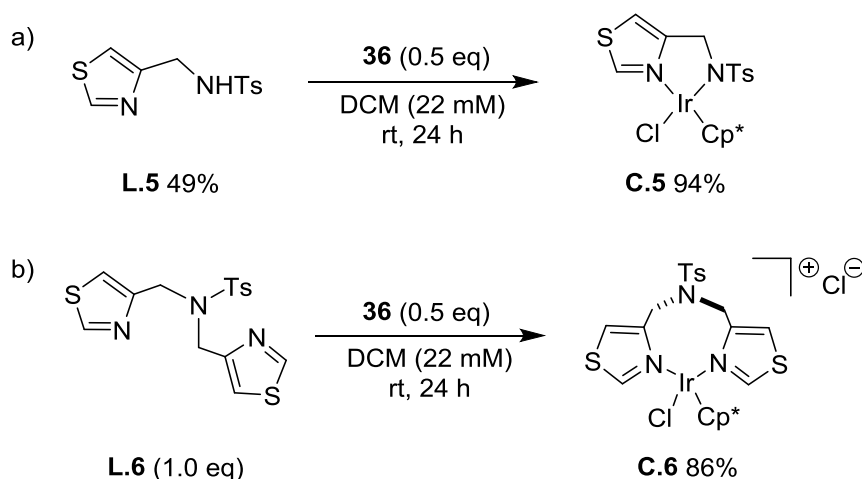
**Scheme 77** The synthesis of quaternary ammonium salt **196** as reported by Lundina and Postovskii.

The ammonium chloride salt **195** was also identified from the reaction to make thiazole compound **197** with 10-camphorsulfonamide (*S*)-**198**. In addition, the

cyclic sulfonylimine (**(S)**-**199**, from the intramolecular condensation of the sulfonamide (**(S)**-**198**, was present in 89% yield (with respect to **198**). The desired product was not observed using  $^1\text{H}$  NMR spectroscopy or LCMS (Scheme 78).



**Scheme 78** The undesired synthesis of ammonium salt **195** and cyclic sulfonylimine (**(S)**-**199**. The yields were determined using  $^1\text{H}$  NMR spectroscopy.



**Scheme 79** The synthesis of bidentate complexes; a) **C.5** and b) **C.6**.

Both thiazole ligands **L.5** and **L.6** were coordinated to the iridium(III) dimer **36** (Scheme 79). The  $^1\text{H}$  NMR spectra and the mass spectroscopic analysis for the *mono*-thiazole complex **C.5** suggest that the thiazole compound has coordinated to the metal centre as a bidentate ligand; the sulfonamide N-H proton signal is absent. The *bis*-thiazole complex **C.6** is more difficult to analyse using  $^1\text{H}$  NMR spectroscopy, however, the C-2 proton signal of the complex is broad when compared to the free ligand (Figure 30). Both rings must have the same bonding, as there is only one set of thiazole signals in the

$^1\text{H}$  NMR spectrum, which suggests that the ligand is bidentate. Also, the mass spectroscopic evidence for complex **C.6** supports that the ligand is bound to the metal.

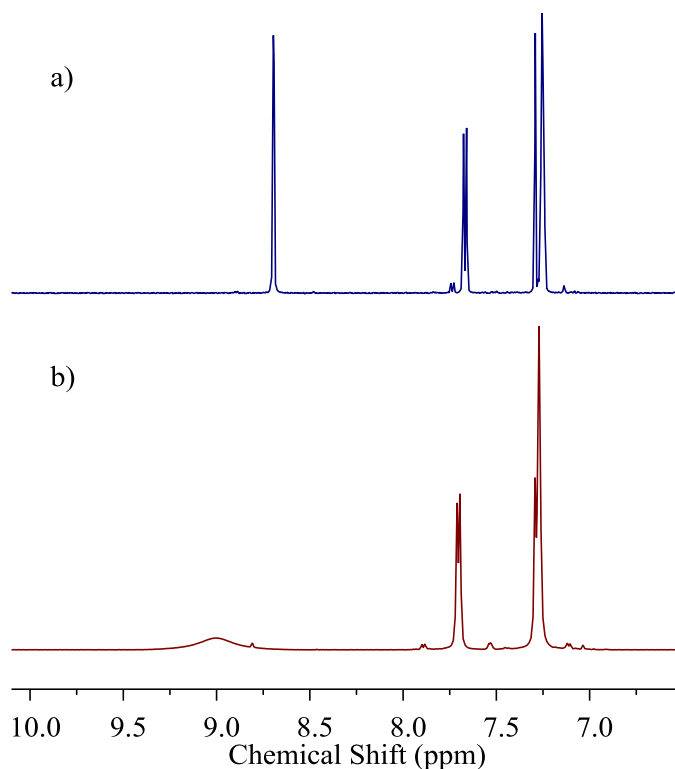


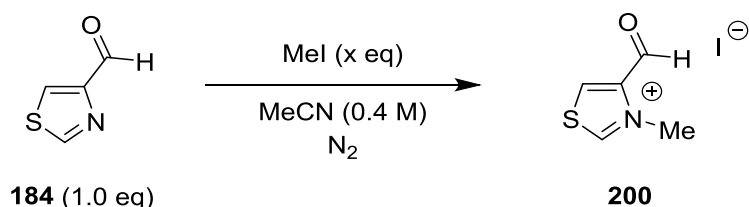
**Figure 30** Stacked  $^1\text{H}$  NMR spectra; a) *bis*-thiazole ligand **L.6**, b) *bis*-thiazole complex **C.6**.

### 2.3.8. Thiazolium Ligands

If the metal is not sufficiently electron poor, the  $\text{pK}_a$  of the thiazole will not be low enough to allow deprotonation, and therefore will not be an active catalyst. Alkylating the thiazole ring at the *N*-atom would increase the acidity of the *C*-2 position considerably ( $\text{pK}_a \sim 17$ ). Synthetic routes to compounds with thiazolium precursors is challenging, especially maintaining a *C*-2 position free from substitution; which is the most acidic and most reactive site on the ring. Alkylation of electron rich thiazoles are facile; however, 4-formyl-1,3-thiazole **184** is electron poor, and very low yields of the novel thiazolium salt **200** were achieved using literature methods.<sup>113</sup> With a large excess of iodomethane and heating at 80 °C, a reasonable yield was achieved (entry 5, Table 8). A second

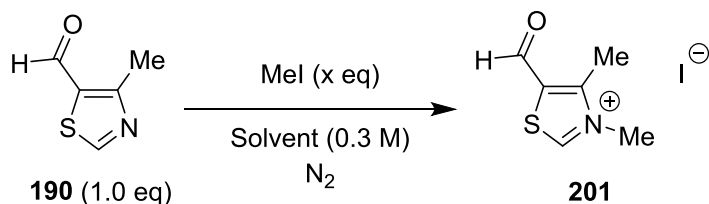
novel thiazolium was prepared from a more electron rich thiazole **190** to produce thiazolium iodide **201** (Table 9). <sup>1</sup>H NMR analysis of **201** in *d*<sub>4</sub>-methanol showed that the hemiacetal **202** had formed with the solvent (Scheme 80). Therefore, the thiazolium aldehydes were analysed for NMR spectroscopy in *d*<sub>6</sub>-DMSO.

**Table 8** Methylation of electron poor thiazole **184** to novel thiazolium **200**.



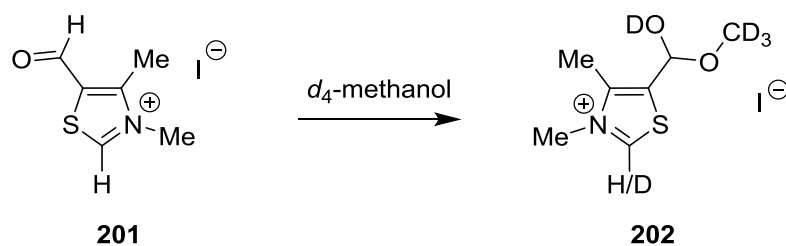
Entry	MeI (x eq)	Time	T (°C)	Yield (%)
1	2.5	24 h	rt	0
2	5.0	7 d	rt	0
3	2.5	16 h	80	11
4	2.5	24 h	80	16
5	10.0	18 h	80	59

**Table 9** Methylation of a more electron rich thiazole **190** (cf. **184**).



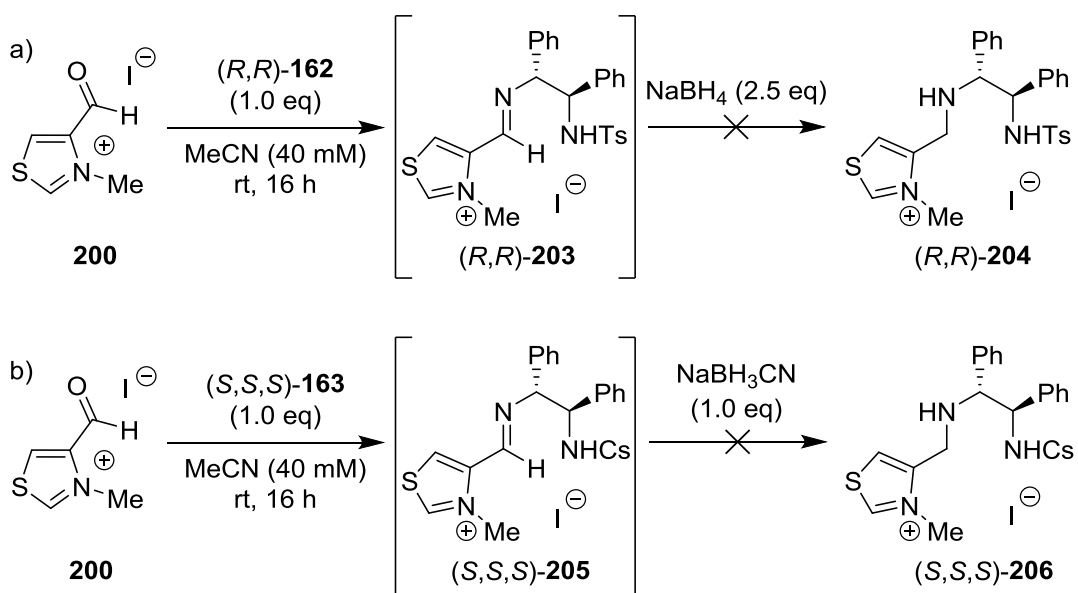
Entry	MeI (x eq)	Solvent	Time (h)	T (°C)	Yield (%)
1	1.5	DCM	24	40	0
2	2.5	MeCN	24	rt	0
3	2.5	MeCN	18	80	18





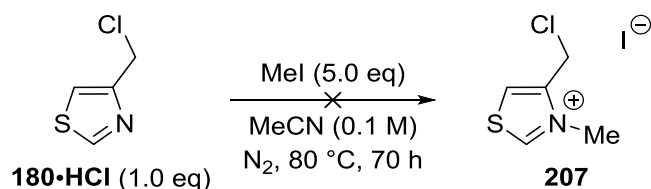
**Scheme 80** Formation of hemiacetal **202** from **201** in  $d_4$ -methanol in an NMR tube at room temperature. Ratio of proton to deuterium at the C-2 position is 1:1.

With the thiazoliums prepared, reductive amination with amines (*R,R*)-**162** and (*S,S,S*)-**163** was attempted (Scheme 81). Both reactions were unsuccessful after the addition of sodium borohydride, suggesting that the thiazolium ring was reduced; due to the absence of downfield thiazole proton signals in the  $^1\text{H}$  NMR spectra.



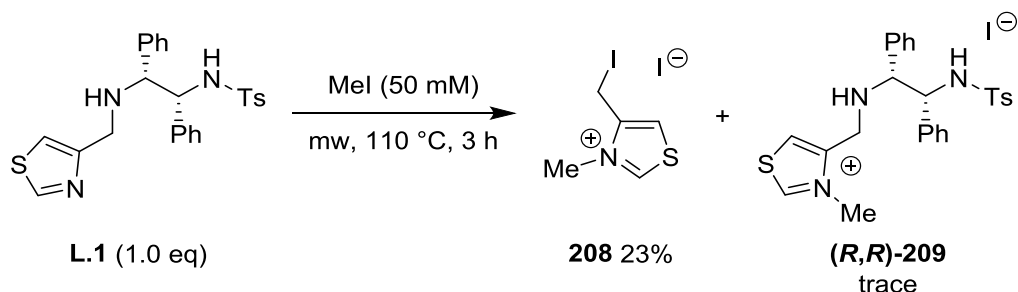
**Scheme 81** Unsuccessful reductive amination of imine thiazolium iodides **203** and **205** to **204** and **206** respectively.

An alternative strategy to synthesise the thiazolium ligands **204** and **206** would be via an  $\text{S}_{\text{N}}2$  reaction with thiazolium salt **207**. However, alkylation of thiazole **180**•HCl was unsuccessful, producing an insoluble black solid (Scheme 82).



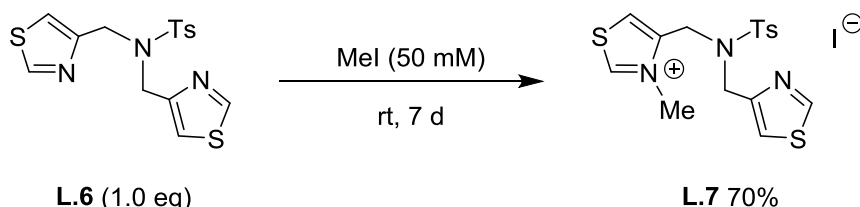
**Scheme 82** Attempted synthesis of thiazolium iodide **207**.

Thiazole ligand **L.1** was stirred in iodomethane at reflux and in a microwave reactor at 110 °C in an attempt to methylate the thiazole *N*-atom (Scheme 83). However, the major product isolated was the eliminated iodomethylthiazolium salt **208**. The desired product **209** was seen in the <sup>1</sup>H NMR and LCMS spectra, but was not isolated from the mixture of other methylated products.



**Scheme 83** Attempted synthesis of thiazolium **209**, forming thiazolium **208** as a side product.

The *bis*-thiazole substituted ligand **L.6** was alkylated at one of the thiazole *N*-atoms using iodomethane to produce thiazole-thiazolium ligand **L.7** (Scheme 84). The thiazole/thiazolium ligand **L.7** was complexed to iridium(III) dimer **36** to produce thiazolium complex **C.7.1**.



**Scheme 84** Methylation of *bis*-thiazole **L.6** to produce thiazolium iodide **L.7**.

The thiazolium ligand **L.7** was only soluble in *d*<sub>6</sub>-DMSO for NMR spectroscopy, therefore the complex **C.7.1** was initially analysed in *d*<sub>6</sub>-DMSO. The crystallisation from the NMR sample yielded orange needles, which was

determined by x-ray crystallography to be an iridium(III) complex with two iodide ligands and a S-coordinated dimethylsulfoxide molecule (Figure 31). A similar structure  $[\text{Cp}^*\text{IrI}_2(d_6\text{-DMSO})]$  is known in the literature and was formed from the attempted analysis of  $[\text{Cp}^*\text{IrI}_2]_2$  in  $d_6\text{-DMSO}$ .<sup>114</sup>

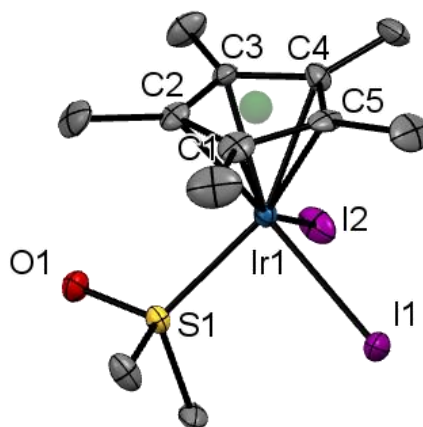


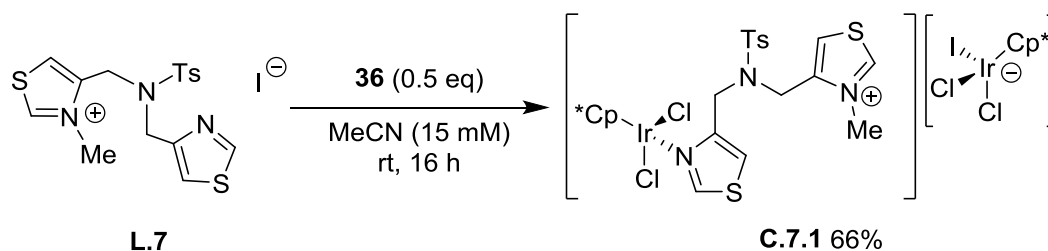
**Figure 31** X-ray crystal structure of  $[\text{Cp}^*\text{IrI}_2(d_6\text{-DMSO})]$  with non-hydrogen atoms displayed as displacement ellipsoids, which are set at the 50% probability level. Hydrogen atoms have been removed for clarity. The centroid of the C(1)–C(5) ring is highlighted (green).

**Table 10** The bond lengths (Å) and angles (°) of the coordinating atoms of  $[\text{Cp}^*\text{IrI}_2(d_6\text{-DMSO})]$ ; Cp\*(1) corresponds to the centroid of ring C(1)–C(5) (green, Figure 31).

Ir(1)-I(1)	2.692(5)	I(1)-Ir(1)-I(2)	92.61(17)
Ir(1)-I(2)	2.689(5)	I(1)-Ir(1)-S(1)	89.20(4)
Ir(1)-S(1)	2.284(16)	I(2)-Ir(1)-S(1)	89.26(4)
Ir(1)-Cp*(1)	1.828	I(1)-Ir(1)-Cp*(1)	123.93
		I(2)-Ir(1)-Cp*(1)	121.83
		S(1)-Ir(1)-Cp*(1)	129.30

The structure indicates that the ligand was displaced by a molecule of dimethylsulfoxide and both chloride ligands were exchanged for iodides. The  $^1\text{H}$  NMR spectrum of the original sample was collected again in  $d_4\text{-MeCN}$ ; as it was assumed the thiazolium iodide ligand would dissolve. As with the  $d_6\text{-DMSO}$  sample, the  $^1\text{H}$  NMR spectrum indicated the ligand **L.7** was no longer coordinated to the metal centre. In  $\text{CDCl}_3$ , in which the sample was surprisingly

soluble (displaying another advantage of a multifunctional catalyst as coordination to the metal improved the solubility of the polar thiazolium in organic solvents), the thiazolium C-2 proton was shifted down field; which suggested complexed ligand (Figure 32). A suitable orange plate-like crystal was obtained from chloroform; the structure was determined using x-ray crystallography and found to exist with an anionic iridate(III) counter-complex (**Scheme 85**). Both complexes display a distorted octahedral geometry about the metal centres (Figure 33).



**Scheme 85** The synthesis of iridium(III)–iridate(III) complex **C.7.1**.

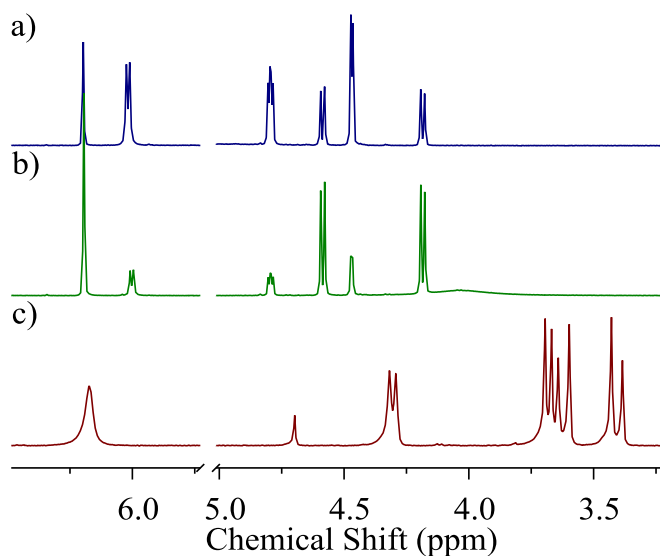


**Figure 32** Stacked  $^1\text{H}$  NMR spectra of thiazole-thiazolium complex **C.7.1** in different solvents; a)  $d_6$ -DMSO, b)  $d_4$ -MeCN, and c)  $\text{CDCl}_3$ .

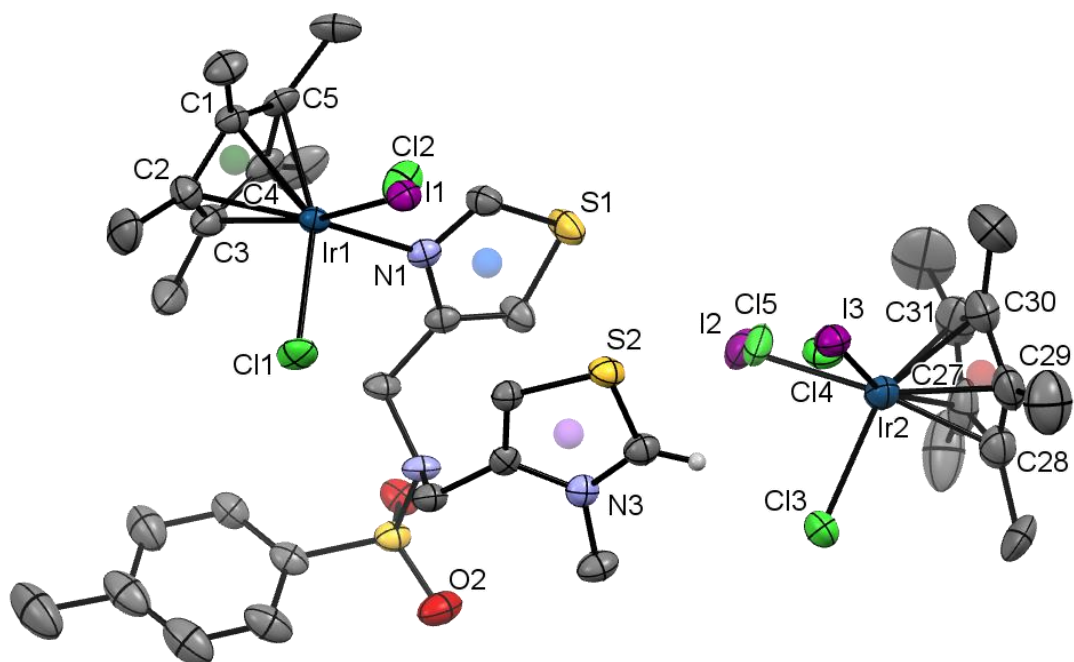


**Figure 33** The x-ray crystal structure of **C.7.1** with four molecules of  $\text{CDCl}_3$  in the asymmetric unit. The compound was modelled as a mixture of halides with ratios of  $\text{Cl}_{1.6}\text{I}_{0.4}$  (Ir1) and  $\text{Cl}_{1.95}\text{I}_{1.05}$  (Ir2). The distance between the centroids of thiazole (N1, S1, blue) and thiazolium (N3, S2, lilac) rings is 3.751 Å. Hydrogen atoms and solvent molecules have been removed for clarity.

**Table 11** The bond lengths (Å) and angles ( $^\circ$ ) of the coordinating atoms of complex **C.7**. Cp\*(1) and Cp\*(2) corresponds to the centroids of rings C(1)–C(5) (green) and C(27)–C(31) (red) respectively (Figure 33).

Ir(1)-Cl(1)	2.410(19)	Cl(1)-Ir(1)-Cl(2)	89.3(3)
Ir(1)-Cl(2)	2.420(8)	Cl(1)-Ir(1)-N(1)	93.10(17)
Ir(1)-N(1)	2.140(7)	Cl(2)-Ir(1)-N(1)	85.5(4)
Ir(1)-Cp*(1)	1.758	N(1)-Ir(1)-Cp*(1)	126.35
		Cl(1)-Ir(1)-Cp*(1)	124.93
		Cl(2)-Ir(1)-Cp*(1)	125.8
Ir(2)-Cl(3)	2.462(2)	Cl(3)-Ir(2)-Cl(4)	90.8(6)
Ir(2)-Cl(4)	2.417(9)	Cl(3)-Ir(2)-Cl(5)	88.7(4)
Ir(2)-Cl(5)	2.411(9)	Cl(4)-Ir(2)-Cl(5)	87.0(8)
Ir(2)-Cp*(2)	1.762	Cl(3)-Ir(2)-Cp*(2)	124.63
		Cl(4)-Ir(2)-Cp*(2)	125.10
		Cl(5)-Ir(2)-Cp*(2)	128.20

Iridate(III) counter-complexes have been previously reported in the literature.<sup>115-118</sup> The crystal structure of **C.7.1** shows that some halide mixing has occurred. Substitution of chloride ligands by iodide anions at iridium(III) is well known in the literature.<sup>119</sup> The orientation of the counter complex is directed at the proton of the C-2 position of the thiazolium ring; which could be explained by hydrogen bonding from the acidic proton to the halide ligands. The distance between the thiazole and thiazolium rings (3.751 Å) is within the constraints of face off-centred  $\pi$ - $\pi$  stacking limits (3.3–3.8 Å).<sup>120</sup>

A variable temperature <sup>1</sup>H NMR experiment of complex **C.7.1** from 213–323 K in CDCl<sub>3</sub> presents differently in three main temperature ranges. In the high temperature region (313–323 K) the thiazole and thiazolium signals (>8 ppm) appear sharp, and the Cp\* ligand appears as one peak (1.6 ppm). In the mid temperature region (263–303 K), the thiazole and thiazolium protons (>8 ppm) appear as broad signals, along with the aromatic, methyl and methylene protons. From 303 K to 263 K the Cp\* ligand splits into five broad peaks, corresponding to each of the five methyl groups, indicating the ring has become less disordered. The low temperature region (253–213 K) shows the sharp thiazole and thiazolium proton signals (>8 ppm) have split into two sets. In addition, the methyl and methylene signals (4–5 ppm) have split into more resolved peaks with more complicated multiplicities. Rotamers could be the cause of the extra sets of peaks which are interconverting more slowly at the low temperature. In addition, the halide ligand scrambling could be the cause for the extra species observed.

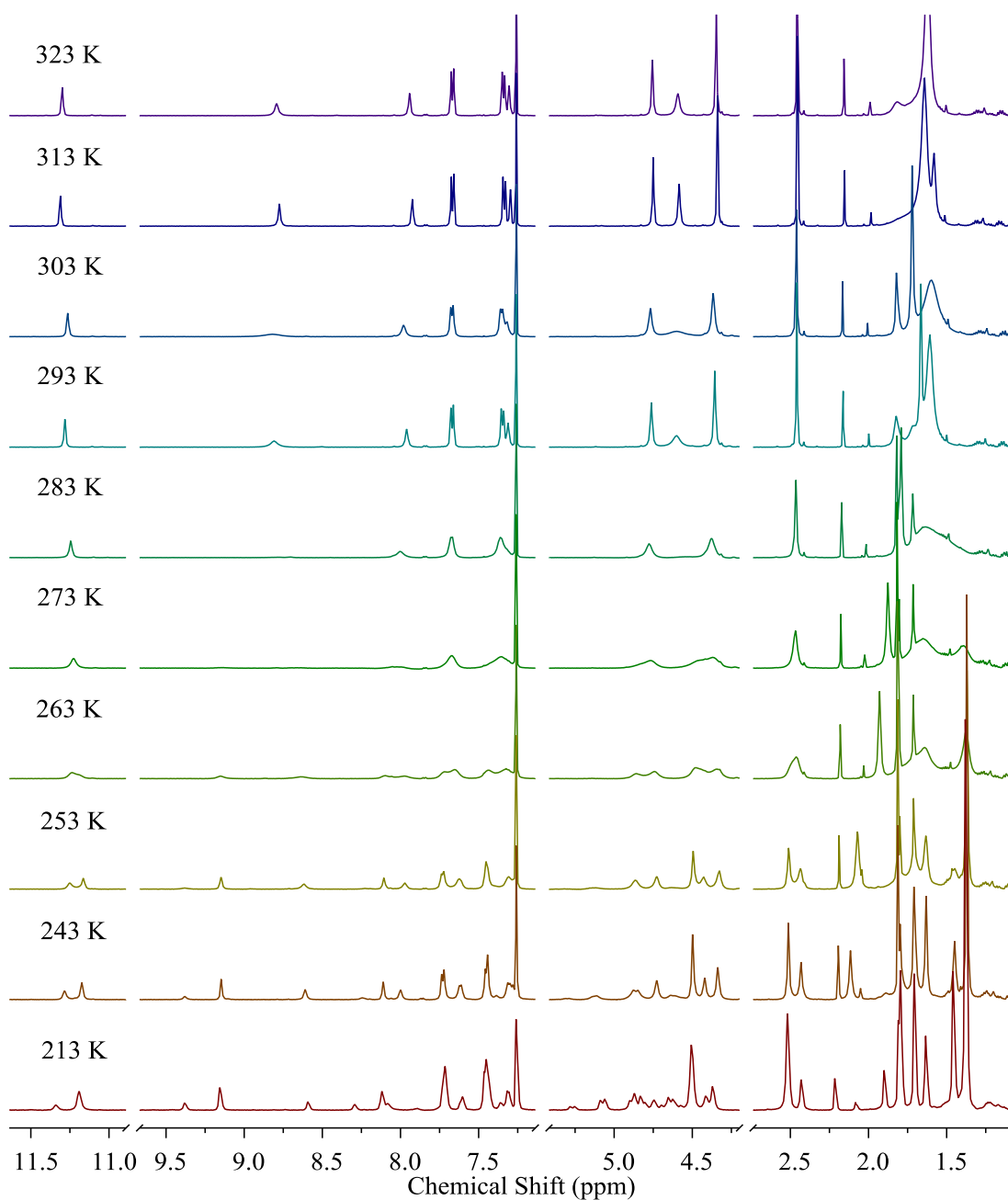
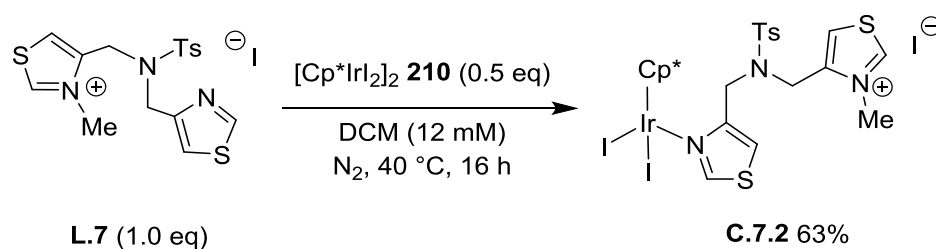


**Figure 34** Variable temperature  $^1\text{H}$  NMR experiment of thiazole-thiazolium iridium(III) complex **C.7.1** in  $\text{CDCl}_3$  from 213–323 K.

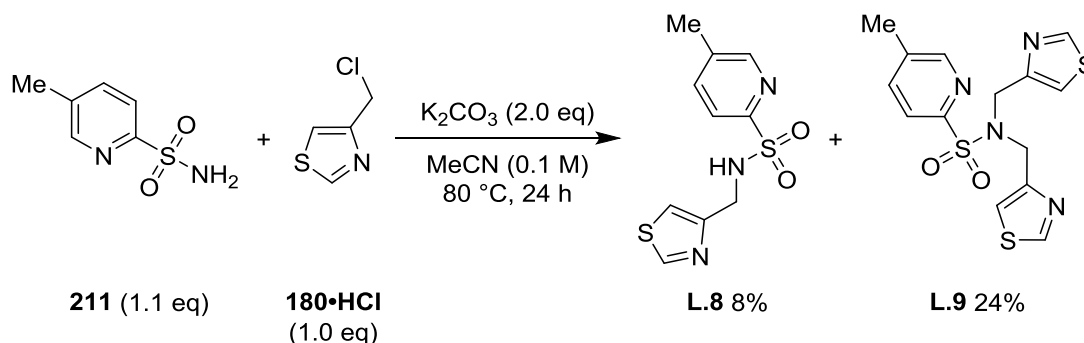
To avoid the halide mixing observed for complex **C.7.1**, analogous complex **C.7.2** was synthesised using the iridium(III) diiodide dimer **210** (Scheme 86).



**Scheme 86** The synthesis of thiazole-thiazolium iridium(III) complex **C.7.2**.

### 2.3.9. Thiazole Tethered Pyridine Iridium(III) Complexes **C.8** and **C.9**

To increase the number of donor atoms in the ligand design, a pyridine sidechain was incorporated into the ligand structure. This will allow both thiazole rings to be methylated whilst maintaining a coordination site to the metal. Pyridine ligands on iridium are well known in the literature.<sup>121</sup> The *mono*- and *bis*- thiazole ligands **L.8** and **L.9** were prepared with 5-methyl-2-pyridinesulfonamide **211** and thiazole **180·HCl** in the same reaction and then separated using column chromatography (Scheme 87). A suitable crystal was obtained for *mono*-thiazole ligand **L.8** and the structure was determined by x-ray crystallography (Figure 35).



**Scheme 87** The synthesis of *mono*-thiazole-pyridine and *bis*-thiazole-pyridine ligands **L.8** and **L.9** respectively.



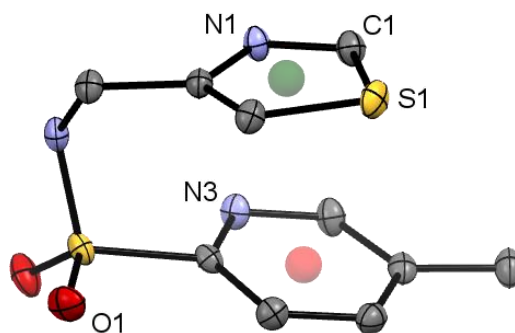
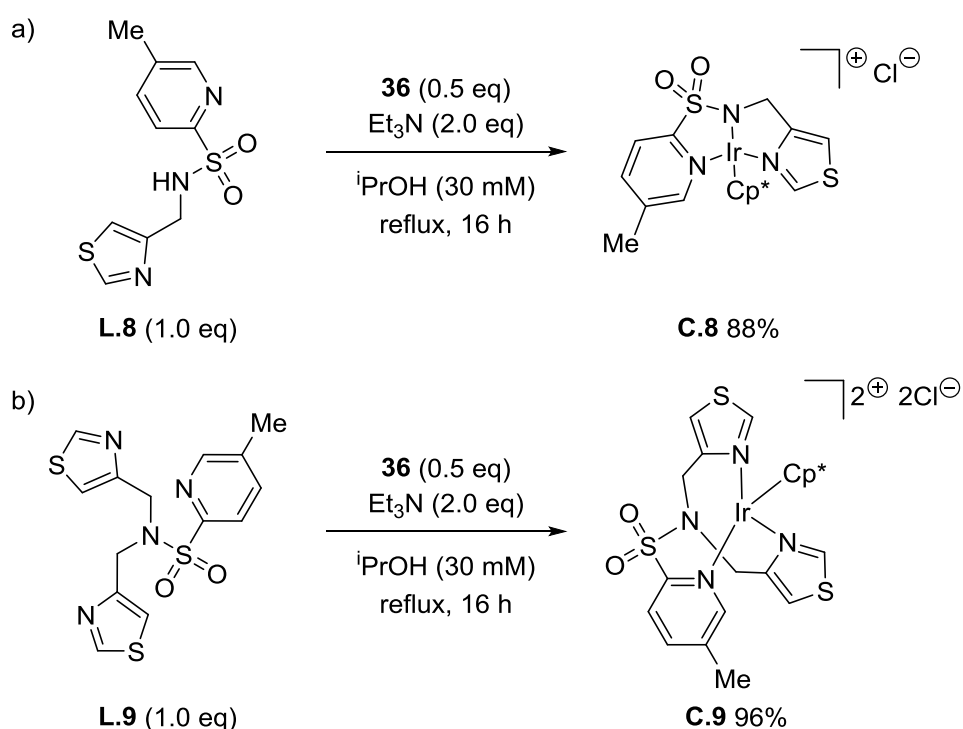


**Figure 35** The x-ray crystal structure of *mono*-thiazole-pyridine ligand **L.8** with non-hydrogen atoms displayed as displacement ellipsoids, which are set at the 50% probability level. Hydrogen atoms have been removed for clarity. The distance between the centroids of thiazole (green) and pyridine (red) rings is 3.589 Å.

The distance between ring centroids of the thiazole and pyridine rings in ligand **L.8** (3.589 Å) is within the constraints of face off-centred  $\pi$ - $\pi$  stacking limits (3.3-3.8 Å).<sup>120</sup> The shape of the ligand could help to define the shape of the metal complex, as all three *N*-donor atoms are directed towards the same point; suggesting the ligand will coordinate in a tridentate fashion. Both ligands **L.8** and **L.9** were complexed to iridium(III) dimer **36** (Scheme 88).



**Scheme 88** Synthesis of thiazole-pyridine complexes; a) **C.8** and b) **C.9**

Analysis of both complexes **C.8** and **C.9** using  $^1\text{H}$  NMR spectroscopy indicates that the ligands are bound to the metal as at least bidentate ligands. However, geometry optimised UFF molecular models of both complexes show that both ligands are capable of binding as tridentate ligands (Figure 36).

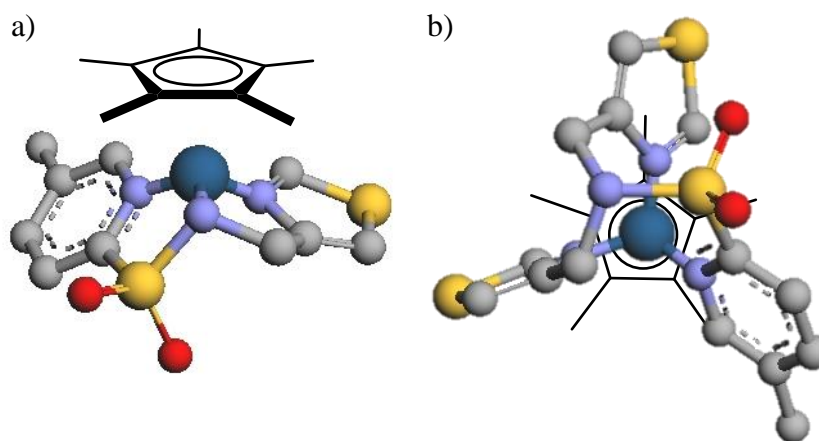
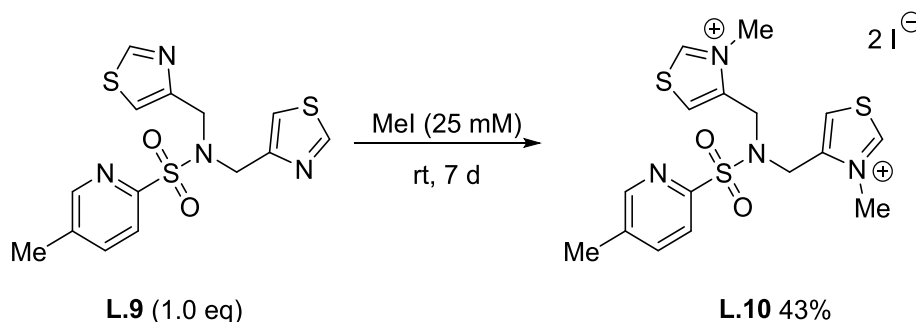
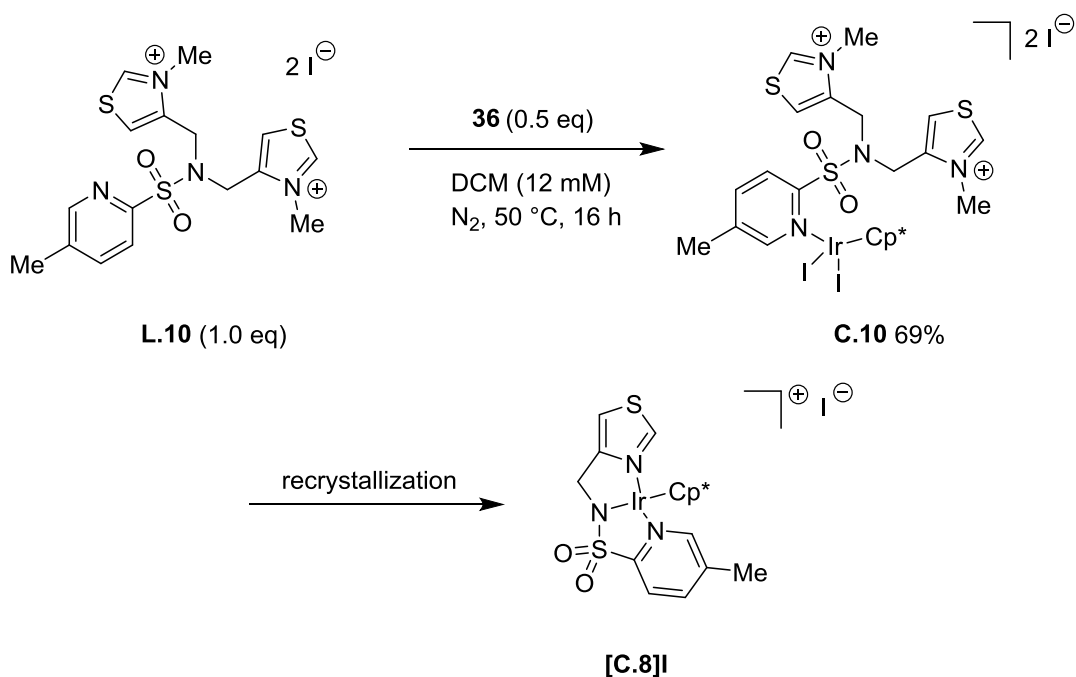


**Figure 36** Molecular models of pyridine-thiazole complexes using a UFF model; a) **C.8** and b) **C.9**



**Scheme 89** The synthesis of *bis*-thiazolium-pyridine ligand **L.10**.

The *bis*-thiazole **L.9** was alkylated with iodomethane to give *bis*-thiazolium **L.10** (Scheme 89). The remaining yield was unreacted starting material. The  $^1\text{H}$  NMR spectrum shows the product as the *bis*-thiazolium ligand; which was surprising as *bis*-thiazole ligand **L.6** only alkylated once under the same conditions. With only a single alkylation, **L.10** would have had two donor atoms to coordinate to the metal centre. The ligand **L.10** can only bind as a monodentate ligand through the pyridine side-chain; however, two thiazole catalysts could improve the rate of the organocatalyzed benzoin condensation reaction. The *bis*-thiazole-pyridine ligand **L.10** was complexed to iridium(III) dimer **36** to give complex **C.10** (Scheme 90).



**Scheme 90** The synthesis of *bis*-thiazolium-pyridine iridium(III) complex **C.10** and the decomposition to **C.8** with an iodide counterion during recrystallization.

The complex was recrystallized from dichloromethane and petrol to produce a suitable crystal for x-ray crystallography (Figure 37); however, the structure was not the desired *bis*-thiazolium complex **C.10**, but the structure expected for *mono*-thiazole complex **C.8** (Scheme 88, a). Both complexes display a distorted octahedral geometry about the metal centre. There are two possibilities for the structure of the complex: either the batch of **L.10** used was impure and the single crystal was recrystallized from the impurity, or a thiazolium molecule and a methyl group were eliminated from the complex via  $\text{S}_{\text{N}}2$  reactions with the iodide ions in solution. During the attempted synthesis of thiazolium **209** from **L.1** (Scheme 83), the eliminated iodomethyl-thiazolium **208** was isolated in 23% yield, which supports the thiazolium elimination to make the crystal structure obtained for **C.10**. The NMR spectra for **C.10** suggested the complex had decomposed to a mixture of other species.

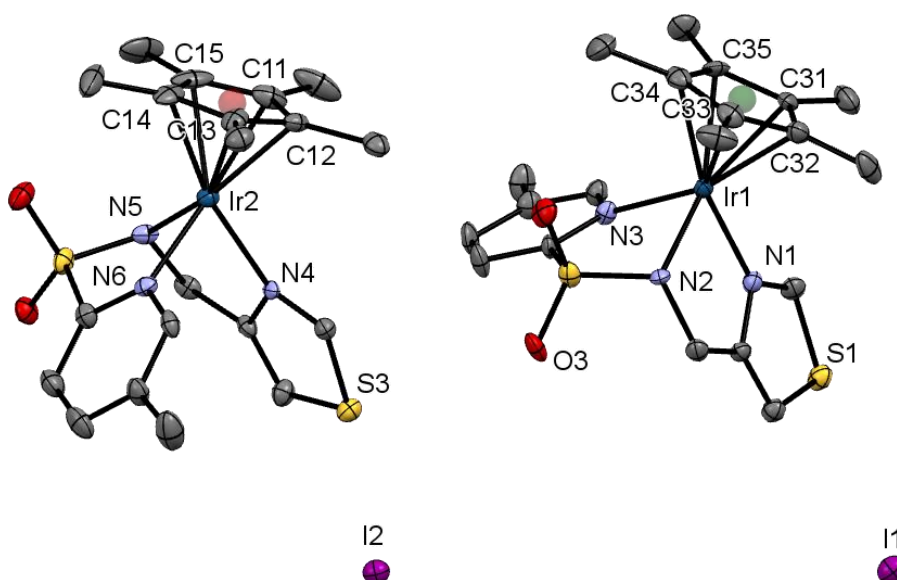


**Figure 37** The x-ray crystal structure of **[C.8]I** with two enantiomers of the complex (***R***<sub>ir</sub>)-**C.8** (Ir1) and (***S***<sub>ir</sub>)-**C.8** (Ir2), two iodide counter ions, and two molecules of DCM in the asymmetric unit; with non-hydrogen atoms displayed as displacement ellipsoids, which are set at the 50% probability level. Hydrogen atoms and solvent molecules have been removed for clarity. The centroids of the C(11)-C(15) and C(31)-C(35) rings are highlighted red and green respectively.

**Table 12** The bond lengths (Å) and angles (°) of the coordinating atoms of complex **C.8**. Cp\*(1) and Cp\*(2) corresponds to the centroids of rings C(31)-C(35) (green) and C(11)-C(15) (red) respectively (Figure 37).

Ir(1)-N(1)	2.088(7)	N(1)-Ir(1)-N(2)	78.3(3)
Ir(1)-N(2)	2.089(7)	N(1)-Ir(1)-N(3)	86.3(3)
Ir(1)-N(3)	2.120(7)	N(2)-Ir(1)-N(3)	80.8(3)
Ir(1)-Cp*(1)	1.793	N(1)-Ir(1)-Cp*(1)	131.99
		N(2)-Ir(1)-Cp*(1)	130.11
		N(3)-Ir(1)-Cp*(1)	130.16
Ir(2)-N(4)	2.080(6)	N(4)-Ir(2)-N(5)	78.8(3)
Ir(2)-N(5)	2.115(7)	N(4)-Ir(2)-N(6)	79.9(3)
Ir(2)-N(6)	2.145(7)	N(5)-Ir(2)-N(6)	81.4(3)
Ir(2)-Cp*(2)	1.787	N(4)-Ir(2)-Cp*(2)	133.32
		N(5)-Ir(2)-Cp*(2)	128.64
		N(6)-Ir(2)-Cp*(2)	134.03

### 2.3.10. Rigid Tether for Thiazolium Iridium(III) Complexes

An alternative ligand design is to use a rigid tether to the organocatalyst to lock the carbene away from the metal centre to prevent coordination of the thiazolium to the metal centre (Figure 38). However, the issue of intermolecular carbene-iridium(III) coordination is still possible.

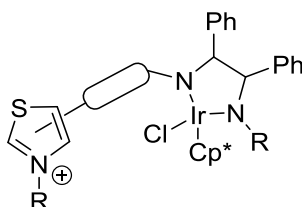
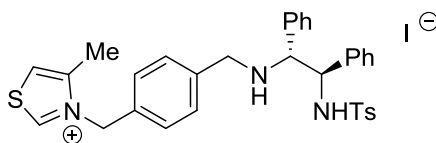


**Figure 38** A new complex design that has a rigid tether to hold the thiazolium component away from the metal centre to avoid carbene coordination.

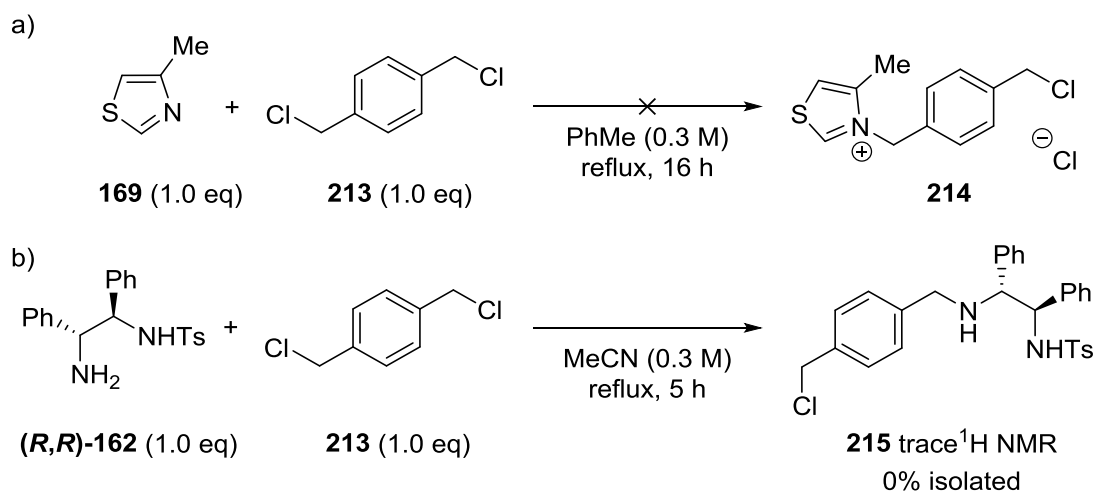
Based on the benzyl control ligand **164**, a thiazole ligand with a rigid benzene tether **212** was designed (Figure 39).



**212**

**Figure 39** Design of a thiazole ligand **212** with a benzene tether to prevent intramolecular carbene-metal binding.

A straight forward route was attempted, from  $\alpha,\alpha'$ -dichloro-*p*-xylene **213** and either thiazole **169** or (*R,R*)-TsDPEN **162** (Scheme 91).



**Scheme 91** Attempted synthesis of rigid benzene-tether components; a) **214** and b) **215**.

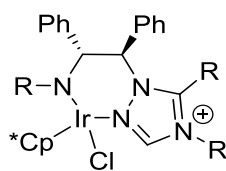
The thiazolium **214** was not identified in the crude reaction mixture. Amine **215** was identified using <sup>1</sup>H NMR spectroscopy of the crude mixture as a trace product with many other side-products; however, the product was unable to be isolated. The focus of the project was shifted away from rigid covalent tethers; as intermolecular thiazolylidene-metal bond formation would be more prevalent.

## 2.4. Triazole Ligands

Triazolium organocatalysts are more acidic than the analogous thiazolium organocatalysts ( $pK_a \sim 16$ , see Chapter 1.10).<sup>73</sup> Therefore, to increase the activity of the organocatalyst, novel triazole iridium(III) complexes have been synthesised.

### 2.4.1. Triazol-1-yl TsDPEN Ligands

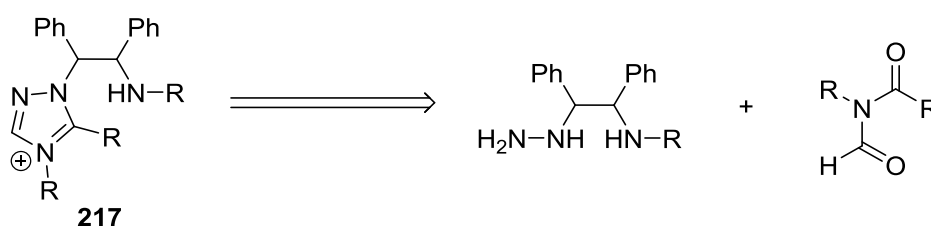
An iridium complex **216** was designed with the triazolium ligand bound in a 6-membered iridacycle to prevent carbene binding to the metal (Figure 40).



**216**

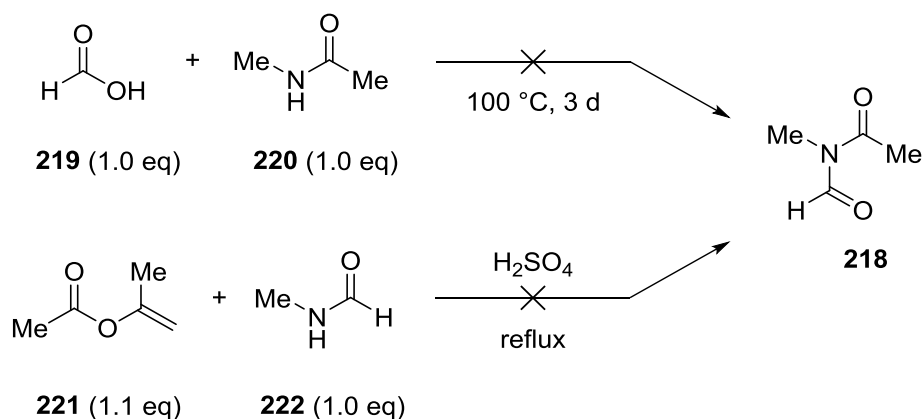
**Figure 40** The design of a triazolium-iridium(III) multifunctional catalyst **216**.

The design only allows one donor atom from the ring to coordinate to the metal centre and prevents a carbene forming at the 5-position. A retrosynthetic route to the ligand was devised and the synthesis attempted (Scheme 92).



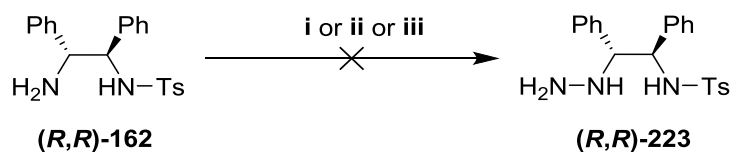
**Scheme 92** Retrosynthesis of the target triazolium ligand **217**.

The imide **218** was not commercially available, therefore the synthesis was attempted via two routes; a neat formic acid **219** condensation reaction with *N*-methylacetamide **220** that was reported as a decomposition product with palladium and DMF,<sup>122</sup> and *iso*-propenyl acetate **221** acetylation reaction with *N*-methylformamide **222** that was reported in a patent (Scheme 93).<sup>123</sup>



**Scheme 93** The attempted synthetic routes to imide **218**.

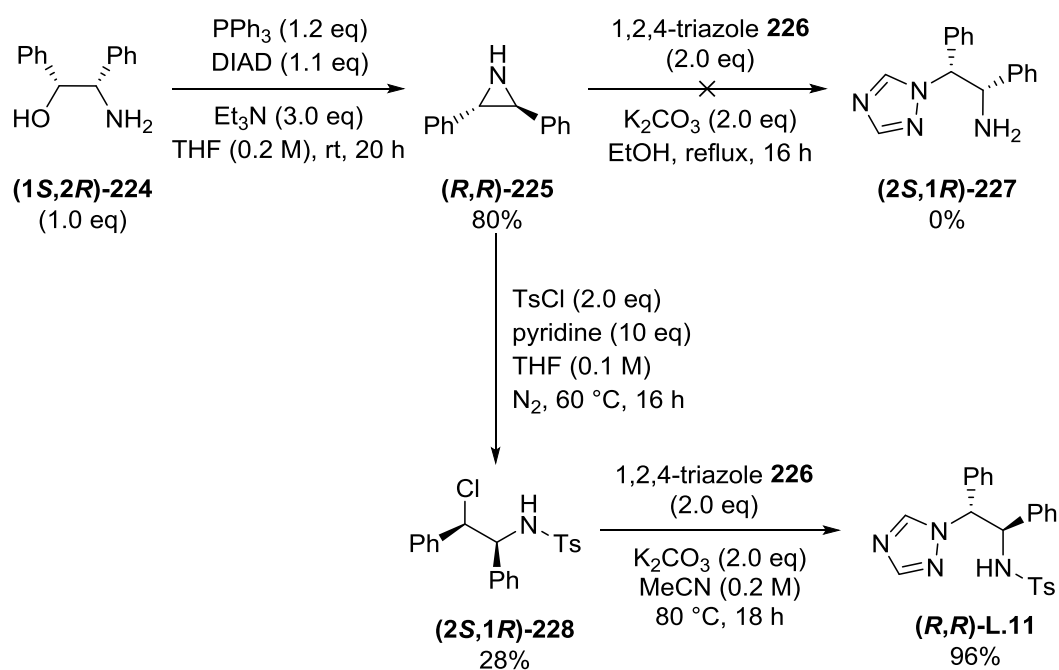
The synthesis of hydrazine **223** was also attempted based on three reported routes to similar compounds; however, all three routes were unsuccessful (Scheme 94).<sup>124-126</sup>



**Scheme 94** Attempted synthesis of hydrazine (*R,R*)-**223**. Conditions: i) 1. (*R,R*)-**162** (1.0 eq), KOH (0.67 eq), H<sub>2</sub>O, 2. H<sub>2</sub>NSO<sub>4</sub>H, H<sub>2</sub>O; ii) KOH (10 eq), H<sub>2</sub>NSO<sub>4</sub>H (2.0 eq), DMF, 50 °C, N<sub>2</sub>, 16 h; iii) KO<sup>t</sup>Bu (15 eq), H<sub>2</sub>NSO<sub>4</sub>H (2.0 eq), MeOH, 0 °C, N<sub>2</sub>, 5 h.

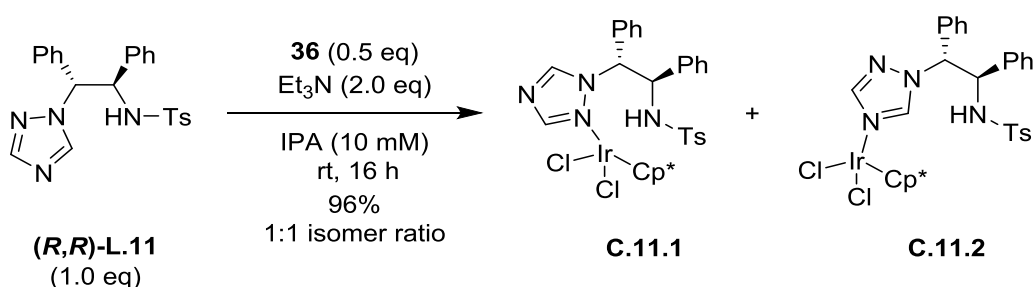
As the initial route was unsuccessful, an alternative route to a triazolium complex was undertaken. Starting from the commercially available aminoethanol (1*S*,2*R*)-**224**, the aziridine **225** was prepared via an intramolecular Mitsunobu reaction. The ring opening reaction with 1,2,4-triazole **226** with potassium carbonate to make triazole **227** was unsuccessful and only starting material was recovered. Instead, the aziridine **225** was made more reactive by tosylating the *N*-atom. The product of the reaction was the ring opened 1-chloro-2-sulfonamide **228**. This was useful, because not only has the tosyl sidechain added to the molecule, the chloride leaving group was now more reactive, making the S<sub>N</sub>2 reaction with **226** possible (Scheme 95).





**Scheme 95** The synthetic route towards triazole (*R,R*)-**L.11** via aziridine (*R,R*)-**225** and 1-chloro-2-sulfonamide (*2S,1R*)-**228**.

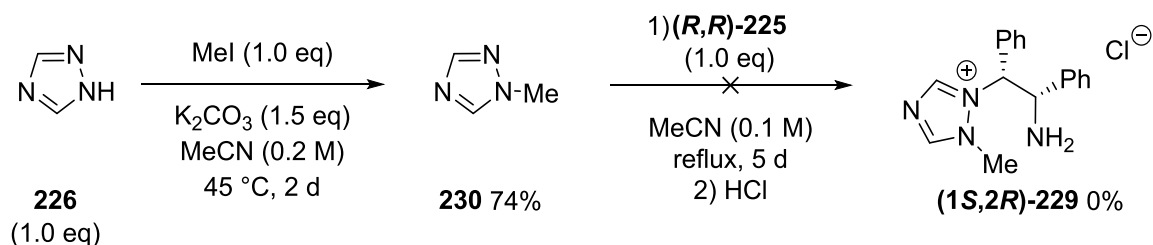
The triazole ligand (*R,R*)-**L.11** was coordinated to the iridium(III) dimer **36** (Scheme 96).  $^1\text{H}$  NMR spectroscopic analysis of the complex shows two species, with a ratio of 1:1, that both have inequivalent triazole proton signals and both have the sulfonamide proton remaining. This suggests the two complex structures **C.11.1** and **C.11.2**. Both complexes have the ligand bound in a monodentate fashion, as the sulfonamide proton signal is still present in the spectrum. This is different to the thiazole complexes that are bound through the sulfonamide *N*-atom under the same conditions.



**Scheme 96** The synthesis of triazole complexes **C.11.1** and **C.11.2**.

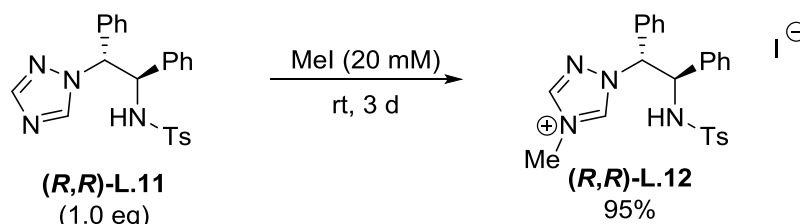
## 2.4.2. Triazol-1-yl-2-ium Ligands

The synthesis of the triazolium ligand (1*S*,2*R*)-**229** was attempted from the ring opening reaction of aziridine (1*S*,2*R*)-**225** with 1-methyl-1,2,4-triazole **230**; which was prepared from **226** and iodomethane with base (Scheme 97).



**Scheme 97** The attempted synthetic route to triazolium chloride (1*S*,2*R*)-**229**.

The reaction did not proceed to the product after five days at reflux, therefore the 2-methyl-1,2,4-triazolium iodide ligand **L.12** was prepared from the alkylation of triazole ligand **L.11** with iodomethane (Scheme 98).



**Scheme 98** The synthesis of triazolium iodide ligand **L.12**.

The position of the positive charge of the triazolium can sit on either alkylated nitrogen atom of the ring (Figure 41). The triazolium ligand **L.12** was complexed to iridium(III) dimer **210** to produce triazolylidene iridium(III) complex **C.12** (Scheme 99).

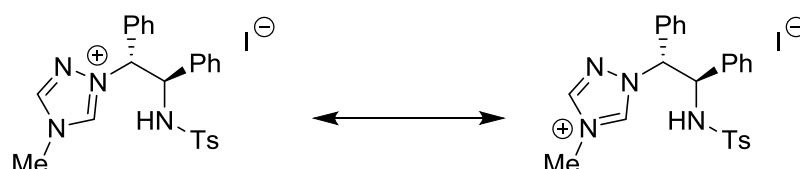
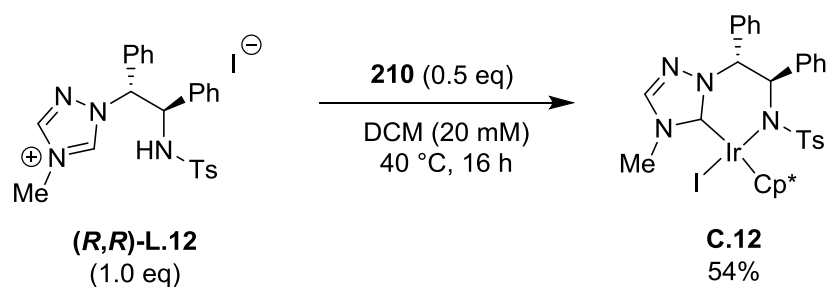


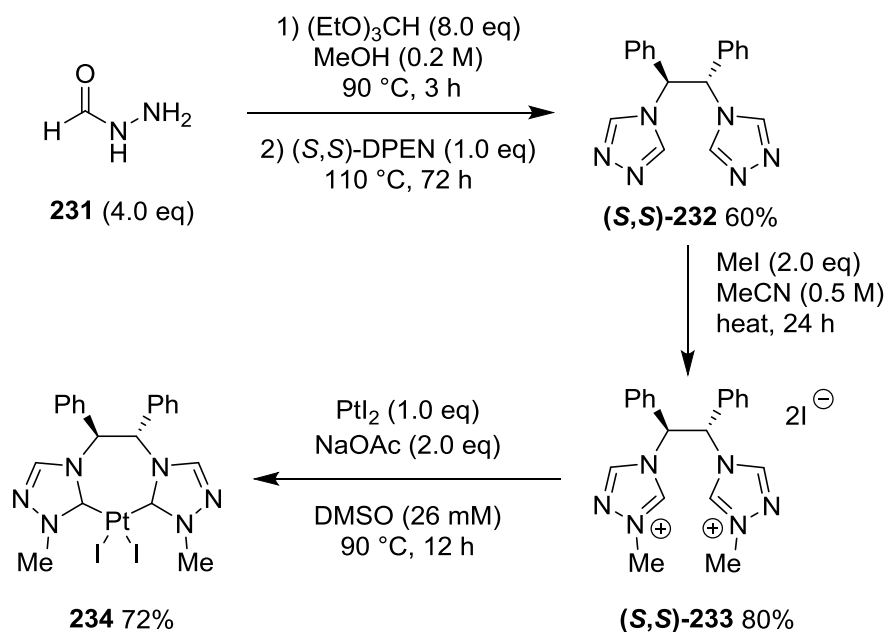
**Figure 41** The resonance structures of triazolium ligand **L.12** showing the two possible positions of the positive charge.



**Scheme 99** The synthesis of triazolylidene iodide complex **C.12**.

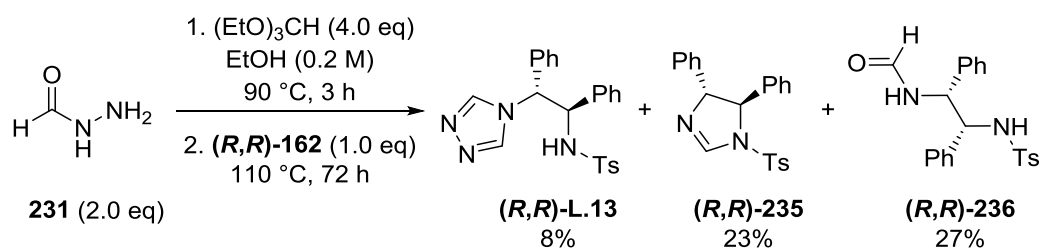
### 2.4.3. Triazol-4-yl TsDPEN ligands

Herrmann and Kühn have developed a *bis*-triazolium ligand system for rhodium and platinum complexes as catalysts for alkene hydrogenation and hydrosilylation reactions respectively (Scheme 100).<sup>127-129</sup>



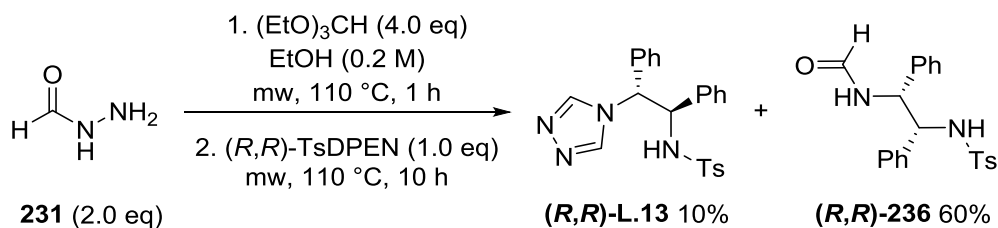
**Scheme 100** The synthetic route to *bis*-triazole ligand  $(R,R)\text{-232}$ , *bis*-triazolium  $(R,R)\text{-233}$  and *bis*-triazolylidene platinum complex **234**.<sup>129</sup>

The *bis*-triazolylidene complexes were designed to coordinate to the metal as bidentate ligands; however, as triazoliums are well known organocatalysts for the benzoin reaction, the carbene position needs to remain unsubstituted for the organocatalysis to occur. A *mono*-triazole analogue of Herrmann and Kühn's ligand **L.13** was synthesised from  $(R,R)\text{-162}$ , formic hydrazide **231** and triethyl orthoformate (Scheme 101).



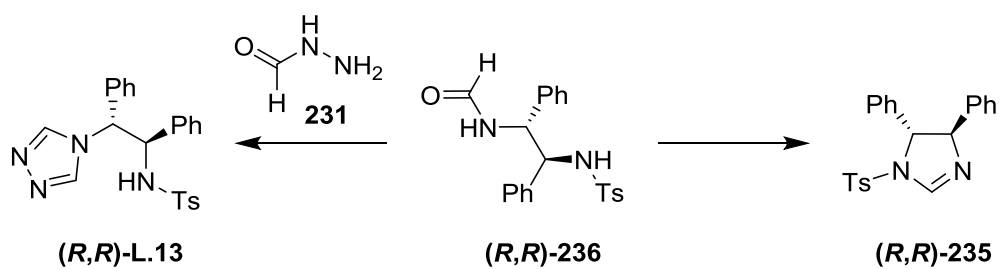
**Scheme 101** The synthesis of triazole ligand  $(R,R)$ -L.13 with major side products imidazoline  $(R,R)$ -235 and  $N$ -formyl-TsDPEN  $(R,R)$ -236.

The reaction was carried out in a sealed pressure tube as was used in the reported process. The reaction was lower yielding than expected and produced two major side products; imidazoline  $(R,R)$ -235 and  $N$ -formyl-TsDPEN  $(R,R)$ -236. The reported yield for the *bis*-triazole compound **232** was 60%, but side products of the reaction were not mentioned. The compounds  $(R,R)$ -235 and  $(R,R)$ -236 were separated using column chromatography, and the remaining pink crude oil was shown to contain the desired product  $(R,R)$ -L.13. Recrystallisation of the crude oil from *iso*-propanol yielded the pure product  $(R,R)$ -L.13 as colourless crystals. In an attempt to improve the reaction conditions and yield of the product, the reaction was repeated in a microwave reactor; reducing the reaction time from 72 to 11 hours and improving the health and safety risks associated with a sealed high temperature reaction (Scheme 102).



**Scheme 102** The synthetic route  $(R,R)$ -L.13 using a microwave reactor.

In this process, the yield of desired product **L.13** remained low, however the formation of  $(R,R)$ -236 improved (27% to 60%) and there was no formation of imidazoline  $(R,R)$ -235. Formation of both  $(R,R)$ -L.13 and  $(R,R)$ -235 can be visualised from  $(R,R)$ -236; via reaction with  $(R,R)$ -231, and intramolecular condensation reactions respectively (Scheme 103).



**Scheme 103** Possible routes to  $(R,R)$ -L.13 and imidazoline  $(R,R)$ -235 from  $(R,R)$ -236.

To further improve the yield and selectivity for the triazole ligand  $(R,R)$ -L.13, increased equivalents of  $(R,R)$ -231 could be used; however, this reaction was not developed further. The molecular structure of  $(R,R)$ -L.13 was determined using x-ray crystallography (Figure 42).

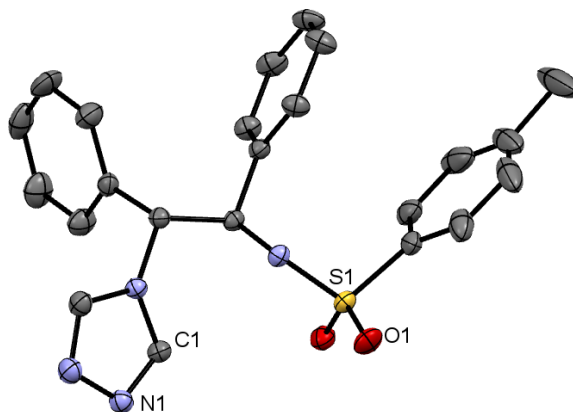
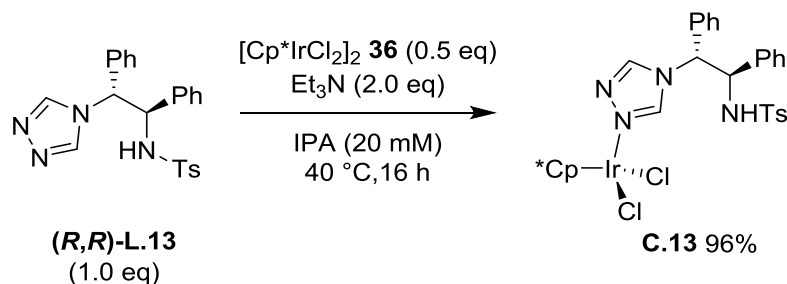


**Figure 42** The x-ray crystal structure of  $(R,R)$ -L.13 with non-hydrogen atoms displayed as displacement ellipsoids, which are set at the 50% probability level. Hydrogen atoms have been removed for clarity.

The triazole ligand (*R,R*)-**L.13** was complexed to the iridium(III) dimer **36** (Scheme 104).



**Scheme 104** The synthesis of triazole iridium(III) complex **C.13**.

The  $^1\text{H}$  NMR spectrum of complex **C.13** shows that two species are present, with a ratio of 1.2:1.0. For both species, the ligand is bound to the metal centre as a monodentate ligand (analogous to **C.11**) through a triazole *N*-donor atom, because the sulfonamide proton signal is still present in the  $^1\text{H}$  NMR spectrum (Figure 43). The two sets of peaks have proton signals that have inequivalent triazole protons. As the triazole is symmetrical, only a single monodentate species should be possible with inequivalent signals; suggesting the ligand has bound in a different way to the metal centre. Possibilities for the second species (Figure 44) could be the ligand coordinated to two metal centres (a), or two ligands bound to a single metal centre (b); however, the integral for the  $\text{Cp}^*$  signal does not allow for these structures. Another possibility could be the neutral (c) and ionic complexes (d). Rotamers could also be the cause for generating two different species with different inequivalent triazole protons (e and f).

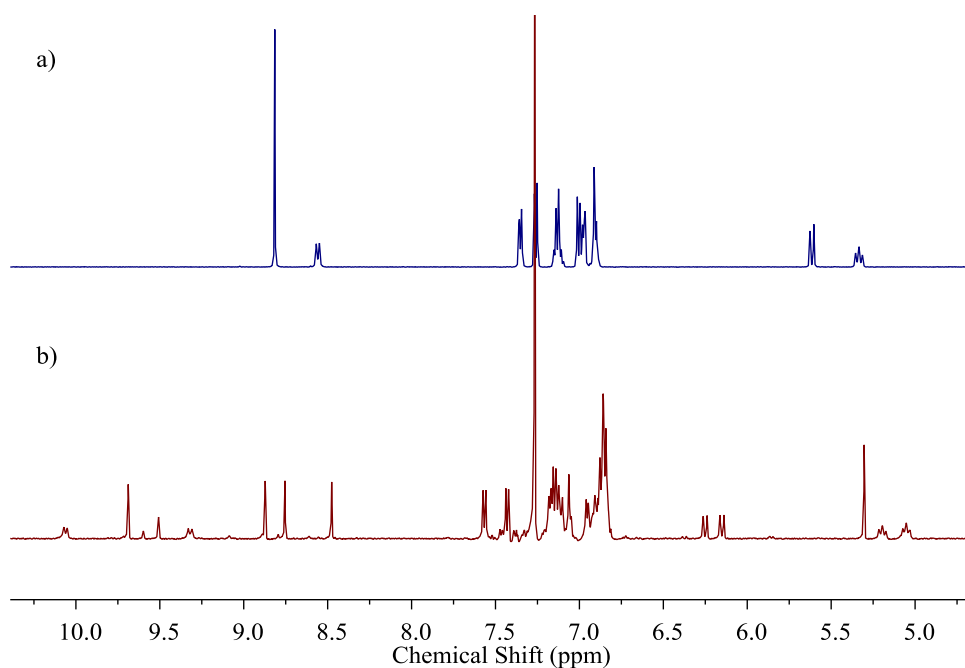


**Figure 43** Stacked  $^1\text{H}$  NMR spectra; a) triazole (*R,R*)-**L.13**, and b) triazole complex **C.13**.

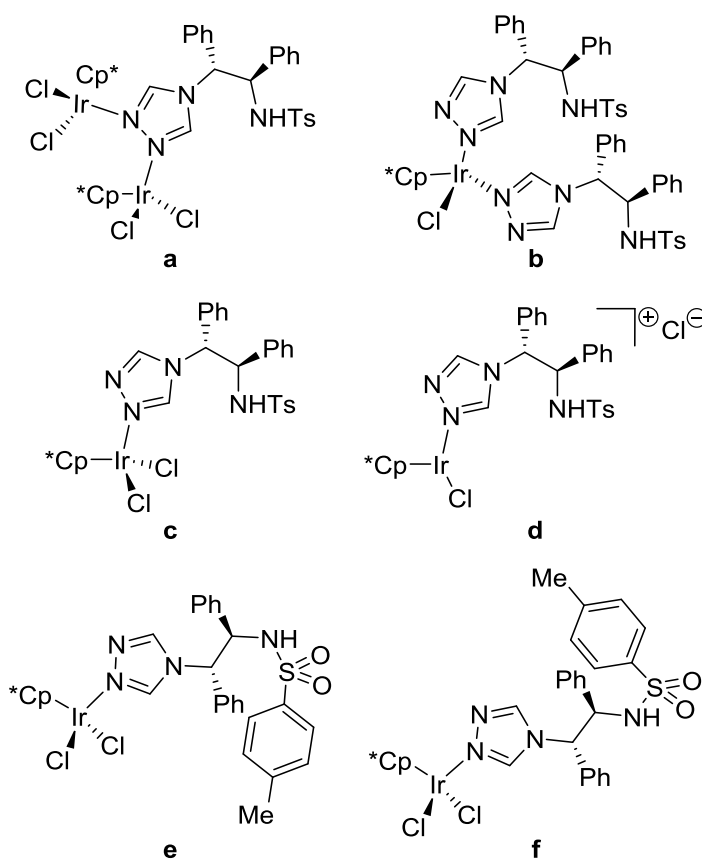
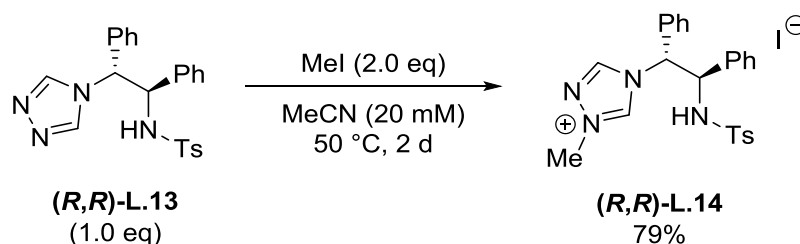


**Figure 44** Possible monodentate structures of **C.13** that would give different sets of inequivalent triazole proton signals in the  $^1\text{H}$  NMR spectrum.

It is surprising neither triazole ligand (*R,R*)-**L.11** or (*R,R*)-**L.13** coordinate as bidentate ligands to the metal centre under the same conditions that were used for complexation of the thiazole ligands. More forcing conditions could form the bidentate complex as a single species.

#### 2.4.4. Triazol-4-yl-1-ium Ligands

The triazole ligand (*R,R*)-**L.13** was alkylated with iodomethane to produce the 1-methyl-1,2,4-triazol-4-yl-1-ium iodide ligand (*R,R*)-**L.14** (Scheme 105).



**Scheme 105** The synthesis of 1-methyl-1,2,4-triazol-4-yl-1-ium iodide ligand (*R,R*)-**L.14**.

As with ligand (*R,R*)-**L.12** (Figure 41), the position of the positive charge of the triazolium can sit on either alkylated nitrogen of the ring (Figure 45).

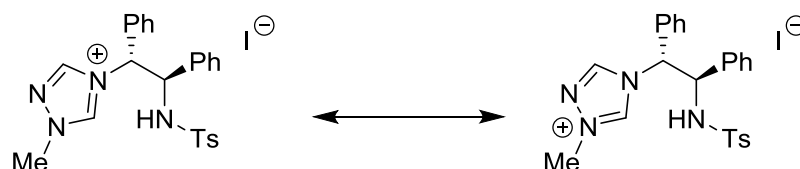
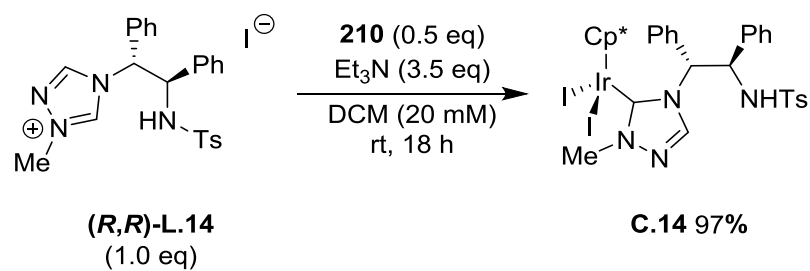


**Figure 45** The resonance structures of triazolium ligand (*R,R*)-**L.14** showing the two positions of the positive charge.

The  $^1\text{H}$  NMR spectra of (*R,R*)-**L.13** and (*R,R*)-**L.14** show the effect that alkylation has on the chemical environment of the ring protons; both shifting downfield (Figure 46). The triazolium iodide (*R,R*)-**L.14** was complexed to iridium(III) dimer **210** to give triazolylidene iridium(III) complex **C.14** (Scheme 106).





**Scheme 106** The synthesis of triazolylidene iridium(III) complex **C.14**.

The  $^1\text{H}$  NMR spectra of ligand  $(R,R)\text{-L.14}$  and complex **C.14** (Figure 46) suggests that the ligand is bound through the carbene; there is only one triazole C-H signal (at 8.6 ppm, spectrum b). Interestingly, the C-H of the DPEN backbone which is bound to the triazole *N*-atom has shifted downfield by 1.6 ppm compared to the ligand  $(R,R)\text{-L.13}$  once the carbene bond to the metal centre has been formed.

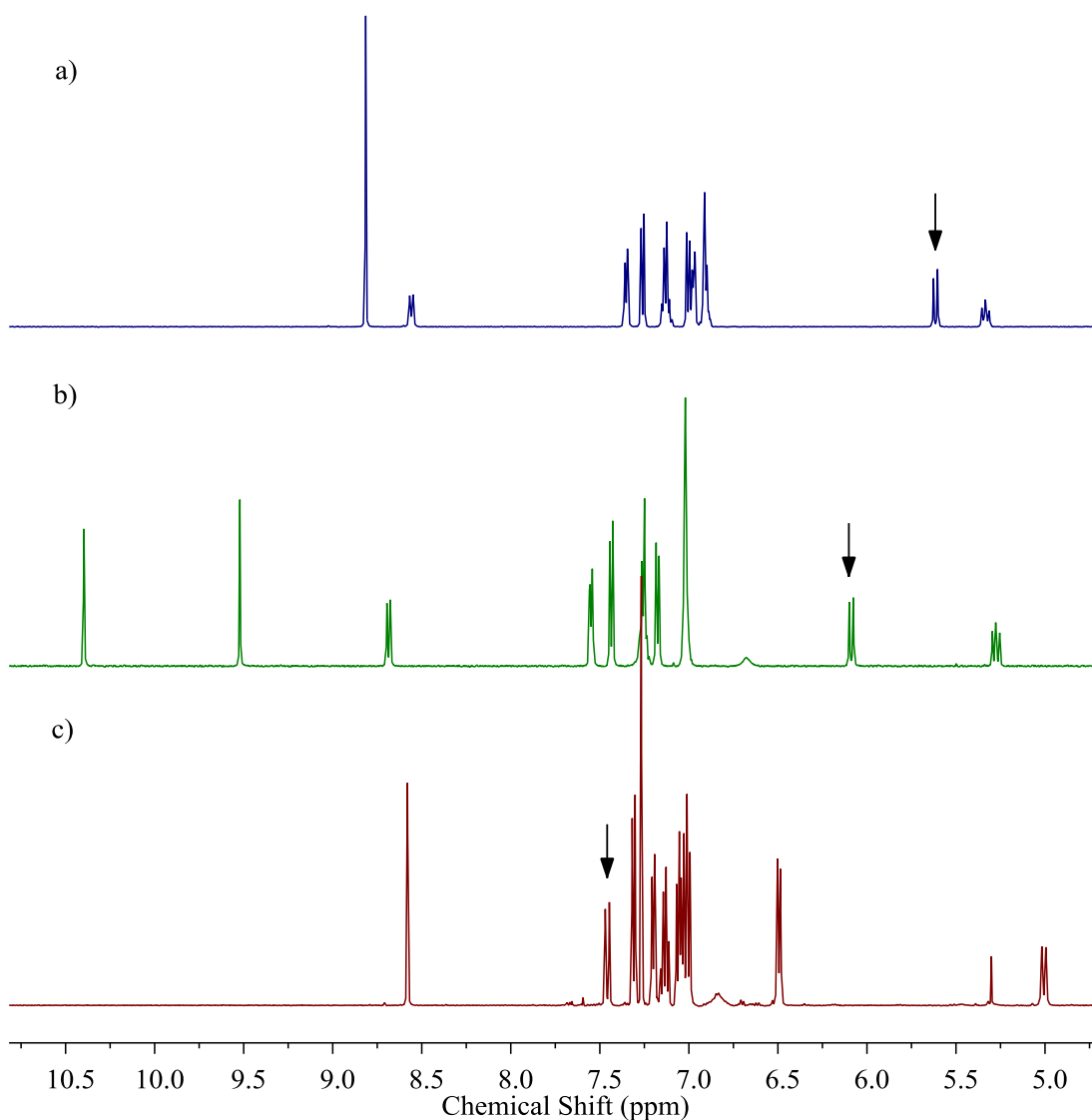


**Figure 46** Stacked  $^1\text{H}$  NMR spectra; a) triazole (*R,R*)-**L.13**, b) triazolium iodide (*R,R*)-**L.14**, and c) triazolylidene complex **C.14**, with the backbone C-H signals indicated with arrows.

A suitable crystal was obtained for the carbene complex **C.14** and the structure was determined by x-ray crystallography (Figure 47). The complex displays a distorted octahedral geometry about the metal centre. The ligand is bound through the carbene only and not through the sulfonamide *N*-donor. It is surprising that the triazolium has been deprotonated under the reaction conditions, yet the sulfonamide proton remains. As with **C.13**, more forcing conditions could generate the 6-membered iridacycle.

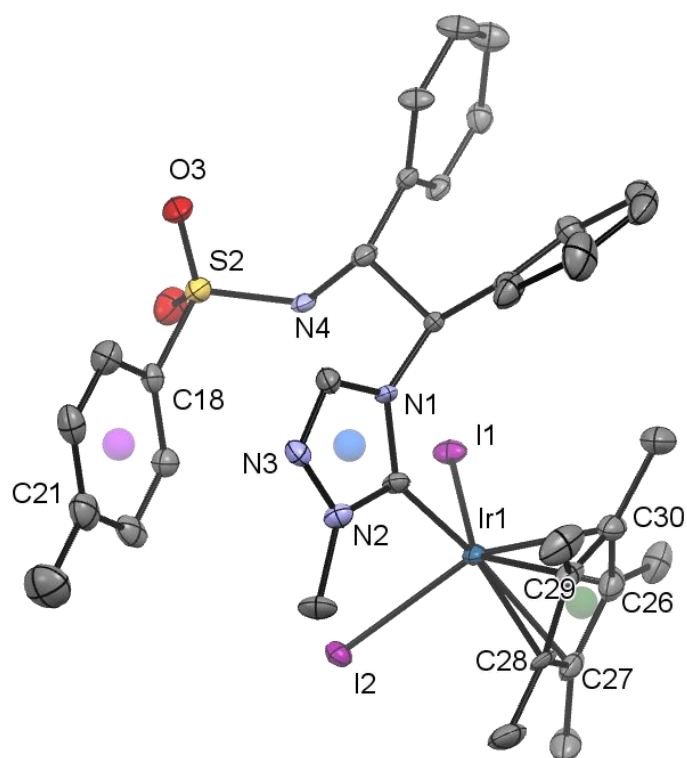


**Figure 47** The x-ray crystal structure of complex **C.14**, with two molecules of dichloromethane and water in the asymmetric unit. Non-hydrogen atoms displayed as displacement ellipsoids, which are set at the 50% probability level. Hydrogen atoms and solvent molecules have been removed for clarity. The centroid of the Cp\* ring is highlighted (C26-C30, green). The distance between the centroids of triazole (C1-N3, blue) and tosyl (C18-C23, red) rings is 3.694 Å.

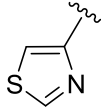
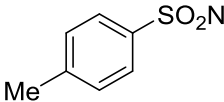
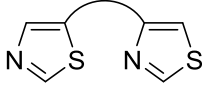
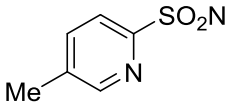
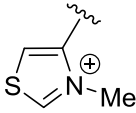
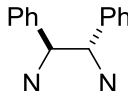
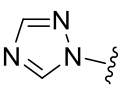
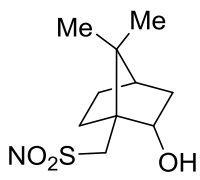
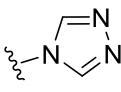
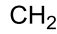
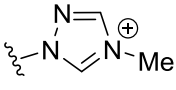
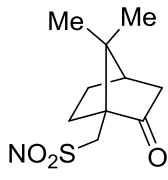
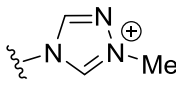
**Table 13** The bond lengths (Å) and angles (°) of the coordinating atoms of complex **C.14**; Cp\*(1) corresponds to the centroid of ring C(26)-C(30) (green, Figure 47).

Ir(1)-I(1)	2.7275(12)	I(1)-Ir(1)-I(2)	85.02(4)
Ir(1)-I(2)	2.7378(12)	I(1)-Ir(1)-C(1)	96.2(4)
Ir(1)-C(1)	2.042(14)	I(2)-Ir(1)-C(1)	92.2(4)
Ir(1)-Cp*(1)	1.837	I(1)-Ir(1)-Cp*(1)	123.07
		I(2)-Ir(1)-Cp*(1)	122.38
		C(1)-Ir(1)-Cp*(1)	126.10

## 2.5. Summary

Chapter 2 has covered the design considerations for a multifunctional catalyst to transform primary alcohols into 1,2-diols through three sequential reactions; transfer dehydrogenation, benzoin condensation, transfer hydrogenation. The synthesis of control catalysts, nine novel thiazole ligands and their corresponding iridium(III) complexes, and four novel triazole ligands and their corresponding complexes has been discussed. The different structural features included in the fourteen ligands are summarised in Table 14.

**Table 14** The different structural features of the novel thiazole and triazole ligands synthesised in Chapter 2.

Rings	Side Chains	Backbones
		
		
		
		
		
		
		

Thiazole ester reduction was achieved with 100% selectivity for the aldehyde product with 0.75 equivalents of reagent, avoiding over-reduction to the thiazole alcohol. It was found that the imine made between TsDPEN and an aldehyde forms an equilibrium with a cyclic aminal, of which only the imine is

observed after 16 hours. An increased steric bulk around the thiazole *N*-atom decreased the coordinating ability of the ligand to the metal centre, resulting in no isolated complexes. 4-(Chloromethyl)-1,3-thiazole was used as a simple route to substituted thiazoles, whilst avoiding the use of reducing agents; however, the yields are typically low, except for the sulfonamide nucleophile to make **L.5** and **L.6**. When triethylamine was used in the reactions with 4-(chloromethyl)-1,3-thiazole or camphorsulfonamide the thiazole triethylammonium salt and the cyclic sulfonylimine products were formed preferentially.

Thiazoles require high temperatures and a high concentration of alkylating agent to make thiazolium salts and still gave low yields. Thiazole aldehydes are more difficult to alkylate and are very reactive, even to weak nucleophiles. The thiazolium rings are completely reduced with sodium borohydride during an attempted reductive amination reaction. Alkylation of 4-(chloromethyl)-1,3-thiazole was unsuccessful, leading to an insoluble black solid. Methylation of **L.1** resulted in an iodide ion eliminating the diamine and forming 4-(iodomethyl)-1,3-thiazolium iodide, which was isolated by filtration. Similarly, **C.10** breaks down to **C.8** with assumed loss of 4-(iodomethyl)-1,3-thiazolium iodide. Triazoles are easier to methylate, with much higher yields than the thiazoles. Synthesis of triazole **L.11** required four steps from the 1,2-aminoalcohol. Synthesis of **L.13** is a single step to the ligand and produces a single isomer; however, the yield was low. The long reaction time was improved by using a microwave reactor, but the yield could be improved further by investigating the ratios of the reagents.

Growing suitable single crystals for x-ray crystallography was challenging, as in most cases the complexes oiled out. Suitable single crystals were generally formed using vapour diffusion with either chloroform in hexane or acetone in pentane. The structures obtained presented the variety of the complexes prepared and that the thiazole and triazole *N*-atoms are strong donors to iridium(III) centres. The majority of the complexes were prepared in good yields and are air and water stable. Complex **C.7.1** was more susceptible to ligand displacement (especially in DMSO) and complex **C.10** was degraded via thiazolium elimination to complex **C.8**. The activity of the 14 novel complexes is discussed in Chapter 3.

## 3. Catalyst Testing

### 3.1. Introduction

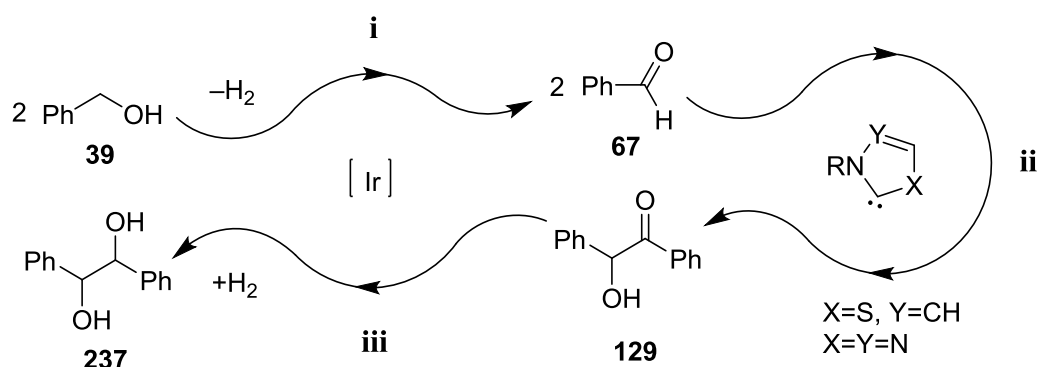
This chapter discusses the catalyst testing of the thiazole and triazole iridium(III) complexes synthesised in Chapter 2. The results are discussed in four sections:

1. Control reactions carried out with known catalysts to validate the target reaction sequence.
2. The initial testing of the complexes **C.1-C.6** and the optimisation of the transfer dehydrogenation reaction and the benzoin condensation catalyst tests.
3. The comparison of all novel thiazole and triazole complexes under the same conditions.
4. The testing of the scope of the reaction with substituted benzylic alcohols.

### 3.2. Control Reactions

#### 3.2.1. Individual Catalyst Tests

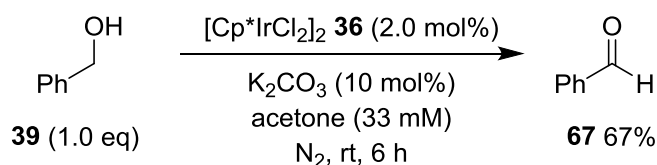
To validate the desired reaction sequence, each step of the sequence was carried out separately. The two catalytic components of the multifunctional complexes must be able to catalyse the hydrogen transfer and benzoin condensation reactions with the organometallic and organocatalysts respectively (Scheme 107).



**Scheme 107** Proposed multicatalytic cycle; i) transfer dehydrogenation, ii) benzoin condensation, iii) transfer hydrogenation.

### 3.2.1.1. Transfer Dehydrogenation of Benzyl Alcohol

The first reaction of the multifunctional catalyst is the dehydrogenation of benzyl alcohol **39** to produce benzaldehyde **67**. The iridium(III) chloride dimer **36** was tested as a control for this reaction with acetone as the hydrogen acceptor (Scheme 108). Acetone was used as the hydrogen acceptor and potassium carbonate as the base in the reaction, following a procedure reported by Fujita.<sup>130</sup> The yield was found to be lower than reported (87%), however, the reaction successfully converted **39** to **67**.

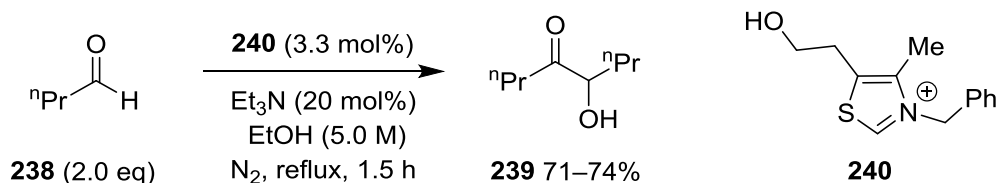


**Scheme 108** The transfer dehydrogenation of benzyl alcohol **39** with catalyst **36**.

### 3.2.1.2. Benzoin Homo-Condensation of Benzaldehyde

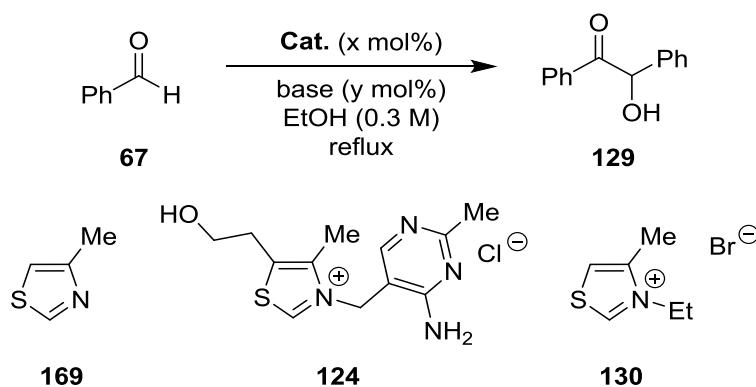
The organocatalysed benzoin condensation has been investigated with **67** (Table 15). The experimental conditions chosen follow a modified procedure that was originally reported by Stetter and Kuhlmann (Scheme 109).<sup>131</sup> 4-Methylthiazole **169** was used as a control catalyst; the unalkylated thiazole ring is unable to catalyse the reaction due to the poor electron withdrawing power of the *N*-atom in thiazole (entries 1 and 2). Thiazolium catalysts are necessary, as the positive charge on the *N*-atom acts as an electron sink and increases

the acidity of the catalyst. Thiamine hydrochloride **124** gave low yields with triethylamine ( $pK_{aH}$  10.8) as a base (entry 3 and 4). With potassium *tert*-butoxide and potassium carbonate there was no conversion to benzoin **129** (entries 5, 6). The thiazolium ring in **124** can be ring opened with a strongly alkaline solution ( $pH > 9.5$ ), which could be the cause of no catalysis.<sup>132</sup> *N*-Ethyl-4-methylthiazolium bromide **130** achieved good conversion at 20 mol% catalyst loading (entry 8). Precious metal catalysts are often reported to reach full conversion in hydrogen transfer reactions with  $<1$  mol% catalyst loadings;<sup>50</sup> the organo/organometallic multifunctional catalyst may require larger loadings to account for the organocatalysis step, therefore the catalyst tests with the multifunctional catalysts will be run at 5 mol% to give the organocatalysis a chance of working. An advantage of multifunctional catalysis can be a decrease in organocatalyst loading, as Schreiner reported a decrease in catalyst loading from 60 mol% to 5.0 mol% as a result of tethering the two catalysts.<sup>33</sup>



**Scheme 109** Benzoin condensation reaction of butyraldehyde with a thiamine analogue catalyst **240**.



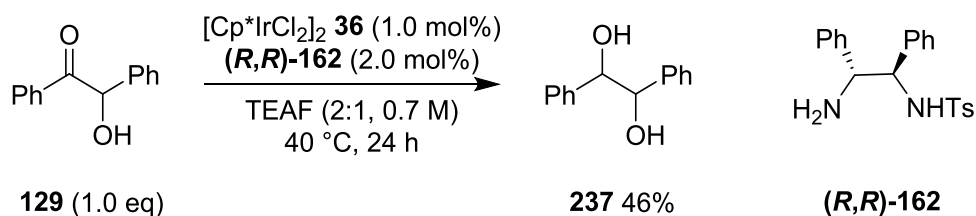
**Table 15** The catalyst tests for the benzoin condensation of **67** to **129**.

Entry	Catalyst	Catalyst Loading (x mol%)	Base	Base Loading (y mol%)	Time (h)	Yield (%)
1	169	5	Et <sub>3</sub> N	30	24	0
2	169	20	DBU	30	24	0
3	124	5	Et <sub>3</sub> N	30	1.5	5
4	124	5	Et <sub>3</sub> N	30	1.5	13
5	124	5	KO <sup>t</sup> Bu	30	4	0
6	130	10	K <sub>2</sub> CO <sub>3</sub>	10	24	0 <sup>a</sup>
7	130	2	Et <sub>3</sub> N	60	5	0
8	130	20	Et <sub>3</sub> N	60	5	68

<sup>a</sup> Reaction carried out in MeCN.

### 3.2.1.3. Hydrogenation of Benzoin to Hydrobenzoin

The final step in the reaction sequence of the multifunctional catalyst is the hydrogenation of benzoin **129** to give hydrobenzoin **237** (Scheme 110).<sup>133</sup> This was achieved with **36** and (*R,R*)-**162**, with TEAF as the hydrogen donor, to produce **237** with 46% yield.

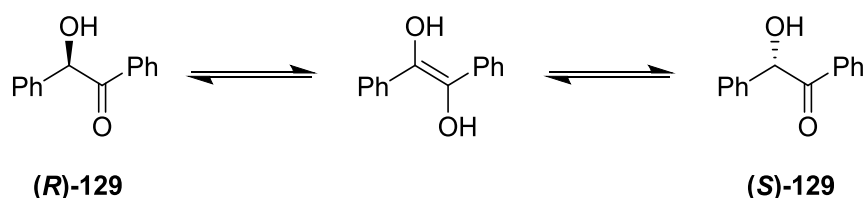


**Scheme 110** Hydrogenation of **129** with an iridium(III) catalyst.

Both hydrogen transfer and benzoin condensation control reactions were successful, which shows that the desired reaction sequence with the chosen combination of catalysts is feasible. As both hydrogen transfers are designed

to occur sequentially, hydrogen borrowing could be employed to remove the need for extra hydrogen acceptors/donors.

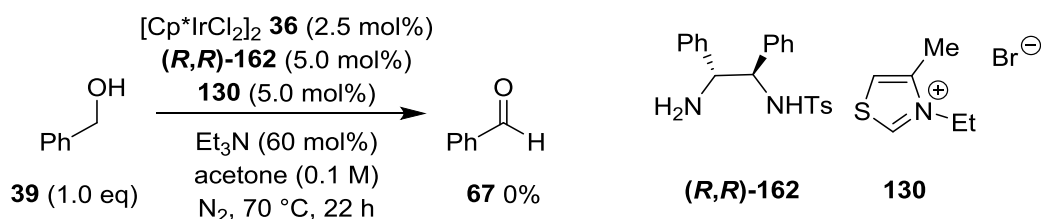
Concerning the asymmetry of the reaction, only the final hydrogenation can influence the stereochemistry of the prochiral centre on **129**, as racemisation of **129** through its enol form is possible (Scheme 111).<sup>134</sup> Due to the close proximity of the thiazolium catalyst to the iridium metal centre, the multifunctional catalyst could hydrogenate the initial enantiomer formed directly after the benzoin condensation before it is able to racemise. This could be a very useful advantage of the catalyst design and allow the production of a specific enantiomer of **237**.



**Scheme 111** The racemisation of **129** via the tautomer.

### 3.2.2. One-pot Test

An experiment to combine both separate catalysts in one-pot was carried out in order to compare the rate of reaction with the multifunctional catalysts. Schreiner and Peris have reported improvements in the rates of reaction with their multifunctional catalysts as compared to separate catalysts under the same conditions (see Chapter 1.8).<sup>33, 36</sup> Orthogonal relay catalysis was attempted to perform the three sequential reactions in one-pot (Scheme 112). This resulted in 0% conversion of **39** to **67**. The cause of no catalysis could be due to the iridium(III) catalyst being inhibited by the thiazolium catalyst **130**.



**Scheme 112** Catalyst test with separate organo and organometallic components.

Sequential catalysis was attempted in order to support the idea of catalyst inhibition. Two parallel reactions in the absence of thiazolium were followed using GC. When the conversion to **67** was observed, a thiazole or thiazolium compound was added to the reaction (Figure 48).

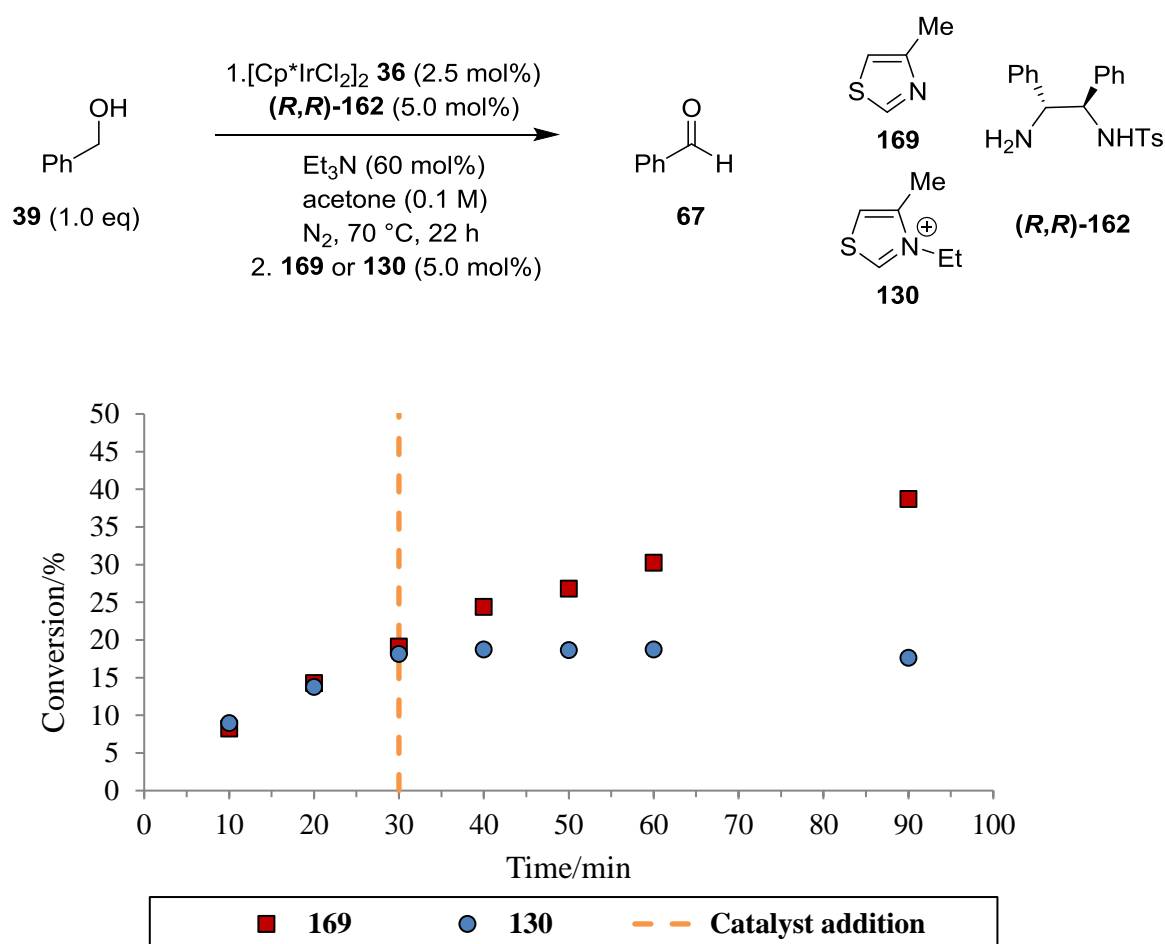
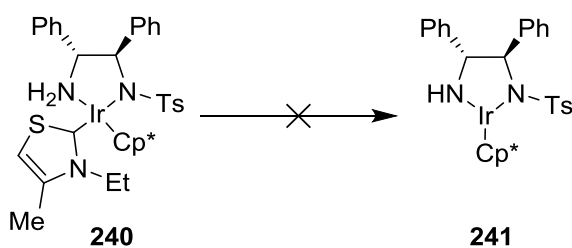


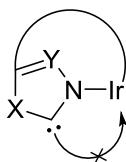
**Figure 48** The conversion (%) of **67** against time (min) for the parallel dehydrogenation reactions of **39** with either thiazole **169** or thiazolium **130** added at 30 minutes. Reactions followed using GC with decane as an internal standard.

The mechanism for the inhibition of the iridium catalyst could be a strong coordination of the thiazolium carbene to the iridium centre. This would block the vacant sites required for an active 16-electron complex, therefore stopping the dehydrogenation of the alcohol substrate (Scheme 113).



**Scheme 113** The proposed inhibited complex **240** preventing formation of the activated iridium catalyst **241**.

The result of the one-pot tests were disheartening; however, the design of the multifunctional catalyst prevents carbene-metal bonding using the *N*-atom as a ligand donor and therefore the observed inhibition should be prevented (Scheme 114).



**Scheme 114** Geometry restricted carbene-iridium bond formation.

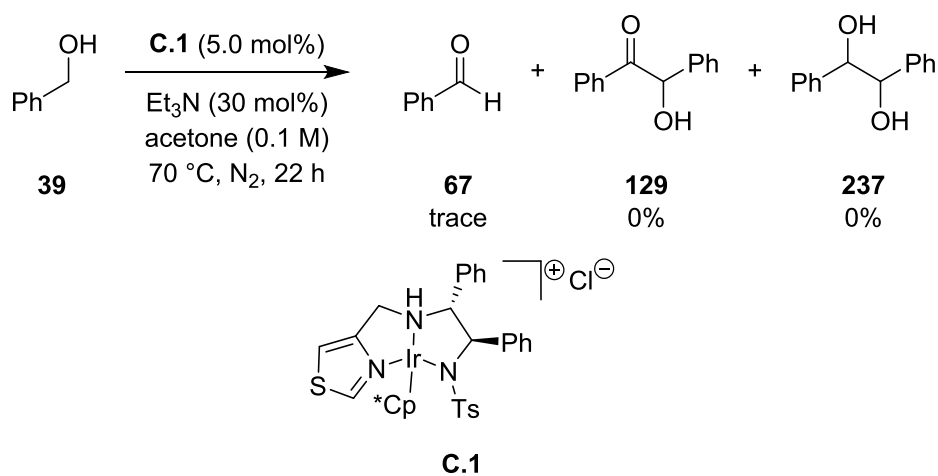
### 3.3. Transfer Dehydrogenation of Benzyl Alcohol

This section discusses the testing of novel iridium(III) complexes presented in Chapter 2, optimisation of reaction conditions, and further catalyst development. The first step in the reaction sequence is the dehydrogenation of benzyl alcohol **39**, however the formation of benzoin and related products were also assessed after each test.

#### 3.3.1. Initial Testing

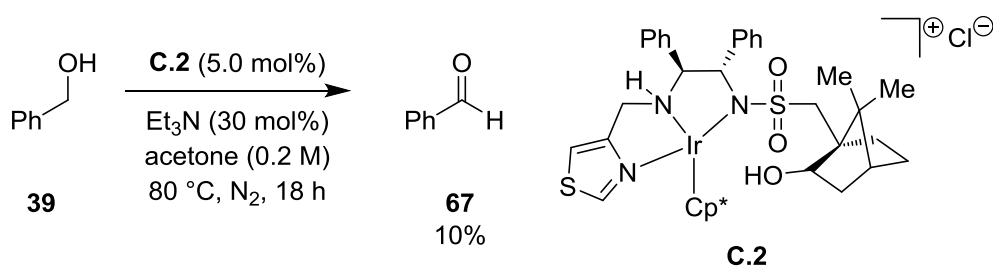
The conditions chosen to test the catalytic activity of the thiazole and triazole complexes **C.1-C.14** were those typically used in the literature, with **39** as a comparable substrate.<sup>130, 135</sup> Acetone is a good hydrogen acceptor and, used in excess as the solvent, is able to drive the equilibrium towards **67**. The thiazole tethered complex **C.1** was found to make only a trace of product **67** and no derivatives **129** or **237** (Scheme 115). This may be because **C.1** is

coordinatively saturated, requiring one of the tridentate coordination sites to show hemi-lability for abstraction of the hydride from **39**.



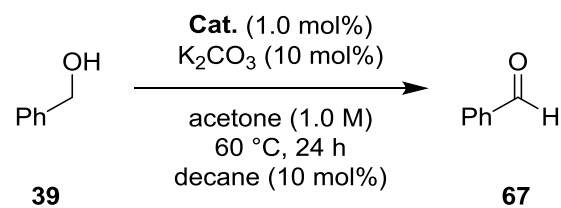
**Scheme 115** Attempted catalytic sequence with iridium(III) complex **C.1**.

The control tests showed that the transfer dehydrogenation worked well in the chosen reaction conditions and that a thiazole ring did not inhibit the catalyst. However, the result with **C.1** suggested that the complex was inactive, where other tethered DPEN ligands have been successful.<sup>136</sup> Complex **C.2** was tested under similar conditions to produce **67** in 10% conversion (Scheme 116).



**Scheme 116** The transfer dehydrogenation of **39** to **67** with novel catalyst **C.2**.

This result indicated that the thiazole side chain was not the cause of inactivity, however, the yield was poor. Following a similar procedure by Fujita,<sup>130</sup> triethylamine was changed for potassium carbonate as the base in the reaction (Table 16).

**Table 16** Catalyst tests with control and novel catalysts.

Entry	Catalyst	Conversion (%) <sup>a</sup>
1	<b>36</b>	16
2	<b>36</b> + ( <i>R,R</i> )- <b>162</b>	18
3	<b>C.2</b>	14

<sup>a</sup> Conversion calculated from the corrected peak integrals using decane as an internal standard for GC at 24 hours.

The yield was improved slightly using potassium carbonate and with a lower catalyst loading (entry 3). The conversion to **67** was almost as good as the control catalysts (entries 1 and 2). As the aim of the project was to carry out reactions in sequence, the benzaldehyde was expected to be used up as it was made, which would give a small concentration. However, the benzoin and hydrobenzoin products were not observed. Surprisingly, the aldehyde yield in the control reactions with the iridium(III) dimer and the iridium(III) complex **62** were lower than seen previously (Scheme 108), and the cause was found to be an unwanted aldol side reaction.

### 3.3.2. Aldol Reaction

It is reported in transfer hydrogenation reactions that the acetone produced can react with the aldehyde substrate to make aldol products, especially with electrophilic substrates. In these reactions the aldol side-reaction has been avoided by slowly feeding in the aldehyde substrate to keep its concentration low, and relying on the faster rate of reduction compared to the aldol.<sup>137</sup> In the case of transfer dehydrogenation, the acetone is in high concentration, increasing the chance of enolate formation. The enolate can attack the aldehyde product as it is formed. After re-analysis of the GC samples using an extended method and using GCMS to identify the compounds, the aldol reaction with acetone was shown to be occurring to produce the aldol products:

4-hydroxy-4-phenylbutan-2-one **242**, benzylidene **243** and dibenzylidene **244** (Figure 49).

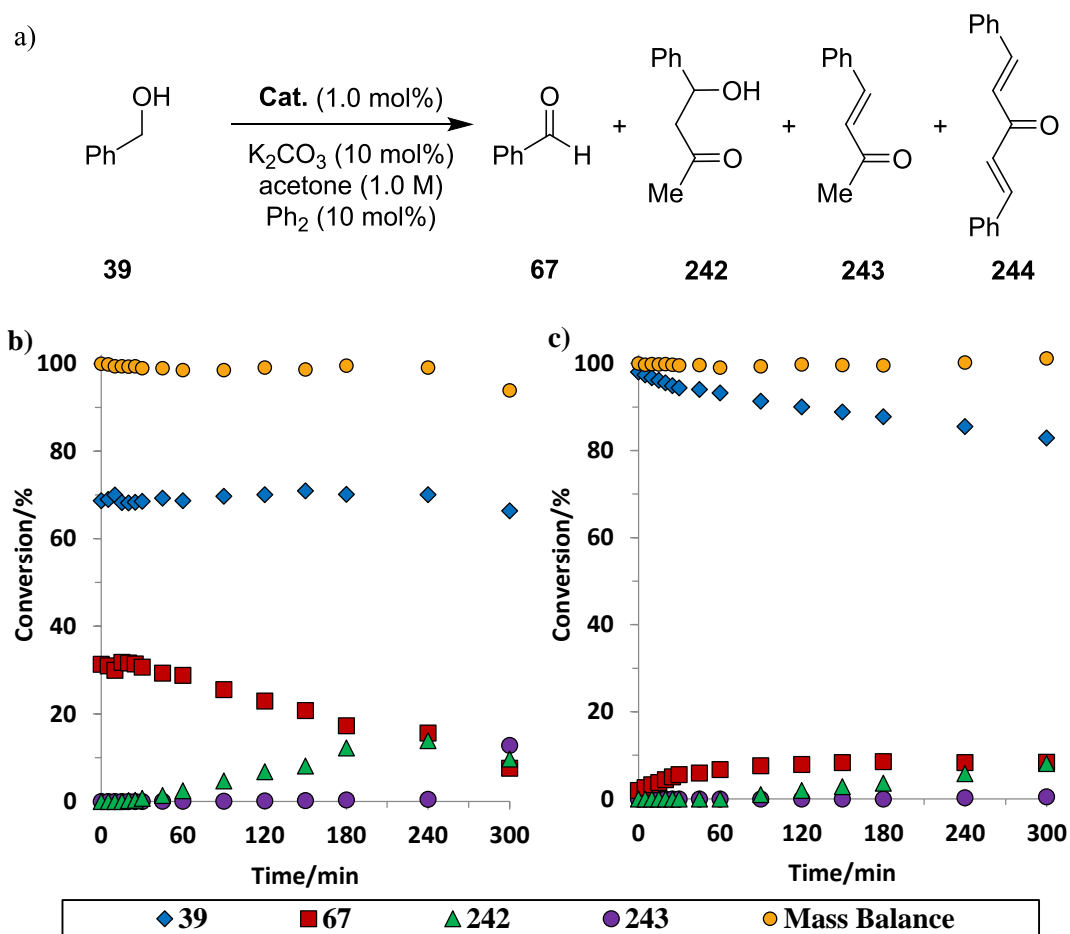
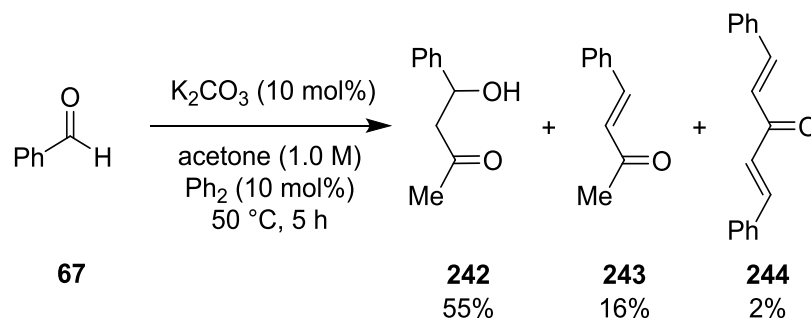


**Figure 49** a) The conversion of **39** to **67** and the aldol reaction of **67** with acetone to give **242** and further products **243** and **244**. b) Catalyst; **36**. c) Catalyst; **C.2**. Samples quantified using GC with biphenyl as an internal standard.

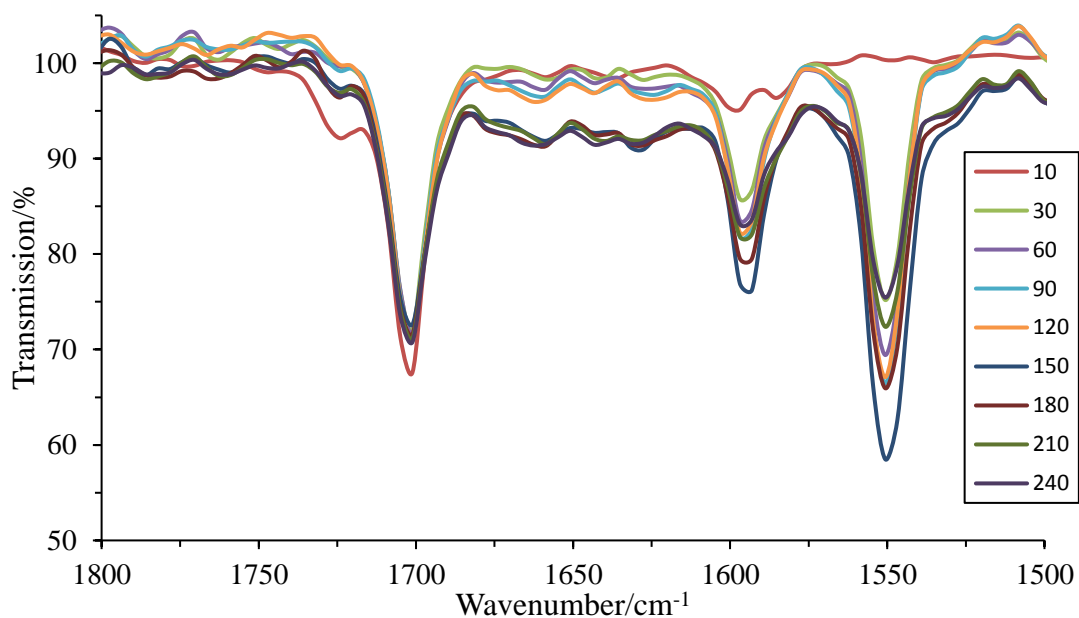
With catalyst **36**, the rate of reaction is very fast, reaching 30% conversion after five minutes. Following the initial accumulation of **67** the aldol reaction begins, but after five hours **67** falls to below 10%. Once the aldol product **242** is present in a high enough concentration, **243** is produced. **244** is present at 4% after 24 hours. The reaction with catalyst **C.2** showed a slower initial rate than **36**, and did not reach equilibrium as quickly, as the substrate continued to decrease. A control reaction of **39** under the same conditions in the absence of catalyst showed only starting material after 24 hours. However, another control reaction with **67** as the substrate, also without catalyst, resulted in

formation of all the aldol products (Scheme 117), showing the aldol side-reaction is not catalysed by **C.2**.



**Scheme 117** The aldol reaction in the absence of catalyst followed using GC with biphenyl as an internal standard.

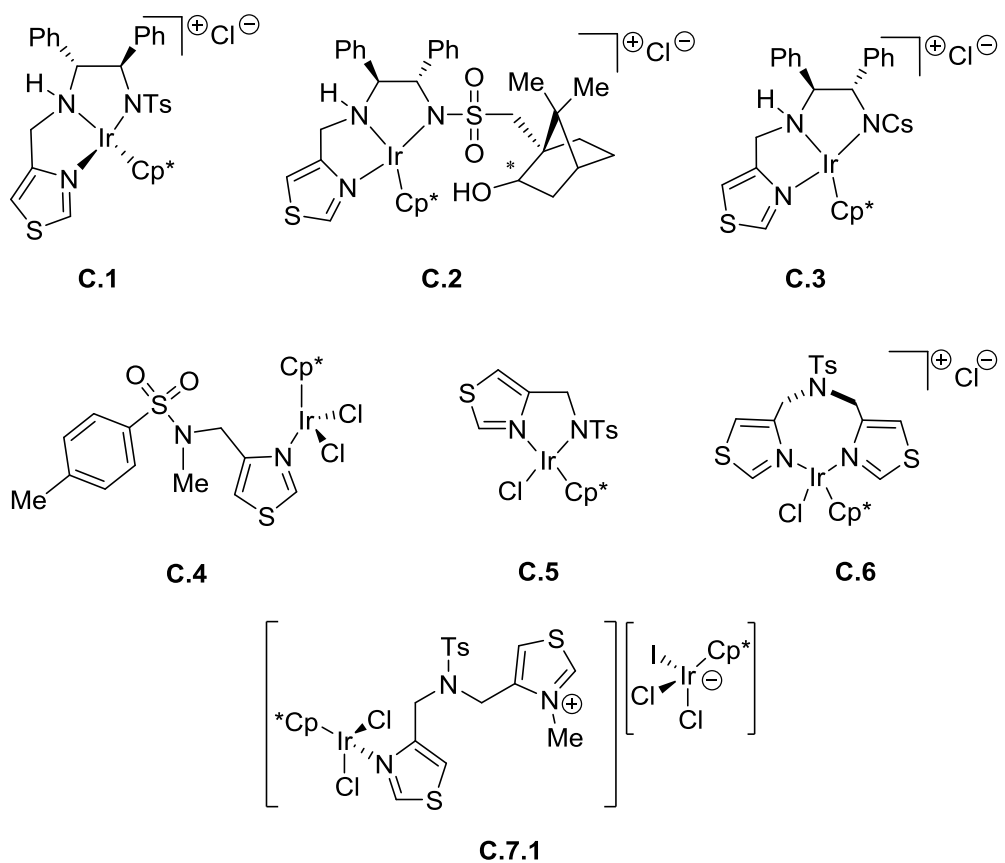
To see whether there are any other background reactions occurring, such as the Tishchenko<sup>138</sup> or Cannizzaro<sup>139</sup> reactions, an IR probe was used to follow a reaction of **67**, **39** and potassium carbonate in acetonitrile in the absence of acetone (Figure 50). The reaction was heated to 50 °C and monitored for five hours, which resulted in no change to the presence of the benzaldehyde carbonyl stretch at 1702  $cm^{-1}$ .



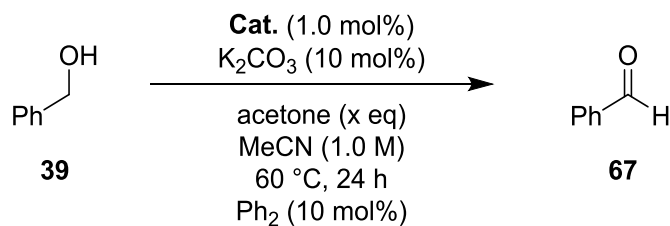
**Figure 50** Overlaid IR spectra (time in minutes) with separate additions of **67** and **39** at 0 and 30 minutes.



To prevent the aldol side reaction, the solvent was changed to acetonitrile; removing the ability to form **242**, but also removing the hydrogen acceptor. As expected, the reaction in absence of acetone gave only 1% conversion to **67** (entry 1, Table 17). Acetone was added back into the reaction in quantities stoichiometric with **39** to try to improve the conversion. Introducing one equivalent improves the conversion (entry 2), whilst five equivalents added over five hours (entry 3) resulted in a slight improvement to 7% conversion. Since acetone has a high vapour pressure, its loss from the reaction would increase the concentration of *iso*-propanol and drive the reverse reaction. The reactions were followed using GC (Figure 52), which shows that after four hours, the rate of conversion to **67** slows and even decreases at 24 hours. With the absence of side-products, this indicates that the dehydrogenation is in equilibrium with the reverse reaction under these conditions. Previously, complex **C.1** was inactive in acetone. With acetonitrile as the solvent the complex gave 3% conversion (entry 4). Surprisingly, dehydrogenation of **39** to **67** with catalyst **C.3** (entry 5) gave a higher conversion than **C.2**. The only structural difference between the complexes is the bicyclic side chain; hydroxyl or ketone for **C.2** and **C.3** respectively. The activity of **C.2** could be hindered due to competitive coordination of the hydroxyl group with the metal centre, which has been suggested is the reason behind an improvement in the enantioselectivity of other catalytic systems that use CsDPEN ligands.<sup>110</sup> The mono- and bidentate thiazole complexes **C.4–C.6** were prepared with the aim of improving the availability of the metal centre for catalysis by increasing the number of vacant/labile sites. All three complexes were able to turn-over, however the conversions were also poor (entries 6–8) (Figure 51).

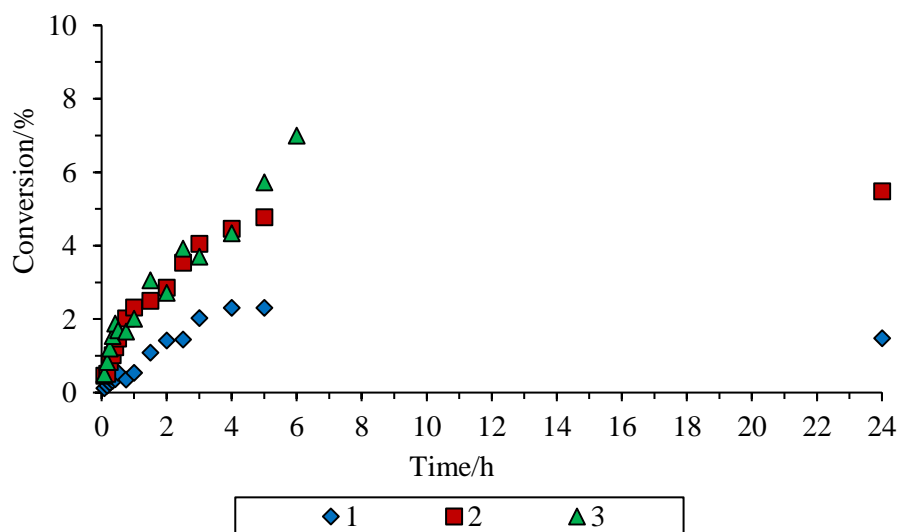


**Figure 51 Complexes C.1–C.7.1**

**Table 17** The conversions to **67** with varied acetone equivalents.

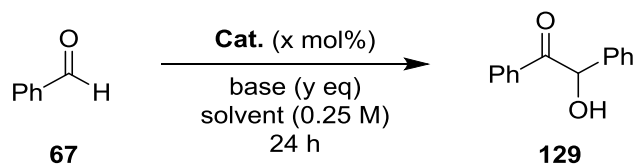
Entry	Catalyst	Acetone (x eq)	Conversion (%) <sup>a</sup>
1	C.2	0	1
2	C.2	1	5
3	C.2	5 <sup>b</sup>	7 <sup>c</sup>
4	C.1	1	3
5	C.3 <sup>d</sup>	2	12
6	C.4	1	5
7	C.5 <sup>d</sup>	2	3
8	C.6 <sup>d</sup>	2	5
9	C.7.1 <sup>d</sup>	2	4

<sup>a</sup> Conversion calculated at 24 hours using GC from the corrected peak integrals with biphenyl as an internal standard. <sup>b</sup> 5 equivalents added evenly over a period of 5 hours. <sup>c</sup> Conversion calculated at 6 hours. <sup>d</sup> 0.5 mol% catalyst.

**Figure 52** Conversion (%) to **67** against reaction time (hours) with three different conditions (entries 1–3, Table 17).

The benzoin products were not observed in any of the catalyst experiments. The cause of this could be due to the unsuccessful deprotonation at the thiazole C-2 position, as the acidity of this proton is dependent on the strength of the coordination of the thiazole *N*-donor to the iridium metal centre. If the metal has a poor electron withdrawing ability, the pK<sub>a</sub> of the thiazole will not be sufficiently decreased to allow the deprotonation and activation of the thiazole catalytic site, therefore the reaction will not occur. In order to correct this, alkylation of the *N*-atom of the thiazole would reduce the pK<sub>a</sub> of the C-2 position to ~17, which is more accessible with mild bases. The complexes **C.1–C.7.1** tested with **67** as the substrate in an attempt to produce **129** (Table 18). The iridium(III) complexes were unsuccessful in transforming **67** to **129**. The *bis*-thiazole ligand **L.6** was alkylated on one of the thiazole rings to make thiazole/thiazolium ligand **L.7**; which was itself a successful organocatalyst for the benzoin condensation (entry 5). However, even though the thiazolium ring in **C.7.1** is pointing away from the metal centre in the x-ray crystal structure, the iridium complex was not able to catalyse the reaction (entry 4). Intermolecular carbene-iridium bond formation could be the problem with the reaction, which would inhibit the organocatalyst.

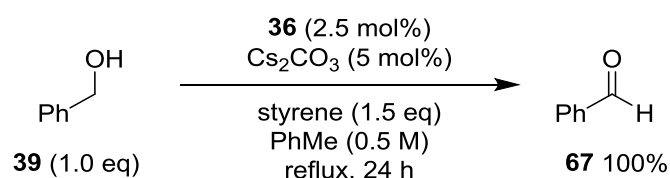
**Table 18** Catalyst tests for the benzoin condensation of **67** to **129**.



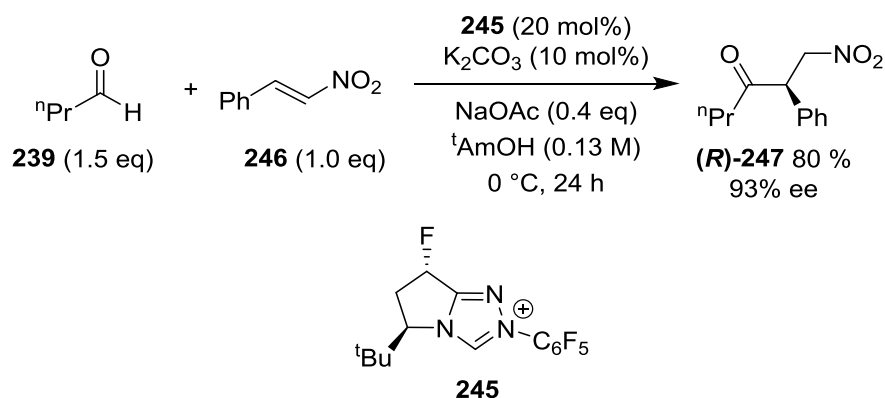
Entry	Catalyst	Catalyst Loading (x mol%)	Base (y eq)	Solvent	Temp (°C)	Yield (%)
1	<b>C.4</b>	1.0	K <sub>2</sub> CO <sub>3</sub> (0.1)	MeCN	40	0
2	<b>C.1</b>	5.0	Et <sub>3</sub> N (0.6)	EtOH	70	0
3	<b>C.1</b>	5.0	Et <sub>3</sub> N (0.6)	<sup>i</sup> PrOH	70	0
4	<b>C.7.1</b>	3.0	Et <sub>3</sub> N (5.0)	MeCN	50	0
5	<b>L.7</b>	5.0	Et <sub>3</sub> N (2.0)	MeCN	80	93

### 3.3.3. Hexamethylacetone (HMA)

Another way in which the aldol and reverse reactions can be avoided is using a hydrogen acceptor which cannot form the aldol products. Williams has used alkenes such as styrene and crotonitrile as successful hydrogen acceptors (Scheme 118);<sup>56, 140-142</sup> however, Rovis has demonstrated that alkenes can be electrophiles for organocatalysed Stetter reactions between an alkene and an aldehyde (Scheme 119).<sup>143</sup>

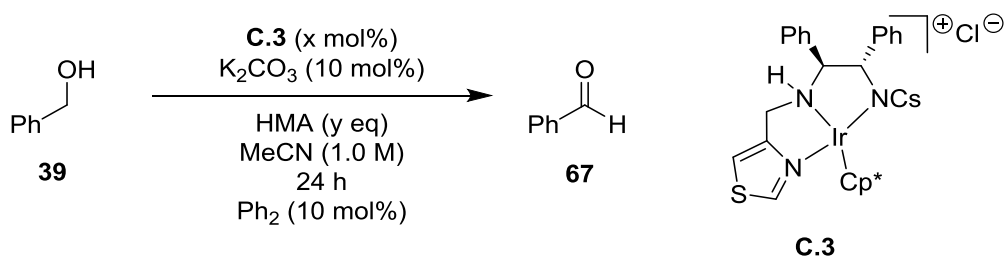


**Scheme 118** The transfer dehydrogenation of benzyl alcohol **39** reported by Williams, with styrene as the hydrogen acceptor.



**Scheme 119** The asymmetric Stetter reaction reported by Rovis with nitrostyrene **246** and butraldehyde **239** using a chiral triazolium organocatalyst **245**.

HMA has a higher boiling point (152 °C) than acetone (56 °C), so higher reaction temperatures and reaction rates are accessible. Furthermore, with the absence of  $\alpha$ -hydrogens, enolate formation is not possible; therefore the aldol reaction cannot occur. Even though at lab-scale it is 2000 times more expensive than acetone, HMA was tested to see if it was a viable hydrogen acceptor. Using **C.3**, the conversions were low (entries 1–3, Table 4), and even using it as a solvent failed to improve the conversion (entry 3). It may be that steric hindrance makes its reduction difficult, or the equilibrium favours the ketone over the alcohol.

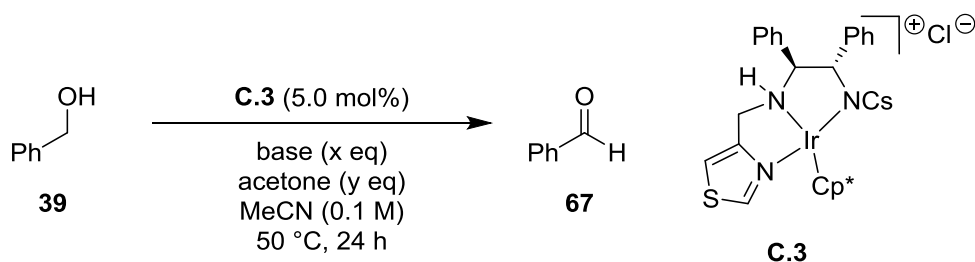
**Table 19** Catalyst tests with HMA as the hydrogen acceptor.

Entry	Catalyst Loading ( $x$ mol%)	HMA ( $y$ eq)	Temperature ( $^{\circ}C$ )	Conversion (%) <sup>a</sup>
<b>1</b>	1.0	2.0	50	5
<b>2</b>	0.7	2.0	75	9
<b>3</b>	0.5	solvent	60	1

<sup>a</sup> Conversion calculated at 24 hours using GC from the corrected peak integrals with biphenyl as an internal standard.

### 3.3.4. Acetone Equivalents

The transfer dehydrogenation reaction was investigated further to improve the conditions. The two main factors that were varied were the base loading and the number of acetone equivalents (Table 5). The type of base was also changed; a heterogeneous inorganic base (potassium carbonate) and a homogenous organic base (triethylamine).

**Table 20** Catalyst tests with varied base, base loading and acetone equivalents.

Entry	Base	Base Loading (x eq)	Acetone (y eq)	Conversion (%) <sup>a</sup>
1	K <sub>2</sub> CO <sub>3</sub>	0.1	5	8 <sup>b</sup>
2	Et <sub>3</sub> N	0.5	5	11 <sup>b</sup>
3	Et <sub>3</sub> N	1.0	10	8
4	Et <sub>3</sub> N	5.0	10	4 <sup>c</sup>
5	Et <sub>3</sub> N	1.0	20	12
6	K <sub>2</sub> CO <sub>3</sub>	1.0	10	11
7	K <sub>2</sub> CO <sub>3</sub>	1.0	20	26
8	K <sub>2</sub> CO <sub>3</sub>	1.0	30	24
9	K <sub>2</sub> CO <sub>3</sub>	1.0	40	25
10	K <sub>2</sub> CO <sub>3</sub>	1.0	50	30
11	KO <sup>t</sup> Bu	1.0	50	4
12	AcOH	1.0	50	3

<sup>a</sup> Conversion calculated at 24 hours using GC from the corrected peak integrals with biphenyl as an internal standard. <sup>b</sup> MeCN (1 mL). <sup>c</sup> Conversion calculated at 4 hours.

Starting from the previous results using 0.1 equivalents of potassium carbonate (entry 1), it was found that changing the base to triethylamine gave a slight improvement (entry 2). Further increasing the amount of triethylamine and acetone equivalents had little effect on the conversion (entries 3–5). Using potassium carbonate and increasing the amount of base and acetone showed a further improvement up to 30% conversion (entry 10). Repeating this reaction with potassium *tert*-butoxide, a stronger base, was detrimental (entry 11). To see what affect an acid would have on the conversion, acetic acid was used instead of a base; however, the conversion was poor (entry 12). The experiments with increasing acetone (entries 6–10) were followed using GC (Figure 53). The initial rate of conversion in the reactions are fast for the first

hour, then the rate slows and conversion decreases over time. With 50 equivalents of acetone in acetonitrile, the conversion continues to increase after its initial peak at 2 hours, highlighting the need for a high acetone concentration. Pleasingly, no aldol side-products were observed during the reactions; the reverse reaction of **67** to **39**, with *iso*-propanol as the hydrogen donor, occurs more quickly. This is surprising, as only 0.25 equivalents of *iso*-propanol are present versus 50 equivalents of acetone.

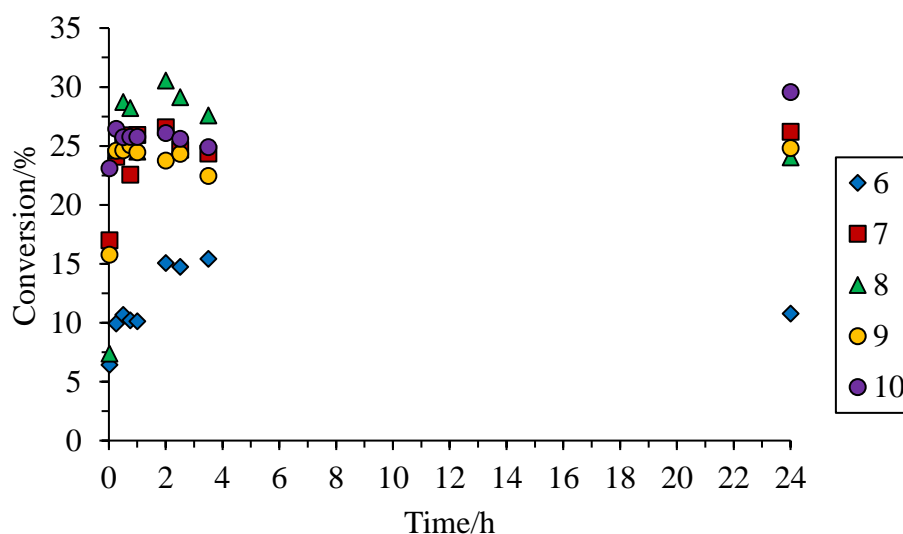
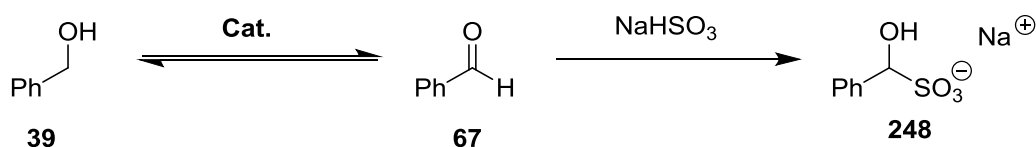


**Figure 53** Conversion (%) against time (hours) for catalyst tests (entries 6–10, Table 20).

### 3.3.5. Sodium Bisulfite Addition

In an attempt to trap any **67** formed during the reaction, sodium bisulfite was added;<sup>144</sup> ideally forming the bisulfite adduct **248** which would precipitate out of the reaction and drive the equilibrium in the forward reaction (Scheme 120).

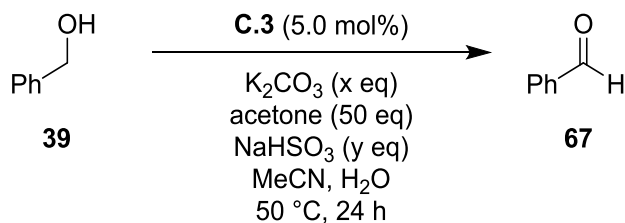


**Scheme 120** Proposed adduct formation to drive the equilibrium to the aldehyde.



Direct addition of bisulfite to the reaction in acetonitrile led to no change, due to its insolubility. Consequently, the reaction was also investigated in a mixture with water, and compared with and without base (Table 21).

**Table 21** Catalyst tests with sodium bisulfite to trap **67**.



Entry	K <sub>2</sub> CO <sub>3</sub> (x eq)	MeCN (mL)	Water (mL)	NaHSO <sub>3</sub> (y eq)	Conversion (%) <sup>a</sup>
1	0	2	0	0	9
2	1	2	0	1	16
3	0	2	0	1	9
4	0	1	1	0	8
5	0	1	1	1	9
6	1	1	1	0	12 <sup>b</sup>
7	1	1	1	1	13

<sup>a</sup> Conversion calculated at 24 hours using GC from the corrected peak integrals with biphenyl as an internal standard. <sup>b</sup> The mass balance was less than 50% of the original substrate concentration.

The addition of water and/or sodium bisulfite to the reactions still allowed the transfer dehydrogenation to proceed; however, the conversions were low. The use of sodium bisulfite during the reaction was unsuccessful in improving the forward reaction.

### 3.3.6. Substrate Addition

To identify if catalyst deactivation was an issue, an experiment was conducted where the substrate was added in ten portions over 5 hours (Figure 54). The catalyst continued to turn-over after each addition. However, after the conversion reached 23% the reaction plateaued.

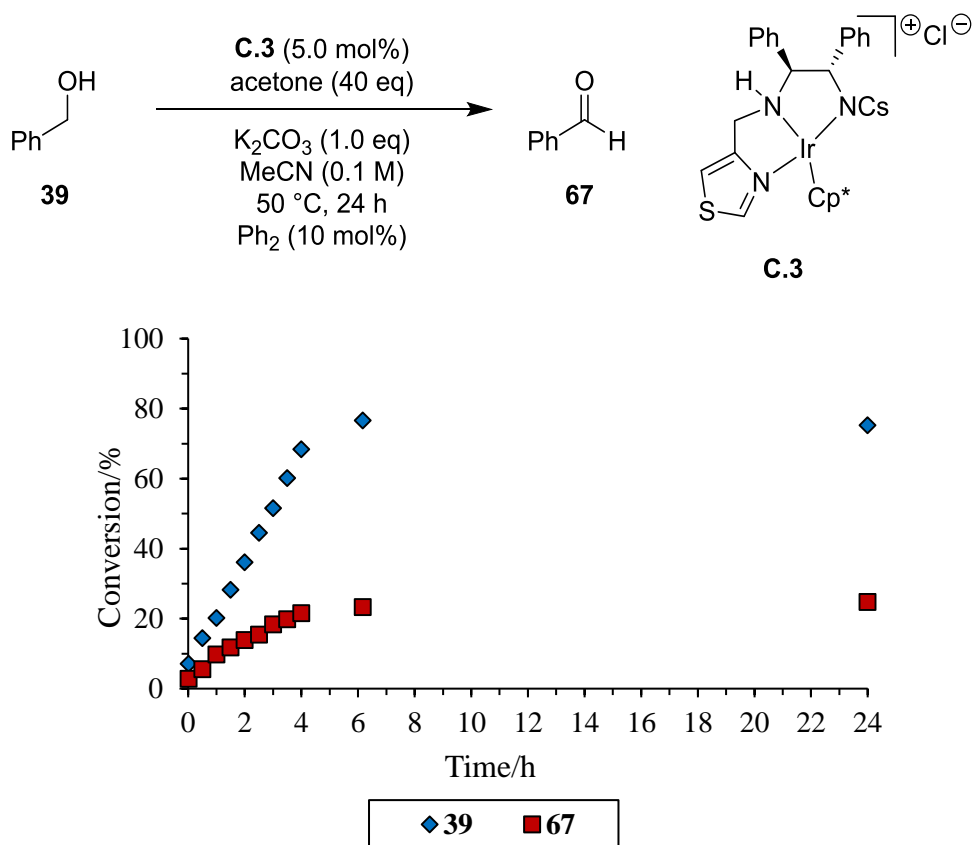


**Figure 54** Conversion (%) against time (hours) with **39** (0.1 eq) added every 30 minutes for 5 hours.

### 3.3.7. Extra Catalyst Addition

An experiment where a second portion of catalyst was added after 1.5 hours resulted in a decrease in conversion to **67**; suggesting that the fresh catalyst was assisting the reverse reaction (Figure 55). From this experiment it seems that the catalyst is not deactivated, otherwise a further increase in conversion would be observed.

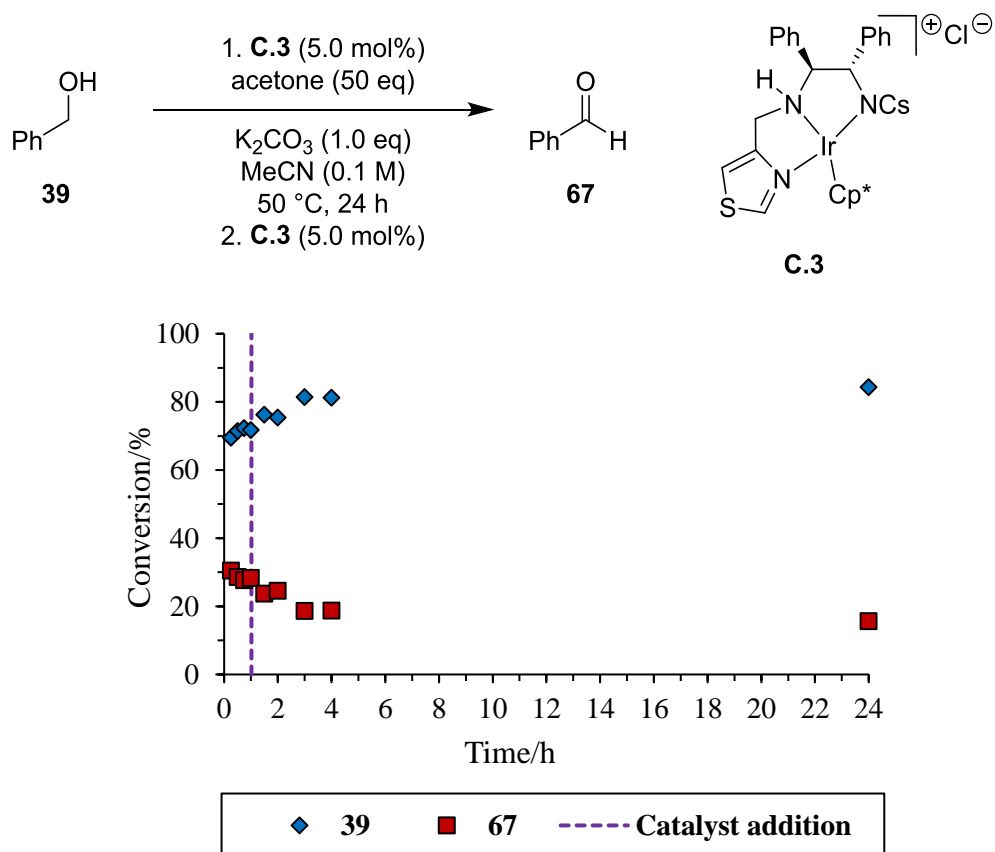
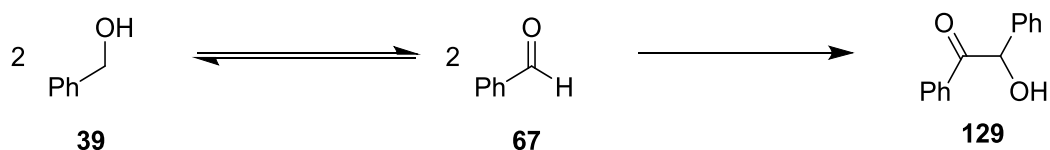


**Figure 55** Catalyst test with a second addition of catalyst (5 mol%) after 1.5 hours.

### 3.3.8. Reaction Equilibrium

The equilibrium between the transfer dehydrogenation and hydrogenation reactions could be the reason for the poor turnover numbers observed with the thiazole iridium(III) complexes. Interestingly, the benzoin condensation reaction would remove **67** and drive the equilibrium to the product (Scheme 121). An experiment starting with an equimolar mixture of **39** and **67** in the transfer dehydrogenation conditions resulted in only a small increase (5%) in the amount of **67** (Figure 56).



Scheme 121 The equilibrium between **39** and **67**, with the benzoin condensation driving the equilibrium.

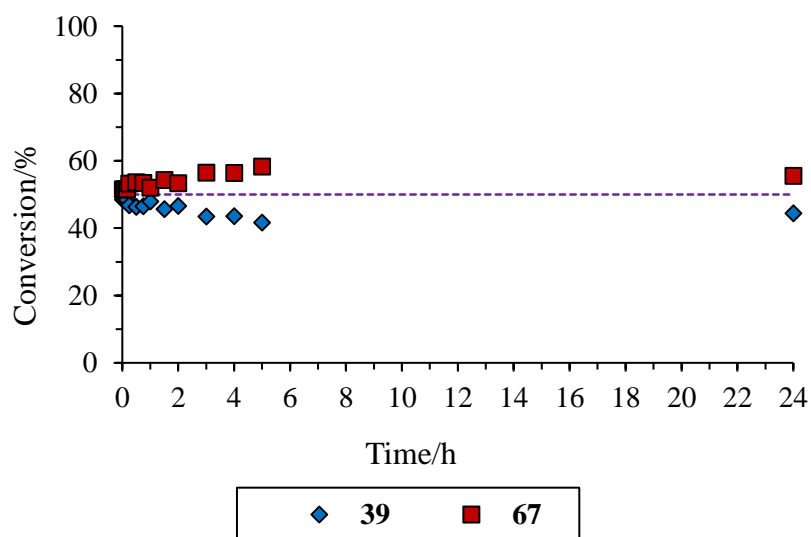
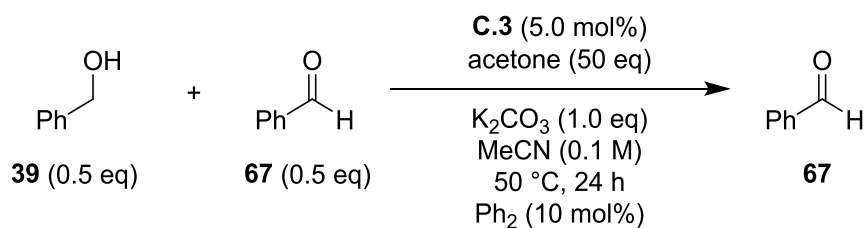
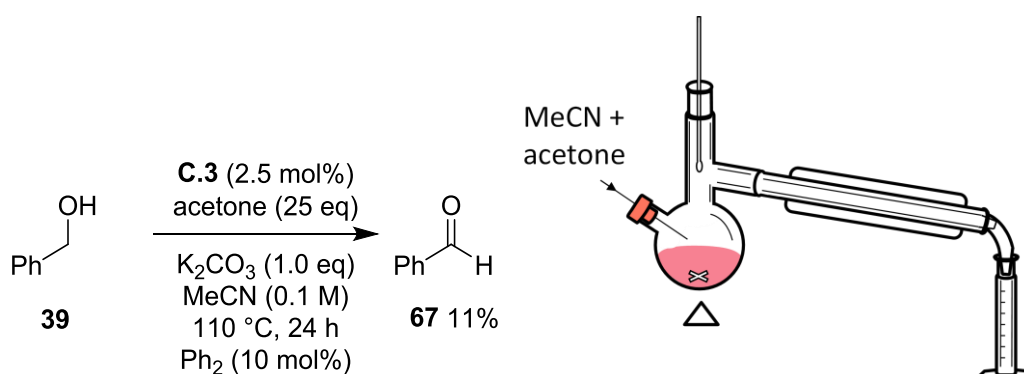
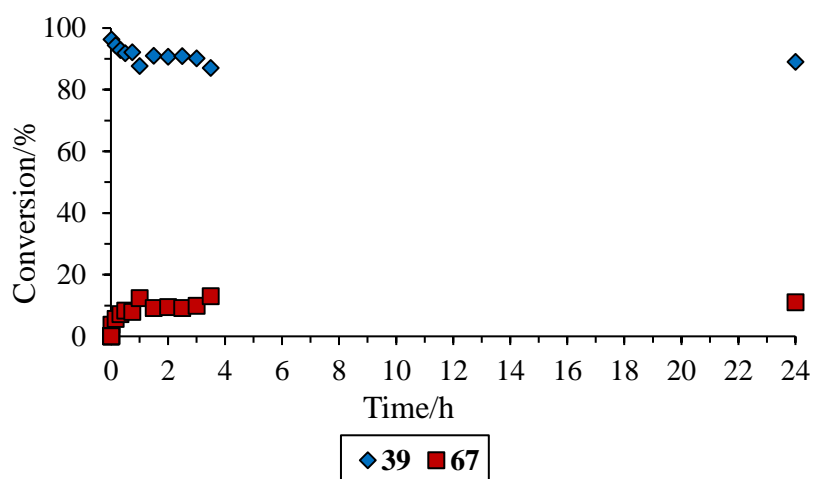


Figure 56 Catalyst test with a starting equimolar mixture of **39** and **67**.

Physical techniques used in transfer hydrogenation reactions that exploit the high volatility of acetone, such as continuous distillation and membrane/mesh reactors using nitrogen to strip, have been shown to overcome the reverse reaction.<sup>145, 146</sup> With its higher boiling point, removing *iso*-propanol in transfer dehydrogenation reactions is significantly more difficult. In an attempt to remove *iso*-propanol from the reaction, a distillation was set up to remove the solvent, acetone and *iso*-propanol. To maintain the acetone concentration and reaction volume, fresh acetone and solvent was added via syringe pump at a rate equal to distillation (Figure 57). The conversion did not exceed previous reactions; however, the temperature was higher and the concentrations of acetone or *iso*-propanol in the reaction were unknown.



**Scheme 122** The reaction conditions and experimental set-up of the distillation catalyst test.

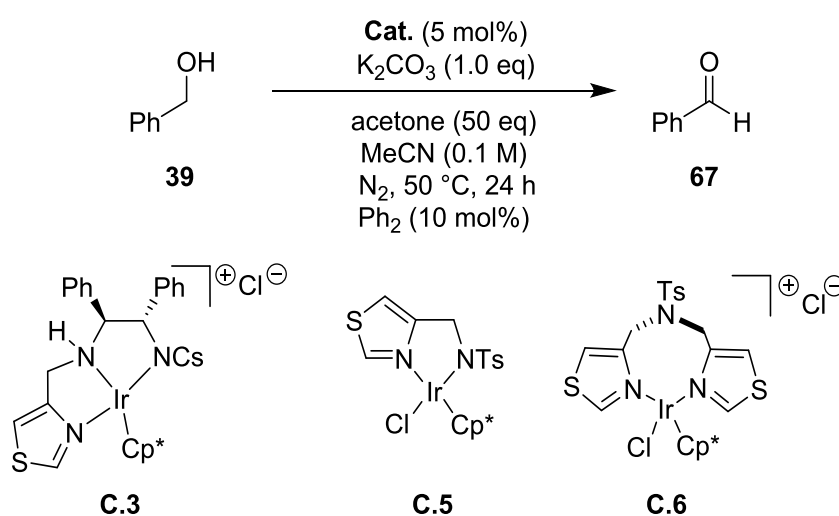


**Figure 57** The distillation reaction was followed using GC with biphenyl as an internal standard. The distillation was stopped after four hours and the reaction was continued at 50 °C.

### 3.3.9. Inert Conditions

The transfer dehydrogenation reaction was carried out previously in aerobic conditions in a round bottomed flask. To investigate whether atmospheric oxygen affects the catalytic activity, Schlenk reaction tubes and a strict nitrogen atmosphere were employed. A comparison of catalysts **C.3**, **C.5** and **C.6** with 50 equivalents of acetone in acetonitrile showed that **C.3** still gave the highest conversion (entry 1, Table 22).

**Table 22** Comparison of catalysts **C.3**, **C.5** and **C.6** under a strict atmosphere of nitrogen.



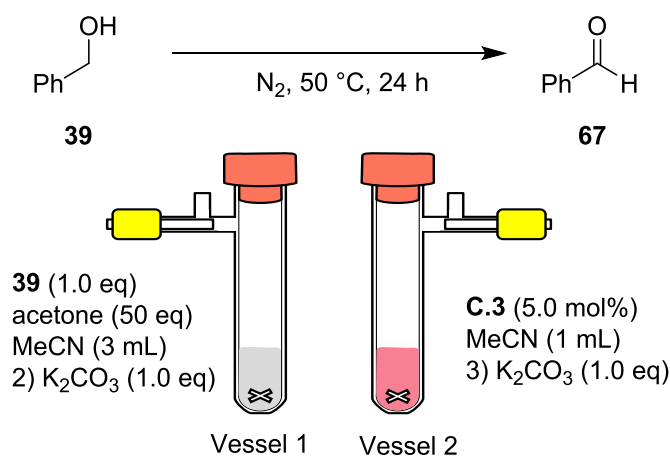
Entry	Catalyst	Conversion (%) <sup>a</sup>
1	<b>C.3</b>	21
2	<b>C.5</b>	7
3	<b>C.6</b>	11

<sup>a</sup> Conversion calculated at 24 hours using GC from the corrected peak integrals with biphenyl as an internal standard.

### 3.3.10. Slow Catalyst Addition

The addition of catalyst to the reaction was investigated. In an experiment without base, the catalyst solution was prepared in a separate vessel to the reaction and added in four equal portions over four hours. The reaction was then repeated with base in the reaction vessel, but not pre-stirred with the catalyst. Then a reaction with only base in the catalyst solution and none in the main reaction vessel (Table 23). The experiment with base in the main reaction vessel gave the highest conversion (entry 2). The conversion is less than when all the catalyst was added at the start of the reaction; suggesting it is not deactivating, and that the equilibrium must be the main issue.

**Table 23** The catalyst and base addition catalyst tests with **C.3**.



Entry	Vessel 1	Vessel 2	Conversion (%) <sup>a</sup>
1	–	–	9
2	K <sub>2</sub> CO <sub>3</sub>	–	17
3	–	K <sub>2</sub> CO <sub>3</sub>	13

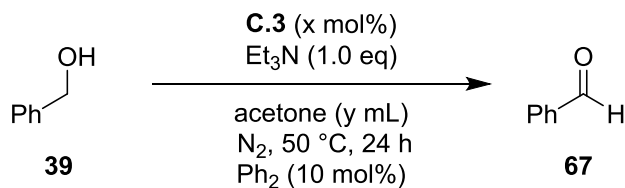
<sup>a</sup> Conversion calculated at 24 hours using GC from the corrected peak integrals with biphenyl as an internal standard.

### 3.3.11. Further Optimisation

After carrying out these reactions, the solubility of the potassium carbonate was considered problematic, as pre-stirring the catalyst in base and transferring it to the reaction still gave a 13% conversion to product. Triethylamine was soluble in this solvent combination and, since it was used successfully for the benzoin condensation (Table 15), would be a useful base in both sequential reactions. Using acetone as the solvent further improved the conversion (entry 4) without producing any aldol products as previously found using less strict inert conditions (Figure 49). Adding base from the start of the reaction gave a higher conversion than a delayed addition (entries 1 and 2). The reaction concentration was investigated and 63 mM of substrate in acetone was the optimal concentration (entry 6). Even at room temperature, the reaction reached 18% conversion (entry 7). The catalyst loading was then investigated, which showed that halving the amount of catalyst more than halved the conversion (entry 10), whilst doubling the amount had little effect (entry 11). With excess catalyst, dimer formation could become a process whereby the amount of active catalyst is decreased, resulting in a poorer yield. However, the solubility of the catalyst may have been a problem, as a further equivalent of base was required to make the reaction homogeneous. The repeat reaction (entry 9) gave a lower conversion than previously (entry 6), which shows that the catalyst may be more sensitive to the reaction conditions than previously thought. This could be due to the sensitivity of the catalyst to oxygen and/or water. The rate of reaction shows almost second order kinetics (Figure 58).



**Table 24** Catalysts tests investigating the amount of acetone and catalyst loading.



Entry	Catalyst Loading (x mol%)	Acetone (y mL)	Conversion (%) <sup>a</sup>
1	5.0	2	47 <sup>b</sup>
2	5.0	2	51
3	5.0	4	62
4	5.0	4	18 <sup>c</sup>
5	5.0	6	58
6	5.0	4	48
7	2.5	4	22
8	10.0	4	47 <sup>d</sup>

<sup>a</sup> Conversion calculated at 24 hours using GC from the corrected peak integrals with biphenyl as an internal standard. <sup>b</sup> Base added after 1 hour. <sup>c</sup> Reaction carried out at room temperature. <sup>d</sup> Reaction turned pale yellow with one equivalent of base, after 1 hour a second equivalent of base added, reaction returned to a pink solution.

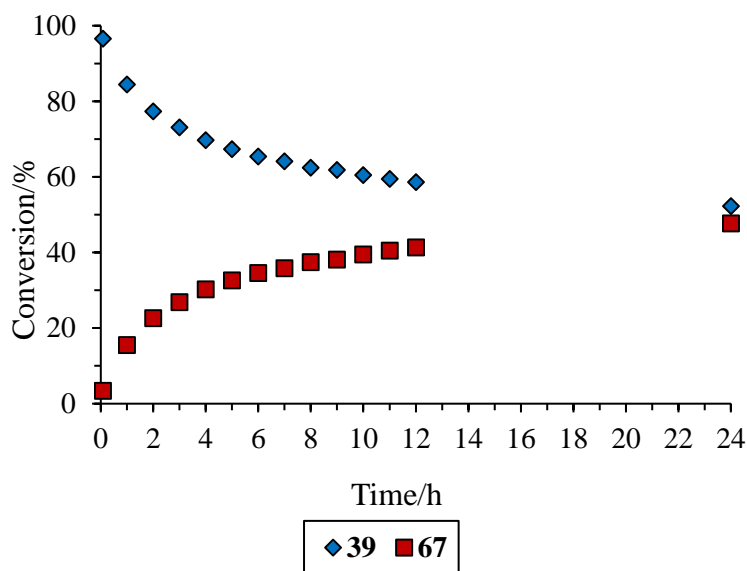


**Figure 58** The optimised catalyst test with **C.3** followed using GC, with biphenyl as an internal standard (entry 6, Table 24).

For comparison, the same reaction with **36** as the catalyst was carried out (Figure 59). The reaction was monitored using GC and the conversion reached 77% after 24 hours. There was a very fast initial rate then the conversion plateaus.

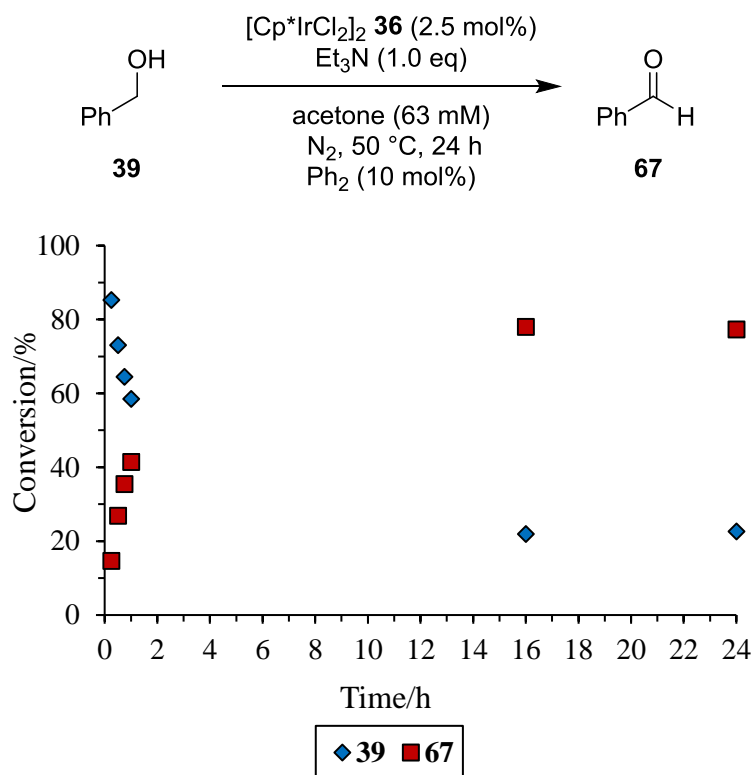


**Figure 59** Catalyst control test with **36** with inert conditions.

To investigate if adding acetonitrile would affect the reaction, an experiment was started in acetone and acetonitrile was added after 1.5 hours; the rate slowed and the conversion after 24 hours was 10% lower (Figure 60). Acetonitrile can coordinate to the metal centre and possibly block the vacant sites needed for catalysis to occur.

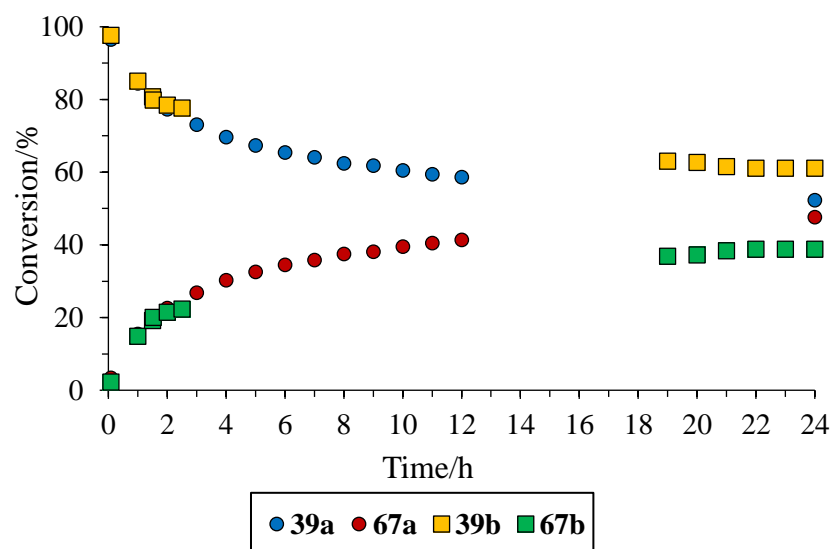


**Figure 60** Transfer dehydrogenation of **39** without (**39a/67a**) and with (**39b/67b**) the addition of MeCN at 1.5 hours.

An experiment was monitored using  $^1\text{H}$  NMR spectroscopy, carried out at room temperature without mixing (Figure 61). The conversion reached 6% after 24 hours and the initial rate is three times faster than the second part of the reaction. This test again shows that the catalyst continues to turn-over at least for 24 hours.

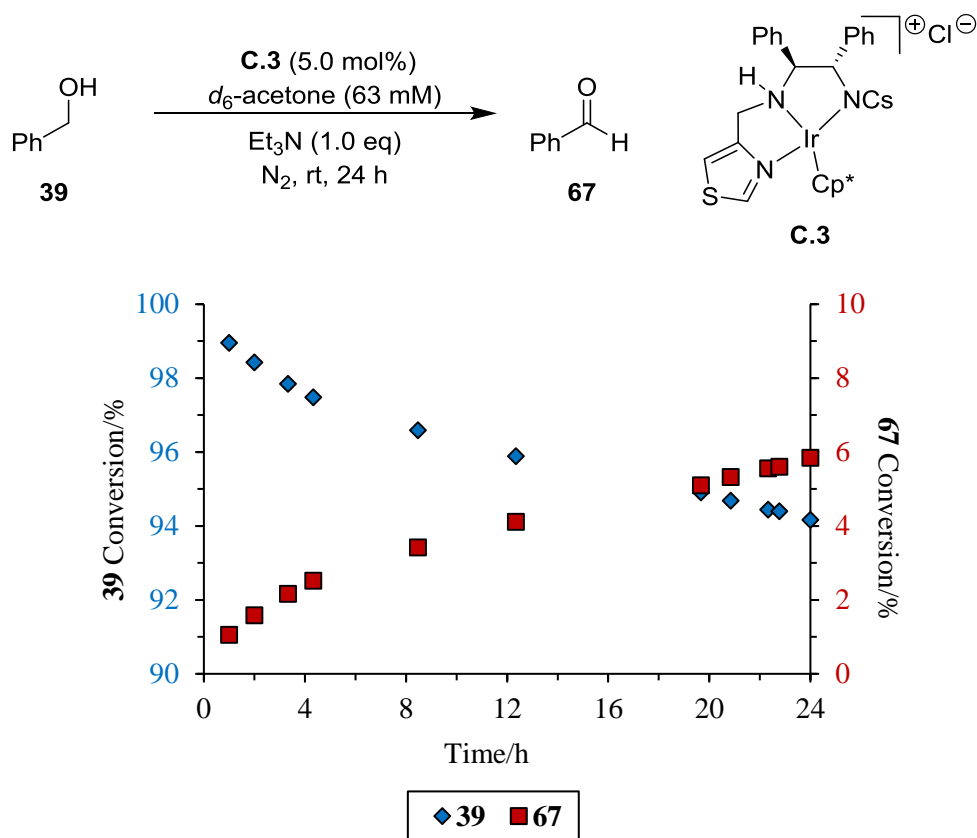


**Figure 61** Transfer dehydrogenation of **39** followed using  $^1\text{H}$  NMR in  $d_6$ -acetone.

### 3.3.12. Transfer Dehydrogenation Comparison of All Complexes

To compare their activities, all of the thiazole, triazole and control complexes that were synthesised in Chapter 2 (Figure 63) were tested with the best conditions identified:  $\text{Et}_3\text{N}$  (1.0 eq), acetone (63 mM),  $\text{N}_2$ ,  $50\text{ }^\circ\text{C}$ , 24 h. The reactions were carried out under a nitrogen atmosphere using a Radleys carousel reactor, which provides even heating and stirring for all the reactions (Figure 62).

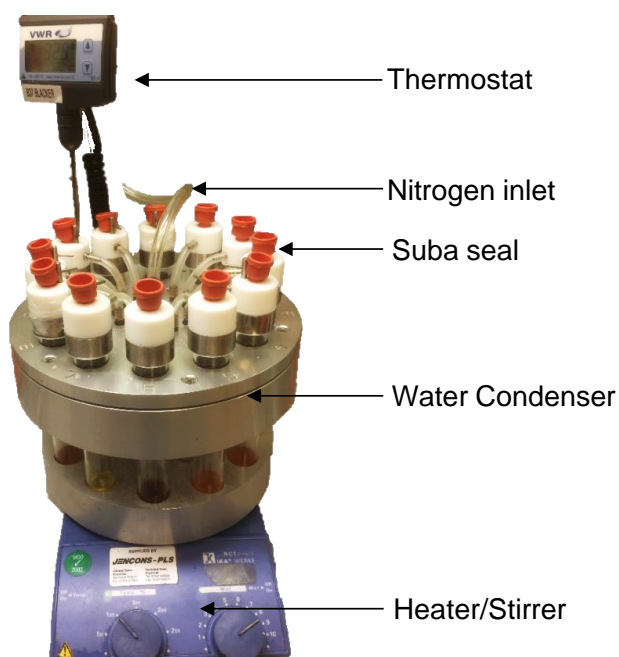


**Figure 62** Radleys carousel reactor with twelve reaction tubes.

Each of the reactions were tested in duplicate and the 24 hour conversion was measured using both GC and  $^1\text{H}$  NMR spectroscopy (Figure 64). Overall, the duplicate results are in good agreement, and the conversion calculated from the GC data is marginally higher compared to the  $^1\text{H}$  NMR spectroscopy data. The control reaction with catalyst **36** gives the best conversion. The CsDPEN complex **62** performs moderately, and the TsDPEN and benzyl tethered complexes **161** and **168** perform poorly. Interestingly, complex **C.3**, which was used to improve the reaction conditions, performed three times less well than previously in a Schlenk tube. This could be due to a less strict nitrogen atmosphere in the carousel tubes. The best catalyst was the monodentate complex **C.4**, with a comparable conversion to **36**. The *bis*-thiazole complex **C.6** and triazole complexes **C.11** and **C.13** performed well, with conversions above 50%. A possible issue with the monodentate complexes is whether the ligand is being displaced and the catalyst **36** is responsible for the high conversion. However, the other monodentate complex **C.7.2** performed badly. All thiazolium/triazolium complexes gave very low conversions, except for **C.12** (10%), and there were no other products observed in the reactions.

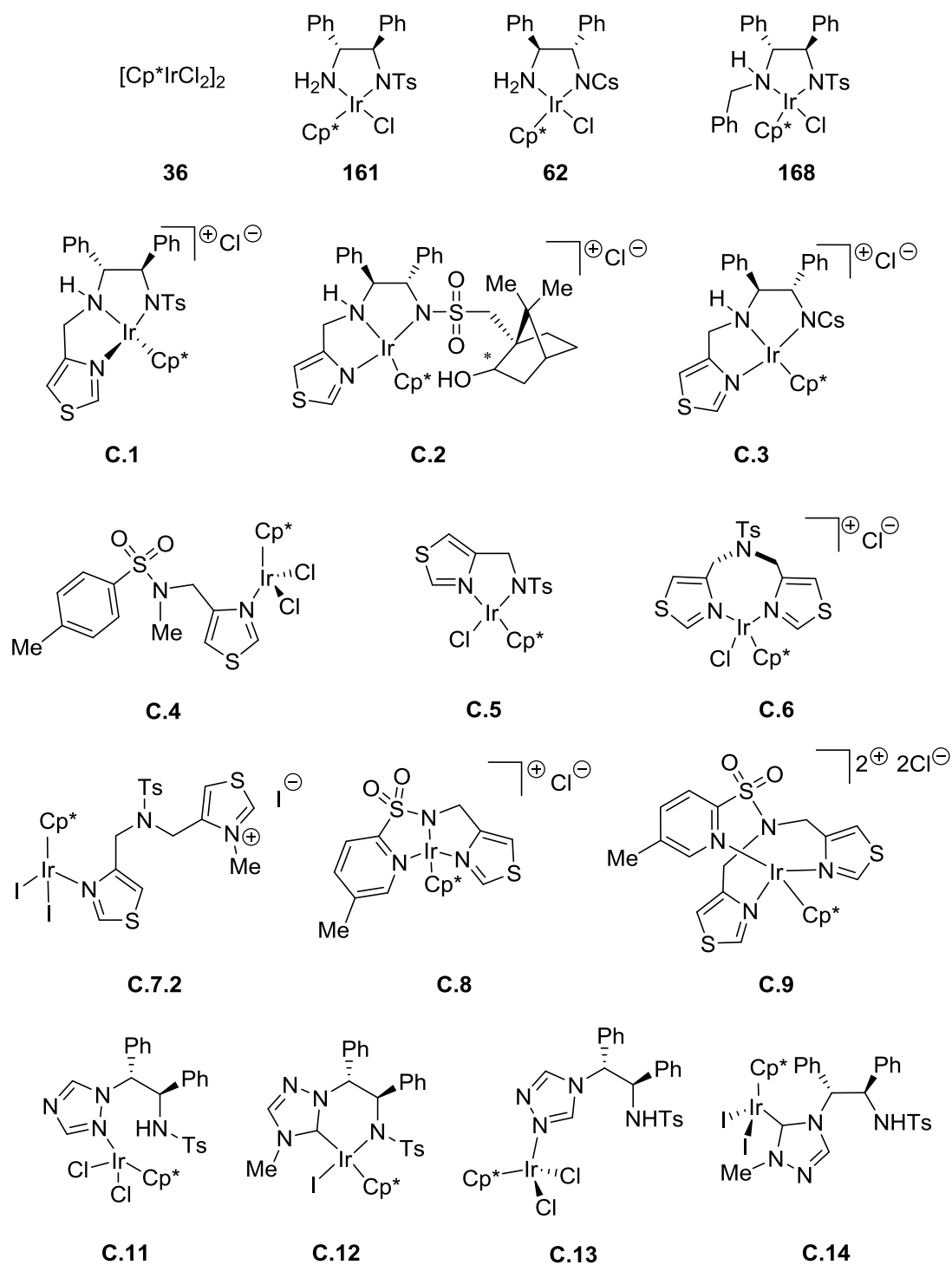


**Figure 63** The control, thiazole and triazole complexes that were compared in the carousel reactions.

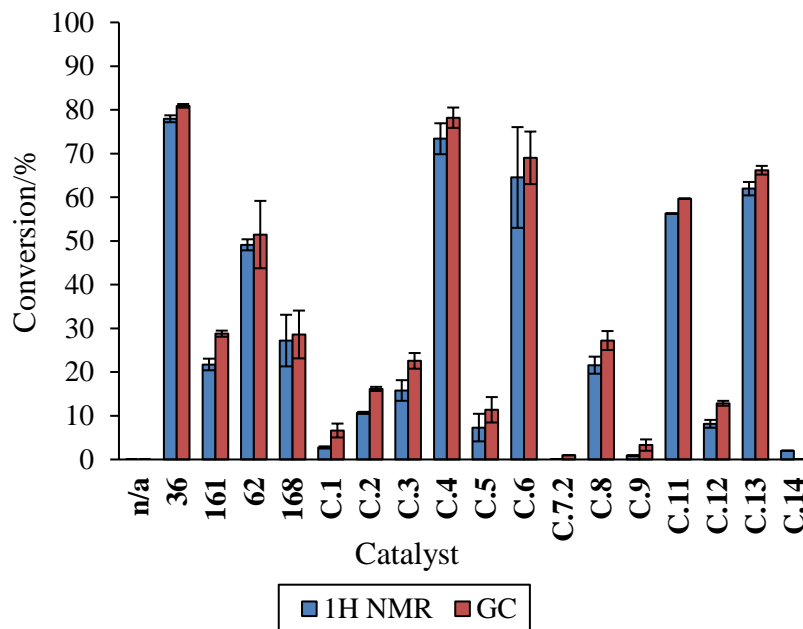
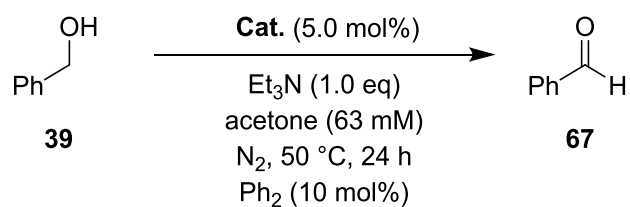


**Figure 64** The average conversions of the duplicate catalyst tests for the transfer dehydrogenation of **39**, analysed using GC (with biphenyl as an internal standard) and <sup>1</sup>H NMR spectroscopy (with mesitylene as an external standard). The error bars are the standard deviation of the duplicate results.

### 3.3.13. Transfer Hydrogenation Comparison with All Complexes

The thiazole, triazole and control complexes were also tested for the transfer hydrogenation of **67** with *iso*-propanol as the hydrogen donor (Figure 65).

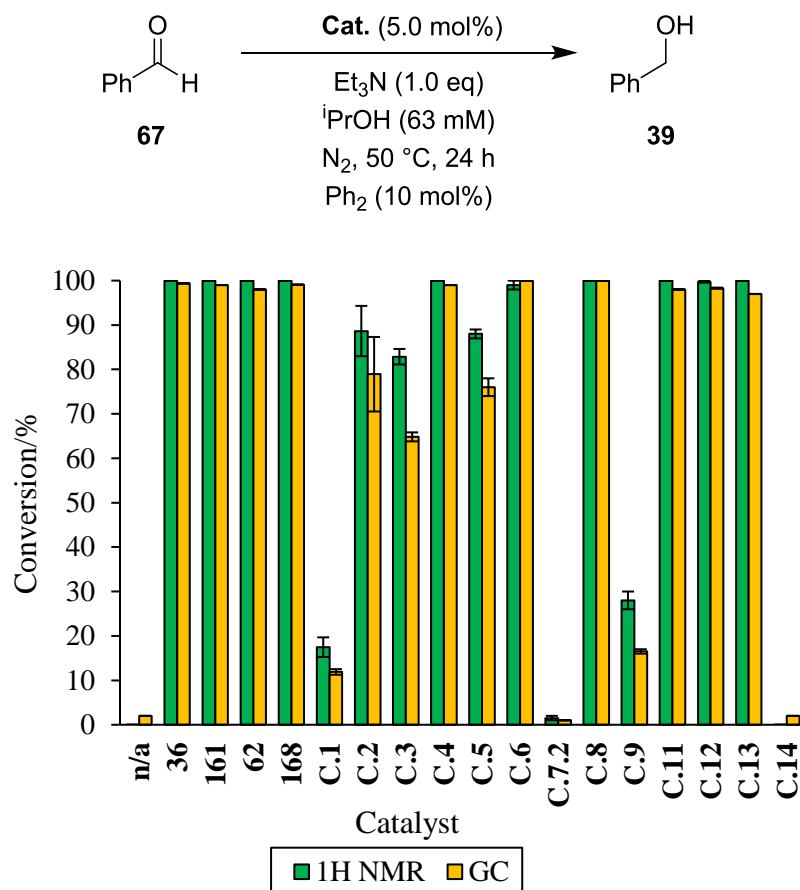


**Figure 65** The average conversions of the duplicate catalyst tests for the transfer hydrogenation of **67**, analysed using GC (with biphenyl as an internal standard) and <sup>1</sup>H NMR spectroscopy (with mesitylene as an external standard). The error bars are the standard deviation of the duplicate results.

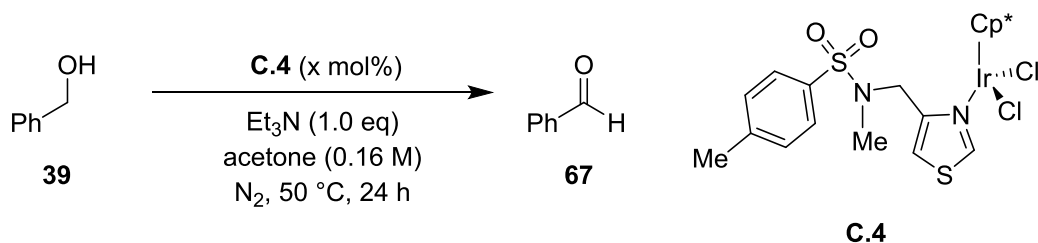
All the control catalysts and most of the novel catalysts transformed **67** to **39** with high to quantitative conversions and the duplicates were in good agreement. Even the triazolium complex **C.12** was successful compared to only 10% conversion in the transfer dehydrogenation reaction (Figure 64). Complexes **C.1**, **C.7.2**, **C.9** and **C.14** gave low conversions, as with the transfer dehydrogenation reaction. These results indicate that the equilibrium between the hydrogen transfer reactions lies towards the primary alcohol, despite a large excess of the hydrogen acceptor in the reactions with acetone as a solvent. Benzoin was not observed in any of these reactions.



### 3.3.14. Transfer Dehydrogenation Catalyst Loading Comparison

As complex **C.4** gave the best results, the catalyst loading was investigated for the transfer dehydrogenation reaction (Table 25). As expected, the conversion decreased with catalyst loading. The reactions were followed using  $^1\text{H}$  NMR spectroscopy (Figure 66).

**Table 25** The catalyst tests with varied catalyst loadings.



Entry	Catalyst Loading (x mol%)	Conversion (%) <sup>a</sup>
1	5.00	73 <sup>b</sup>
2	3.60	62
3	0.90	55
4	0.18	37

<sup>a</sup> Conversion calculated from the  $^1\text{H}$  NMR spectra with 0.17 M mesitylene in  $\text{CDCl}_3$  as an external standard.

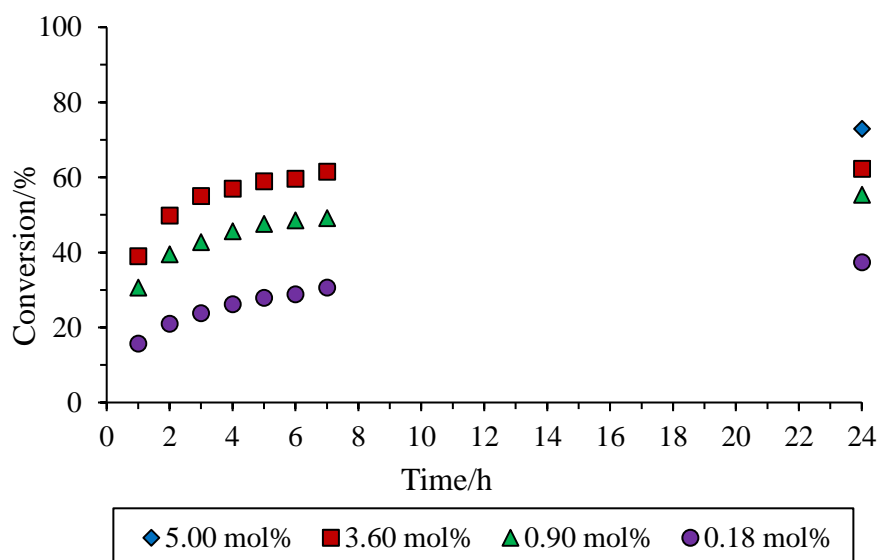
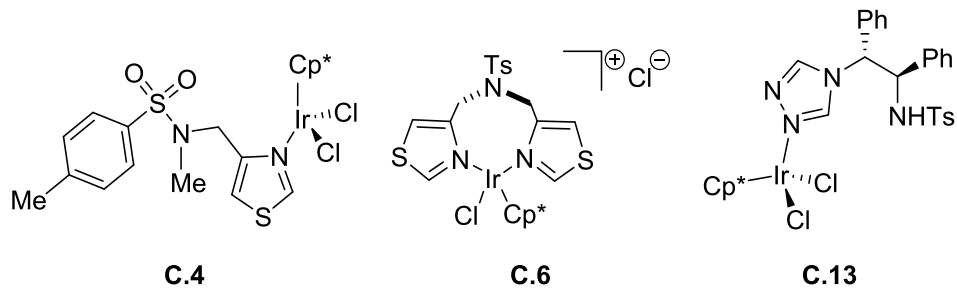
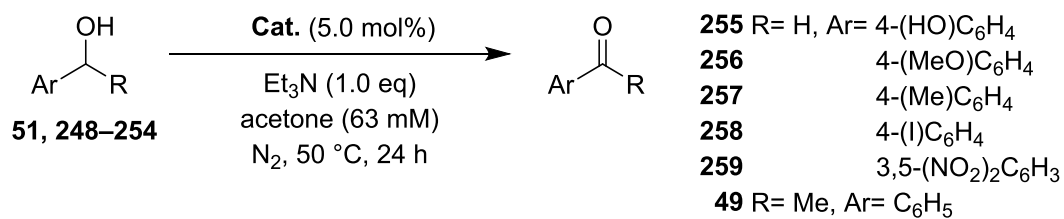


**Figure 66** The conversion calculated from  $^1\text{H}$  NMR spectroscopy with mesitylene as an external standard of **39** to **67** with varied catalyst loading (mol%). The 5.00 mol% result was taken from a previous experiment (Figure 64).

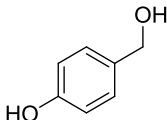
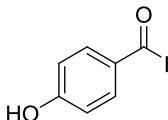
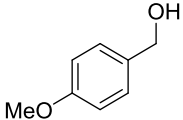
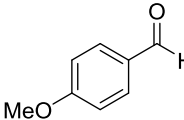
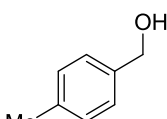
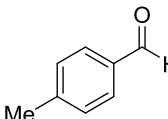
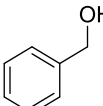
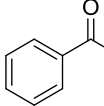
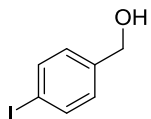
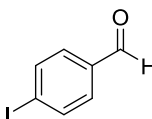
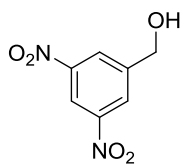
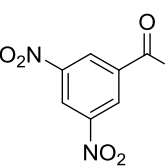
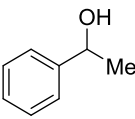
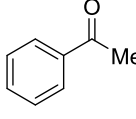
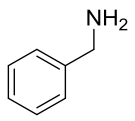
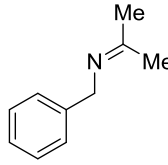
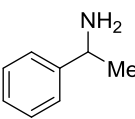
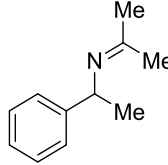
### 3.4. Transfer Dehydrogenation of Benzyl Alcohol Derivatives

Having identified the best performing catalysts, a range of substituted benzylic alcohols were tested to look at the effect of increasing the electron donating or withdrawing power of the substituents on the ring (Scheme 123, Table 26). The conversion is higher for electron rich substrates (entries 1–3) and had a decreasing trend towards the electron poor alcohols with 1,3-dinitrobenzyl alcohol failing to give any product (entry 6); this trend follows that reported by Fujita.<sup>130</sup> The conversions with **C.13** were lower than **C.4** and **C.6**, however the trend showed similar electronic effects. The results for the hydroxyl and methyl substrates were lower than expected, based on the conversion of **39**. A secondary alcohol, 1-phenylethanol **51**, was also tested and reached quantitative conversion with catalyst **C.4** (entry 7). This result was interesting, as the extra methyl group is only a small steric difference, but the redox potential of primary alcohol oxidation is higher than secondary alcohols.<sup>147</sup> The reverse reaction could be slower with acetophenone as it is less electrophilic than benzaldehyde, with the equilibrium in favour of the product.



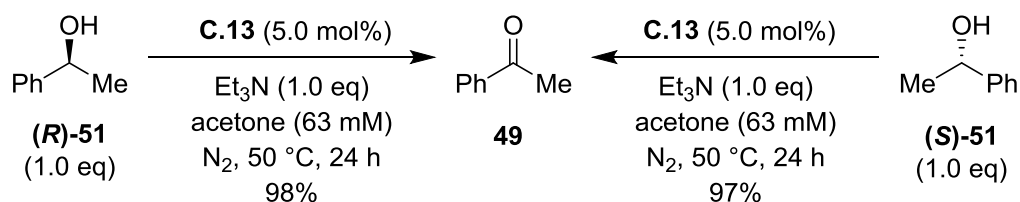
**Scheme 123** The catalysts and conditions used to test the varied benzylic alcohols **248–254** in Table 26.

**Table 26** Transfer dehydrogenation with catalysts **C.4**, **C.6** and **C.13**.

Entry	Substrate	Product	Conversion (%) <sup>a</sup>		
			C.4	C.6	C.13
1			99 <sup>b</sup>	97 <sup>b</sup>	60 <sup>b</sup>
2			97	97	69
3			89	84	45
4			78	69	60
5			50	40	13
6			0 <sup>b</sup>	0 <sup>b</sup>	0 <sup>b</sup>
7			100	-	52
8			0 <sup>c</sup>	-	-
9			0 <sup>c</sup>	-	-

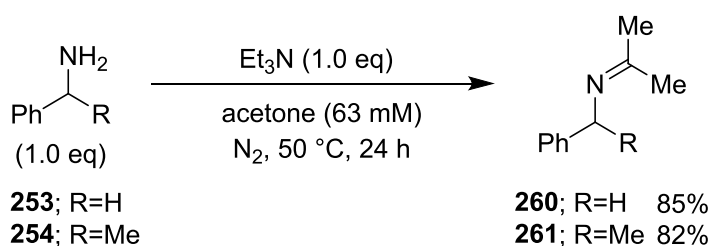
<sup>a</sup> Conversion calculated from the <sup>1</sup>H NMR spectra with 0.17 M mesitylene in CDCl<sub>3</sub> as an external standard. <sup>b</sup> 0.17 M mesitylene in d<sub>6</sub>-acetone used as an external standard. <sup>c</sup> Substrate condensed with acetone; no oxidation product observed.

With catalyst **C.13** the conversion only reaches 52% (entry 7); this is interesting, because **C.13** has a chiral backbone, and since a racemic mixture of 1-phenylethanol was used, a selective catalyst would only give a 50% conversion. Two parallel reactions were carried out with the different enantiomers of the substrate and both reached the same conversion, suggesting the oxidation was not enantioselective (Scheme 124). The conversions were higher in these reactions as they were carried out in Schlenk tubes with a strict nitrogen atmosphere, again suggesting there is a possible sensitivity of the complexes to air or moisture.



**Scheme 124** Catalyst tests with the two enantiomers of **51**, both reaching near quantitative conversion with catalyst **C.13** in Schlenk tubes.

Benzylamine **253** and 1-phenethylamine **254** did not react as hoped, however, they did react with acetone to produce benzyl ketimines **260** and **261** (entries 8 and 9). However, the same reactions were repeated without catalyst and shown to give the same conversions (Scheme 125).

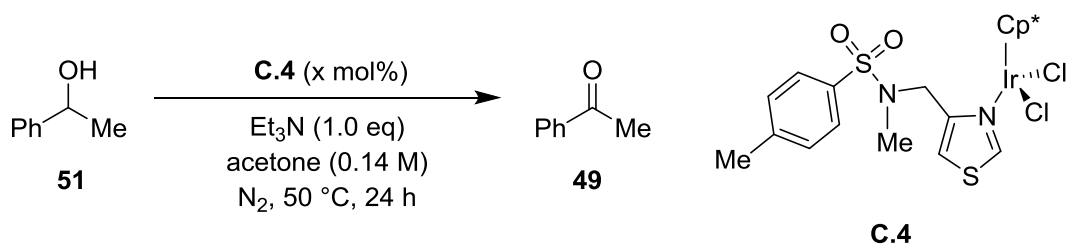


**Scheme 125** Control test for the background reaction of substrates **253** and **254** with acetone in the absence of a catalyst to produce imines **260** and **261** respectively.

### 3.4.1. Transfer Dehydrogenation of 1-Phenylethanol **51**

For comparison against **39**, the catalyst loading was investigated with **51** (Table 27). With only 0.2 mol% of catalyst **C.4**, the reaction proceeded to 93% after 24 hours (entry 3). The reactions were followed using  $^1\text{H}$  NMR spectroscopy (Figure 67). The initial rates of the dehydrogenation reactions for both the production of **49** and **67** were plotted against the concentration of catalyst **C.4** (Figure 68). The initial rates of reaction to make **49** were three times higher than for making **67** at low catalyst concentration. At higher concentrations of catalyst the rate of reaction is much lower for both products, again suggesting catalyst dimer formation could be limiting the rate of reaction.

**Table 27** The transfer dehydrogenation of **51** with catalyst **C.4** with varied catalyst loadings.



Entry	Catalyst Loading (x mol%)	Conversion (%) <sup>a</sup>
1	5.00	100
2	1.00	97 <sup>b</sup>
3	0.20	93

<sup>a</sup> Conversion calculated from the  $^1\text{H}$  NMR spectra with 0.17 M mesitylene in  $\text{CDCl}_3$  as an external standard. <sup>b</sup> The average conversion of two results.

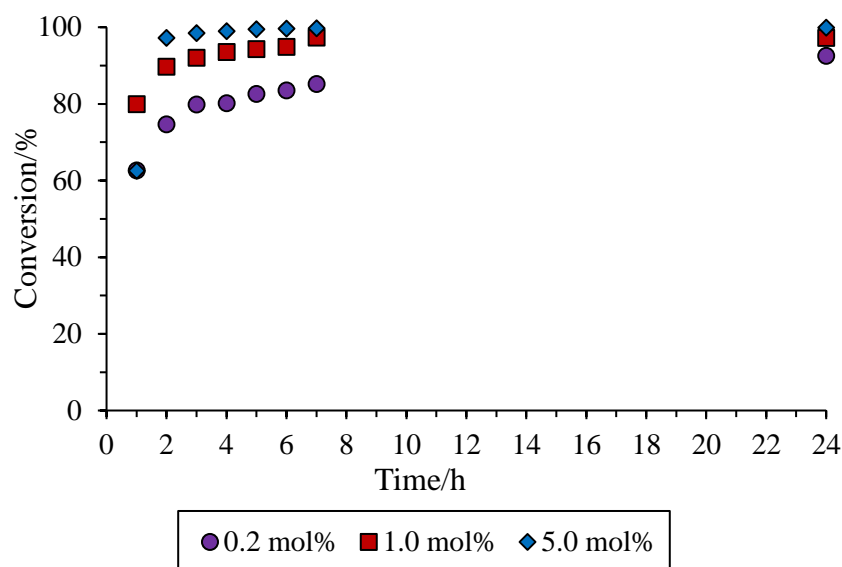


**Figure 67** The conversion calculated from  $^1\text{H}$  NMR spectroscopy with mesitylene as an external standard of **51** to **49** with varied catalyst loading (mol%).

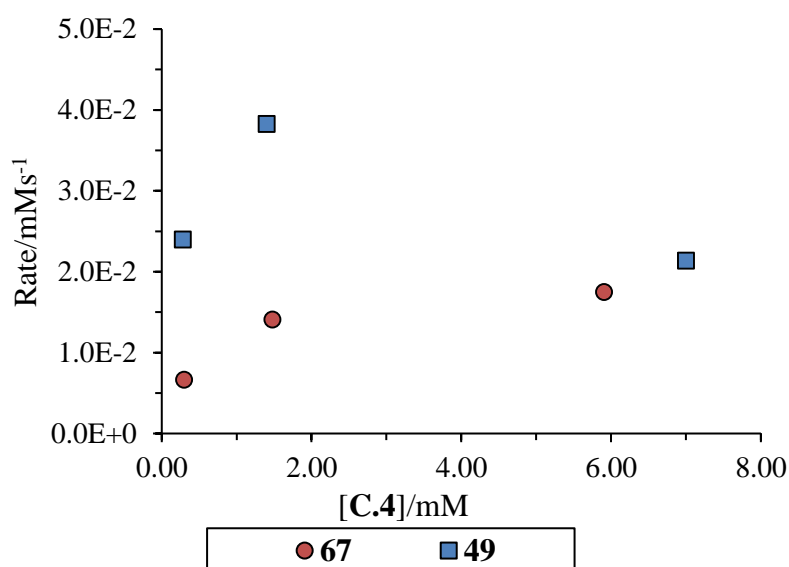


**Figure 68** The initial rate ( $\text{mM}\cdot\text{s}^{-1}$ ) of the dehydrogenation reactions to produce **67** or **49** against the concentration of catalyst **C.4** used (mM).

These results highlight how difficult the transfer dehydrogenation of **39** is in comparison to **51**. The equilibrium must be responsible for the difference in conversion. Frustratingly, the benzoin condensation reaction requires an aldehyde substrate to work, meaning the multifunctional catalysis sequence cannot be carried out from **51**.

### 3.5. Summary

This chapter has discussed the testing of the novel complexes synthesised in Chapter 2 for the transfer dehydrogenation of benzyl alcohol. Control tests were carried out to validate the reaction sequence for multicycatalysis, and the one-pot reaction showed that thiazolium compounds inhibit the transfer dehydrogenation of benzyl alcohol. The competition between the transfer dehydrogenation reaction and the aldol background reaction was investigated. The amount of acetone in the reactions was decreased to prevent the aldol reaction, however the conversion suffered. Experiments were conducted with increasing amounts acetone, which prevented the aldol reaction from occurring. The benzoin reaction was not successful with the iridium(III) complexes, even though the thiazole/thiazolium ligand **L.7** was a good organocatalyst for the reaction.

Hexamethylacetone was investigated as an alternative hydrogen acceptor, but performed poorly, even at higher temperatures. An experiment to trap the aldehyde product to drive the equilibrium to the aldehyde using sodium bisulfite was attempted, however the solubility of the salt prevented any adduct formation. The possibility of catalyst deactivation was negated with a substrate addition experiment showing a continually increasing concentration of aldehyde. Distillation to remove *iso*-propanol from the reaction was attempted, however the conversion was low.

Switching the solvent back to acetone under strictly inert and dry conditions prevented the aldol reaction from occurring and increased the conversion to 50% with **C.3**. Using soluble triethylamine improved the conversion over using potassium carbonate. Using the best conditions, all of the complexes prepared in Chapter 2 were compared against the control catalysts, and the highest conversion was found with monodentate thiazole complex **C.4**. A small substrate scoping set of reactions was carried out with the best three complexes and the more electron rich benzylic alcohols were found to be more easily oxidised. A secondary alcohol, which is unable to be used as a substrate for the organocatalyst, was also tested and found to give quantitative conversion; suggesting that the reverse reaction is slower than compared to benzaldehyde. Neither benzylamine nor 1-phenethylamine were converted to the desired imines (or dimers as expected), but reacted with acetone to form



benzyl ketimines. The catalyst loadings for the dehydrogenation of benzyl alcohol and 1-phenylethanol were investigated, with the conversion decreasing with catalyst loading. 1-Phenylethanol can reach 93% conversion with only 0.2 mol% of catalyst **C.4**. The initial rates of reaction for benzyl alcohol were found to be three times slower compared to 1-phenylethanol. At 5 mol% catalyst loading, both substrates showed a slower initial rate.

## 4. Conclusions and Future Work

The ability to use a single multifunctional catalyst to compress multiple steps into a single catalysed reaction is advantageous, and would improve the removal and recyclability of the catalyst from a reaction. There is an inherent challenge in creating a multifunctional catalyst, due to the nature of combining different catalysts that are aimed specifically at a selected reaction sequence, and the need to prevent intermediates reacting with the wrong active site. In addition, the substrate scope is narrowed, as only the substrates that can enter both catalytic cycles will give the desired products and both catalysts have to work in the same reaction conditions. There are very few examples of successful multifunctional catalysts in the literature, and those reported are made up of organo-organo-catalysts<sup>33</sup> or metal-metal catalysts<sup>35</sup>.

This project has developed an organo-organometallic multifunctional catalyst based on an iridium(III) hydrogen transfer catalysts and a thiazolium or triazolium benzoin condensation catalysts. A family of novel thiazole iridium(III) complexes and a family of triazole iridium(III) complexes were prepared and analysed using mass spectroscopy and NMR techniques, with x-ray crystal structures obtained where possible.

The complexes were shown to be active for the dehydrogenation of benzyl alcohol to benzaldehyde, with monodentate thiazole complex **C.4** performing on par with the control catalyst  $[\text{Cp}^*\text{IrCl}_2]_2$ . However, the benzoin condensation was not catalysed by any of the complexes. The structural features of the early complexes were based on well-studied TsDPEN and CsDPEN organometallic catalysts, which are bidentate, and transformed into tridentate complexes with a tethered thiazole ring. These complexes are coordinatively and electronically saturated, and therefore catalyst activity requires one of the donors to dissociate to allow the dehydrogenation of the alcohol substrate. Following on from this design, monodentate and bidentate complexes were prepared with less steric encumbrance around the metal centre. However, the chelate strength of the ligands suffers with fewer donors. A pyridine side chain was then introduced to add another donor that could coordinate to the metal centre and allow a thiazolium to be available; however, the *bis*-thiazolium-pyridine

complex was unstable and decomposed. This highlighted the unfortunate leaving group ability of thiazoliums, as found during the synthesis of other thiazolium salts.

X-ray crystallography confirmed that the thiazole ring coordinated to the metal centre as designed, which was hoped that the  $pK_a$  of the thiazole would drop as electron density was donated to the metal centre. The acidity of the thiazole was believed to be one of the main reasons that the benzoin condensation reaction failed to work, therefore the ligand designs were focussed on thiazolium rings, which have a more accessible  $pK_a$ . This was confirmed with a successful benzoin condensation using thiazolium ligand **L.7**. Unfortunately, the thiazolium-iridium(III) complexes were not organo-catalytically active. To further increase the acidity of the organocatalyst, triazole and triazolium complexes were made. The triazoliums both formed carbene complexes with the metal centre and therefore unable to catalyse the benzoin condensation.

The transfer dehydrogenation reactions were investigated and the limited conversions were believed to be the result of an equilibrium that was heavily one-sided towards the substrate, and methods to push the equilibrium to the product were unsuccessful. The distillation set-up used to remove *iso*-propanol from the reaction using acetonitrile as the solvent, could be further developed with acetone as the solvent and allow addition of acetone only. This could help to drive off *iso*-propanol and stop the reverse reaction. Catalyst deactivation or dimerization could be a cause of low turn-over numbers, therefore improving the complex robustness or the steric bulk about the metal centre could increase the amount of active catalyst in the reactions. Kinetic modelling could be employed to investigate the mechanism of the dehydrogenation reaction with these complexes under these conditions. The results of the transfer hydrogenation tests were interesting, as the majority of the novel complexes reached quantitative conversions. This suggests the catalysts are able to turn-over effectively under these conditions and demonstrated the difficulty faced with the equilibrium for the dehydrogenation reactions.

The substrate scope identified that the more electron rich benzylic alcohols were more easily oxidised. The amines tested in the substrate scope did not form imines as desired, but reacted with acetone to form ketimines. However, cyclic amines could be dehydrogenated more readily, as they should not react favourably with acetone in the reactions.

Since the first step in the reaction sequence had been developed, the future work of this project would be the development of the benzoin condensation, possibly by designing a complex with a more defined steric bulk around the organocatalyst centre that would completely prevent carbene-iridium coordination or dimerization, which was believed to be a cause of inactivity.

The organocatalyst has other reactivities that could be utilized with a working multifunctional catalyst for other reaction sequences. Decarboxylation reactions can be catalysed with TPP in enzyme reactions, which could be coupled with hydrogen transfer reactions to make aromatic aldehydes from  $\alpha$ -hydroxy-carboxylic acids. The aldehydes could then follow the benzoin condensation route and achieve a four-step reaction sequence.

Enzymes have been developed by nature over time, and the ability of allosteric enzymes to alter their shape and conformation with specific receptors is yet to be adopted by organometallic catalysis. A carbene that is available at the centre of a catalyst could act as a receptor for aldehydes or ketones whilst a metal catalysed reaction occurs at another functional group on the substrate, perhaps aiding C-H activation for alkane dehydrogenation.

Another route that could be ventured could be the combination of two immobilised catalysts, on either the same surface or separate surfaces, and conducting reactions in batch or continuous flow apparatus. This method could allow for the exchange and/or mixing of the types of catalyst required.

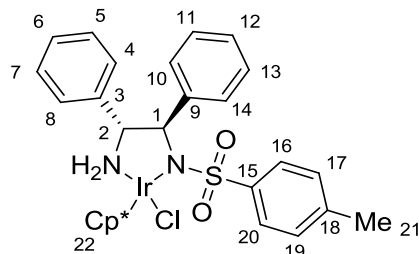
## 5. Experimental

### 5.1. General Experimental

All reagents were used as received from commercial suppliers. NMR spectra were recorded on a Bruker DX300 spectrometer operating at 300 MHz ( $^1\text{H}$  NMR), or on a Bruker AVANCE III 300 operating at 300 MHz ( $^1\text{H}$  NMR), or on a Bruker AVANCE III HD-400 spectrometer, operating at 400 MHz ( $^1\text{H}$  NMR) and 101 MHz ( $^{13}\text{C}$  NMR), or on a Bruker Avance 500 spectrometer operating at 500 MHz ( $^1\text{H}$  NMR) and 126 MHz ( $^{13}\text{C}$  NMR). High resolution mass spectra were recorded on a Bruker MaXis Impact ESI spectrometer or on an Agilent 1200 LC and Bruker Daltonics HCT Ultra Ion Trap MS LCMS system. Elemental analyses were carried out in a Carlo Erba 1108 Elemental Analyzer. Melting point analysis was carried out on a Stuart Melting Point SMP30 and infra-red spectroscopy was carried out on a Bruker Platinum-ATR Alpha. Specific rotations were measured on a Schmidt & Haensch Polartronic H532. Gas chromatography was carried out with a HP6890 series GC system, with an FID detector and hydrogen flow gas. Gas chromatography mass spectrometry was carried out with a HP6890 series GC system with a HP5973 mass selective detector and helium flow gas. A 30 m long, 320  $\mu\text{m}$  diameter HP-5 column was used for both GC and GCMS with an oven temperature of 60  $^\circ\text{C}$ , a ramp of 15  $^\circ\text{C}/\text{min}$  to 140  $^\circ\text{C}$  and then 30  $^\circ\text{C}/\text{min}$  to 280  $^\circ\text{C}$ . Heterogeneous GC samples were filtered through a plug of celite prior to loading. HPLC data was obtained using an Agilent 1100 HPLC with a DAD and the data was processed with Chemstation software. X-ray measurements were carried out at 120K on an Agilent SuperNova diffractometer equipped with an Atlas CCD detector and connected to an Oxford Cryostream low temperature device using mirror monochromated Mo  $K_\alpha$  radiation ( $\lambda = 0.7107 \text{ \AA}$ ) or Cu  $K_\alpha$  radiation ( $\lambda = 1.54184 \text{ \AA}$ ) from a Microfocus Mova X-ray source. Petrol refers to petroleum ether (40–60  $^\circ\text{C}$ ). Assignment of NMR signals for novel compounds were aided with the following techniques:  $^{13}\text{C}$   $\{^1\text{H}\}$  DEPT135,  $^1\text{H}$  COSY, HMQC and HMBC. Carbon atoms are numbered to aid NMR assignment. All solvents in reactions carried out under nitrogen were collected from a solvent purification system and degassed prior to use.

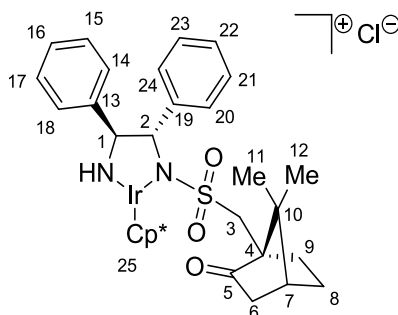
## 5.2. Control Compounds

### 5.2.1. Synthesis of Chloro[(*R,R*)-*N*-{(1,2-diphenyl-2-amino)-ethyl}-*p*-toluenesulfonamide]( $\eta^5$ -pentamethylcyclopentadienyl)iridium(III) **161**



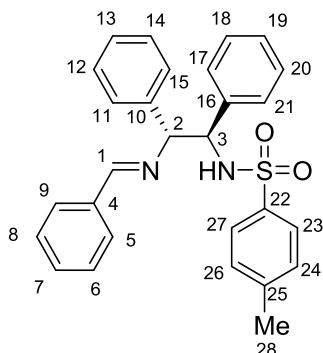
Following a modified procedure from Blacker and Mellor,<sup>47</sup> triethylamine (39  $\mu$ L, 0.28 mmol, 4.00 eq) was added to a stirred solution of (*R,R*)-**162** (50 mg, 0.14 mmol, 2.00 eq) and **36** (54 mg, 0.07 mmol, 1.00 eq) in *iso*-propanol (5 mL) and stirred at 40 °C for 16 hours. The solvent was removed from the brown solution to give a brown crystalline solid (60 mg, 0.08 mmol, 59%). mp; 130.3–131.6 °C. ESIMS  $m/z = M^+ - Cl$  693.2020, Theoretical Mass = 693.2127. <sup>1</sup>H NMR (500 MHz, CDCl<sub>3</sub>)  $\delta$ : 7.40 (d,  $J = 8.1$  Hz, 2H, *CH*-16/20), 7.22 – 7.06 (m, 2H, *CH*-5/7), 6.92 – 6.78 (m, 8H, *CH*-Ph), 6.64 (d,  $J = 7.4$  Hz, 2H, *CH*-10/14), 4.52 – 4.31 (m, 2H, *NH*<sub>2</sub>), 4.30 (d,  $J = 10.8$  Hz, 1H, *CH*-1), 3.68 (t,  $J = 10.8$  Hz, 1H, *CH*-2), 2.23 (s, 3H, *CH*<sub>3</sub>-21), 1.84 (s, 15H, *CH*<sub>3</sub>-22). <sup>13</sup>C NMR {<sup>1</sup>H} (126 MHz, CDCl<sub>3</sub>)  $\delta$ : 140.62 (*C*-15), 139.55 (*C*-18), 138.91 (*C*-9), 138.69 (*C*-3), 128.76 (*C*-10/14), 128.61 (*C*-5/7), 128.50 (*C*-6), 128.44 (*C*-16/20), 127.87 (*C*-17/19), 127.13 (*C*-4/8), 127.03 (*C*-11/13), 126.54 (*C*-12), 85.59 (*C*-22), 74.09 (*C*-2), 69.58 (*C*-1), 21.23 (*C*-21), 8.76 (*C*-22). IR (cm<sup>-1</sup>): 3226, 3028, 2978, 2914, 2603, 2497, 1598, 1475, 1445, 1331, 1159. Spectral data is consistent with the literature.<sup>148</sup>

### 5.2.2. Synthesis of Chloro[(*S,S,S*)-*N*-{(1,2-diphenyl-2-amino)-ethyl}-camphorsulfonamide]( $\eta^5$ -pentamethylcyclopentadienyl)iridium(III) **62**



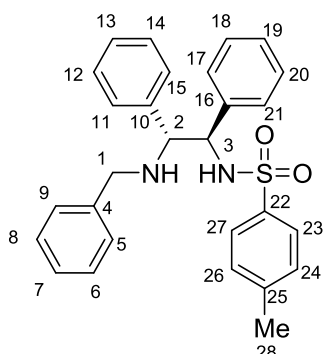
Following a modified procedure from Blacker and Mellor,<sup>47</sup> Triethylamine (33  $\mu$ L, 0.24 mmol, 4.00 eq) was added to a stirred solution (*S,S,S*)-**163** (50 mg, 0.12 mmol, 2.00 eq) and **36** (47 mg, 0.06 mmol, 1.00 eq) in *iso*-propanol (5 mL) and stirred at 40 °C for 16 hours. The solvent was removed from the brown solution to give a brown crystalline solid (91 mg, 0.11 mmol, 96%). mp; 164.4–167.5 °C. ESIMS  $m/z = M^+ - Cl$  753.2569, Theoretical Mass = 753.2696. <sup>1</sup>H NMR (500 MHz, CDCl<sub>3</sub>)  $\delta$ : 7.26 – 7.07 (m, 10H, *CH*-Ph), 5.17 (s, 1H, *NH*), 4.86 (d,  $J = 9.8$  Hz, 1H, *CH*-1), 4.77 (s, 1H, *CH*-2), 3.35 (d,  $J = 14.7$  Hz, 1H, *CHH*-3), 2.69 (d,  $J = 14.7$  Hz, 1H, *CHH*-3), 2.36 – 2.20 (m, 2H, *CH*-6/9), 2.03 (t,  $J = 4.3$  Hz, 1H, *CH*-7), 1.99 – 1.91 (m, 2H, *CH*-6/8), 1.57 – 1.43 (m, 16H, *CH*<sub>3</sub>-25, *CH*-8), 0.85 (s, 3H, *CH*<sub>3</sub>-12), 0.74 (s, 3H, *CH*<sub>3</sub>-11). <sup>13</sup>C NMR {<sup>1</sup>H} (126 MHz, CDCl<sub>3</sub>)  $\delta$ ; 215.96 (*C*-5), 139.08 (*C*-19), 133.00 (*C*-13), 128.82 (*C*-21/23), 128.71 (*C*-22), 128.53 (*C*-20/24), 128.44 (*C*-14/18), 127.91 (*C*-16), 127.74 (*C*-15/17), 85.27 (*C*-25), 63.00 (*C*-1), 62.34 (*C*-2), 58.49 (*C*-4), 51.06 (*C*-3), 48.58 (*C*-10), 42.83 (*C*-6), 42.56 (*C*-7), 27.00 (*C*-8), 24.73 (*C*-9), 19.73 (*C*-11), 19.38 (*C*-12), 9.03 (*C*-25). IR (cm<sup>-1</sup>): 3470, 3216, 3062, 2958, 2916, 1742, 1576, 1495, 1454, 1376, 1143. The complex is known, but the spectral data has not been reported in the literature.<sup>48</sup>

### 5.2.3. Synthesis of (*R,R*)-*N*-{1,2-diphenyl-2-[(phenyl)methanimine]-ethyl}-*p*-toluenesulfonamide 166



**67** (300  $\mu$ L, 3.00 mmol, 1.1 eq) was added to a solution of (*R,R*)-**162** (1 g, 2.73 mmol, 1 eq) in toluene (10 mL) and stirred at reflux under nitrogen for 2 hours. The solvent was removed from the yellow solution to give a pale yellow solid (1.15 g, 2.53 mmol, 93% yield). ESIMS  $m/z = M^+ + H$  455.1802, Theoretical Mass = 455.1788.  $^1\text{H NMR}$  (500 MHz,  $\text{CDCl}_3$ )  $\delta$ : 7.82 (d,  $J = 7.5$  Hz, 2H, *CH*-23/27), 7.71 (d,  $J = 8.2$  Hz, 2H, *CH*-Ph), 7.43 (t,  $J = 7.7$  Hz, 2H, *CH*-Ph), 7.38 – 7.34 (m, 1H, *CH*-Ph), 7.27 (d,  $J = 8.1$  Hz, 2H, *CH*-Ph), 7.20 – 7.15 (m, 1H, *CH*-Ph), 7.13 (m, 5H, *CH*-Ph), 7.01 – 6.95 (m, 2H, *CH*-Ph), 6.88 (d,  $J = 7.5$  Hz, 2H, *CH*-Ph), 6.19 (s, 1H, *CH*-1), 4.59 (d,  $J = 7.8$  Hz, 1H, *CH*-2), 4.18 (d,  $J = 7.8$  Hz, 1H, *CH*-3), 4.04 (br s, 1H, S-NH), 2.44 (s, 3H, *CH*<sub>3</sub>-28).

### 5.2.4. Synthesis of (*R,R*)-*N*-{1,2-diphenyl-2-(benzylamino)-ethyl}-*p*-toluenesulfonamide 164

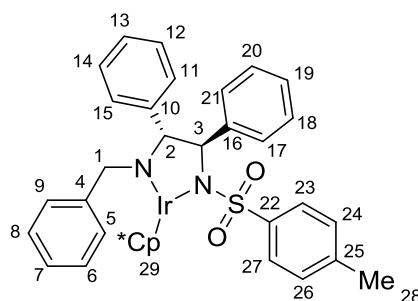


This compound is known in the literature. **67** (600  $\mu$ L, 6.00 mmol, 1.10 eq) was added to a solution of (*R,R*)-**162** (2.0 g, 5.45 mmol, 1.00 eq) in EtOH (20 mL) and stirred at reflux (82  $^{\circ}\text{C}$ ) under nitrogen. The reaction was followed by TLC



until the imine was formed after 2 hours. The reaction was cooled to room temperature, diluted with EtOH (20 mL) and NaBH<sub>4</sub> (311 mg, 8.72 mmol, 1.60 eq) was slowly added. The reaction was stirred for 16 hours, quenched with water (30 mL) and the organics were extracted with ethyl acetate (2 x 40 mL). The organic layer was dried with MgSO<sub>4</sub> and the solvent was removed *in vacuo* to give a colourless solid. The solid was recrystallized from ethyl acetate and petrol to give the product as colourless fine needles (1.87 g, 4.10 mmol, 75%). *R*<sub>f</sub> = 0.62 (ethyl acetate/petrol, 1:3), mp; 126.3–127.2 °C (Lit. 136–138 °C). ESIMS *m/z* = *M*<sup>+</sup>+*H* 457.1986, Theoretical Mass = 457.1944. <sup>1</sup>H NMR (300 MHz; CDCl<sub>3</sub>) δ: 7.36 (d, *J* = 8.3 Hz, 2H, *CH*-23/27), 7.27 (t, *J* = 6.9 Hz, 3H, *CH*-Ph), 7.22 – 7.11 (m, 5H, *CH*-Ph), 7.09 – 6.87 (m, 9H, *CH*-Ph), 6.17 (br s, 1H, *S*-*NH*), 4.31 (d, *J* = 7.7 Hz, 1H, *CH*-3), 3.68 (d, *J* = 7.7 Hz, 1H, *CH*-2), 3.62 (d, *J* = 13.2 Hz, 1H, *CHH*-1), 3.41 (d, *J* = 13.2 Hz, 1H, *CHH*-1), 2.31 (s, 3H, *CH*<sub>3</sub>-28), 1.68 (br s, 1H, amine-*NH*). <sup>13</sup>C NMR {<sup>1</sup>H} (126 MHz, CDCl<sub>3</sub>) δ; 142.72 (C<sub>0</sub>-Ph), 140.77 (C<sub>0</sub>-Ph), 139.38 (C<sub>0</sub>-Ph), 138.91 (C<sub>0</sub>-Ph), 138.27 (C<sub>0</sub>-Ph), 129.10 (C-Ph), 128.48 (C-Ph), 128.43 (C-Ph), 128.04 (C-Ph), 127.95 (C-Ph), 127.62 (C-*p*-Ph), 127.56 (C-Ph), 127.51 (C-Ph), 127.32 (C-*p*-Ph), 127.18 (C-*p*-Ph), 127.11 (C-Ph), 66.81 (C-2), 63.09 (C-3), 50.88 (C-1), 21.43 (C-28). IR (cm<sup>-1</sup>); 3246, 3060, 3026, 2926, 2846, 2815, 1600, 1489, 1456, 1433, 1322, 1156. Spectral data is consistent with the literature.<sup>97</sup>

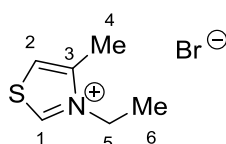
### 5.2.5. Synthesis of [(*R,R*)-*N*{1,2-diphenyl-2-(benzylamino)-ethyl}-*p*-toluenesulfonamide](η<sup>5</sup>-pentamethylcyclopentadienyl)iridium(III) **168**



Following a modified procedure from Wills,<sup>98</sup> triethylamine (14 μL, 0.10 mmol, 2.00 eq) was added to a red solution of **164** (23 mg, 0.05 mmol, 1.00 eq) and **36** (20 mg, 0.03 mmol, 0.50 eq, 1.00 eq Ir) in *iso*-propanol (1 mL) and stirred at 40 °C for 16 hours. The solvent was removed from the deep red solution *in*

*vacuo* to give a dark red powder. The powder was washed with water (1 mL) and dried *in vacuo* to give the product as a dark red powder (33 mg, 0.04 mmol, 84%). mp; 110.3–113.9 °C. ESIMS:  $m/z = M^+ + H$  783.2590, Theoretical Mass = 783.2591.  $^1H$  NMR (500 MHz,  $CDCl_3$ )  $\delta$ ; 7.58 (d,  $J = 7.2$  Hz, 2H, *CH*-23/27), 7.30 – 7.19 (m, 6H, *CH*-Ph), 7.10 – 7.05 (m, 4H, *CH*-Ph), 7.00 – 6.95 (m, 1H, *CH*-Ph), 6.86 (t,  $J = 7.6$  Hz, 2H, *CH*-Ph), 6.76 (d,  $J = 8.0$  Hz, 2H, *CH*-24/26), 6.43 (d,  $J = 7.5$  Hz, 2H, *CH*-Ph), 5.00 (d,  $J = 16.3$  Hz, 1H, *CH*-3), 4.29 (s, 1H, *CHH*-1), 3.98 (d,  $J = 16.3$  Hz, 1H, *CH*-2), 3.57 (s, 1H, *CHH*-1), 2.23 (s, 3H, *CH*<sub>3</sub>-28), 1.82 (s, 15H, *CH*<sub>3</sub>-29).  $^{13}C$  NMR  $\{^1H\}$  (126 MHz,  $CDCl_3$ )  $\delta$ ; 145.69 (*C*<sub>0</sub>-Ph), 142.78 (*C*<sub>0</sub>-Ph), 140.88 (*C*<sub>0</sub>-Ph), 140.19 (*C*<sub>0</sub>-Ph), 140.01 (*C*<sub>0</sub>-Ph), 128.41 (*C*-*p*-Ph), 128.27 (*C*-Ph), 128.00 (*C*-Ph), 127.89 (*C*-Ph), 127.33 (*C*-Ph), 127.28 (*C*-*p*-Ph), 127.08 (*C*-Ph), 127.04 (*C*-Ph), 126.62 (*C*-Ph), 126.15 (*C*-*p*-Ph), 125.91 (*C*-Ph), 86.29 (*C*-3), 85.54 (*C*-29), 64.27 (*C*-2), 45.92 (*C*-1), 25.35 (*C*-28), 8.71 (*C*-29). IR ( $cm^{-1}$ ); 3058, 3026, 2978, 2917, 2603, 2496, 1600, 1489, 1478, 1444, 1278, 1189.

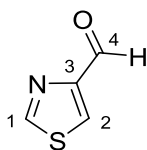
### 5.2.6. Synthesis of 3-Ethyl-4-methyl-1,3-thiazol-3-ium bromide **130**



**169** (5.0 mL, 55.0 mmol, 1.00 eq) was added to 1-bromoethane (4.5 mL, 60.0 mmol, 1.09 eq) and stirred at reflux under nitrogen for 20 hours. The white slurry was washed with EtOH (10 mL) to give a colourless solid, which was recrystallized in methanol to give **130** as colourless cubic crystals (2.77 g, 13.3 mmol, 24%). HPLC; 99% ( $t_R = 5.688$  min). mp; 172.3–174.4 °C (Lit. 170–171 °C).<sup>77</sup> ESIMS:  $m/z = M^+ - Br$  128.0535, Theoretical Mass = 128.0534.  $^1H$  NMR (300 MHz;  $d_6$ -DMSO)  $\delta$ : 10.17 (d,  $J = 2.0$  Hz, 1H, *CH*-1), 8.04 (d,  $J = 2.0$  Hz, 1H, *CH*-2), 4.47 (q,  $J = 7.3$  Hz, 2H, *CH*<sub>2</sub>-5), 2.56 (s, 3H, *CH*<sub>3</sub>-4), 1.46 (t,  $J = 7.3$  Hz, 3H, *CH*<sub>3</sub>-6).  $^{13}C$  NMR  $\{^1H\}$  (126 MHz,  $d_6$ -DMSO)  $\delta$ ; 158.62 (*C*-1), 145.74 (*C*-3), 121.89 (*C*-2), 47.86 (*C*-5), 14.51 (*C*-4), 12.59 (*C*-6). IR ( $cm^{-1}$ ): 3045.28, 2976.36, 2957.18, 2873.38, 1580.79. Spectral data is consistent with the literature.<sup>149</sup>

## 5.3. Thiazole Compounds

### 5.3.1. Synthesis of 1,3-Thiazole-4-carboxaldehyde **184**



#### 5.3.1.1. Method 1

General procedure for the synthesis of **184**; DIBALH (1.0 M in DCM, x eq) was added dropwise to **183** (1.00 g, 6.36 mmol, 1.00 eq) in DCM (40 mL) under nitrogen at  $-78\text{ }^{\circ}\text{C}$  and stirred for 2 hours. The reaction was quenched slowly with MeOH (30 mL), and stirred for 3 hours at room temperature. The solvent was removed *in vacuo* to give a crude solid, which was washed with ethyl acetate (20 mL) to give the products described (Table 28). The product (entry 3) was recrystallized from DCM and petrol to give colourless needles (663 mg, 5.86 mmol, 92%).

**Table 28** The selectivity of the reduction of ethyl-4-thiazolecarboxylate **183** to the product aldehyde **184** by varying the number of equivalents of DIBAL-H.

Entry	DIBALH (eq)	Product Distribution (%) <sup>a</sup>		
		Ester	Aldehyde	Alcohol
1	1.50	0	17	83
2	0.95	0	25	75
3	0.33	93	7	0
4	0.50	14	86	0
5	0.75	0	100	0

#### 5.3.1.2. Method 2

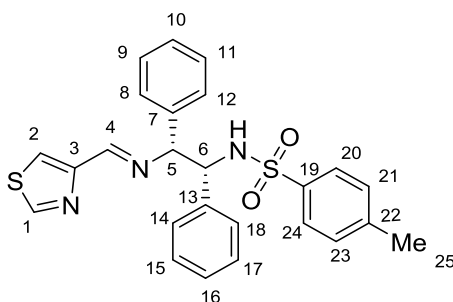
<sup>n</sup>BuLi (1.6 M in hexanes, 4.0 mL, 6.35 mmol, 1.50 eq) was added dropwise to a solution of 4-bromo-2-(trimethylsilyl)-1,3-thiazole (725  $\mu\text{L}$ , 4.23 mmol, 1.00 eq) in dry THF (25 mL) at  $-78\text{ }^{\circ}\text{C}$  under nitrogen and stirred for 0.5 hours. 4-Formylmorpholine (636  $\mu\text{L}$ , 6.35 mmol, 1.00 eq) in THF (5 mL) was added dropwise and stirred at  $-78\text{ }^{\circ}\text{C}$  under nitrogen for 1 hour. HCl (1 M, 10 mL, 10

mmol, 2.36 eq) was added dropwise and stirred for 16 hours whilst the reaction was allowed to warm to room temperature. The brown solution was washed with DCM (10 mL) and extracted with brine (30 mL). The solvent was removed *in vacuo* from the organic layer to give a brown solid (crude mass 553 mg, 0% yield). <sup>1</sup>H NMR gave trace conversion only.

### 5.3.1.3. Analytical Data

mp; 62.4–63.3 °C (Lit. 59–61 °C)<sup>150</sup>. LCMS: *m/z* = *M*<sup>+</sup>+*H* 114.0, Theoretical Mass = 114.0. <sup>1</sup>H NMR (300 MHz, CDCl<sub>3</sub>) δ; 10.13 (s, 1H, *CH*-4), 9.18 (d, *J* = 0.8 Hz, 1H, *CH*-1), 8.07 (s, *J* = 0.8 Hz, 1H, *CH*-2). <sup>13</sup>C NMR {<sup>1</sup>H} (126 MHz, CDCl<sub>3</sub>) δ; 184.83 (*C*-4), 155.72 (*C*-3), 154.01 (*C*-1), 126.66 (*C*-2). IR (cm<sup>-1</sup>); 3074, 2860, 2799, 2727, 2699, 1682. Spectral data is consistent with the literature.<sup>150</sup>

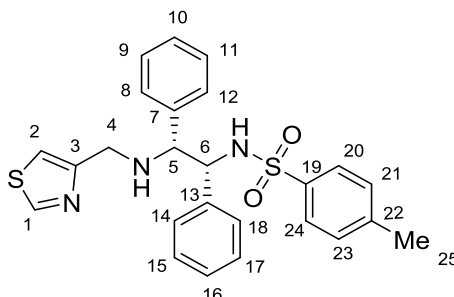
### 5.3.2. Synthesis of (*R,R*)-*N*-{1,2-diphenyl-2-[(1,3-thiazol-4-yl)methanimine]-ethyl}-*p*-toluenesulfonamide **188**



**184** (100 mg, 0.88 mmol, 1.10 eq) and (*R,R*)-**162** (294 mg, 0.80 mmol, 1.00 eq) were stirred at reflux in ethanol (5 mL) for 2 hours. The homogenous yellow solution was cooled to room temperature and the solvent was removed *in vacuo* to give yellow powder (370 mg, 0.80 mmol 91% yield). ESIMS: *m/z* = *M*<sup>+</sup> 462.2270, Theoretical Mass = 462.1304. <sup>1</sup>H NMR (300 MHz, CDCl<sub>3</sub>) δ; 8.91 (d, *J* = 2.0 Hz, 1H, *CH*-1), 7.72 (d, *J* = 2.0 Hz, 1H, *CH*-2), 7.50 (d, *J* = 8.3 Hz, 2H, *CH*-20/24), 7.27 – 7.17 (m, 8H, *CH*-Ph), 7.15 (d, *J* = 8.3 Hz, 2H, *CH*-21/23), 7.05 (m, 2H, *CH*-Ph), 6.15 (s, 1H, *CH*-4), 4.71 (d, *J* = 6.8 Hz, 1H, *CH*-5), 4.49 (d, *J* = 6.8 Hz, 1H, *CH*-6), 2.41 (s, 3H, *CH*<sub>3</sub>-25), 2.23 (br s, 1H, S-NH). <sup>13</sup>C NMR {<sup>1</sup>H} (126 MHz, CDCl<sub>3</sub>) δ; 153.41 (*C*-1), 148.61 (*C*-3), 143.70 (*C*-22), 139.25 (*C*<sub>0</sub>-Ph), 138.21 (*C*<sub>0</sub>-Ph), 134.80 (*C*-19), 129.49 (*C*-Ph), 128.57 (*C*-Ph),

128.33 (C-Ph), 127.84 (C-Ph), 127.74 (C-Ph), 127.64 (C-Ph), 127.41 (C-Ph), 126.92 (C-Ph), 117.99 (C-2), 74.89 (C-4), 71.51 (C-6), 69.97 (C-5), 21.57 (C-25).

### 5.3.3. Synthesis of (*R,R*)-*N*-{1,2-diphenyl-2-[(1,3-thiazol-4-ylmethyl)-amino]-ethyl}-*p*-toluenesulfonamide **L.1**



#### 5.3.3.1. Method 1

**184** (250 mg, 2.21 mmol, 1.00 eq) and (*R,R*)-**162** (811 mg, 2.21 mmol, 1.00 eq) were stirred in ethanol (10 mL) at reflux for 4 hours. The reaction to **188** was complete by TLC. NaBH<sub>4</sub> (126 mg, 3.32 mmol, 1.5 eq) was added to the yellow solution and stirred for 16 hours at room temperature. The solvent was removed *in vacuo* from the cloudy solution and the solid was dissolved in DCM (2 x 10 mL) and extracted with brine (2 x 20 mL). The organic layers were combined, dried with MgSO<sub>4</sub>, filtered and the solvent was removed *in vacuo* to give a yellow amorphous solid. The product was purified with column chromatography (ethyl acetate/petrol, 1:2) and recrystallized from ethyl acetate in petrol to give the product as colourless needles (830 mg, 1.79 mmol, 81% yield).

#### 5.3.3.2. Method 2

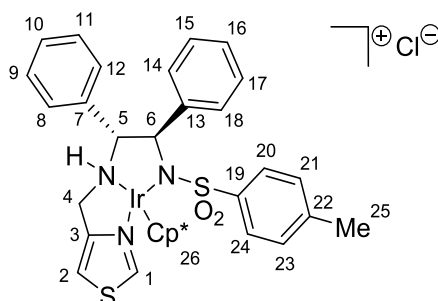
(*R,R*)-**162** (2.16 g, 5.88 mmol, 1.00 eq), **180·HCl** (1.00g, 5.88 mmol, 1.00 eq) and K<sub>2</sub>CO<sub>3</sub> (812 mg, 5.88 mmol, 1.00 eq) were stirred in ethanol (50 mL) at reflux for 48 hours. The solvent was removed *in vacuo* to give a yellow solid, which was transferred to a separating funnel with DCM (10 mL). The organics were washed with DCM (2 x 40 mL) and extracted with a saturated solution of NaHCO<sub>3</sub> (2 x 50 mL). The organic layers were combined, dried with MgSO<sub>4</sub>, filtered and the solvent was removed *in vacuo* to give a yellow amorphous

solid. The product was purified with column chromatography (ethyl acetate/petrol, 1:2) and recrystallized from ethyl acetate in petrol to give the product as colourless needles (806 mg, 1.74 mmol, 30%).

### 5.3.3.3. Analytical Data

$R_f$  = 0.40 (ethyl acetate/petrol, 1:3), mp; 142–145 °C. ESIMS  $m/z$  =  $M^+ + H$  464.1463, Theoretical Mass = 464.1461. Anal. Calcd for  $C_{25}H_{25}N_3O_2S_2$ : C, 64.77; H, 5.43; N, 9.06; S, 13.84. Found: C, 63.75; H, 5.40; N, 8.80; S, 14.00.  $^1H$  NMR (500 MHz,  $CDCl_3$ )  $\delta$ : 8.66 (d,  $J$  = 1.7 Hz, 1H, CH-1), 7.30 (d,  $J$  = 8.0 Hz, 2H, CH-20/24), 7.08 – 7.05 (m, 3H, CH-9–11), 7.02 – 6.88 (m, 8H, CH-2/Ph), 6.86 (d,  $J$  = 7.6 Hz, 2H, CH-15/17), 6.13 (s, 1H, S-NH), 4.27 (d,  $J$  = 7.4 Hz, 1H, CH-6), 3.72 (d,  $J$  = 14.3 Hz, 1H, CH-4), 3.67 (d,  $J$  = 7.4 Hz, 1H, CH-5), 3.58 (d,  $J$  = 14.3 Hz, 1H, CH-4), 2.26 (s, 3H, CH-25), 2.00 (br s, 1H, amine-NH).  $^{13}C$  NMR  $\{^1H\}$  (126 MHz,  $CDCl_3$ )  $\delta$ : 155.95 (C-3), 152.93 (C-1), 142.70 (C-22), 138.85 (C-13), 138.38 (C-7), 137.14 (C-19), 129.12 (C-21/23), 128.38 (C-8/12), 127.97 (C-14/18), 127.61 (C-9/11), 127.59 (C-10), 127.46 (C-15/17), 127.31 (C-16), 127.09 (C-20/24), 114.36 (C-2), 67.16 (C-5), 63.10 (C-6), 46.85 (C-4), 21.43 (C-25). IR ( $cm^{-1}$ ); 3304, 2957, 2935, 2872, 2854, 1613, 1583, 1511, 1454, 1437, 1248, 1148. X-ray crystal data for this compound can be found in the appendix.

### 5.3.4. Synthesis of [(*R,R*)-*N*{1,2-diphenyl-2-[(1,3-thiazol-4-ylmethyl)-amino]-ethyl}-*p*-toluenesulfonamide}( $\eta^5$ -pentamethylcyclopentadienyl)iridium(III) chloride **C.1**



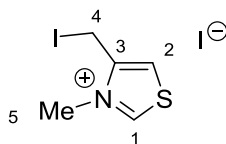
Triethylamine (70  $\mu$ L, 0.50 mmol, 4.00 eq) was added to a solution of (*R,R*)-**L.1** (116 mg, 0.25 mmol, 1.00 eq) and **36** (100 mg, 0.13 mmol, 0.50 eq, 1.00 eq Ir) in *iso*-propanol (5 mL) and stirred at room temperature for 18 hours. The solvent was removed *in vacuo* to give a light brown powder, which was

recrystallized in DCM and petrol to give brown microcrystals (108 mg, 0.14 mmol, 55% yield). mp; 203.7–206.2 °C. ESIMS:  $m/z = M^+$  790.2096, Theoretical Mass = 790.2113.  $^1\text{H}$  NMR (500 MHz,  $\text{CDCl}_3$ )  $\delta$ : 9.53 (br s, 1H, amine-NH), 9.32 (d,  $J = 1.9$  Hz, 1H, CH-1), 7.50 (s, 1H, CH-2), 7.39 (d,  $J = 7.6$  Hz, 2H, CH-20/24), 7.24 – 7.14 (m, 3H, CH-15–17), 7.07 (d,  $J = 8.1$  Hz, 2H, CH-21/23), 6.75 – 6.56 (m, 7H, CH-9–12/14/18), 4.59 (d,  $J = 12.2$  Hz, 1H, CH-6), 4.53 (dd,  $J = 12.2, 3.3$  Hz, 1H, CH-5), 4.42 (d,  $J = 17.0$  Hz, 1H, CH-4), 4.19 (d,  $J = 17.0$  Hz, 1H, CH-4), 2.13 (s, 3H,  $\text{CH}_3$ -25), 2.02 (s, 15H,  $\text{CH}_3$ -26).  $^{13}\text{C}$  NMR  $\{^1\text{H}\}$  (126 MHz,  $\text{CDCl}_3$ )  $\delta$ : 159.48 (C-3), 155.62 (C-1), 140.45 (C-19), 140.03 (C-22), 137.70 (C-13), 132.36 (C-7), 131.28 (C-20/24), 128.79 (C-15/18), 128.25 (C-Ph), 128.11 (C-16), 128.03 (C-Ph), 127.41 (C-Ph), 127.08 (C-21/23), 126.45 (C-10), 112.29 (C-2), 88.42 (C-26), 79.96 (C-6), 64.19 (C-5), 47.32 (C-4), 21.03 (C-25), 9.68 (C-26). IR ( $\text{cm}^{-1}$ ): 3376, 3029, 2977, 2916, 2529, 2495, 1600, 1489, 1267, 1133.

### 5.3.5. Synthesis of (*R,R*)-*N*-{1,2-diphenyl-2-[(3-methyl-1,3-thiazol-3-ium-4-ylmethyl)-amino]-ethyl}-*p*-toluenesulfonamide iodide **209** and *N*-Methyl-4-(iodomethyl)-1,3-thiazol-3-ium iodide **208**

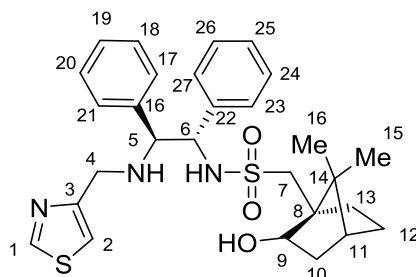
(*R,R*)-**L.1** (100 mg, 0.21 mmol, 1.00 eq) was stirred in iodomethane (4 mL) at 110 °C in a microwave for 3 hours. The precipitate was filtered from the solution and washed with DCM (5 mL) to give **208** as a spectroscopically pure orange powder (18 mg, 0.05 mmol, 23%).

#### 5.3.5.1. Analytical Data for *N*-Methyl-4-(iodomethyl)-1,3-thiazol-3-ium iodide **208**



mp; 175.6–177.3 °C. ESIMS  $m/z = M^+ - \text{I}$  239.9347, Theoretical Mass = 239.9344.  $^1\text{H}$  NMR (500 MHz,  $d_6$ -DMSO)  $\delta$ : 10.12 (d,  $J = 2.4$  Hz, 1H, CH-1), 8.30 (d,  $J = 2.6$  Hz, 1H, CH-2), 4.81 (s, 2H,  $\text{CH}_2$ -4), 4.15 (s, 3H,  $\text{CH}_3$ -5).  $^{13}\text{C}$  NMR  $\{^1\text{H}\}$  (126 MHz,  $d_6$ -DMSO)  $\delta$ : 161.88 (C-1), 146.31 (C-3), 123.97 (C-2), 39.60 (C-5), –9.20 (C-4). IR ( $\text{cm}^{-1}$ ): 3073, 3005, 2848, 1563, 1456.

**5.3.6. Synthesis of (S,S,S,R)-C-(7,7-Dimethyl-2-hydroxy-bicyclo[2.2.1]hept-1-yl)-N-{1,2-diphenyl-2-[(1,3-thiazol-4-ylmethyl)-amino]-ethyl}-methanesulfonamide L.2**

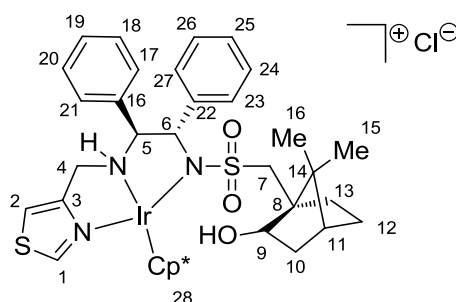


(S,S,S)-**163** (189 mg, 0.44 mmol, 1.00 eq) and **184** (50 mg, 0.44 mmol, 1.00 eq) were dissolved in ethanol (10 mL) and stirred at reflux for 20 hours. The reaction was allowed to cool to room temperature and NaBH<sub>4</sub> (42 mg, 1.10 mmol, 2.5 eq) was added and stirred at room temperature for 20 hours. The solvent was removed *in vacuo* to give an orange amorphous solid, which was dissolved in DCM (50 mL) and extracted with an aqueous HCl solution (2 M, 50 mL). The organic layer was neutralized with a saturated aqueous solution of NaHCO<sub>3</sub> (50 mL) and the organics extracted with DCM (50 mL), dried with MgSO<sub>4</sub>, filtered and the solvent was removed *in vacuo* to give an orange solid. The product was purified with column chromatography (ethyl acetate/petrol, 1:1) and recrystallized from ethyl acetate and petrol to give the product as a colourless powder (118 mg, 0.36 mmol, 82% yield). *R*<sub>f</sub> = 0.57 (ethyl acetate/petrol, 1:1). mp; 73.3–75.1 °C. ESIMS: *m/z* = M<sup>+</sup>+H 526.2192, Theoretical Mass = 526.2193. <sup>1</sup>H NMR (500 MHz, CDCl<sub>3</sub>) δ; 8.73 (s, 1H, CH-1), 7.37 – 7.12 (m, 10H, CH-Ph), 7.00 (s, 1H, CH-2), 6.22 (br s, 1H, S-NH), 4.59 (d, *J* = 7.3 Hz, 1H, CH-6), 3.97 – 3.92 (m, 2H, CH-5/9), 3.87 (d, *J* = 14.3 Hz, 1H, CHH-4), 3.70 (d, *J* = 14.3 Hz, 1H, CHH-4), 2.99 (br s, 1H, OH), 2.63 (d, *J* = 13.9 Hz, 1H, CHH-7), 2.21 (d, *J* = 13.9 Hz, 1H, CHH-7), 2.10 (br s, 1H, amine-NH), 1.74 – 1.57 (m, 4H, CH-10–12), 1.56 – 1.48 (m, 1H, CHH-13), 1.46 – 1.31 (m, 1H, CHH-13), 1.11 – 0.92 (m, 1H, CH-12), 0.72 (s, 3H, CH<sub>3</sub>-15), 0.56 (s, 3H, CH<sub>3</sub>-16). <sup>13</sup>C NMR {<sup>1</sup>H} (126 MHz, CDCl<sub>3</sub>) δ; 155.80 (C-3), 153.11 (C-1), 139.13 (C-16), 138.86 (C-22), 128.64 (C-Ph), 128.08 (C-*p*-Ph), 128.02



(C-*p*-Ph), 127.78 (C-Ph), 127.53 (C-Ph), 114.57 (C-2), 76.24 (C-9), 66.42 (C-5), 63.37 (C-6), 53.24 (C-7), 50.17 (C-8), 48.43 (C-14), 46.70 (C-4), 44.29 (C-11), 38.79 (C-10), 30.31 (C-13), 27.34 (C-12), 20.33 (C-16), 19.47 (C-15). IR (cm<sup>-1</sup>); 3515, 3264, 3063, 2951, 2879, 1467, 1444, 1311, 1133.

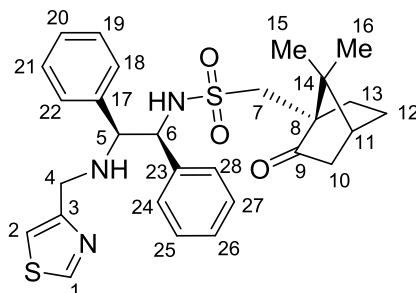
**5.3.7. Synthesis of [(S,S,S,R)-C-(7,7-Dimethyl-2-hydroxy-bicyclo[2.2.1]hept-1-yl)-N-{1,2-diphenyl-2-[(1,3-thiazol-4-ylmethyl)-amino]-ethyl}-methanesulfonamide](η<sup>5</sup>-pentamethylcyclopentadienyl)iridium(III) chloride C.2**



Triethylamine (70 μL, 0.50 mmol, 4.00 eq) was added to a yellow solution of **L.2** (132 mg, 0.25 mmol, 1.00 eq) and **36** (100 mg, 0.13 mmol, 1.00 eq) in *iso*-propanol (5 mL) and stirred at room temperature for 16 hours. The solvent was removed *in vacuo* to give a dark brown powder (164 mg, 0.19 mmol, 77% yield). mp; 171.6–175.8 °C. ESIMS; *m/z* = M<sup>+</sup>-Cl 852.2587, Theoretical Mass = 852.2845. <sup>1</sup>H NMR (500 MHz, CDCl<sub>3</sub>) δ; 9.77 (s, 1H, NH), 9.29 (d, *J* = 2.0 Hz, 1H, CH-1), 7.47 (d, *J* = 7.5 Hz, 2H, CH-23/27), 7.36 (s, 1H, CH-2), 7.28 – 7.23 (m, 2H, CH-24/26), 7.25 – 7.12 (m, 5H, CH-Ph), 7.11 – 7.06 (m, 1H, CH-19), 4.67 (dd, *J* = 12.5, 4.0 Hz, 1H, CH-5), 4.53 (d, *J* = 12.5 Hz, 1H, CH-6), 4.28 (dd, *J* = 17.8, 7.4 Hz, 1H, CHH-4), 4.11 (d, *J* = 17.8 Hz, 1H, CHH-4), 3.81 (s, 1H, CH-9), 3.29 (d, *J* = 2.4 Hz, 1H, OH), 1.98 (s, 15H, CH<sub>3</sub>-28), 1.94 (s, 2H, CH<sub>2</sub>-7), 1.58 – 1.44 (m, 6H, CH-10–13), 0.97 (t, *J* = 8.3 Hz, 1H, CHH-10), 0.51 (s, 3H, CH<sub>3</sub>-16), 0.46 (s, 3H, CH<sub>3</sub>-15). <sup>13</sup>C NMR {<sup>1</sup>H} (126 MHz, CDCl<sub>3</sub>) δ; 158.48 (C-3), 156.00 (C-1), 139.62 (C-22), 132.24 (C-16), 131.38 (C-23/27), 128.94 (C-25), 128.78 (C-Ph), 128.57 (C-Ph), 128.34 (C-24/26), 128.06 (C-19), 113.05 (C-2), 88.18 (C-28), 79.04 (C-5), 76.08 (C-9), 64.39 (C-6), 57.37 (C-7), 51.33 (C-8), 48.10 (C-14), 47.64 (C-4), 44.33 (C-11), 38.43 (C-13),

31.58 (C-12), 27.36 (C-10), 20.31 (C-16), 19.39 (C-15), 9.98 (C-28). IR (cm<sup>-1</sup>); 3445, 3031, 2928, 2878, 2602, 2495, 1476, 1453, 1291, 1106.

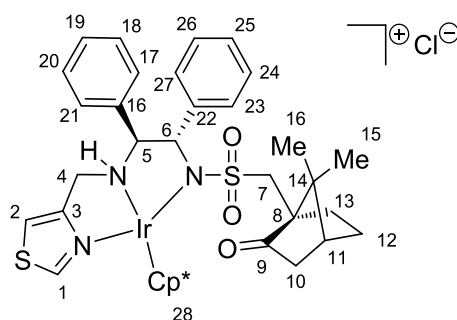
### 5.3.8. Synthesis of (S,S,S)-N-{1,2-diphenyl-2-[(1,3-thiazol-4-ylmethyl)-amino]-ethyl}-camphorsulfonamide L.3



**180·HCl** (500 mg, 2.94 mmol, 1.00 eq), (**S,S,S**)-**163** (1.26 g, 2.94 mmol, 1.00 eq) and K<sub>2</sub>CO<sub>3</sub> (812 mg, 5.88 mmol, 2.00 eq) were stirred in acetonitrile (15 mL) at reflux for 48 hours. The reaction was cooled to room temperature, washed with DCM (25 mL x 3) and extracted with a saturated solution of NaHCO<sub>3</sub> (25 mL x 3). The combined organics were extracted with brine (2 x 20 mL) and the organic layer was dried with MgSO<sub>4</sub> and filtered. The solvent was removed *in vacuo* to give a pale yellow amorphous solid, which was purified using column chromatography (ethyl acetate/petrol, 2:1) to give a colourless amorphous solid. The solid was recrystallized from 2% ethyl acetate in petrol solution to give the product as colourless needles (550 mg, 1.06 mmol, 36%). *R*<sub>f</sub> = 0.63 (petrol:ethyl acetate, 1:2). mp; 68.4–72.1 °C. ESIMS *m/z* = M<sup>+</sup> 524.2105, Theoretical Mass = 524.2036. <sup>1</sup>H NMR (500 MHz, CDCl<sub>3</sub>) δ: 8.72 (d, *J* = 1.9 Hz, 1H, CH-1), 7.29 – 7.17 (m, 10H, CH-Ph), 7.02 (d, *J* = 1.9 Hz, 1H, CH-2), 6.33 (d, *J* = 3.7 Hz, 1H, S-NH), 4.70 (dd, *J* = 6.9, 4.3 Hz, 1H, CH-6), 3.91 (d, *J* = 7.2 Hz, 1H, CH-8), 3.84 (d, *J* = 14.2 Hz, 1H, CHH-4), 3.69 (d, *J* = 14.2 Hz, 1H, CHH-4), 3.01 (d, *J* = 15.0 Hz, 1H, CHH-7), 2.46 (d, *J* = 15.0 Hz, 1H, CHH-7), 2.35 – 2.26 (m, 2H, CH-11/12), 2.03 (t, *J* = 4.4 Hz, 1H, CHH-10), 1.99 – 1.89 (m, 1H, CHH-13), 1.84 (d, *J* = 18.4 Hz, 1H, CHH-10), 1.66 – 1.59 (m, 2H, CHH-20, amine-NH), 1.35 – 1.26 (m, 1H, CHH-13), 0.93 (s, 3H, CH<sub>3</sub>-15), 0.73 (s, 3H, CH<sub>3</sub>-16). <sup>13</sup>C NMR {<sup>1</sup>H} (126 MHz, CDCl<sub>3</sub>) δ; 155.9 (C-3), 152.86 (C-1), 139.48 (C-23), 139.34 (C-17), 128.53 (C-21/19), 128.40 (C-25/27), 127.88 (C-18/22), 127.78 (C-20), 127.67 (C-26), 127.38 (C-24/28),

114.40 (C-2), 67.03 (C-4), 63.32 (C-6), 58.58 (C-8), 50.10 (C-7), 46.85 (C-14), 42.73 (C-10), 42.70 (C-11), 26.92 (C-13), 25.29 (C-12), 19.81 (C-15), 19.62 (C-16). IR (cm<sup>-1</sup>): 3265, 3063, 3029, 2957, 1741, 1602, 1494, 1454, 1321, 1145.

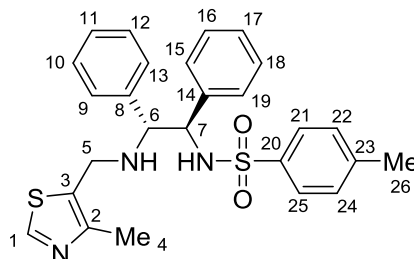
### 5.3.9. Synthesis of [(S,S,S)-N-{1,2-diphenyl-2-[(1,3-thiazol-4-ylmethyl)-amino]-ethyl}-camphorsulfonamide]( $\eta^5$ -pentamethylcyclopentadienyl)iridium(III) chloride **C.3**



Triethylamine (30  $\mu$ L, 0.21 mmol, 4.00 eq) was added to a solution of **L.3** (56 mg, 0.11 mmol, 2.00 eq) and **36** (42 mg, 0.05 mmol, 1.00 eq) in *iso*-propanol (2 mL) at room temperature for 24 hours. The solvent was removed *in vacuo* from the deep red solution to give dark red microcrystals (83 mg, 0.10 mmol, 89%). mp; 207.2–211.1 °C. ESIMS  $m/z$  =  $M^+$ -Cl 850.2400, Theoretical Mass = 850.2688. <sup>1</sup>H NMR (500 MHz, CDCl<sub>3</sub>)  $\delta$ : 9.59 (s, 1H, NH), 9.26 (d,  $J$  = 2.2 Hz, 1H, CH-1), 7.46 (d,  $J$  = 7.5 Hz, 2H, CH-17/21), 7.38 (s, 1H, CH-2), 7.24 (t,  $J$  = 7.5 Hz, 2H, CH-18/20), 7.20 – 7.09 (m, 5H, CH-Ph), 7.05 (t,  $J$  = 7.1 Hz, 1H, CH-19), 4.66 (dd,  $J$  = 12.5, 5.5 Hz, 1H, CH-5), 4.58 (d,  $J$  = 12.5 Hz, 1H, CH-6), 4.24 (dd,  $J$  = 17.3, 5.5 Hz, 1H, CHH-4), 4.09 (d,  $J$  = 17.3 Hz, 1H, CHH-4), 2.23 – 2.16 (m, 2H, CH-7/10), 2.13 – 2.04 (m, 2H, CH<sub>2</sub>-13), 1.96 (s, 15H, CH<sub>3</sub>-28), 1.92 (s, 1H, CHH-7), 1.89 (t,  $J$  = 4.4 Hz, 1H, CH-11), 1.86 – 1.78 (m, 2H, CH<sub>2</sub>-12), 1.66 (d,  $J$  = 18.8 Hz, 1H, CHH-10), 0.98 (s, 3H, CH<sub>3</sub>-16), 0.71 (s, 3H, CH<sub>3</sub>-15). <sup>13</sup>C NMR {<sup>1</sup>H} (126 MHz, CDCl<sub>3</sub>)  $\delta$ : 215.20 (C-9), 158.97 (C-3), 155.97 (C-1), 139.48 (C-22), 132.41 (C-16), 131.35 (C-17/21), 129.12 (C-23/27), 128.98 (C-19), 128.39 (C-24/26), 128.33 (C-18/20), 127.71 (C-25), 112.18 (C-2), 88.12 (C-28), 79.03 (C-5), 64.33 (C-6), 59.45 (C-8), 53.57 (C-7), 47.54 (C-4), 47.01 (C-14), 43.51 (C-11), 42.61 (C-10), 26.58 (C-12), 26.39 (C-13), 19.97 (C-16), 19.82 (C-15), 9.93 (C-28). IR (cm<sup>-1</sup>): 3360, 3030, 2956,

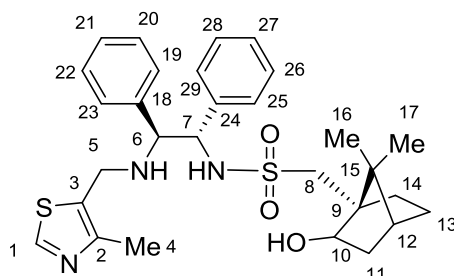
2919, 1738, 1625, 1493, 1452, 1280, 1117. X-ray crystal data for this compound can be found in the appendix.

### 5.3.10. Synthesis of (*R,R*)-*N*-{1,2-diphenyl-2-[(4-methyl-1,3-thiazol-5-ylmethyl)-amino]-ethyl}-*p*-toluenesulfonamide **191**



**190** (100 mg, 0.79 mmol, 1.00 eq) and (*R,R*)-**162** (289 mg, 0.79 mmol, 1.00 eq) were stirred in ethanol (5 mL) at reflux for 16 hours. The formation of the imine was complete by  $^1\text{H}$  NMR. The reaction was cooled to room temperature and  $\text{NaBH}_4$  (76 mg, 1.97 mmol, 2.50 eq) was added and stirred for 48 hours. The solvent was removed *in vacuo* and the yellow solid was dissolved in DCM (5 mL) and transferred to a separating funnel. The organic layer was washed with DCM (2 x 10 mL) and extracted with brine (2 x 10 mL). The organic layers were combined, dried with  $\text{MgSO}_4$ , filtered and the solvent was removed *in vacuo* to give a pale yellow solid. The solid was purified by recrystallisation from ethyl acetate and petrol to give the product as colourless microcrystals (284 mg, 0.60 mmol, 75%). mp; 157.9–160.2 °C. ESIMS  $m/z = M^+ + H$  478.1634, Theoretical Mass = 478.1617.  $^1\text{H}$  NMR (500 MHz,  $\text{CDCl}_3$ )  $\delta$ : 8.63 (s, 1H, *CH*-1), 7.36 (d,  $J = 8.2$  Hz, 1H, *CH*-21/25), 7.19 – 7.14 (m, 3H, *CH*-10–12), 7.06 (t,  $J = 7.2$  Hz, 1H, *CH*-17), 7.04 – 6.98 (m, 4H, *CH*-16/18/22/24), 6.97 – 6.92 (m, 1H, *CH*-9/13), 6.87 (d,  $J = 7.0$  Hz, 1H, *CH*-15/19), 5.90 (s, 1H, S-NH), 4.32 (d,  $J = 7.9$  Hz, 1H, *CH*-7), 3.75 (d,  $J = 14.3$  Hz, 1H, CHH-5), 3.68 (d,  $J = 7.9$  Hz, 1H, *CH*-6), 3.59 (d,  $J = 14.3$  Hz, 1H, CHH-5), 2.32 (s, 3H,  $\text{CH}_3$ -26), 2.13 (s, 3H,  $\text{CH}_3$ -4), 1.82 (br s, 1H, amine-NH).  $^{13}\text{C}$  NMR  $\{^1\text{H}\}$  (126 MHz,  $\text{CDCl}_3$ )  $\delta$ : 150.77 (C-1), 149.51 (C-2), 142.84 (C-23), 138.26 (C-8), 137.92 (C-14), 136.97 (C-20), 130.14 (C-3), 129.13 (C-22/24), 128.53 (C-10/12), 128.02 (C-16/18), 127.88 (C-17), 127.58 (C-9/13), 127.43 (C-11/15/19), 127.10 (C-21/25), 66.44 (C-6), 63.00 (C-7), 42.17 (C-5), 21.43 (C-26), 14.91 (C-4). IR ( $\text{cm}^{-1}$ ): 3214, 3067, 3029, 2925, 2850, 1600, 1554, 1493, 1331, 1152.

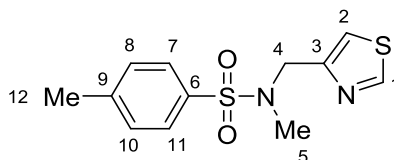
**5.3.11. Synthesis of (S,S,S)-C-(7,7-Dimethyl-2-hydroxy-bicyclo[2.2.1]hept-1-yl)-N-{1,2-diphenyl-2-[(4-methyl-1,3-thiazol-5-ylmethyl)-amino]-ethyl}-methanesulfonamide **192****



**190** (50 mg, 0.39 mmol, 1.00 eq) and (S,S,S)-**163** (168 mg, 0.39 mmol, 1.00 eq) were dissolved in ethanol (5 mL) and stirred at reflux for 18 hours. The formation of the imine was complete by  $^1\text{H}$  NMR. The reaction was cooled to room temperature and  $\text{NaBH}_4$  (37 mg, 0.98 mmol, 2.5 eq) was added and stirred for 16 hours. The solvent was removed *in vacuo* and the white solid was dissolved in DCM (5 mL) and water (5 mL) and transferred to a separating funnel. The organic layer was washed with DCM (2 x 10 mL) and extracted with brine (2 x 10 mL). The organic layers were combined, dried with  $\text{MgSO}_4$ , filtered and the solvent was removed *in vacuo* to give an off-white solid. The solid was purified by recrystallisation from ethyl acetate and petrol to give the product as colourless microcrystals (143 mg, 0.26 mmol, 67%). mp; 78.6–80.8 °C. ESIMS  $m/z = M^+ + H$  540.2361, Theoretical Mass = 540.2349.  $^1\text{H}$  NMR (500 MHz,  $\text{CDCl}_3$ )  $\delta$ : 8.64 (s, 1H, CH-1), 7.33 – 7.09 (m, 10H, CH-Ph), 5.97 (s, 1H, S-NH), 4.56 (d,  $J = 7.3$  Hz, 1H, CH-7), 3.98 – 3.91 (m, 1H, CH-10), 3.87 – 3.78 (m, 2H, CH-5/6), 3.65 (d,  $J = 14.3$  Hz, 1H, CHH-5), 2.60 (d,  $J = 13.9$  Hz, 1H, CHH-8), 2.24 (d,  $J = 13.9$  Hz, 1H, CHH-8), 2.16 (s, 4H,  $\text{CH}_3$ -4/OH), 1.69 – 1.49 (m, 5H, CH-11–14), 1.40 – 1.32 (m, 1H, CHH-11), 1.09 – 0.96 (m, 1H, CHH-14), 0.70 (s, 3H,  $\text{CH}_3$ -17), 0.57 (s, 3H,  $\text{CH}_3$ -16).  $^{13}\text{C}$  NMR  $\{^1\text{H}\}$  (126 MHz,  $\text{CDCl}_3$ )  $\delta$ : 150.90 (C-1), 149.66 (C-2), 138.47 (C-18), 138.34 (C-24), 130.08 (C-3), 128.76 (C-*m*-Ph), 128.70 (C-*m*-Ph), 128.27 (C-*p*-Ph), 128.24 (C-*p*-Ph), 127.71 (C-19/23), 127.63 (C-25/29), 76.24 (C-10), 65.64 (C-6), 63.17 (C-7), 53.42 (C-8), 50.17 (C-9), 48.44 (C-15), 44.28 (C-12), 42.02 (C-5), 38.76 (C-13), 30.28 (C-11), 27.34 (C-14), 20.34 (C-16), 19.42 (C-17), 14.95 (C-4). IR

(cm<sup>-1</sup>): 3520, 3262, 3062, 3029, 2952, 2878, 1629, 1602, 1541, 1494, 1454, 1314, 1139.

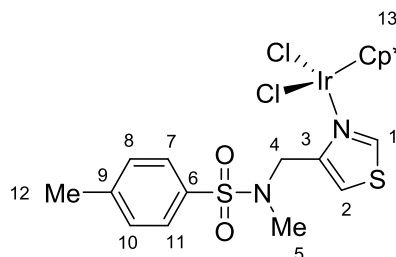
### 5.3.12. Synthesis of *N*-methyl-*N*-(1,3-thiazol-4-ylmethyl)-*p*-toluene sulfonamide L.4



**194** (111 mg, 0.60 mmol, 2.00 eq) and NaOH (24 mg, 0.60 mmol, 2.00 eq) were dissolved in ethanol (10 mL) and stirred at room temperature for 1 hour. **180•HCl** (51 mg, 0.30 mmol, 1.00 eq) was added and the reaction was stirred at reflux for 16 hours. The reaction was cooled to room temperature and the solvent was removed in vacuo. The crude material was washed with brine (2 x 10 mL) and extracted with DCM (2 x 10 mL). The organics were collected and the solvent was removed *in vacuo* to give a white solid. The product was purified by column chromatography (ethyl acetate/petrol, 1:1) and recrystallized from ethyl acetate and petrol to give colourless needles (50 mg, 0.18 mmol, 59%).

HPLC: 99% ( $t_R$  = 15.417 min).  $R_f$  = 0.21 (ethyl acetate/petrol, 1:1). mp; 77.7–81.3 °C. ESIMS  $m/z$  =  $M^+ + H$  283.0568, Theoretical Mass = 283.0569. <sup>1</sup>H NMR (500 MHz, CDCl<sub>3</sub>)  $\delta$ : 8.73 (d,  $J$  = 2.0 Hz, 1H, CH-1), 7.70 (d,  $J$  = 8.4 Hz, 2H, CH-7/11), 7.33 (s, 1H, CH-2), 7.32 (d,  $J$  = 8.4 Hz, 2H, CH-8/10), 4.42 (s, 2H, CH<sub>2</sub>-4), 2.79 (s, 3H, CH<sub>3</sub>-5), 2.44 (s, 3H, CH<sub>3</sub>-12). <sup>13</sup>C NMR {<sup>1</sup>H} (126 MHz, CDCl<sub>3</sub>)  $\delta$ : 153.01 (C-1), 152.90 (C-3), 143.50 (C-6), 134.63 (C-9), 129.72 (C-8/10), 127.49 (C-7/11), 116.45 (C-2), 50.07 (C-4), 35.33 (C-5), 21.52 (C-12). IR (cm<sup>-1</sup>): 3100, 3056, 2922, 2856, 1600, 1522, 1489, 1329, 1157.

### 5.3.13. Synthesis of Dichloro[*N*-methyl-*N*-(1,3-thiazol-4-ylmethyl)-*p*-toluenesulfonamide]( $\eta^5$ -pentamethylcyclopentadienyl)iridium(III) **C.4**

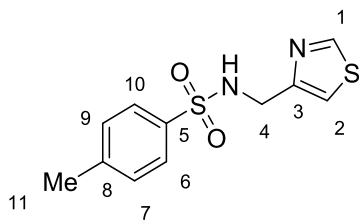


**L.4** (25 mg, 0.09 mmol, 2.00 eq) and **36** (35 mg, 0.04 mmol, 1.00 eq) were stirred in DCM (5 mL) at room temperature for 16 hours. The solvent was removed *in vacuo* to give a yellow powder. Recrystallization from chloroform and hexane gave the product as yellow plates (53 mg, 0.08 mmol, 91%). mp; 229.6–232.2 °C. ESIMS  $m/z = M^+ - Cl$  645.0968, Theoretical Mass = 645.0988.  $^1H$  NMR (500 MHz,  $CDCl_3$ )  $\delta$ : 9.38 (br s, 1H, *CH*-1), 7.72 (d,  $J = 8.1$  Hz, 2H, *CH*-7/11), 7.54 (s, 1H, *CH*-2), 7.36 (d,  $J = 8.1$  Hz, 2H, *CH*-8/10), 4.84 (s, 2H,  $CH_2$ -4), 2.83 (s, 3H,  $CH_3$ -5), 2.47 (s, 3H,  $CH_3$ -12), 1.56 (s, 15H,  $CH_3$ -13).  $^{13}C$  NMR  $\{^1H\}$  (126 MHz,  $CDCl_3$ )  $\delta$ : 158.23 (br, C-1), 154.79 (C-3), 143.90 (C-6), 134.82 (C-9), 129.94 (C-8/10), 127.28 (C-9/11), 117.12 (C-2), 86.08 (C-13), 50.81 (C-4), 35.64 (C-5), 21.57 (C-12), 8.98 (C-13). IR ( $cm^{-1}$ ): 3122, 3089, 2967, 2922, 1600, 1533, 1444, 1373, 1160. X-ray crystal data for this compound can be found in the appendix.

### 5.3.14. Synthesis of *N*-(1,3-thiazol-4-ylmethyl)-*p*-toluenesulfonamide **L.5** and *N,N*-bis-(1,3-thiazol-4-ylmethyl)-*p*-toluenesulfonamide **L.6**

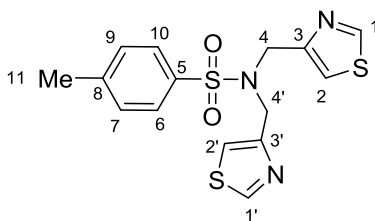
Following a modified procedure from Caldwell;<sup>103</sup> **194** (402 mg, 2.35 mmol, 2.00 eq), **180·HCl** (200 mg, 1.18 mmol, 1.00 eq) and  $K_2CO_3$  (650 mg, 4.71 mmol, 4.00 eq) were stirred at reflux in acetonitrile (10 mL) for 24 hours. The white homogeneous solution was washed with ether (3 x 40 mL) and extracted with water (3 x 40 mL). The combined organics were dried with  $MgSO_4$ , filtered and the solvent was removed *in vacuo* to give a pale yellow solid. Both title compounds were separated and purified using column chromatography (petrol:ethyl acetate, 1:1) and recrystallized from ethyl acetate and petrol.

### 5.3.14.1. Analytical Data for *N*-(1,3-thiazol-4-ylmethyl)-*p*-toluene sulfonamide L.5



Product isolated as colourless plates (155 mg, 0.58 mmol, 49 %).  $R_f = 0.42$  (petrol:ethyl acetate, 1:1). mp; 123.9–124.7 °C. ESIMS  $m/z = M^+$  269.0470, Theoretical Mass = 269.0412.  $^1\text{H}$  NMR (500 MHz,  $\text{CDCl}_3$ )  $\delta$ : 8.69 (d,  $J = 1.9$  Hz, 1H, CH-1), 7.68 (d,  $J = 8.2$  Hz, 2H, CH-6/10), 7.23 (d,  $J = 8.2$  Hz, 2H, CH-7/9), 7.10 (d,  $J = 1.9$  Hz, 1H, CH-2), 5.59 (t,  $J = 6.0$  Hz, 1H, NH), 4.32 (d,  $J = 6.0$  Hz, 2H,  $\text{CH}_2$ -4), 2.40 (s, 3H,  $\text{CH}_3$ -11).  $^{13}\text{C}$  NMR  $\{^1\text{H}\}$  (126 MHz,  $\text{CDCl}_3$ )  $\delta$ ; 153.49 (C-1), 152.41 (C-3), 143.44 (C-5), 136.89 (C-8), 129.62 (C-6/10), 127.14 (C-7/9), 115.67 (C-2), 43.02 (C-4), 21.50 (C-11). IR ( $\text{cm}^{-1}$ ): 3062, 2849, 1599, 1523, 1308, 1146.

### 5.3.14.2. Analytical Data for *N,N*-bis-(1,3-thiazol-4-ylmethyl)-*p*-toluene sulfonamide L.6



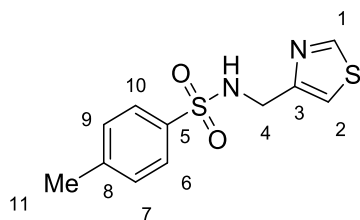
Product isolated as colourless plates (61 mg, 0.17 mmol, 29%).  $R_f = 0.23$  (petrol:ethyl acetate, 1:1). mp; 133.3–135.5 °C. ESIMS  $m/z = M^+$  366.0451, Theoretical Mass = 366.0399.  $^1\text{H}$  NMR (500 MHz,  $\text{CDCl}_3$ )  $\delta$ : 8.66 (d,  $J = 2.0$  Hz, 2H, CH-1/1'), 7.64 (d,  $J = 8.3$  Hz, 2H, CH-6/10), 7.27 – 7.23 (m, 4H, CH-2/2'/7/9), 4.68 (s, 4H,  $\text{CH}_2$ -4/4'), 2.40 (s, 3H,  $\text{CH}_3$ -11).  $^{13}\text{C}$  NMR  $\{^1\text{H}\}$  (126 MHz,  $\text{CDCl}_3$ )  $\delta$ ; 152.87 (C-3/3'), 152.82 (C-1/1'), 143.23 (C-5), 137.06 (C-8), 129.50 (C-6/10), 127.29 (C-7/9), 116.92 (C-2/2'), 47.05 (C-4/4'), 21.51 (C-11). IR ( $\text{cm}^{-1}$ ): 3109, 3067, 2971, 2921, 2857, 1601, 1525, 1498, 1338, 1160.



### 5.3.15. Synthesis of *N,N*-bis-(1,3-thiazol-4-ylmethyl)-*p*-toluene sulfonamide L.6

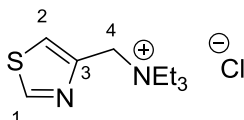
**194** (101 mg, 0.59 mmol, 1.00 eq), **180•HCl** (200 mg, 1.18 mmol, 2.00 eq) and  $K_2CO_3$  (324 mg, 2.35 mmol, 4.00 eq) were stirred at reflux in acetonitrile (5mL) for 16 hours. The reaction was cooled to room temperature and the solvent was removed *in vacuo*. The white solid was washed with DCM (2 x 10 mL) and extracted with brine (2 x 10 mL). The combined organics were dried with  $MgSO_4$ , filtered and the solvent removed *in vacuo* to give a white powder (181 mg, 0.44 mmol, 84%) (see 5.3.14.2 for analytical data).

### 5.3.16. Attempted synthesis of *N*-(1,3-thiazol-4-ylmethyl)-*p*-toluenesulfonamide L.5



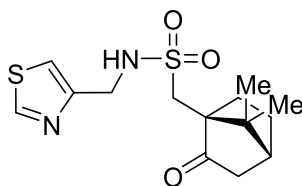
Triethylamine (163  $\mu$ L, 1.18 mmol, 2.00 eq) was added to a solution of **194** (101 mg, 0.59 mmol, 1.00 eq) and **180•HCl** (100 mg, 0.59 mmol, 1.00 eq) in acetonitrile (5 mL). The reaction was stirred at reflux for 16 hours. The solvent was removed *in vacuo* to give a white solid.  $^1H$  NMR shows the product of the  $S_N2$  reaction of the **180•HCl** with triethylamine to give salt **195**.

#### 5.3.16.1. Analytical Data for triethyl[(1,3-thiazol-4-yl)methyl]azanium chloride **195**



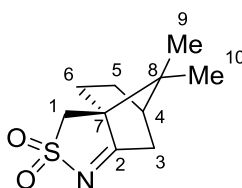
LCMS:  $M^+$  = 199.1, Theoretical Mass = 199.1.  $^1H$  NMR (500 MHz,  $CDCl_3$ )  $\delta$ : 8.82 (d,  $J$  = 1.9 Hz, 1H, CH-1), 8.33 (d,  $J$  = 1.9 Hz, 1H, CH-2), 4.80 (s, 2H, CH<sub>2</sub>-4), 3.35 (q,  $J$  = 7.2 Hz, 6H, CH<sub>2</sub>-Et), 1.37 (t,  $J$  = 7.2 Hz, 9H, CH<sub>3</sub>-Et).

### 5.3.17. Attempted synthesis of (S)-N-(1,3-thiazol-4-ylmethyl)camphorsulfonamide **197**



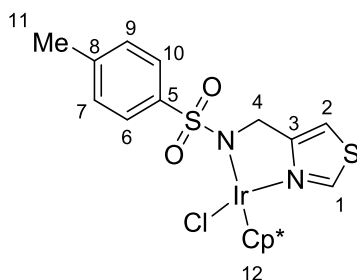
Triethylamine (163  $\mu\text{L}$ , 1.18 mmol, 2.00 eq) was added to a solution of 10-camphorsulfonamide (136 mg, 0.59 mmol, 1.00 eq) and **180** $\cdot\text{HCl}$  (100 mg, 0.59 mmol, 1.00 eq) in acetonitrile (5 mL). The reaction was stirred at reflux for 16 hours. The solvent was removed *in vacuo* to give a white solid.  $^1\text{H}$  NMR shows the intramolecular reaction of the starting material to the sulfonyl imine (**S**)-**199** and the product of the  $\text{S}_{\text{N}}2$  reaction of the **180** $\cdot\text{HCl}$  with triethylamine to give salt **195** (see 5.3.16.1 for analytical data).

#### 5.3.17.1. Analytical Data for (S)-Camphorsulfonylimine **199**



$^1\text{H}$  NMR (500 MHz,  $\text{CDCl}_3$ )  $\delta$ : 3.18 (d,  $J = 13.3$  Hz, 1H), 2.97 (d,  $J = 13.3$  Hz, 1H), 2.77 (ddd,  $J = 19.1, 4.7, 2.4$  Hz, 1H), 2.44 (ddd,  $J = 19.1, 4.7, 2.4$  Hz, 1H), 2.26 (t,  $J = 4.3$  Hz, 1H), 2.15 (d,  $J = 4.3$  Hz, 1H), 1.79 (t,  $J = 9.1$  Hz, 1H), 1.52 – 1.43 (m, 2H), 1.09 (s, 3H), 0.87 (s, 3H). Spectral data is consistent with the literature.<sup>151</sup>

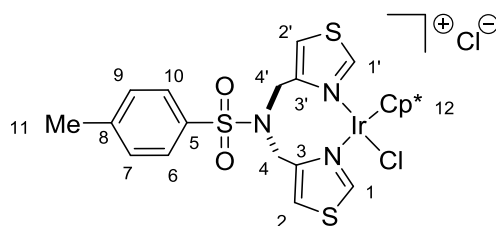
### 5.3.18. Synthesis of Chloro[*N*-(1,3-thiazol-4-ylmethyl)-*p*-toluene sulfonamide]( $\eta^5$ -pentamethylcyclopentadienyl)iridium(III) **C.5**



**L.5** (30 mg, 0.11 mmol, 2.00 eq) and **36** (45 mg, 0.06 mmol, 1.00 eq) were stirred in DCM (5 mL) at 40 °C for 16 hours. The solvent was removed *in vacuo* to give a yellow powder. The powder was washed with DCM (10 mL) and extracted with water (10 mL). The solvent was removed to give the product as a yellow powder (65 mg, 0.10 mmol, 94%). mp; 209.5–212.3 °C. ESIMS  $m/z$  =  $M^+ - Cl$  595.1022, Theoretical Mass = 595.1065.  $^1H$  NMR (500 MHz,  $CDCl_3$ )  $\delta$ : 8.80 (d,  $J$  = 2.0 Hz, 1H,  $CH-1$ ), 7.89 (d,  $J$  = 8.1 Hz, 2H,  $CH-6/10$ ), 7.11 (d,  $J$  = 8.1 Hz, 2H,  $CH-7/9$ ), 7.02 (d,  $J$  = 2.0 Hz, 1H,  $CH-2$ ), 4.25 (s, 2H,  $CH_2-4$ ), 2.30 (s, 3H,  $CH_3-11$ ), 1.76 (s, 15H,  $CH_3-12$ ).  $^{13}C$  NMR { $^1H$ } (126 MHz,  $CDCl_3$ )  $\delta$ ; 159.59 (C-3), 151.70 (C-1), 140.51 (C-8), 139.97 (C-5), 128.75 (C-7/9), 128.26 (C-6/10), 110.70 (C-2), 86.50 (C-12), 49.99 (C-4), 21.33 (C-11), 9.59 (C-12). IR ( $cm^{-1}$ ): 3059, 2978, 2914, 2822, 2603, 2497, 1598, 1548, 1475, 1268, 1132.

### 5.3.19. Synthesis of Chloro[*N,N*-bis-(1,3-thiazol-4-ylmethyl)-*p*-toluene sulfonamide]( $\eta^5$ -pentamethylcyclopentadienyl)iridium(III) chloride

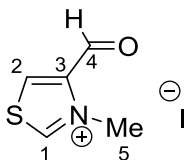
#### C.6



Triethylamine (11  $\mu$ L, 0.08 mmol, 2.00 eq) was added to a stirred solution of **L.6** (30 mg, 0.08 mmol, 2.00 eq) and **36** (33 mg, 0.04 mmol, 1.00 eq) were stirred in DCM (5 mL) and stirred at 40 °C under nitrogen for 16 hours. The solvent was removed *in vacuo* to give a yellow powder. The powder was washed with DCM (10 mL) and extracted with water (10 mL). The solvent was removed *in vacuo* to give the product as a yellow powder (25 mg, 0.07 mmol, 86%). mp; 208.1–210.3 °C. ESIMS  $m/z$  =  $M^+ - Cl_2$  346.5559, Theoretical Mass = 346.5565.  $^1H$  NMR (500 MHz,  $CDCl_3$ )  $\delta$ ; 9.00 (br s, 2H,  $CH-1/1'$ ), 7.70 (d,  $J$  = 7.7 Hz, 2H,  $CH-6/10$ ), 7.29–7.27 (m, 4H,  $CH-2/2'/7/9$ ), 4.90 (br s, 4H,  $CH_2-4/4'$ ), 2.43 (s, 3H,  $CH_3-11$ ), 1.50 (s, 15H,  $CH_3-12$ ).  $^{13}C$  NMR { $^1H$ } (126 MHz,  $CDCl_3$ )  $\delta$ ; 159.37 (1/1'), 145.22 (C-3/3'), 141.17 (C-8), 136.96 (C-5), 129.76 (7/9), 127.30 (8/10), 116.89 (C-2/2'), 86.11 (C-12), 50.18 (C-4/4'), 21.57 (C-

11), 8.96 (C-12). IR (cm<sup>-1</sup>): 3093, 2963, 2916, 1596, 1490, 1448, 1408, 1378, 1155.

### 5.3.20. Synthesis of 3-Methyl-4-formyl-1,3-thiazol-3-ium iodide **200**



The general procedure for the synthesis of **200**; Iodomethane (x eq) was added to a stirred solution of **184** (100 mg, 0.88 mmol, 1.00 eq) in acetonitrile (5 mL) and stirred under nitrogen. The solvent was removed *in vacuo* and the crude solid was washed with DCM (10 mL) and the precipitate filtered out to give the product as a spectroscopically pure orange powder in the yields described (Table 29).

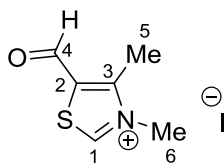
**Table 29** Methylation of electron poor thiazole **184** to novel thiazolium **200**.

Entry	MeI (x eq)	Time	T (°C)	Yield (%)
1	2.5	24 h	rt	0
2	5.0	7 d	rt	0
3	2.5	16 h	80	11
4	2.5	24 h	80	16
5	10.0	18 h	80	59

#### 5.3.20.1. Analytical Data

mp; 149.6–150.8 °C. ESIMS  $m/z = M^+(+H_2O)(-I)$  146.0068, Theoretical Mass = 146.1824. <sup>1</sup>H NMR (500 MHz, *d*<sub>6</sub>-DMSO) δ: 10.25 (d, *J* = 2.5 Hz, 1H, CH-1), 10.01 (s, 1H, CH-4), 9.17 (d, *J* = 2.5 Hz, 1H, CH-2), 4.37 (s, 3H, CH<sub>3</sub>-5). <sup>13</sup>C NMR {<sup>1</sup>H} (126 MHz, *d*<sub>6</sub>-DMSO) δ; 180.85 (C-4), 163.52 (C-1), 142.97 (C-3), 137.79 (C-2), 41.73 (C-5). IR (cm<sup>-1</sup>): 3088, 2933, 2856, 1698.

### 5.3.21. Synthesis of 3,4-Dimethyl-5-formyl-1,3-thiazol-3-ium iodide **201**



The general procedure for the synthesis of **201**; Iodomethane (x eq) was added to a stirred solution of (200 mg, 1.57 mmol, 1.00 eq) in solvent (5 mL) and stirred under nitrogen. The reaction was quenched with ethanol (1 mL) and the solvent was removed *in vacuo*. The brown solid was washed with DCM (10 mL) and the yellow precipitate was filtered to give a yellow solid in the yields described (Table 30).

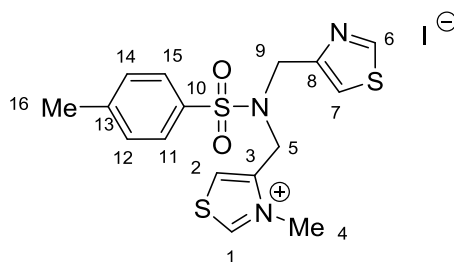
**Table 30** Methylation of a more electron rich thiazole **190** (cf. **184**).

Entry	MeI (x eq)	Solvent	Time (h)	T (°C)	Yield (%)
1	1.5	DCM	24	40	0
2	2.5	MeCN	24	rt	0
3	2.5	MeCN	18	80	18

#### 5.3.21.1. Analytical Data

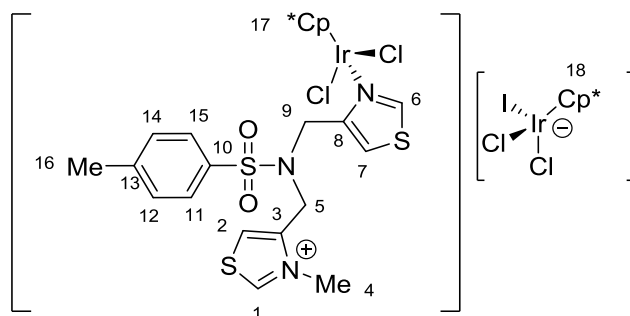
HPLC: 98% ( $t_R$  = 6.752 min). mp; 72.1–74.1 °C. ESIMS  $m/z$  =  $M^+$ +MeOH 174.0583, Theoretical Mass = 174.0589.  $^1\text{H}$  NMR (500 MHz,  $d_6$ -DMSO)  $\delta$ : 10.36 (s, 1H, CH-1), 10.21 (s, 1H, CH-4), 4.16 (s, 3H,  $\text{CH}_3$ -6), 2.84 (s, 3H,  $\text{CH}_3$ -5).  $^{13}\text{C}$  NMR  $\{^1\text{H}\}$  (126 MHz,  $d_6$ -DMSO)  $\delta$ ; 183.87 (C-4), 163.97 (C-1), 153.33 (C-2), 134.61 (C-3), 40.16 (C-6), 12.22 (C-5). IR ( $\text{cm}^{-1}$ ): 3100, 3044, 2999, 1652.

### 5.3.22. Synthesis of *N*-(3-methyl-1,3-thiazol-3-ium-4-ylmethyl)-*N*-(1,3-thiazol-4-ylmethyl)-*p*-toluenesulfonamide iodide L.7



**L.6** (100 mg, 0.27 mmol, 1.00 eq) was stirred in iodomethane (5 mL) at room temperature for 7 days. The solvent was removed *in vacuo* and recrystallized in chloroform, and the precipitate filtered to give the product as a yellow powder (95 mg, 0.19 mmol, 70%). HPLC; 87% ( $t_R = 8.072$  min). mp; 182.0–183.9 °C. ESIMS  $m/z = M^+ - I$  380.0592, Theoretical Mass = 380.0561.  $^1H$  NMR (500 MHz,  $d_6$ -DMSO)  $\delta$ : 10.04 (d,  $J = 1.9$  Hz, 1H, CH-1), 8.86 (d,  $J = 1.4$  Hz, 1H, CH-6), 8.04 (d,  $J = 1.9$  Hz, 1H, CH-2), 7.78 (d,  $J = 8.2$  Hz, 2H, CH-11/15), 7.51 – 7.42 (m, 3H, CH-7/12/14), 4.75 (s, 2H, CH<sub>2</sub>-5), 4.48 (s, 2H, CH<sub>2</sub>-9), 4.16 (s, 3H, CH<sub>3</sub>-4), 2.44 (s, 3H, CH<sub>3</sub>-16).  $^{13}C$  NMR { $^1H$ } (126 MHz, CDCl<sub>3</sub>)  $\delta$ : 160.90 (C-1), 154.55 (C-6), 151.60 (C-8), 144.14 (C-3), 143.99 (C-13), 134.45 (C-10), 130.00 (C-12/14), 127.27 (C-11/15), 125.71 (C-2), 117.84 (C-7), 47.54 (C-9), 44.94 (C-5), 39.92 (C-4), 21.02 (C-16). IR (cm<sup>-1</sup>): 3116, 3085, 3065, 2969, 1600, 1579, 1336, 1158.

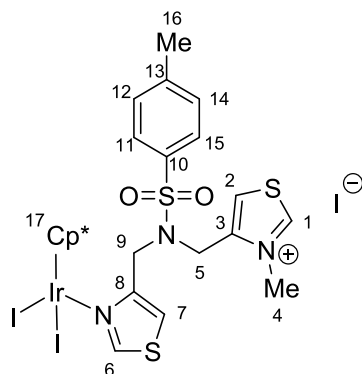
### 5.3.23. Synthesis of Dichloro[*N*-(3-methyl-1,3-thiazol-3-ium-4-ylmethyl)-*N*-(1,3-thiazol-4-ylmethyl)-*p*-toluenesulfonamide]( $\eta^5$ -pentamethylcyclopentadienyl)iridium(III) dichloroiodoiodate(III) C.7.1



**L.7** (15 mg, 0.03 mmol, 1.00 eq) and **36** (24 mg, 0.03 mmol, 1.00 eq) were stirred in acetonitrile (2 mL) at room temperature for 16 hours. The solvent was

removed from the orange solution *in vacuo* to give an orange powder, which was recrystallized from chloroform and petrol to give orange needles (23 mg, 0.02 mmol, 66%). ESIMS  $m/z = 496.1106$  [ $M^+ - C_{11}H_{13}N_2S_2O_2 + MeCN$ ], Theoretical Mass = 496.1398,  $m/z = 455.0757$  [ $M^+ - C_{11}H_{13}N_2S_2O_2$ ], Theoretical Mass = 455.1133,  $m/z = 367.2219$  [ $IrL.7CII$ ] $^{2+}$ , Theoretical Mass = 367.4462.  $^1H$  NMR (500 MHz,  $CDCl_3$ )  $\delta$ : 11.29 (s, 1H, *CH*-1), 8.81 (br s, 1H, *CH*-6), 7.96 (s, 1H, *CH*-2), 7.67 (d,  $J = 7.9$  Hz, 2H, *CH*-11/15), 7.35 (d,  $J = 7.9$  Hz, 2H, *CH*-12/14), 7.32 (s, 1H, *CH*-7), 4.77 (s, 2H, *CH*<sub>2</sub>-5), 4.60 (br s, 2H, *CH*<sub>2</sub>-9), 4.36 (s, 3H, *CH*<sub>3</sub>-4), 2.46 (s, 3H, *CH*<sub>3</sub>-16), 1.77 – 1.51 (m, 30H, *CH*<sub>3</sub>-17/18).  $^{13}C$  NMR ( $\{^1H\}$ ) (126 MHz,  $CDCl_3$ )  $\delta$ : 164.65 (*C*-1), 155.40 (br, *C*-6) 151.34 (*C*-8), 144.73 (*C*-13), 143.38 (*C*-3), 134.57 (*C*-10), 130.24 (*C*-12/14), 127.36 (*C*-11/15), 125.33 (*C*-2), 118.96 (*C*-7), 85.56 (br, *C*-17/18), 47.37 (*C*-9), 44.70 (*C*-5), 40.98 (*C*-4), 21.65 (*C*-16), 9.39 (br, *C*-17/18). X-ray crystal data for this compound can be found in the appendix.

### 5.3.24. Synthesis of Diiodo[*N*-(3-methyl-1,3-thiazol-3-ium-4-ylmethyl)-*N*-(1,3-thiazol-4-ylmethyl)-*p*-toluenesulfonamide]( $\eta^5$ -pentamethylcyclopentadienyl)iridium(III) **C.7.2**



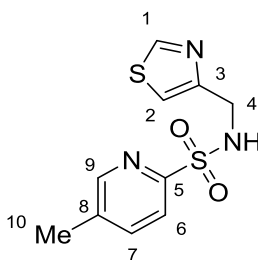
**L.7** (30 mg, 0.06 mmol, 2.00 eq) and **210** (34mg, 0.03 mmol, 1.00 eq) were stirred in DCM (5 mL) at 40 °C under nitrogen for 16 hours. The solvent was removed from the dark red solution *in vacuo* and the red solid was recrystallized from chloroform and pentane to give the product as red needles (41 mg, 0.04 mmol, 63%). mp; 175.7–182.8 °C. ESIMS  $m/z = 496.0098$  [ $Cp^*IrI + MeCN$ ], Theoretical Mass = 496.1398,  $m/z = 454.9843$  [ $Cp^*IrI$ ], Theoretical Mass = 455.1133,  $m/z = 380.0575$  [**L.7**], Theoretical Mass = 380.0561.  $^1H$

NMR (500 MHz, CDCl<sub>3</sub>)  $\delta$ : 10.95 (d,  $J$  = 2.4 Hz, 1H, CH-1), 8.60 (s, 1H, CH-6), 7.83 (d,  $J$  = 2.4 Hz, 1H, CH-2), 7.57 (d,  $J$  = 8.3 Hz, 2H, CH-11/15), 7.26 (d,  $J$  = 8.3 Hz, 2H, CH-12/14), 7.19 (s, 1H, CH-7), 4.66 (s, 2H, CH<sub>2</sub>-5), 4.41 (s, 2H, CH<sub>2</sub>-9), 4.29 (s, 3H, CH<sub>3</sub>-4), 2.38 (s, 3H, CH<sub>3</sub>-16), 1.84 (s, 15H, CH<sub>3</sub>-17). <sup>13</sup>C NMR {<sup>1</sup>H} (126 MHz, CDCl<sub>3</sub>)  $\delta$ : 162.39 (C-1), 155.89 (C-6), 150.76 (C-8), 144.70 (C-13), 144.22 (C-3), 134.70 (C-10), 130.20 (C-12/14), 127.36 (C-11/15), 124.45 (C-2), 118.51 (C-7), 88.86 (C-17), 47.18 (C-9), 44.75 (C-5), 41.16 (C-4), 21.65 (C-16), 10.76 (C-17). IR (cm<sup>-1</sup>): 3111, 3088, 3064, 2967, 2905, 1599, 1578, 1449, 1331, 1155.

### 5.3.25. Synthesis of *N*-(1,3-Thiazol-4-ylmethyl)-5-methylpyridine-2-sulfonamide L.8 and *N,N*-bis-(1,3-Thiazol-4-ylmethyl)-5-methylpyridine-2-sulfonamide L.9

**211** (100 mg, 0.58 mmol, 1.00 eq), **180•HCl** (200 mg, 1.16 mmol, 2.00 eq) and K<sub>2</sub>CO<sub>3</sub> (160 mg, 1.16 mmol, 2.00 eq) were stirred in acetonitrile (5 mL) at 80 °C for 16 hours. The reaction was cooled to room temperature and the solvent was removed *in vacuo*. The white solid was washed with DCM (2 x 20 mL) and extracted with a saturated aqueous solution of NaHCO<sub>3</sub> (2 x 20 mL). The combined organics were washed with brine (20 mL), dried with MgSO<sub>4</sub> and filtered. The solvent was removed *in vacuo* to give a white solid, from which the two title compounds were isolated and purified using column chromatography (ethyl acetate/petrol, 1:1) and recrystallized from ethyl acetate and petrol.

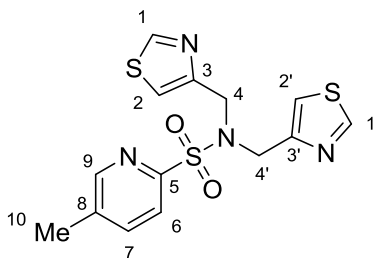
#### 5.3.25.1. Analytical Data for *N*-(1,3-Thiazol-4-ylmethyl)-5-methylpyridine-2-sulfonamide L.8





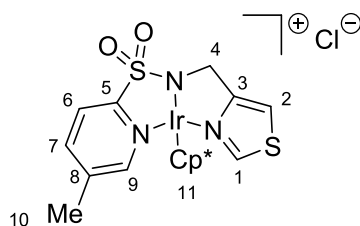
Product isolated as colourless blocks (34 mg, 0.13 mmol, 22%). *R*<sub>f</sub>: 0.29 (ethyl acetate/petrol, 3:1). HPLC; 96% (*t*<sub>R</sub> = 7.355 min). mp; 180.1–185.9 °C. ESIMS *m/z* = *M*<sup>+</sup>+*H* 270.0369, Theoretical Mass = 270.0365. <sup>1</sup>H NMR (500 MHz, *d*<sub>6</sub>-DMSO) δ: 8.98 (d, *J* = 1.9 Hz, 1H, *CH*-1), 8.54 (d, *J* = 1.6 Hz, 1H, *CH*-9), 8.39 (t, *J* = 5.1 Hz, 1H, *NH*), 7.85 (dd, *J* = 8.0, 1.6 Hz, 1H, *CH*-7), 7.80 (d, *J* = 8.0 Hz, 1H, *CH*-6), 7.43 (d, *J* = 1.9 Hz, 1H, *CH*-2), 4.30 (d, *J* = 5.1 Hz, 2H, *CH*<sub>2</sub>-4), 2.40 (s, 3H, *CH*<sub>3</sub>-10). <sup>13</sup>C NMR {<sup>1</sup>H} (126 MHz, *d*<sub>6</sub>-DMSO) δ; 155.26 (*C*-5), 154.01 (*C*-1), 153.72 (*C*-3), 150.04 (*C*-9), 138.31 (*C*-7), 136.92 (*C*-8), 121.18 (*C*-6), 115.95 (*C*-2), 42.93 (*C*-4), 17.84 (*C*-10). IR (cm<sup>-1</sup>): 3105, 3082, 3025, 2822, 1459, 1416, 1314, 1132. X-ray crystal data for this compound can be found in the appendix.

### 5.3.25.2. Analytical Data for *N,N*-bis-(1,3-Thiazol-4-ylmethyl)-5-methylpyridine-2-sulfonamide L.9



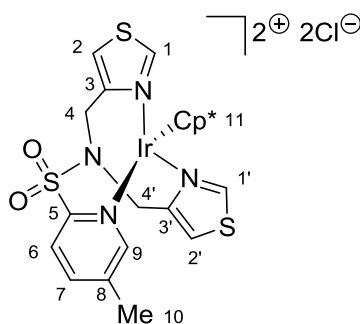
Product isolated as colourless needles (24 mg, 0.07 mmol, 11%). *R*<sub>f</sub>: 0.16 (ethyl acetate/petrol, 3:1). HPLC; 86% (*t*<sub>R</sub> = 8.392 min). mp; 172.1–176.2 °C. ESIMS *m/z* = *M*<sup>+</sup>+*H* 367.0384, Theoretical Mass = 367.0352. <sup>1</sup>H NMR (500 MHz, *d*<sub>6</sub>-DMSO) δ: 8.93 (d, *J* = 1.8 Hz, 2H, *CH*-1/1'), 8.44 (s, 1H, *CH*-9), 7.78 (d, *J* = 7.6 Hz, 1H, *CH*-7), 7.71 (d, *J* = 7.6 Hz, 1H, *CH*-6), 7.45 (d, *J* = 1.8 Hz, 2H, *CH*-2/2'), 4.72 (s, 4H, *CH*<sub>2</sub>-4/4'), 2.38 (s, 3H, *CH*<sub>3</sub>-10). <sup>13</sup>C NMR {<sup>1</sup>H} (126 MHz, *d*<sub>6</sub>-DMSO) δ; 154.87 (*C*-5), 154.15 (*C*-1/1'), 152.03 (*C*-3/3'), 150.01 (*C*-9), 138.09 (*C*-7), 136.99 (*C*-8), 121.60 (*C*-6), 117.50 (*C*-2/2'), 47.31 (*C*-4/4'), 17.86 (*C*-10). IR (cm<sup>-1</sup>): 3108, 3067, 3023, 2821, 1458, 1414, 1315, 1169.

**5.3.26. Synthesis of [N-(1,3-Thiazol-4-ylmethyl)-5-methylpyridine-2-sulfonamide]( $\eta^5$ -pentamethylcyclopentadienyl)iridium(III) chloride **C.8****



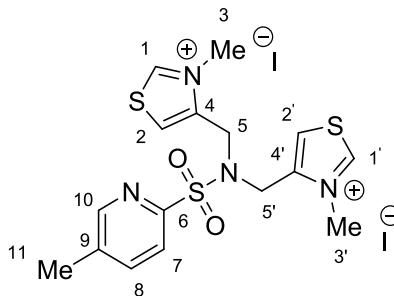
Triethylamine (13  $\mu$ L, 0.09 mmol, 1.00 eq) was added to a stirred solution of **L.8** (25 mg, 0.09 mmol, 2.00 eq) and **36** (37 mg, 0.05 mmol, 1.00 eq) in DCM (3 mL) and stirred at 40  $^{\circ}$ C for 24 hours. The solvent was removed from the orange solution *in vacuo* to give the product as orange crystals (50 mg, 0.08, 88%). mp; 168.0–176.5  $^{\circ}$ C. ESIMS  $m/z = M^+ - Cl$  596.0951, Theoretical Mass = 596.1017.  $^1H$  NMR (500 MHz,  $CDCl_3$ )  $\delta$ : 11.21 (s, 1H, CH-1), 9.83 (s, 1H, CH-9), 7.69 (d,  $J = 7.5$  Hz, 1H, CH-7), 7.60 (d,  $J = 7.5$  Hz, 1H, CH-6), 7.04 (s, 1H, CH-2), 4.81 (d,  $J = 17.3$  Hz, 1H, CHH-4), 4.22 (dd,  $J = 17.3, 1.6$  Hz, 1H, CHH-4), 2.60 (s, 3H,  $CH_3$ -10), 2.17 (s, 15H,  $CH_3$ -11).  $^{13}C$  NMR  $\{^1H\}$  (126 MHz,  $CDCl_3$ )  $\delta$ : 160.23 (C-1), 158.45 (C-3), 155.22 (C-5), 154.61 (C-9), 141.39 (C-7), 141.28 (C-8), 121.23 (C-6), 111.26 (C-2), 89.92 (C-11), 51.64 (C-4), 18.53 (C-10), 9.23 (C-11). IR ( $cm^{-1}$ ): 2978, 2946, 2916, 2739, 2531, 1632, 1475, 1444, 1332, 1171. X-ray crystal data for this compound, which was collected from a single crystal in the preparation of **C.10**, can be found in the appendix.

**5.3.27. Synthesis of [N,N-bis-(1,3-Thiazol-4-ylmethyl)-5-methylpyridine-2-sulfonamide]( $\eta^5$ -pentamethylcyclopentadienyl)iridium(III) dichloride **C.9****



**L.9** (41 mg, 0.11 mmol, 2.00 eq) and **36** (45 mg, 0.06 mmol, 1.00 eq) were stirred in DCM (3 mL) at 40 °C for 24 hours. The solvent was removed from the yellow solution *in vacuo* to give the product as yellow crystals (77 mg, 0.10 mmol, 96%). mp; 172.9–185.2 °C. ESIMS  $m/z$  = 596.0971 [ $M^+$ -C<sub>4</sub>H<sub>4</sub>NSCl<sub>2</sub>], Theoretical Mass = 596.1017,  $m/z$  = 367.0362 [**L.9**+H], Theoretical Mass = 367.0352. <sup>1</sup>H NMR (500 MHz, CDCl<sub>3</sub>) δ: 9.09 (br s, 2H, CH-1/1'), 8.43 (s, 1H, CH-9), 7.92 (d,  $J$  = 7.9 Hz, 1H, CH-7), 7.68 (d,  $J$  = 7.9 Hz, 1H, CH-6), 7.45 (s, 2H, CH-2/2'), 5.09 (br s, 4H, CH<sub>2</sub>-4/4'), 2.45 (s, 3H, CH<sub>3</sub>-10), 1.56 (s, 15H, CH<sub>3</sub>-11). <sup>13</sup>C NMR {<sup>1</sup>H} (126 MHz, CDCl<sub>3</sub>) δ; 161.26 (br, C-1/1'), 155.19 (C-3/3'), 155.00 (C-5), 150.18 (C-9), 138.21 (C-6), 137.48 (C-8), 122.91 (C-7), 117.65 (C-2/2'), 86.06 (C-11), 49.91 (br, C-4/4'), 18.59 (C-10), 9.03 (C-11). IR (cm<sup>-1</sup>): 2978, 2946, 2882, 2603, 2531, 2497, 1572, 1475, 1444, 1335, 1168.

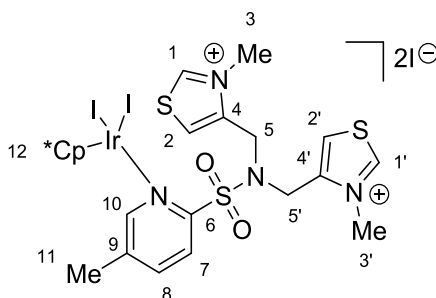
### 5.3.28. Synthesis of *N*-bis-(3-Methyl-1,3-thiazol-3-ium-4-ylmethyl)-5-methylpyridine-2-sulfonamide diiodide **L.10**



**L.9** (43 mg, 0.12 mmol, 1.00 eq) was stirred in iodomethane (2 mL, excess) at 40 °C for 16 hours. The solvent was removed *in vacuo* and washed with DCM, and the yellow precipitate filtered and dried in air to give the product as yellow crystals (32 mg, 0.06 mmol, 53%). ESIMS  $m/z$  = 395.1023 [ $M^+$ -HI<sub>2</sub>], Theoretical Mass = 395.0670. <sup>1</sup>H NMR (500 MHz, *d*<sub>6</sub>-DMSO) δ: 10.07 (s, 2H, CH-1/1'), 8.69 (s, 1H, CH-10), 8.07 – 8.01 (m, 3H, CH-2/2'/8), 7.98 (d,  $J$  = 8.0 Hz, 1H, CH-7), 4.92 (s, 4H, CH<sub>2</sub>-5/5'), 4.19 (s, 6H, CH<sub>3</sub>-3/3'), 2.48 (s, 3H, CH<sub>3</sub>-11). <sup>13</sup>C NMR {<sup>1</sup>H} (101 MHz, *d*<sub>6</sub>-DMSO) δ; 161.95 (C-1/1'), 152.83 (C-6), 151.40 (C-10), 144.72 (C-4/4'), 139.77 (C-8), 139.43 (C-9), 125.28 (C-2/2'),

123.26 (C-7), 46.23 (C-5/5'), 40.56 (C-3/3'), 18.52 (C-11). IR (cm<sup>-1</sup>): 2981, 2959, 2904, 1573, 1455, 1370, 1158.

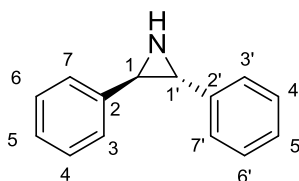
**5.3.29. Synthesis of Diiodo[*N,N*-bis-(3-methyl-1,3-thiazol-3-ium-4-ylmethyl)-5-methylpyridine-2-sulfonamide]( $\eta^5$ -pentamethylcyclopentadienyl)iridium(III) diiodide **C.10****



**L.10** (16 mg, 0.02 mmol, 1.00 eq) and **210** (12 mg, 0.01 mmol, 1.00 eq) in DCM (2 mL) and stirred at 40 °C for 16 hours. The solvent was removed from the red solution *in vacuo* to give a red powder, which was recrystallized in acetone and pentane to give the product as a red crystalline powder (17 mg, 0.01 mmol, 69%). mp; 192.5–195.7 °C. ESIMS  $m/z = 596.0962$  [ $M^+ - C_6H_{10}NSI_2$ ], Theoretical Mass = 596.1017,  $m/z = 496.0102$  [ $Cp^*IrI + MeCN$ ], Theoretical Mass = 496.1398,  $m/z = 454.9847$  [ $Cp^*IrI$ ], Theoretical Mass = 455.1133,  $m/z = 381.0515$  [**L.10**-CH<sub>3</sub>], Theoretical Mass = 381.0514,  $m/z = 284.0518$  [**L.10**-C<sub>5</sub>H<sub>7</sub>NS], Theoretical Mass = 284.0527,  $m/z = 198.0378$  [**L.10**], Theoretical mass, 198.0374. The complex decomposed before suitable NMR spectra could be collected.

## 5.4. Triazole Compounds

### 5.4.1. Synthesis of (*R,R*)-2,3-Diphenylaziridine **225**



#### 5.4.1.1. Method 1

Following a procedure by Fang,<sup>152</sup> DIAD (506  $\mu\text{L}$ , 2.57 mmol, 1.10 eq) was added to a solution triphenylphosphine (737 mg, 2.81 mmol, 1.20 eq) in THF (5 mL) at room temperature under nitrogen with vigorous stirring for 20 minutes. A solution of (*1S,2R*)-**224** (500 mg, 2.34 mmol, 1.00 eq) and triethylamine (971  $\mu\text{L}$ , 7.02 mmol, 3.00 eq) in THF (7.5 mL) was added and stirred at room temperature for 20 hours. The solvent was removed *in vacuo* to give a yellow oil, which was then directly purified using column chromatography (ethyl acetate/petrol, 1:3) to give the product as a white solid (356 mg, 1.82 mmol, 78%).

#### 5.4.1.2. Method 2

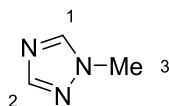
DIAD (506  $\mu\text{L}$ , 2.57 mmol, 1.10 eq) and triethylamine (971  $\mu\text{L}$ , 7.02 mmol, 3.00 eq) were added to a stirred solution of triphenylphosphine (737 mg, 2.81 mmol, 1.20 eq) and (*1S,2R*)-**224** (500 mg, 2.34 mmol, 1.00 eq) in THF (15 mL) under nitrogen at room temperature with vigorous stirring for 20 minutes. The dark yellow solution was then stirred at room temperature for 20 hours. The solvent was removed *in vacuo* to give a viscous yellow oil, which was then directly purified using column chromatography (ethyl acetate/petrol, 1:3) to give the product as a colourless oil. The product was recrystallized from ethyl acetate to give a white solid (367 mg, 1.88 mmol, 80%).

#### 5.4.1.3. Analytical Data

$R_f$ : 0.83 (ethyl acetate/petrol, 1:3). mp; 49.8–50.6  $^{\circ}\text{C}$  (Lit. 56–58  $^{\circ}\text{C}$ ). ESIMS  $m/z = M^+ + H$  196.1123, Theoretical Mass = 196.1121.  $^1\text{H}$  NMR (500 MHz,  $\text{CDCl}_3$ )  $\delta$ : 7.38 – 7.32 (m, 4H,  $\text{CH-Ph}$ ), 7.30 – 7.24 (m, 6H,  $\text{CH-Ph}$ ), 3.10 (s,

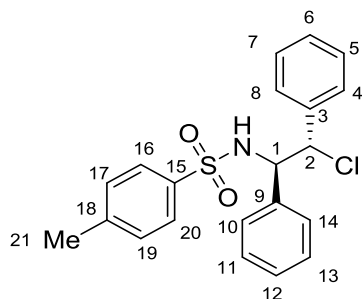
2H, CH-1/1'), 1.49 (s, 1H, NH).  $^{13}\text{C}$  NMR  $\{^1\text{H}\}$  (126 MHz,  $\text{CDCl}_3$ )  $\delta$ : 139.68 (C-2/2'), 128.64 (C-4/4'/6/6'), 127.34 (C-3/3'/7/7'), 125.52 (C-5/5'), 43.81 (C-1/1'). IR ( $\text{cm}^{-1}$ ): 3257, 3216, 3058, 3032, 2982, 1601, 1599, 1490, 1449. Spectral data is consistent with the literature.<sup>153</sup>

#### 5.4.2. Synthesis of 1-Methyl-1,2,4-triazole 230



Iodomethane (448  $\mu\text{L}$ , 7.2 mmol, 1.00 eq) was added to a solution of **226** (500 mg, 7.2 mmol, 1.00 eq) and  $\text{K}_2\text{CO}_3$  (1.49 g, 10.8 mmol, 1.50 eq) in acetonitrile (40 mL) and stirred at 45  $^\circ\text{C}$  for 2 days. The reaction was cooled to room temperature and the solvent was removed *in vacuo* to give a white solid. The solid was washed with DCM and the white precipitate was filtered out to give a colourless solution. The solvent was removed *in vacuo* to give the product as a colourless oil (444 mg, 5.34 mmol, 74%). % ( $t_{\text{R}}$  = min). ESIMS  $m/z$  =  $\text{M}^+ + \text{H}$  84.0660, Theoretical Mass = 84.0556.  $^1\text{H}$  NMR (500 MHz,  $\text{CDCl}_3$ )  $\delta$ : 8.09 (s, 1H, CH-1), 7.93 (s, 1H, CH-2), 3.95 (s, 3H,  $\text{CH}_3$ -3). IR ( $\text{cm}^{-1}$ ): 3111, 2948, 1674, 1513. Spectral data is consistent with the literature.<sup>154</sup>

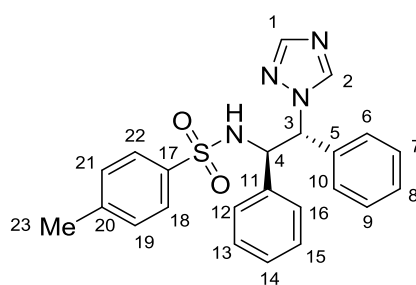
#### 5.4.3. Synthesis of *N*-(2*S*,1*R*)-(2-Chloro-1,2-diphenylethyl)-*p*-toluene sulfonamide 228



Following a modified procedure from Mattay,<sup>155</sup> a solution *p*-toluenesulfonyl chloride (259 mg, 1.36 mmol, 2.00 eq) in THF (2.5 mL) was slowly added to a stirred solution of (*R,R*)-**225** (132 mg, 0.68 mmol, 1.00 eq) and pyridine (550  $\mu\text{L}$ , 6.80 mmol, 10.0 eq) in THF (2.5 mL) at 60  $^\circ\text{C}$  under nitrogen and stirred

for 16 hours. The bright yellow opaque solution was poured directly into a slurry of ice and water (100 mL) and stirred for 10 minutes. The mixture was washed with DCM (2 x 50 mL) and extracted with brine (2 x 50 mL). The organics were collected, dried with MgSO<sub>4</sub>, filtered and the solvent was removed *in vacuo* to give a yellow oil. The product was purified with column chromatography (ethyl acetate/petrol, 1:3) to give a white solid (73 mg, 0.19 mmol, 28%). HPLC; 86% (*t<sub>r</sub>* = 10.606 min). *R<sub>f</sub>*: 0.44 (ethyl acetate/petrol, 1:3). mp; 120.1–121.7 °C (Lit. 122–123 °C).<sup>156</sup> ESIMS *m/z* = *M*<sup>+</sup> 408.0795, Theoretical Mass = 408.0801. <sup>1</sup>H NMR (500 MHz, CDCl<sub>3</sub>) δ: 7.49 (d, *J* = 8.3 Hz, 2H, *CH*-16/20), 7.32 – 7.26 (m, 1H, *CH*-6), 7.23 (t, *J* = 7.2 Hz, 2H, *CH*-5/7), 7.17 (t, *J* = 7.4 Hz, 1H, *CH*-12), 7.11 – 7.05 (m, 4H, *CH*-11/13/17/19), 7.00 (d, *J* = 7.2 Hz, 2H, *CH*-4/8), 6.81 (d, *J* = 7.3 Hz, 2H, *CH*-10/14), 5.20 (d, *J* = 5.0 Hz, 1H, *CH*-2), 5.18 (d, *J* = 8.3 Hz, 1H, *NH*), 4.81 (dd, *J* = 8.3, 5.0 Hz, 1H, *CH*-1), 2.34 (s, 1H, *CH*<sub>3</sub>-21). <sup>13</sup>C NMR {<sup>1</sup>H} (126 MHz, CDCl<sub>3</sub>) δ; 143.30 (C-18), 137.20 (C-15), 136.40 (C-3), 135.30 (C-9), 129.34 (C-17/19), 128.80 (C-6), 128.34 (C-11/13), 128.17 (C-5/7), 128.01 (C-12), 127.92 (C-10/14), 127.76 (C-4/8), 127.06 (C-16/20), 66.64 (C-2), 63.21 (C-1), 21.44 (C-21). IR (cm<sup>-1</sup>): 3278, 3064, 3032, 2983, 1598, 1495, 1457, 1437, 1326, 1168. Spectral data is consistent with the literature.<sup>157</sup>

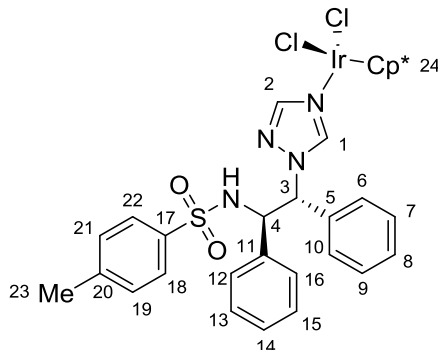
#### 5.4.4. Synthesis of (*R,R*)-*N*-{1,2-Diphenyl-2-(1,2,4-triazol-1-yl)-ethyl}-*p*-toluenesulfonamide L.11



(2*S*,1*R*)-**228** (73 mg, 0.19 mmol, 1.00 eq), 1,2,4-triazole (26 mg, 0.38 mmol, 2.00 eq) and K<sub>2</sub>CO<sub>3</sub> (52 mg, 0.38 mmol, 2.00 eq) were refluxed in acetonitrile (10 mL) for 18 hours. The reaction was cooled to room temperature and the solvent was removed *in vacuo* to give a white solid. The solid was transferred to a separating funnel, washed with DCM (10 mL), and extracted with a saturated aqueous solution of NaHCO<sub>3</sub> (10 mL). The organics were collected,

dried with MgSO<sub>4</sub>, filtered and the solvent was removed *in vacuo* to give a white powder (76 mg, 0.18 mmol, 96%). mp; 216.4–219.8 °C. ESIMS *m/z* = M<sup>+</sup>+H 419.1545, Theoretical Mass = 419.1536. <sup>1</sup>H NMR (500 MHz, *d*<sub>6</sub>-DMSO) δ: 8.49 (d, *J* = 10.9 Hz, 1H, NH), 8.36 (s, 1H, CH-1), 7.77 (s, 1H, CH-2), 7.65 (dd, *J* = 7.0, 2.3 Hz, 2H, CH-18/22), 7.40 – 7.31 (m, 3H, CH-19/21/*p*-Ph), 7.17 (d, *J* = 8.2 Hz, 2H, CH-Ph), 7.11 – 7.06 (m, 2H, CH-Ph), 7.02 – 6.96 (m, 5H, CH-Ph), 5.73 (d, *J* = 10.9 Hz, 1H, CH-3), 5.29 (t, *J* = 10.9 Hz, 1H, CH-4), 2.25 (s, 3H, CH<sub>3</sub>-23). <sup>13</sup>C NMR {<sup>1</sup>H} (101 MHz, *d*<sub>6</sub>-DMSO) δ; 161.02 (C-1/2), 142.13 (C-20), 139.96 (C-5), 138.95 (C-17), 138.91 (C-11), 129.27 (C-19/21), 128.31 (C-7/9), 127.97 (C-Ph), 127.82 (C-Ph), 127.79 (C-Ph), 127.36 (C-8), 127.12 (C-14), 126.56 (C-18/22), 62.49 (C-4), 56.54 (C-3), 21.30 (C-23). IR (cm<sup>-1</sup>): 3147, 3108, 2898, 1595, 1510, 492, 1454, 1323, 1151.

#### 5.4.5. Synthesis of Dichloro[(*R,R*)-*N*{1,2-diphenyl-2-(1,2,4-triazol-1-yl)ethyl}-*p*-toluenesulfonamide](η<sup>5</sup>-pentamethylcyclopentadienyl) iridium(III) C.11

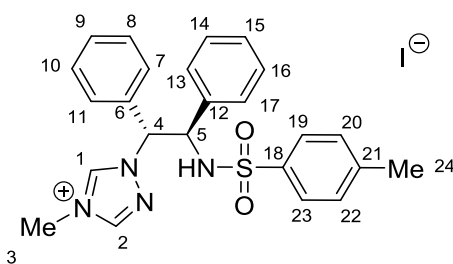


Triethylamine (8 μL, 0.06 mmol, 2.00 eq) was added to a stirred solution of (*R,R*)-L.11 (25 mg, 0.06 mmol, 2.00 eq) and **36** (24 mg, 0.03 mmol, 1.00 eq) in *iso*-propanol (5 mL) and stirred at 40 °C under nitrogen for 16 hours. The solvent was removed from the yellow solution and the orange solid was recrystallized from DCM in petrol to give orange microcrystals (47 mg, 0.06 mmol, 96%). mp; 171.9–179.2 °C. ESIMS *m/z* = M<sup>+</sup>(-Cl) 781.1972, Theoretical Mass = 781.1954. <sup>1</sup>H NMR (500 MHz, CDCl<sub>3</sub>) δ: 8.54 (s, 1H, CH-1), 7.95 (s, 1H, CH-2), 7.45 – 6.87 (m, 14H, CH-Ph), 5.72 (d, *J* = 9.3 Hz, 1H, CH-3), 5.62 (br s, 1H, NH), 5.20 (d, *J* = 9.3 Hz, 1H, CH-4), 2.32 (s, 3H, CH<sub>3</sub>-23), 1.37 (s, 15H, CH<sub>3</sub>-24). <sup>13</sup>C NMR {<sup>1</sup>H} (500 MHz, CDCl<sub>3</sub>) δ; 156.31 (C-1), 149.04 (C-2),



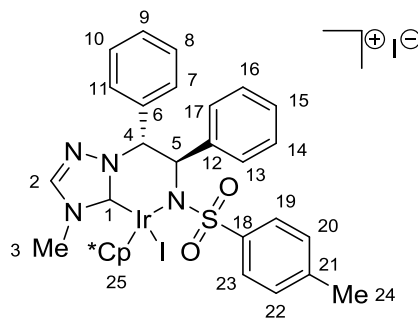
144.79 (C-20), 139.16 (C-5), 134.08 (C-17), 132.30 (C-11) 130.22 (C-19/21), 129.21 (C-12/16), 128.50 (C-Ph), 128.26 (C-Ph), 127.34 (C-18/22), 127.07 (C-Ph), 125.77 (C-Ph), 124.93 (C-6/10), 85.97 (C-24), 43.99 (C-3), 40.92 (C-4), 21.65 (C-23), 9.34 (C-24). IR (cm<sup>-1</sup>): 3062, 2978, 2920, 2604, 2498, 1599, 1523, 1455, 1327, 1156.

#### 5.4.6. Synthesis of (*R,R*)-*N*-{1,2-Diphenyl-2-(4-methyl-1,2,4-triazol-4-ium-1-yl)-ethyl}-*p*-toluenesulfonamide iodide L.12



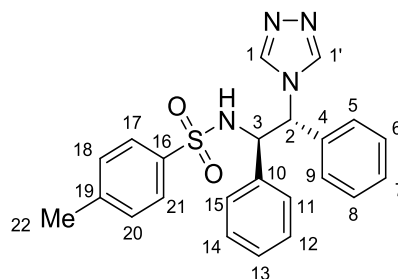
(*R,R*)-**L.11** (13 mg, 0.03 mmol, 1.00 eq) was stirred in an excess of iodomethane (2 mL) at room temperature for 3 d. The yellow solution was diluted with acetonitrile (5 mL) and the solvent was removed *in vacuo* to give the product as a yellow powder (16 mg, 0.03 mmol, 95%). mp; 116.5–119.7 °C. ESIMS *m/z* = *M*<sup>+</sup>-I 433.1688, Theoretical Mass = 433.1698. <sup>1</sup>H NMR (500 MHz, *d*<sub>6</sub>-DMSO) δ: 9.99 (s, 1H, *CH*-1), 9.03 (s, 1H, *CH*-2), 8.65 (d, *J* = 10.0 Hz, 1H, *NH*), 7.70 – 7.61 (m, 2H, *CH*-8/10), 7.46 – 7.40 (m, 2H, *CH*-7/11), 7.21 (d, *J* = 8.4 Hz, 2H, *CH*-19/23), 7.19 – 7.05 (m, 6H, *CH*-Ph), 7.02 (d, *J* = 8.4 Hz, 2H, *CH*-20/22), 6.09 (d, *J* = 10.7 Hz, 1H, *CH*-4), 5.32 (t, *J* = 10.7 Hz, 1H, *CH*-5), 3.67 (s, 3H, *CH*<sub>3</sub>-3), 2.25 (s, 3H, *CH*<sub>3</sub>-24). <sup>13</sup>C NMR {<sup>1</sup>H} (101 MHz, *d*<sub>6</sub>-DMSO) δ: 146.33 (C-2), 143.48 (C-1), 142.52 (C-21), 138.36 (C-18), 137.29 (C-12), 134.38 (C-6), 129.43 (C-8/10), 129.33 (C-20/22), 129.08 (C-Ph), 128.69 (C-7/11), 128.13 (C-9), 127.56 (C-Ph), 127.51 (C-15), 126.51 (C-19/23), 69.04 (C-4), 59.51 (C-5), 34.66 (C-3), 21.31 (C-24). IR (cm<sup>-1</sup>): 3062, 2958, 2922, 2854, 1598, 1577, 1496, 1324, 1153.

**5.4.7. Synthesis of Iodo[(*R,R*)-1-{1',2'-Diphenyl-2'-(*p*-toluenesulfonamido)-ethyl}-1,2,4-triazol-2-ylidene]( $\eta^5$ -pentamethylcyclopentadienyl) iridium(III) iodide **C.12****



(*R,R*)-**L.12** (45 mg, 0.08 mmol, 2.00 eq) and **210** (47 mg, 0.04 mmol, 1.00 eq) in DCM (5 mL) and stirred at 40 °C for 16 hours. The solvent was removed from the red solution to give a red crystalline solid, which was recrystallized from DCM and petrol to give the product as dark orange crystals (44 mg, 0.04 mmol, 54%). mp; 110.9–113.8 °C. ESIMS  $m/z = 538.0295 [M^+ - C_{21}H_{21}NO_2S]$ , Theoretical Mass = 538.0331,  $m/z = 496.0100 [M^+ - \mathbf{L.12} + MeCN]$ , Theoretical Mass = 496.0113,  $m/z = 454.9845 [M^+ - \mathbf{L.12}]$ , Theoretical Mass = 454.9848,  $m/z = 434.1726 [\mathbf{L.12} + H]$ , Theoretical Mass = 434.1771.  $^1H$  NMR (500 MHz,  $CDCl_3$ )  $\delta$ : 10.80 (s, 1H, *CH*-2), 7.94 – 7.73 (m, 2H, *CH*-Ph), 7.41 – 7.19 (m, 8H, *CH*-Ph), 7.09 – 6.94 (m, 2H, *CH*-Ph), 6.90 (d,  $J = 7.4$  Hz, 2H, *CH*-Ph), 6.73 (d,  $J = 10.0$  Hz, 1H, *CH*-4), 5.38 (t,  $J = 10.0$  Hz, 1H, *CH*-5), 3.75 (s, 1H,  $CH_3$ -3), 2.26 (s, 1H,  $CH_3$ -24), 1.85 (s, 1H,  $CH_3$ -25).  $^{13}C$  NMR  $\{^1H\}$  (101 MHz,  $CDCl_3$ )  $\delta$ : 150.58 (C-2), 144.32 (C-1), 142.90 (C-21), 137.04 (C-18), 135.73 (C-12), 132.95 (C-6), 129.71 (C-*p*-Ph), 129.62 (C-Ph), 129.38 (C-Ph), 129.10 (C-Ph), 128.83 (C-Ph), 128.73 (C-Ph), 128.26 (C-*p*-Ph), 127.87 (C-Ph), 126.82 (C-Ph), 88.04 (C-25), 68.68 (C-4), 60.67 (C-5), 32.70 (C-3), 21.41 (C-24), 10.66 (C-25). IR ( $cm^{-1}$ ): 3396, 3029, 2908, 1668, 1576, 1549, 1454, 1373, 1154.

#### 5.4.8. Synthesis of (*R,R*)-*N*-{1,2-Diphenyl-2-(1,2,4-triazol-4-yl)-ethyl}-*p*-toluenesulfonamide L.13



##### 5.4.8.1. Method 1

Following a modified route from Herrmann and Kühn,<sup>129</sup> triethyl orthoformate (3.1 mL, 18.8 mmol, 4.00 eq) was added to a stirred solution of **231** (565 mg, 9.40 mmol, 2.00 eq) in ethanol (20 mL) and stirred at 90 °C in a sealed Ace pressure tube for 3 hours. The reaction was cooled to room temperature and (*R,R*)-**162** (1.72 g, 4.70 mmol, 1.00 eq) was added to the reaction mixture. The reaction was resealed and stirred at 100 °C for 66 hours. The solvent was removed *in vacuo* to give a crude colourless oil. Compounds **L.13**, **235** and **236** were isolated and purified using column chromatography (ethyl acetate/petrol 1:1). The fractions for **L.13** resulted in an impure pink oil. The oil was recrystallized from *iso*-propanol to give the product as colourless prisms (165 mg, 0.39 mmol, 8%). The remaining compounds were recrystallized from ethyl acetate and petrol to give **236** as colourless needles (499 mg, 1.27 mmol, 27%), and **235** as colourless plates (409 mg, 1.09 mmol, 23%).

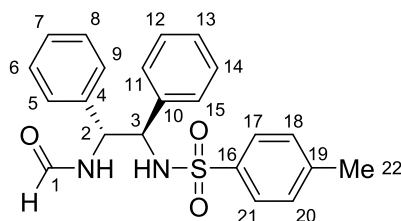
##### 5.4.8.2. Method 2

Triethyl orthoformate (3.1 mL, 18.8 mmol, 4.00 eq) was added to a stirred solution of **231** (565 mg, 9.40 mmol, 2.00 eq) in ethanol (20 mL) and heated in a microwave to 110 °C for 1 hour. (*R,R*)-**162** (1.72 g, 4.70 mmol, 1.00 eq) was added to the reaction mixture and reacted in a microwave at 110 °C for 10 hours. The solvent was removed *in vacuo* to give a crude colourless oil, which was purified by recrystallization from *iso*-propanol and ethyl acetate, to give the product as colourless prisms (201 mg, 0.48 mmol, 10%). The ethyl acetate filtrate was treated with petrol to recrystallize **236** as colourless needles (1.14 g, 2.88 mmol, 60%)

#### 5.4.8.3. Analytical Data for L.13

HPLC; 95% ( $t_R = 8.931$  min).  $R_f$ : 0.10 (ethyl acetate : petrol, 1:1). mp; 246.1–249.7 °C. ESIMS  $m/z = M^+$  419.1555, Theoretical Mass = 419.1536.  $^1\text{H}$  NMR (500 MHz,  $d_6$ -DMSO)  $\delta$ : 8.82 (s, 2H, CH-1), 8.56 (d,  $J = 10.4$  Hz, 1H, S-NH), 7.35 (dd,  $J = 7.9, 1.5$  Hz, 2H, CH-5/9), 7.26 (d,  $J = 8.2$  Hz, 2H, CH-17/21), 7.18 – 7.08 (m, 3H, CH-6–8), 7.00 (d,  $J = 8.2$  Hz, 2H, CH-18/20), 6.98 (dd,  $J = 7.4, 2.0$  Hz, 2H, CH-11/15), 6.94 – 6.87 (m, 3H, CH-12–14), 5.61 (d,  $J = 10.4$  Hz, 1H, CH-2), 5.33 (t,  $J = 10.4$  Hz, 1H, CH-3), 2.22 (s, 3H, CH<sub>3</sub>-11).  $^{13}\text{C}$  NMR ( $^1\text{H}$ ) (101 MHz,  $d_6$ -DMSO)  $\delta$ : 142.82 (C-1/1'), 142.35 (C-19), 138.65 (C-16), 137.70 (C-4), 137.27 (C-10), 129.30 (C-18/20), 128.89 (C-6/8), 128.63 (C-7), 128.56 (C-5/9), 128.15 (C-12/14), 128.00 (C-11/15), 127.49 (C-13), 126.58 (C-17/21), 64.05 (C-2), 60.42 (C-3), 21.29 (C-22). IR ( $\text{cm}^{-1}$ ): 3143, 3123, 3071, 2880, 1600, 1516, 1457, 1457, 1329, 1160. X-ray crystal data for this compound can be found in the appendix.

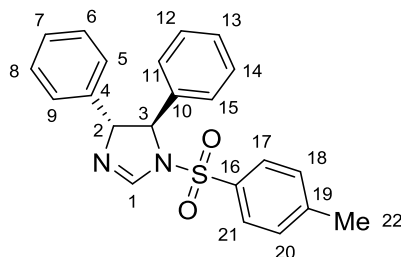
#### 5.4.8.4. Analytical Data for *N*[(*R,R*)-2-(*p*-Toluenesulfonamido)-1,2-diphenylethyl]formamide 236



HPLC; 72% ( $t_R = 9.424$  min).  $R_f$ : 0.23 (ethyl acetate/petrol, 1:1). mp; 136.6–143.8 °C. ESIMS  $m/z = M^+$  395.1426, Theoretical Mass = 395.1424.  $^1\text{H}$  NMR (500 MHz,  $\text{CDCl}_3$ )  $\delta$ : 8.19 (s, 1H, CH-1), 7.41 (d,  $J = 8.3$  Hz, 2H, CH-17/21), 7.13 – 7.06 (m, 3H, CH-6–8), 7.02 – 6.96 (m, 3H, CH-13/18/20), 6.95 – 6.89 (m, 4H, CH-5/9/12/14), 6.71 (d,  $J = 7.2$  Hz, 2H, CH-11/15), 6.50 (d,  $J = 7.9$  Hz, 1H, amide-NH), 5.80 (d,  $J = 8.1$  Hz, 1H, S-NH), 5.18 (dd,  $J = 10.0, 7.9$  Hz, 1H, CH-2), 4.50 (dd,  $J = 10.0, 8.1$  Hz, 1H, CH-3), 2.25 (s, 1H, CH<sub>3</sub>-22).  $^{13}\text{C}$  NMR ( $^1\text{H}$ ) (126 MHz,  $\text{CDCl}_3$ )  $\delta$ : 161.91 (C-1), 143.17 (C-19), 137.67 (C-16), 137.56 (C-4), 137.34 (C-10), 129.32 (C-18/20), 128.67 (C-6/8), 128.30 (C-12/14), 128.10 (C-13), 127.79 (C-7), 127.39 (C-5/9), 127.32 (C-11/15), 126.90 (C-

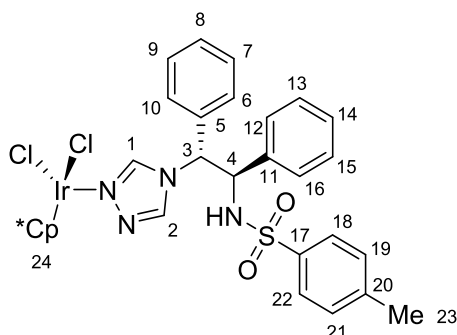
17/21), 63.17 (C-3), 57.43 (C-2), 21.42 (C-22). IR (cm<sup>-1</sup>): 3302, 3110, 3034, 2917, 2800, 2706, 1661, 1602, 1497, 1456, 1322, 1156.

#### 5.4.8.5. Analytical Data for (*R,R*)-1-(*p*-Toluenesulfonyl)-4,5-diphenyl-4,5-dihydroimidazole 235



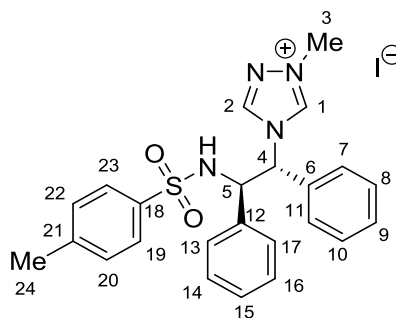
HPLC; 91% ( $t_R$  = 9.433 min).  $R_f$ : 0.68 (ethyl acetate/petrol, 1:1). mp; 181.3–182.8 °C. ESIMS  $m/z$  = 417.1245 [ $M^+$ +MeCN], Theoretical Mass = 417.1511,  $m/z$  = 395.1430 [ $M^+$ +H<sub>3</sub>O], Theoretical Mass = 395.1429. <sup>1</sup>H NMR (500 MHz, CDCl<sub>3</sub>)  $\delta$ : 7.79 (d,  $J$  = 2.0 Hz, 1H, CH-1), 7.53 (d,  $J$  = 8.3 Hz, 2H, CH-17/21), 7.40 – 7.20 (m, 8H, CH-Ph), 7.19 – 7.09 (m, 2H, CH-5/9), 6.85 (d,  $J$  = 7.8 Hz, 2H, CH-11/15), 5.07 (dd,  $J$  = 7.4, 2.0 Hz, 1H, CH-2), 4.54 (d,  $J$  = 7.4 Hz, 1H, CH-3), 2.45 (s, 3H, CH-22). <sup>13</sup>C NMR {<sup>1</sup>H} (126 MHz, CDCl<sub>3</sub>)  $\delta$ : 148.48 (C-1), 144.67 (C-19), 140.76 (C-4), 139.16 (C-10), 134.49 (C-16), 129.83 (C-18/20), 128.85 (C-*m*-Ph), 128.72 (C-*m*-Ph), 128.24 (C-*p*-Ph), 127.89 (C-*p*-Ph), 127.41 (C-17/21), 126.88 (C-5/9), 126.31 (C-11/15), 82.25 (C-2), 69.83 (C-3), 21.57 (C-22). IR (cm<sup>-1</sup>): 3350, 3309, 3066, 3037, 2929, 1661, 1597, 1500, 1325, 1158.

#### 5.4.9. Synthesis of Dichloro[(*R,R*)-*N*-(1,2-Diphenyl-2-(1,2,4-triazol-4-yl)ethyl)-*p*-toluenesulfonamide]( $\eta^5$ -pentamethylcyclopentadienyl) iridium(III) C.13



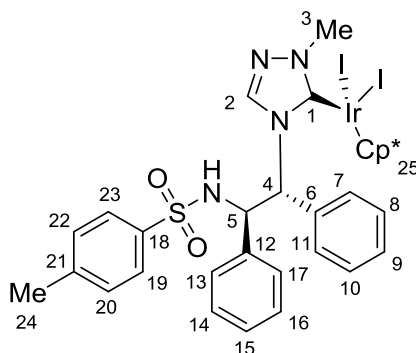
Triethylamine (17  $\mu$ L, 0.12 mmol, 2.00 eq) was added to a stirred solution of (*R,R*)-**L.13** (50 mg, 0.12 mmol, 2.00 eq) and **36** (48 mg, 0.06 mmol, 1.00 eq) in *iso*-propanol (5 mL) and stirred at 40  $^{\circ}$ C for 16 hours. The solvent was removed from the red solution to give a brown crystalline solid (94 mg, 0.12 mmol, 96%). mp; 196.8–202.7  $^{\circ}$ C. ESIMS  $m/z$  =  $M^+$ -Cl 781.1777, Theoretical Mass = 781.1955. NMR spectra contains a mixture of a major and minor species at 1.15:1.00 respectively. The signals were separated where possible. Major:  $^1\text{H}$  NMR (500 MHz,  $\text{CDCl}_3$ )  $\delta$ : 9.32 (d,  $J$  = 11.1 Hz, 1H, NH), 8.87 (s, 1H, CH-1), 8.75 (s, 1H, CH-2), 7.43 (d,  $J$  = 8.2 Hz, 2H, CH-18/22), 6.15 (d,  $J$  = 11.1 Hz, 1H, CH-3), 5.05 (t,  $J$  = 11.1 Hz, 1H, CH-4), 2.20 (s, 3H,  $\text{CH}_3$ -23), 1.74 (s, 15H,  $\text{CH}_3$ -24).  $^{13}\text{C}$  NMR  $\{^1\text{H}\}$  (126 MHz,  $\text{CDCl}_3$ )  $\delta$ : 145.86 (C-1), 141.74 (C-17), 141.67 (C-20), 141.31 (C-2), 135.66 (C-5), 135.32 (C-11), 128.66 (C-19/21), 128.27 (C-12/16), 127.98 (C-6/10), 126.73 (C-18/22), 88.01 (C-24), 63.87 (C-3), 61.15 (C-4), 21.29 (C-23), 8.85 (C-24). Minor:  $^1\text{H}$  NMR (500 MHz,  $\text{CDCl}_3$ )  $\delta$ : 10.06 (d,  $J$  = 10.5 Hz, 1H, NH), 9.69 (s, 1H, CH-1), 8.48 (s, 1H, CH-2), 7.57 (d,  $J$  = 8.2 Hz, 2H, CH-18/22), 6.25 (d,  $J$  = 10.5 Hz, 1H, CH-3), 5.20 (t,  $J$  = 10.5 Hz, 1H, CH-4), 2.22 (s, 3H,  $\text{CH}_3$ -23), 1.83 (s, 15H,  $\text{CH}_3$ -24).  $^{13}\text{C}$  NMR  $\{^1\text{H}\}$  (126 MHz,  $\text{CDCl}_3$ )  $\delta$ : 146.41 (C-1), 141.74 (C-17), 141.67 (C-20), 142.03 (C-2), 135.66 (C-5), 135.32 (C-11), 128.68 (C-19/21), 128.46 (C-12/16), 127.42 (C-6/10), 127.10 (C-18/22), 89.45 (C-24), 64.99 (C-3), 61.63 (C-4), 21.29 (C-23), 9.49 (C-24). IR ( $\text{cm}^{-1}$ ): 3030, 2979, 2863, 2604, 2497, 1598, 1534, 1495, 1325, 1156. Unassigned signals:  $^1\text{H}$  NMR (500 MHz,  $\text{CDCl}_3$ )  $\delta$ : 7.24 – 7.01 (m, CH-Ph), 6.99 – 6.80 (m, CH-Ph).  $^{13}\text{C}$  NMR  $\{^1\text{H}\}$  (126 MHz,  $\text{CDCl}_3$ )  $\delta$ : 128.94 (C-Ph), 128.89 (C-Ph), 128.85 (C-Ph), 128.68 (C-Ph), 128.04 (C-Ph), 127.74 (C-Ph).

#### 5.4.10. Synthesis of (*R,R*)-*N*-{1,2-Diphenyl-2-(1-methyl-1,2,4-triazol-1-ium-4-yl)-ethyl}-*p*-toluenesulfonamide iodide L.14



Iodomethane (15  $\mu$ L, 0.24 mmol, 2.00 eq) was added to a stirred solution of (*R,R*)-**L.13** (50 mg, 0.12 mmol, 1.00 eq) in acetonitrile (5 mL) and stirred at 50  $^{\circ}$ C for 2 days. The reaction was cooled to room temperature and the solvent was removed *in vacuo* to give the product as yellow crystals (53 mg, 0.09 mmol, 79%). mp; 123.1–125.4  $^{\circ}$ C. ESIMS  $m/z$  =  $M^+ - I$  433.1690, Theoretical Mass = 433.1698.  $^1\text{H}$  NMR (500 MHz,  $d_6$ -DMSO)  $\delta$ : 10.40 (s, 1H, *CH*-1), 9.52 (s, 1H, *CH*-2), 8.69 (d,  $J$  = 9.2 Hz, 1H, *NH*), 7.55 (d,  $J$  = 7.6 Hz, 2H, *CH*-7/11), 7.44 (d,  $J$  = 8.2 Hz, 2H, *CH*-19/23), 7.32 – 7.22 (m, 3H, *CH*-8–10), 7.18 (d,  $J$  = 8.2 Hz, 2H, *CH*-20/22), 7.07 – 6.98 (m, 5H, *CH*-13–17), 6.09 (d,  $J$  = 11.3 Hz, 1H, *CH*-4), 5.28 (dd,  $J$  = 11.3, 9.2 Hz, 1H, *CH*-5), 4.11 (s, 3H,  $\text{CH}_3$ -3), 2.31 (s, 3H,  $\text{CH}_3$ -24).  $^{13}\text{C}$  NMR  $\{^1\text{H}\}$  (101 MHz,  $d_6$ -DMSO)  $\delta$ ; 144.45 (C-2), 143.20 (C-21), 142.92 (C-1), 138.16 (C-18), 136.57 (C-12), 133.92 (C-6), 129.83 (C-9), 129.68 (C-20/22), 129.37 (C-8/10), 129.24 (C-7/11), 128.57 (C-14/16), 128.27 (C-15), 128.06 (C-13/17), 126.78 (C-19/23), 66.44 (C-4), 60.25 (C-5), 39.56 (C-24), 21.36 (C-11). IR ( $\text{cm}^{-1}$ ): 3031, 2926, 2859, 1657, 1596, 1573, 1494, 1330, 1156.

**5.4.11. Synthesis of Diiodo[(*R,R*)-4-{1',2'-Diphenyl-2'-(*p*-toluene sulfonamido)-ethyl}-1,2,4-triazol-2-ylidene]( $\eta^5$ -pentamethylcyclopentadienyl)iridium(III) **C.14****

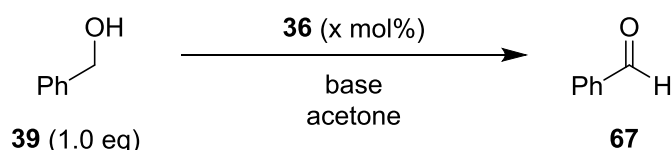


Triethylamine (20  $\mu$ L, 0.14 mmol, 3.50 eq) was added to a stirred solution of (*R,R*)-**L.14** (43 mg, 0.08 mmol, 2.00 eq) and **210** (47 mg, 0.04 mmol, 1.00 eq) in DCM (5 mL) and stirred at room temperature for 18 hours. The solvent was removed from the dark red solution to give the product as red crystals (66 mg, 0.07 mmol, 93%). mp; 189.1–191.2 °C. ESIMS  $m/z$  =  $M^+ - I$  887.1194, Theoretical Mass = 887.1468.  $^1\text{H}$  NMR (500 MHz,  $\text{CDCl}_3$ )  $\delta$ : 8.51 (s, 1H, *CH*-2), 7.39 (d,  $J$  = 11.4 Hz, 1H, *CH*-4), 7.24 (d,  $J$  = 8.3 Hz, 2H, *CH*-19/23), 7.12 (d,  $J$  = 7.2 Hz, 2H, *CH*-13/17), 7.07 (dd,  $J$  = 15.5, 7.6 Hz, 2H, *CH*-8/10), 7.02 – 6.91 (m, 6H, *CH*-9/14–16/20/22), 6.78 (br s, 1H, *NH*), 6.42 (d,  $J$  = 7.6 Hz, 2H, *CH*-7/11), 4.94 (d,  $J$  = 11.4 Hz, 1H, *CH*-5), 4.14 (s, 3H, *CH*,  $\text{CH}_3$ -3), 2.23 (s, 3H,  $\text{CH}_3$ -24), 1.48 (s, 15H,  $\text{CH}_3$ -25).  $^{13}\text{C}$  NMR  $\{^1\text{H}\}$  (101 MHz,  $\text{CDCl}_3$ )  $\delta$ ; 156.24 (*C*-1), 142.67 (*C*-2), 142.35 (*C*-21), 138.05 (*C*-18), 137.01 (*C*-12), 135.65 (*C*-6), 129.23 (*C*-20/22), 128.85 (*C*-13/17), 128.41 (*C*-15), 128.17 (*C*-8/10), 127.96 (*C*-9), 127.94 (*C*-14/16), 127.46 (*C*-7/11), 126.33 (*C*-19/23), 90.97 (*C*-25), 65.27 (*C*-4), 63.51 (*C*-5), 45.64 (*C*-3), 21.40 (*C*-24), 10.50 (*C*-25). IR ( $\text{cm}^{-1}$ ): 3179, 3032, 3914, 2667, 2476, 1662, 1597, 1553, 1493, 1331, 1156. X-ray crystal data for this compound can be found in the appendix.



## 5.5. Catalyst Testing Experiments

### 5.5.1. Transfer Dehydrogenation of Benzyl Alcohol 39



**39** (103  $\mu\text{L}$ , 1.00 mmol, 1.00 eq) was added to a solution of **36** (8 mg, 10.0  $\mu\text{mol}$ , 1.0 mol%, 2.0 mol% Ir) and  $\text{K}_2\text{CO}_3$  (14 mg, 0.10 mmol, 10 mol%) in acetone (30 mL) and stirred at room temperature under nitrogen for 6 hours. The solvent was removed *in vacuo* from the yellow solution to give a brown oil. The reaction was analysed using  $^1\text{H}$  NMR, which gave 67% conversion to product.

#### 5.5.1.1. Orthogonal-Relay Catalysis Experiment

Triethylamine (21  $\mu\text{L}$ , 0.15 mmol, 30 mol%) was added to a solution of **36** (10 mg, 12.5  $\mu\text{mol}$ , 2.5 mol%, 5.0 mol% Ir), (*R,R*)-**162** (9 mg, 25.0  $\mu\text{mol}$ , 5.0 mol%) and **130** (5 mg, 25  $\mu\text{mol}$ , 5.0 mol%) in acetone (5 mL) at 60  $^\circ\text{C}$  for 30 minutes. **39** (52  $\mu\text{L}$ , 0.50 mmol, 1.00 eq) was added to the yellow solution and stirred at 60  $^\circ\text{C}$  under nitrogen for 16 hours. The reaction was analysed using GC. 0% conversion after 16 hours.

#### 5.5.1.2. Sequential Catalysis Experiment – Thiazolium Addition

Triethylamine (150  $\mu\text{L}$ , 1.20 mmol, 50 mol%) and decane (97  $\mu\text{L}$ , 0.50 mmol, 20 mol%) were added to a solution of **36** (50 mg, 0.06 mmol, 2.5 mol%, 5.0 mol% Ir) and (*R,R*)-**162** (44 mg, 0.12 mmol, 5.0 mol%) in acetone (5 mL) and stirred at 40  $^\circ\text{C}$  for 30 minutes. **39** (250  $\mu\text{L}$ , 2.40 mmol, 1.00 eq) was added to the orange solution and stirred at 40  $^\circ\text{C}$  in air for 6 hours. **130** (25 mg, 0.12 mmol, 5.0 mol%) was added after the reaction had proceeded for 30 minutes. The reaction was followed using GC (Figure 69). 18% conversion after 90 minutes.

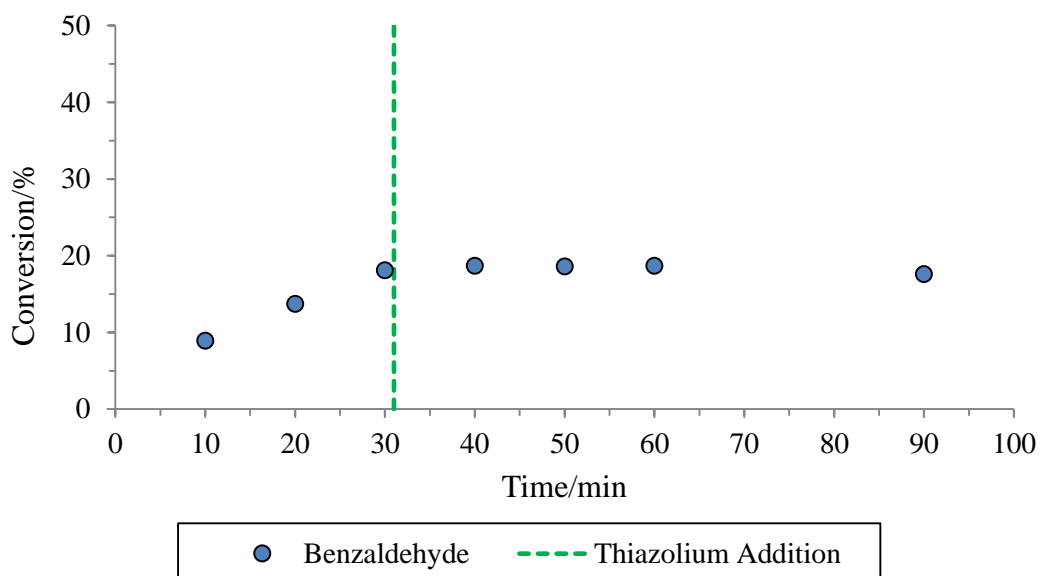


**Figure 69** The conversion (%) of **67** against time (min) for the transfer dehydrogenation reaction of **39** with thiazolium **130** added at 30 minutes. The reaction was followed using GC with decane as an internal standard.

### 5.5.1.3. Sequential Catalysis Experiment – Thiazole Addition

Triethylamine (150  $\mu\text{L}$ , 1.20 mmol, 50 mol%) and decane (97  $\mu\text{L}$ , 0.50 mmol, 20 mol%) were added to a solution of **36** (50 mg, 0.06 mmol, 2.5 mol%, 5.0 mol% Ir) and (*R,R*)-**162** (44 mg, 0.12 mmol, 5.0 mol%) in acetone (5 mL) and stirred at 40  $^{\circ}\text{C}$  for 30 minutes. **39** (250  $\mu\text{L}$ , 2.40 mmol, 1.00 eq) was added to the orange solution and stirred at 40  $^{\circ}\text{C}$  for 6 hours. **169** (11  $\mu\text{L}$ , 0.12 mmol, 5.0 mol%) was added after the reaction had proceeded for 30 minutes. The reaction was followed using GC (Figure 70). 39% conversion after 90 minutes.

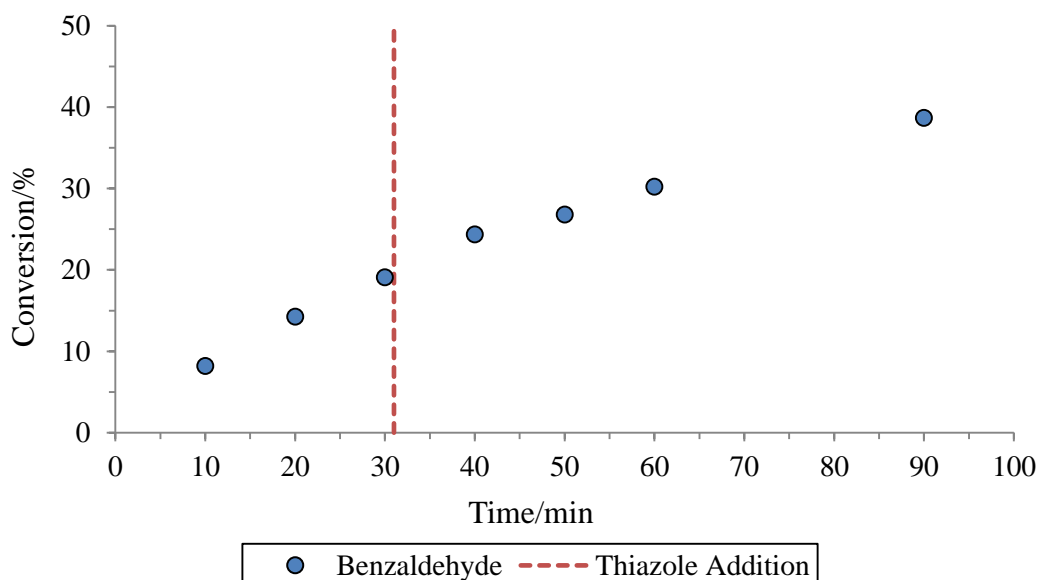
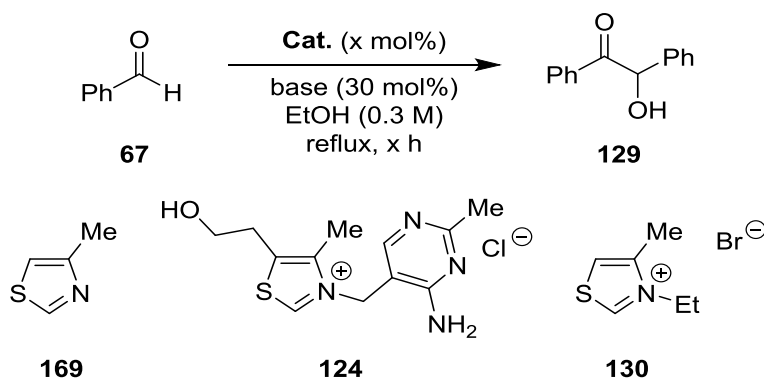


Figure 70 The conversion (%) of **67** against time (min) for the transfer dehydrogenation reaction of **39** with thiazole **169** added at 30 minutes. The reaction was followed using GC with decane as an internal standard.

### 5.5.2. Benzoin Condensation of Benzaldehyde **67**



#### 5.5.2.1. General procedure

**67** (1.00 eq) was added to a solution of catalyst (x mol%) in EtOH (30 mL). Base (x eq) was added to the reaction and stirred at reflux. The reaction was cooled to room temperature and concentrated *in vacuo*. The crude was washed with DCM (2x 20 mL) and extracted with water (2 x 20 mL) and brine (20 mL). The combined organics were dried with MgSO<sub>4</sub>, filtered and the solvent was removed *in vacuo* to give the product as a yellow oil. The oil was

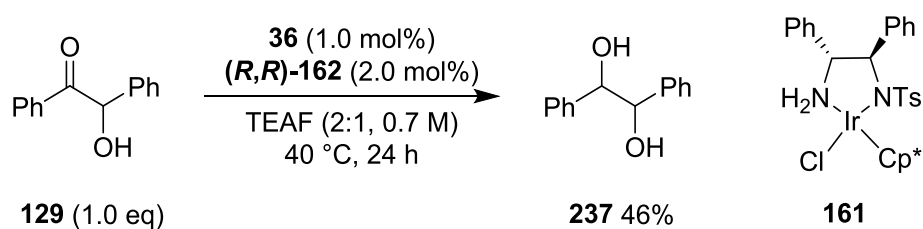
recrystallized from DCM and petrol to give the product as yellow needles (Table 31).

**Table 31** The catalyst tests for the benzoin condensation of **67** to **129**

Entry	Catalyst	Catalyst Loading (mol%)	Base	Base Loading (mol%)	Time (h)	Yield (%)
1	<b>169</b>	5	Et <sub>3</sub> N	30	24	0
2	<b>169</b>	20	DBU	30	24	0
3	<b>124</b>	5	Et <sub>3</sub> N	30	1.5	5
4	<b>124</b>	5	Et <sub>3</sub> N	30	1.5	13
5	<b>124</b>	5	KO <sup>t</sup> Bu	30	4	0
6	<b>130</b>	10	K <sub>2</sub> CO <sub>3</sub>	10	24	0 <sup>a</sup>
7	<b>130</b>	2	Et <sub>3</sub> N	60	5	0
8	<b>130</b>	20	Et <sub>3</sub> N	60	5	68

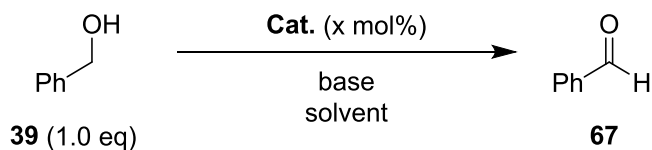
<sup>a</sup> Reaction carried out in MeCN.

### 5.5.3. Transfer Hydrogenation of Benzoin **129**



**129** (212 mg, 1.00 mmol, 1.00 eq), **36** (8 mg, 10.0  $\mu$ mol, 1.0 mol%, 2.0 mol% Ir) and (*R,R*)-**162** (7 mg, 20.0  $\mu$ mol, 2.0 mol%) in a mixture of formic acid and triethylamine (1.5 mL, 2:1 v/v respectively), at 40 °C under nitrogen for 24 hours. The reaction was allowed to cool to room temperature and diluted with water (5 mL). The precipitate was filtered and washed with water (10 mL). The brown solid was dried for 16 hours to give a brown powder, which was washed with DCM (10 mL) and dried in air to give a colourless powder (62 mg, 0.29 mmol, 29%). <sup>1</sup>H NMR gave 46% conversion after 24 hours.

## 5.6. Transfer Dehydrogenation Experiments



### 5.6.1. Initial Test with TsDPEN Iridium(III) Catalyst 161

**36** (10 mg, 12.5  $\mu\text{mol}$ , 2.5 mol%, 5.0 mol% Ir) and (*R,R*)-**162** (9 mg, 25.0  $\mu\text{mol}$ , 5.0 mol%) were dissolved in acetone (2 mL) and stirred under nitrogen at room temperature. **39** (52  $\mu\text{L}$ , 0.50 mmol, 1.00 eq) and triethylamine (25  $\mu\text{L}$ , 0.15 mmol, 30 mol%) were added to the orange solution and stirred at 70 °C under nitrogen for 20 hours. The reaction was analysed using GC-MS. 54% conversion after 20 hours.

### 5.6.2. Initial Test with C.1

**39** (52  $\mu\text{L}$ , 0.50 mmol, 1.00 eq) and triethylamine (25  $\mu\text{L}$ , 0.15 mmol, 30 mol%) were added to a solution of **C.1** (20 mg, 25.0  $\mu\text{mol}$ , 5.0 mol%) in acetone (5 mL) and stirred under nitrogen at 70 °C under nitrogen for 22 hours. The reaction was analysed using GC-MS. 0% conversion after 22 hours.

### 5.6.3. Initial Test with C.2

Triethylamine (42  $\mu\text{L}$ , 0.30 mmol, 30 mol%) was added to a solution of **C.2** (43 mg, 50.0  $\mu\text{mol}$ , 5.0 mol%) in acetone (5 mL) and stirred at 40 °C for 30 minutes. **39** (103  $\mu\text{L}$ , 1.00 mmol, 1.00 eq) was added to the orange solution and stirred at 80 °C for 18 hours. The reaction was analysed using  $^1\text{H}$  NMR. 10% conversion after 18 hours.

### 5.6.4. General Procedure for Parallel Control Reactions

Decane (97  $\mu\text{L}$ , 0.50 mmol, 10 mol%) was added to a solution of catalyst (43 mg, 50.0  $\mu\text{mol}$ , 1.0 mol%) and  $\text{K}_2\text{CO}_3$  (70 mg, 0.50 mmol, 10 mol%) in acetone

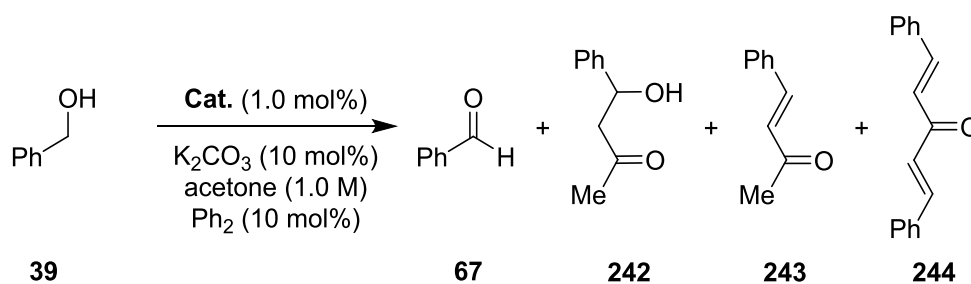
(5 mL) and stirred at room temperature for 30 minutes. **39** (514  $\mu$ L, 5.00 mmol, 1.00 eq) was added and the reaction was stirred at 60 °C for 24 hours. The reaction was analysed using GC (Table 32).

**Table 32** Catalyst tests with control and novel catalysts.

Entry	Catalyst	Conversion (%) <sup>a</sup>
1	<b>36</b>	16
2	<b>36</b> + ( <i>R,R</i> )- <b>162</b>	18
3	<b>C.2</b>	14

<sup>a</sup> Conversion calculated from the corrected peak integrals using decane as an internal standard for GC at 24 hours.

### 5.6.5. Aldol Experiment with C.2



**C.2** (43 mg, 50.0  $\mu$ mol, 1.0 mol%),  $\text{K}_2\text{CO}_3$  (70 mg, 0.50 mmol, 10 mol%) and biphenyl (77 mg, 0.50 mmol, 10 mol%) were stirred in acetone (5 mL) at 40 °C for 30 minutes. **39** (514  $\mu$ L, 5.00 mmol, 1.00 eq) was added and the reaction was stirred at 60 °C for 24 hours. The reaction was followed using GC (Figure 71). **67**; 8%, **242**; 8%, after 5 hours.

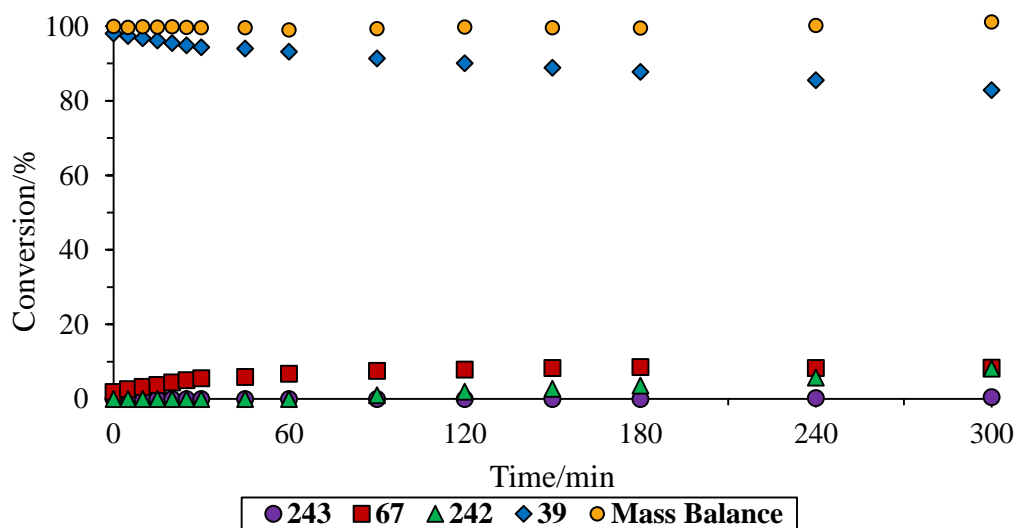


**Figure 71** The conversion of **39** to **67** and the aldol reaction of **67** with acetone to give **242** and further products **243** and **244** with catalyst **C.2**. Samples quantified using GC with biphenyl as an internal standard.

#### 5.6.6. Aldol Experiment with $[\text{Cp}^*\text{IrCl}_2]_2$ **36**

**36** (20 mg, 25.0  $\mu\text{mol}$ , 1.0 mol% Ir),  $\text{K}_2\text{CO}_3$  (70 mg, 0.50 mmol, 10 mol%) and biphenyl (77 mg, 0.50 mmol, 10 mol%) were stirred in acetone (5 mL) at 40  $^\circ\text{C}$  for 30 minutes. **39** (514  $\mu\text{L}$ , 5.00 mmol, 1.00 eq) was added and the reaction was stirred at 60  $^\circ\text{C}$  for 24 hours. The reaction was followed using GC (Figure 72). **67**; 16%, **242**; 14%, **243**; <1% after 5 hours.

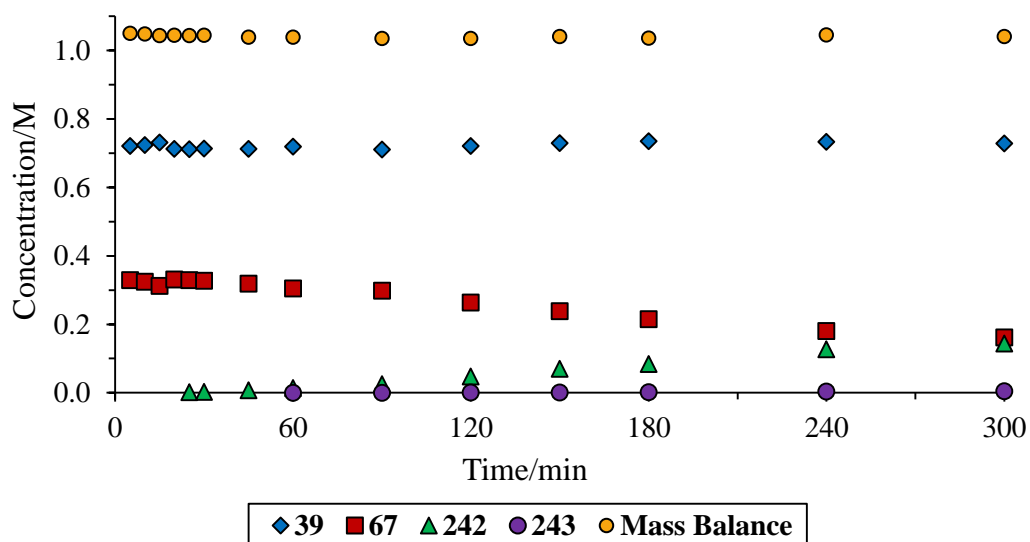
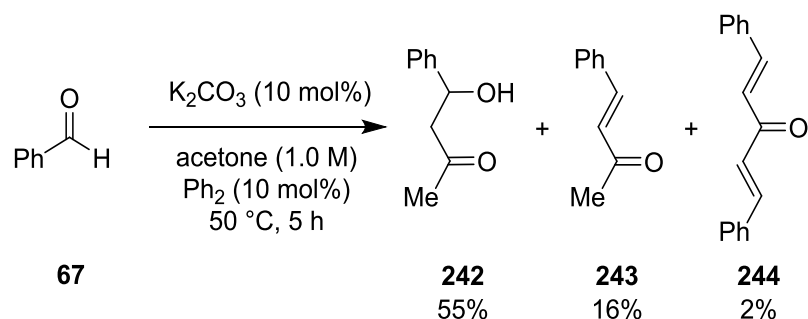


**Figure 72** The conversion of **39** to **67** and the aldol reaction of **67** with acetone to give **242** and further products **243** and **244** with catalyst **36**. Samples quantified using GC with biphenyl as an internal standard.

### 5.6.7. 39 Control Test

$K_2CO_3$  (70 mg, 0.50 mmol, 10 mol%) and biphenyl (77 mg, 0.50 mmol, 10 mol%) were stirred in acetone (5 mL) at 40 °C for 30 minutes. **39** (514  $\mu$ L, 5.00 mmol, 1.00 eq) was added and the reaction was stirred at 60 °C for 5 hours. The reaction was analysed using GC. 0% conversion after 5 hours.

### 5.6.8. Aldol Background Experiment

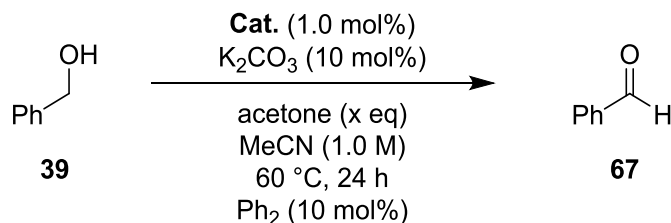


$K_2CO_3$  (70 mg, 0.50 mmol, 10 mol%) and biphenyl (77 mg, 0.50 mmol, 10 mol%) were stirred in acetone (5 mL) at 40 °C for 30 minutes. **67** (514  $\mu$ L, 5.00 mmol, 1.00 eq) was added and the reaction was stirred at 60 °C for 5 hours.



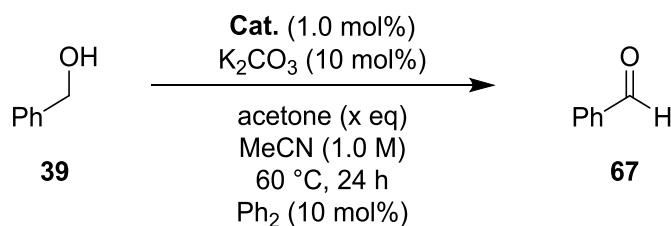
The reaction was analysed using GC. **67**; 27%, **242**; 55%, **243**; 16%, **244**; 2%, after 5 hours.

### 5.6.9. General Procedure – Acetone Experiments



Catalyst (1.0 mol%), K<sub>2</sub>CO<sub>3</sub> (70 mg, 0.50 mmol, 10 mol%) and biphenyl (77 mg, 0.50 mmol, 10 mol%) were stirred in acetonitrile (5 mL) at 40 °C for 30 minutes. **39** (514 μL, 5.00 mmol, 1.00 eq) and acetone (x eq) were added and the reaction was stirred at 60 °C for 24 hours. The reaction was followed with GC (Table 33, Figure 73).

**Table 33** The conversions to **67** with varied acetone equivalents.



Entry	Catalyst	Acetone (eq)	Conversion (%) <sup>a</sup>
1	C.2	0	1
2	C.2	1	5
3	C.2	5 <sup>b</sup>	7 <sup>c</sup>
4	C.1	1	3
5	C.3 <sup>d</sup>	2	12
6	C.4	1	5
7	C.5 <sup>d</sup>	2	3
8	C.6 <sup>d</sup>	2	5
9	C.7.1 <sup>d</sup>	2	4

<sup>a</sup> Conversion calculated at 24 hours using GC from the corrected peak integrals with biphenyl as an internal standard. <sup>b</sup> 5 equivalents added evenly over a period of 5 hours. <sup>c</sup> Conversion calculated at 6 hours. <sup>d</sup> 0.5 mol% catalyst.

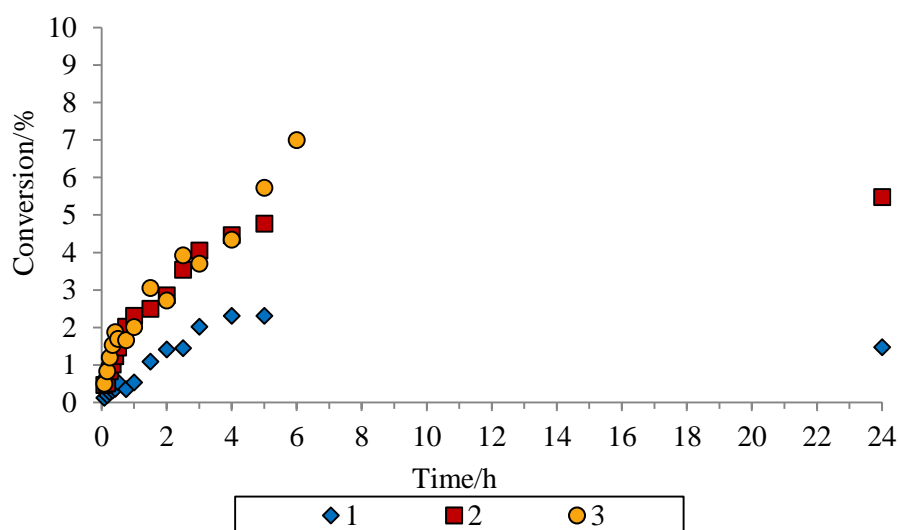
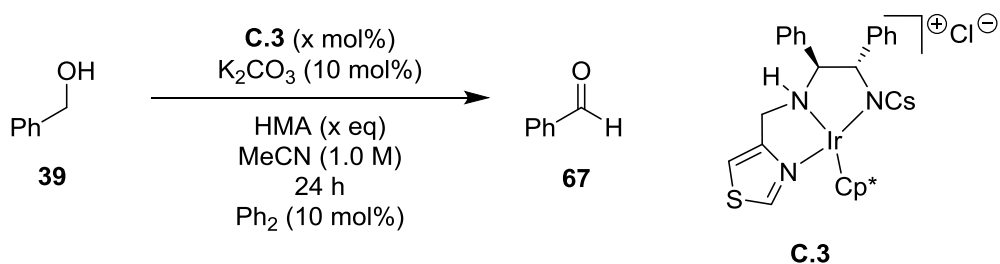


**Figure 73** Conversion (%) to **67** against reaction time (hours) with three different conditions (entries 1–3, Table 33).

### 5.6.10. General Procedure – Comparison of Catalysts

Catalyst (x mol%), K<sub>2</sub>CO<sub>3</sub> (35 mg, 0.25 mmol, 10 mol%) and biphenyl (39 mg, 0.25 mmol, 10 mol%) were stirred in acetonitrile (2.5 mL) at 40 °C for 30 minutes. HMA (x eq) and **39** (257 μL, 2.50 mmol, 1.00 eq) were added to the reaction and stirred at 50 °C for 24 hours. The reaction was followed with GC (Table 34).

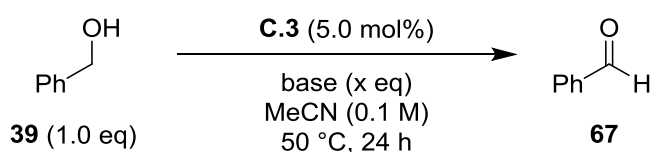
**Table 34** Catalyst tests with HMA as the hydrogen acceptor.



Entry	Catalyst Loading (mol%)	HMA (eq)	Temperature (°C)	Conversion (%) <sup>a</sup>
1	1.0	2.0	50	5
2	0.7	2.0	75	9
3	0.5	solvent	60	1

<sup>a</sup> Conversion calculated at 24 hours using GC from the corrected peak integrals with biphenyl as an internal standard.

### 5.6.11. General Procedure – Acetone and Base Optimisation



**C.3** (11 mg, 0.013 mmol, 5.0 mol%), base (x eq) and biphenyl (4 mg, 25.0  $\mu\text{mol}$ , 10 mol%) were stirred in acetonitrile (2 mL) at 40  $^\circ\text{C}$  for 30 minutes. Acetone (x eq) and **39** (27  $\mu\text{L}$ , 0.26 mmol, 1.00 eq) were added to the reaction and stirred at 50  $^\circ\text{C}$  for 24 hours. The reaction was followed using GC (Table 35, Figure 74).

**Table 35** Catalyst tests with varied base, base loading and acetone equivalents.

Entry	Base	Base Loading (eq)	Acetone (eq)	Conversion (%) <sup>a</sup>
1	$\text{K}_2\text{CO}_3$	0.1	5	8 <sup>b</sup>
2	$\text{Et}_3\text{N}$	0.5	5	11 <sup>b</sup>
3	$\text{Et}_3\text{N}$	1.0	10	8
4	$\text{Et}_3\text{N}$	5.0	10	4 <sup>c</sup>
5	$\text{Et}_3\text{N}$	1.0	20	12
6	$\text{K}_2\text{CO}_3$	1.0	10	11
7	$\text{K}_2\text{CO}_3$	1.0	20	26
8	$\text{K}_2\text{CO}_3$	1.0	30	24
9	$\text{K}_2\text{CO}_3$	1.0	40	25
10	$\text{K}_2\text{CO}_3$	1.0	50	30
11	$\text{KO}^t\text{Bu}$	1.0	50	4
12	$\text{AcOH}$	1.0	50	3

<sup>a</sup> Conversion calculated from the corrected peak integrals using biphenyl as an internal standard for GC at 24 hours. <sup>b</sup> MeCN (1 mL). <sup>c</sup> Conversion calculated at 4 hours.

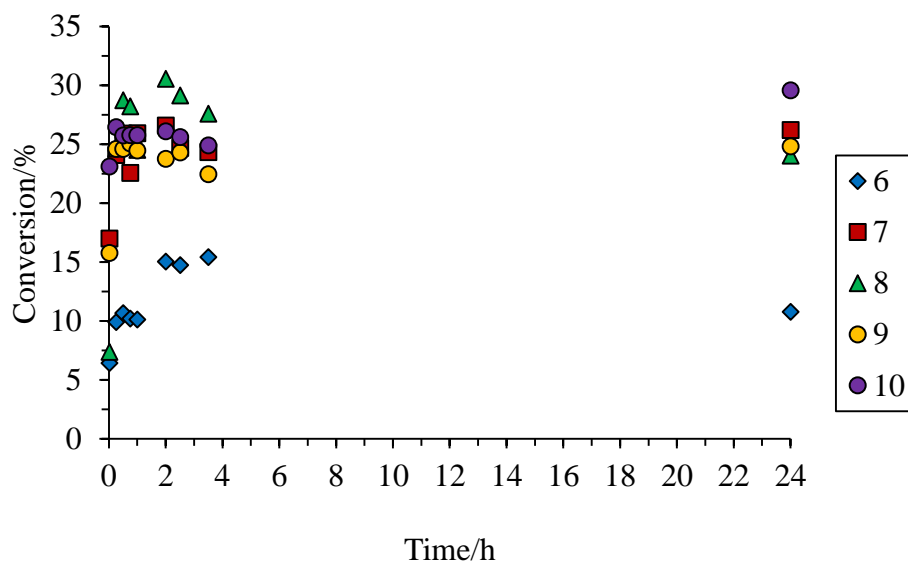
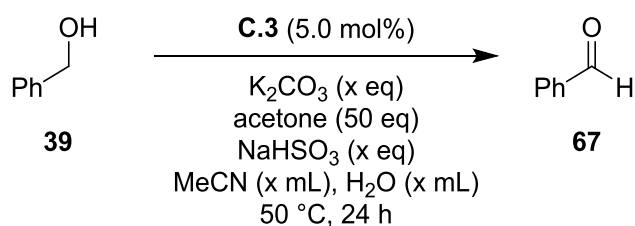


**Figure 74** Conversion (%) against time (hours) for catalyst tests (entries 6–10, Table 35).

### 5.6.12. General Procedure – Water and NaHSO<sub>3</sub> Addition



A solution of **39** (27  $\mu\text{L}$ , 0.26 mmol, 1.00 eq) and acetone (955  $\mu\text{L}$ , 13.0 mmol, 50.0 eq) was added to a solution of **C.3** (11 mg, 13.0  $\mu\text{mol}$ , 5.0 mol%), K<sub>2</sub>CO<sub>3</sub> (x eq), sodium bisulfite (x eq) and biphenyl (4 mg, 25.0  $\mu\text{mol}$ , 10 mol%) in acetonitrile (x mL) and water (x mL) at 50 °C and stirred for 24 hours. The coloured reaction was analysed using GC (Table 36).

**Table 36** Catalyst tests with sodium bisulfite to trap **67**.

Entry	K <sub>2</sub> CO <sub>3</sub> (eq)	MeCN (mL)	Water (mL)	NaHSO <sub>3</sub> (eq)	Conversion (%) <sup>a</sup>
1	0	2	0	0	9
2	1	2	0	1	16
3	0	2	0	1	9
4	0	1	1	0	8
5	0	1	1	1	9
6	1	1	1	0	12 <sup>b</sup>
7	1	1	1	1	13

<sup>a</sup> Conversion calculated from the corrected peak integrals using biphenyl as an internal standard for GC at 24 hours.

### 5.6.13. Experiment with a Second Addition of Catalyst

**C.3** (11 mg, 12.5  $\mu\text{mol}$ , 5.0 mol%),  $\text{K}_2\text{CO}_3$  (36 mg, 0.26 mmol, 1.00 eq) and biphenyl (4 mg, 25.0  $\mu\text{mol}$ , 10 mol%) were stirred in acetonitrile (2 mL) at 40  $^\circ\text{C}$  for 30 minutes. Acetone (764  $\mu\text{L}$ , 10.4 mmol, 40.0 eq) and **39** (27  $\mu\text{L}$ , 0.26 mmol, 1.00 eq) were added and the reaction was stirred at 50  $^\circ\text{C}$ . After 1 hour, a second portion of catalyst was added (11 mg, 12.5  $\mu\text{mol}$ , 5.0 mol%) and the reaction was stirred at 50  $^\circ\text{C}$  for 23 hours. The reaction was followed using GC (Figure 75). 16% conversion after 24 hours.

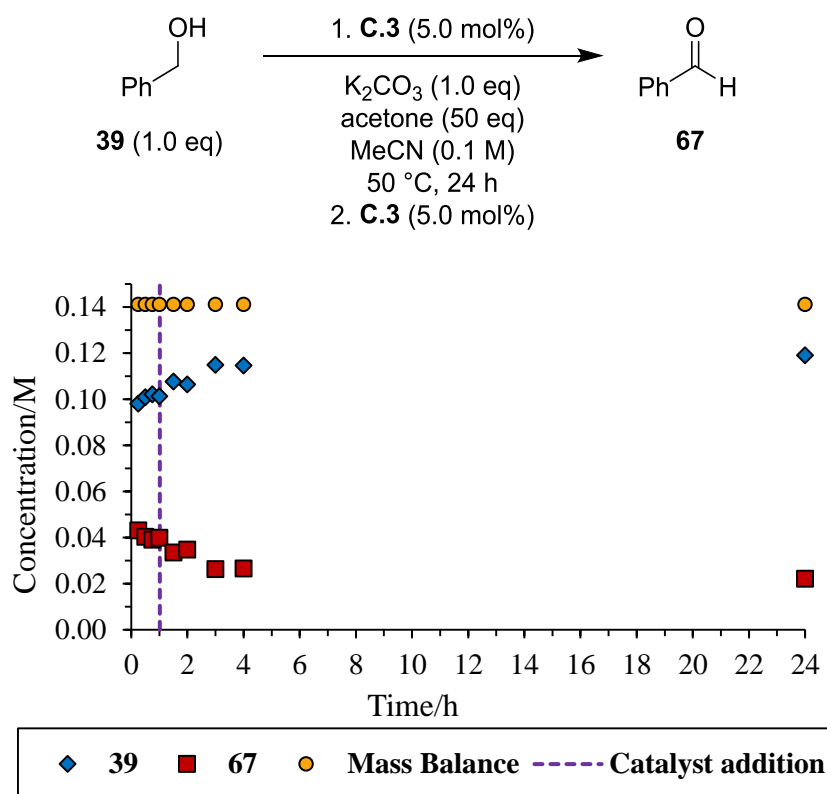


**Figure 75** Catalyst test with a second addition of catalyst (5 mol%) after 1.5 hours.

### 5.6.14. Portioned Addition of Substrate

**C.3** (22 mg, 26.0  $\mu\text{mol}$ , 5.0 mol%),  $\text{K}_2\text{CO}_3$  (72 mg, 0.52 mmol, 1.00 eq) and biphenyl (8 mg, 52.0  $\mu\text{mol}$ , 10 mol%) were stirred in acetonitrile (4 mL) at 40

°C for 30 minutes. Acetone (1.5 mL, 20.8 mmol, 40.0 eq) and **39** (6  $\mu$ L, 52.0  $\mu$ mol, 10 mol%) were added to the reaction and stirred at 50 °C for 24 hours. A further 9 portions of substrate (6  $\mu$ L, 52.0  $\mu$ mol, 10 mol%) were added after 30 minutes with intervals of 30 minutes. The reaction was followed using GC. 32% conversion after 24 hours (Figure 76).

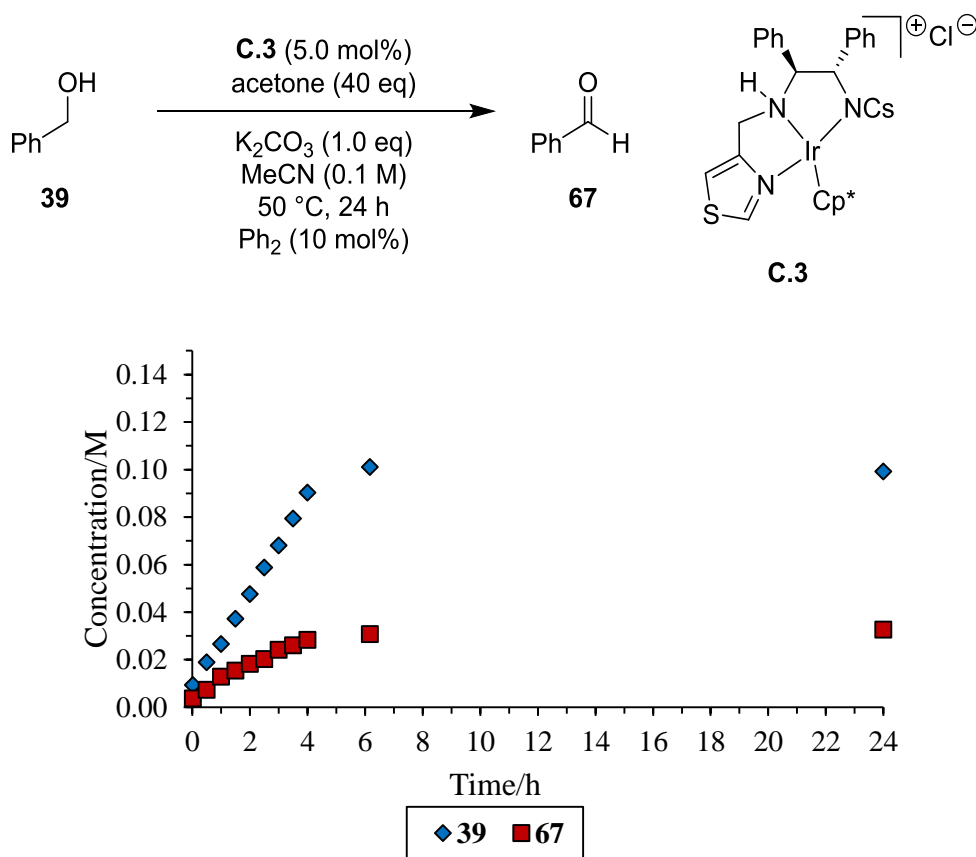


**Figure 76** Conversion (%) against time (hours) with **39** (0.1 eq) added every 30 minutes for 5 hours.

### 5.6.15. Experiment Starting with 1:1 Substrate/Product

A solution of **39** (14  $\mu$ L, 0.13 mmol, 0.50 eq) and **67** (13  $\mu$ L, 0.13 mmol, 0.50 eq) in acetone (955  $\mu$ L, 13.0 mmol, 50.0 eq) was added to a solution of **C.3** (11 mg, 13.0  $\mu$ mol, 5.0 mol%),  $K_2CO_3$  (36 mg, 0.26 mmol, 1.00 eq) and biphenyl (4 mg, 25.0  $\mu$ mol, 10 mol%) in acetonitrile (2 mL) at 50 °C and stirred

for 24 hours. The reaction was followed using GC; 10% increase in **67** concentration and 10% decrease in **39** after 24 hours (Figure 77).

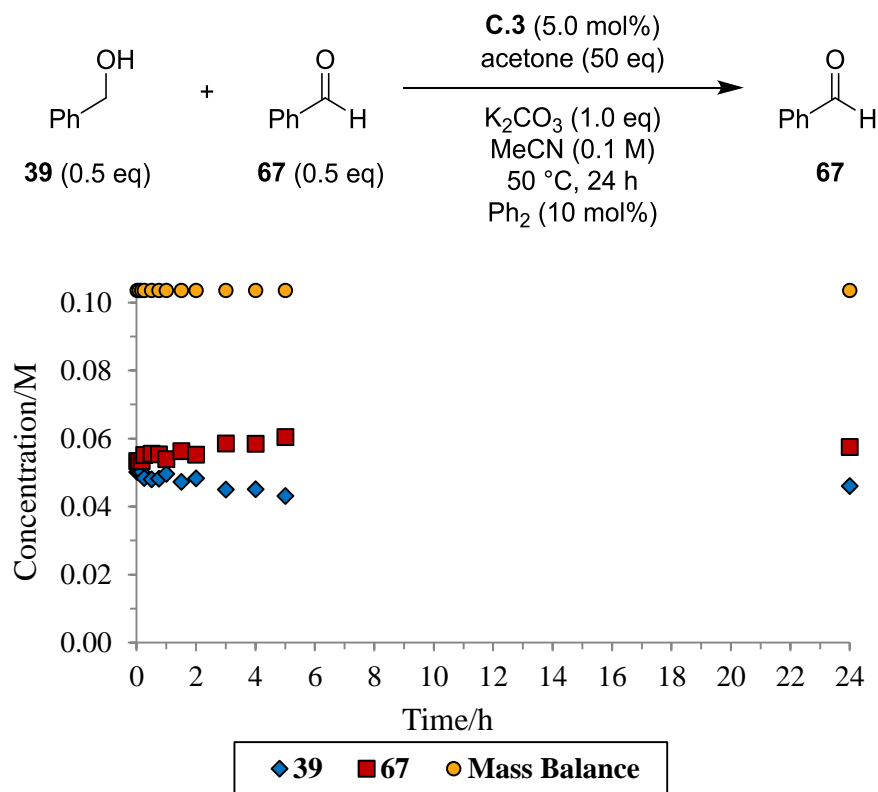


**Figure 77** Catalyst test with a starting equimolar mixture of **39** and **67**.

#### 5.6.16. Distillation Experiment with Syringe Pump Addition

A solution of **39** (270  $\mu\text{L}$ , 2.90 mmol, 1.00 eq) and acetone (4.8 mL, 65.0 mmol, 25 eq) was added to a solution of **C.3** (55 mg, 65  $\mu\text{mol}$ , 2.5 mol%),  $\text{K}_2\text{CO}_3$  (360 mg, 2.60 mmol, 1.00 eq) and biphenyl (40 mg, 0.26 mmol, 10 mol%) in acetonitrile (20 mL) and heated at 110  $^\circ\text{C}$  (distillation temperature; 70  $^\circ\text{C}$ ). A solution of acetonitrile and acetone (8:1, v/v) was continuously added to the reaction via syringe pump at a rate equalling the rate of distillation ( $\sim 200 \mu\text{L}$



per minute). The reaction was followed using GC; 11% conversion after 24 hours (Figure 78).

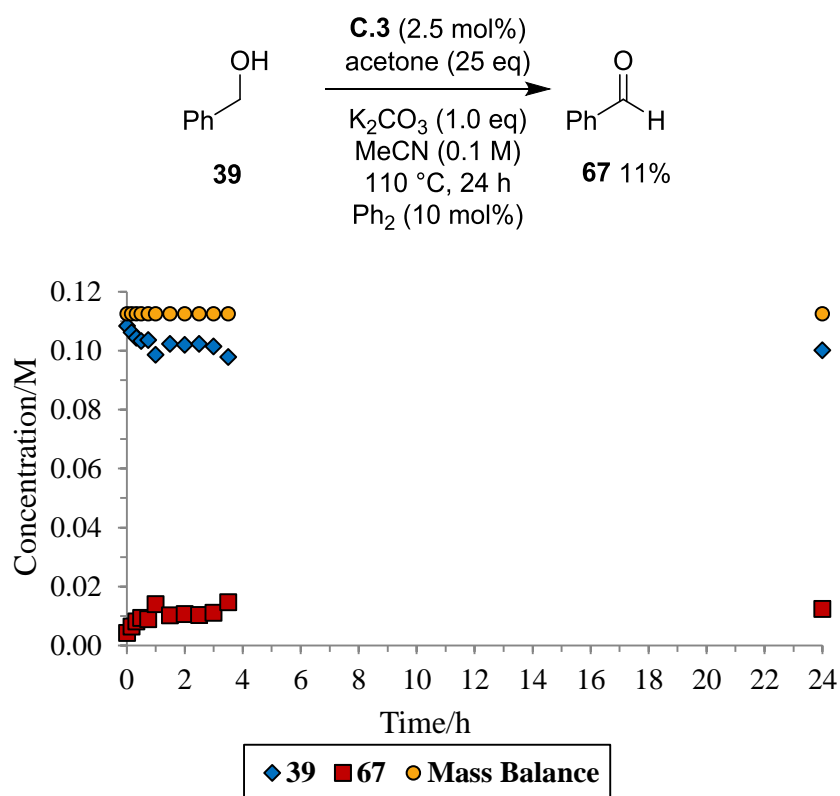


**Figure 78** The distillation reaction was followed using GC with biphenyl as an internal standard. The distillation was stopped after four hours and the reaction was continued at 50 °C.

### 5.6.17. Catalyst Addition Experiment – No Base

In a flame dried Schlenk tube, a solution of **39** (26  $\mu\text{L}$ , 0.25 mmol, 1.00 eq) and acetone (918  $\mu\text{L}$ , 12.5 mmol, 50.0 eq) was added to a solution of biphenyl (4 mg, 25.0  $\mu\text{mol}$ , 10 mol%) in acetonitrile (2 mL) at 50 °C and stirred for 1 hour. A solution of catalyst **C.3** (11 mg, 12.5  $\mu\text{mol}$ , 5.0 mol%) in acetonitrile (1 mL) was prepared in a flame dried Schlenk tube under nitrogen and the solution was added to the reaction in four equal portions with one hour intervals. The reaction was analysed with GC. 9% conversion after 24 hours.

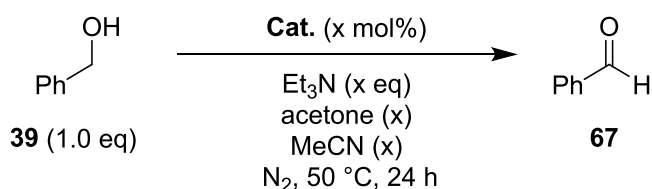
### 5.6.18. Catalyst Addition Experiment – Base in Reaction

In a flame dried Schlenk tube, a solution of **39** (26  $\mu$ L, 0.25 mmol, 1.00 eq) and acetone (918  $\mu$ L, 12.5 mmol, 50.0 eq) was added to a solution of  $K_2CO_3$  (35 mg, 0.25 mmol, 1.00 eq) and biphenyl (4 mg, 25.0  $\mu$ mol, 10 mol%) in acetonitrile (2 mL) at 50  $^\circ$ C and stirred for 1 hour. A solution of catalyst **C.3** (11 mg, 12.5  $\mu$ mol, 5.0 mol%) in acetonitrile (1 mL) was prepared in a flame dried Schlenk tube under nitrogen and the solution was added to the reaction in four equal portions with one hour intervals. The reaction was followed using GC. 17% conversion after 24 hours.

### 5.6.19. Catalyst Addition Experiment – Pre-stirred with Base

In a flame dried Schlenk tube, a solution of **39** (26  $\mu$ L, 0.25 mmol, 1.00 eq) and acetone (918  $\mu$ L, 12.5 mmol, 50.0 eq) was added to a solution of biphenyl (4 mg, 25.0  $\mu$ mol, 10 mol%) in acetonitrile (2 mL) at 50  $^\circ$ C under nitrogen and stirred for 1 hour. A solution of catalyst **C.3** (11 mg, 12.5  $\mu$ mol, 5.0 mol%) and  $K_2CO_3$  (35 mg, 0.25 mmol, 1.00 eq) in acetonitrile (1 mL) was prepared in a flame dried Schlenk tube under nitrogen and the solution was added to the reaction in four equal portions with one hour intervals. The reaction was analysed using GC. 13% conversion after 24 hours.

### 5.6.20. General Procedure for Condition Optimisation

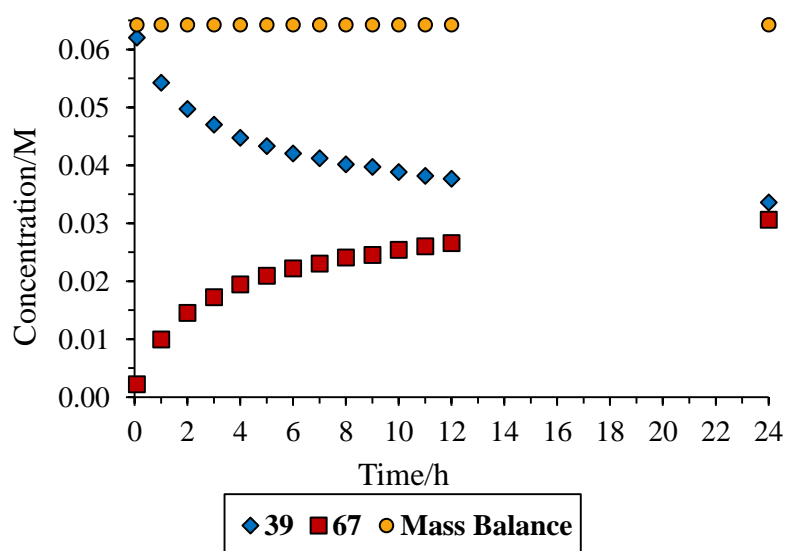


In a flame dried Schlenk tube, triethylamine (35  $\mu$ L, 0.25 mmol, 1.00 eq) was added to a solution of **C.3** (x mol%) and biphenyl (4 mg, 25.0  $\mu$ mol, 10 mol%) in acetonitrile (x mL) and acetone (x mL) under nitrogen at 50  $^\circ$ C and stirred for 1 hour. **39** (27  $\mu$ L, 0.26 mmol, 1.00 eq) was added to the reaction and stirred for 24 hours. The pink homogeneous reaction was analysed using GC (Table 37).

**Table 37** Catalysts tests investigating the amount of acetone and catalyst loading.

Entry	Catalyst	Catalyst Loading (mol%)	Base	Acetone (mL)	MeCN (mL)	Conversion (%) <sup>a</sup>
1	C.3	5.0	K <sub>2</sub> CO <sub>3</sub>	1	2	21
2	C.5	5.0	K <sub>2</sub> CO <sub>3</sub>	1	2	7
3	C.6	5.0	K <sub>2</sub> CO <sub>3</sub>	1	2	11
4	C.3	5.0	Et <sub>3</sub> N	2	-	47 <sup>b</sup>
5	C.3	5.0	Et <sub>3</sub> N	2	-	51
6	C.3	5.0	Et <sub>3</sub> N	4	-	62
7	C.3	5.0	Et <sub>3</sub> N	4	-	18 <sup>c</sup>
8	C.3	5.0	Et <sub>3</sub> N	6	-	58
9	C.3	5.0	Et <sub>3</sub> N	4	-	48
10	C.3	2.5	Et <sub>3</sub> N	4	-	22
11	C.3	10.0	Et <sub>3</sub> N	4	-	47 <sup>d</sup>

<sup>a</sup> Conversion calculated from the corrected peak integrals using biphenyl as an internal standard for GC at 24 hours. <sup>b</sup> Base added after 1 hour. <sup>c</sup> Reaction carried out at room temperature. <sup>d</sup> Reaction turned pale yellow with one equivalent of base, after 1 hour a second equivalent of base added, reaction returned to a pink solution.

**Figure 79** Concentration (M) against time (h) for the transfer dehydrogenation of **67** (entry 9, Table 37).

### 5.6.21. Transfer Dehydrogenation with $[\text{Cp}^*\text{IrCl}_2]_2$ **36**

Triethylamine (35  $\mu\text{L}$ , 0.25 mmol, 1.00 eq) was added to a solution of **36** (5 mg, 6.25  $\mu\text{mol}$ , 2.5 mol%, 5.0 mol% Ir) and biphenyl (4 mg, 25.0  $\mu\text{mol}$ , 10 mol%) in acetone (4 mL) at 50  $^\circ\text{C}$  and stirred for 1 hour. **39** (27  $\mu\text{L}$ , 0.26 mmol, 1.00 eq) was added to the reaction and stirred for 24 hours. The orange homogeneous reaction was followed with GC; 77% conversion after 24 hours (Figure 80).

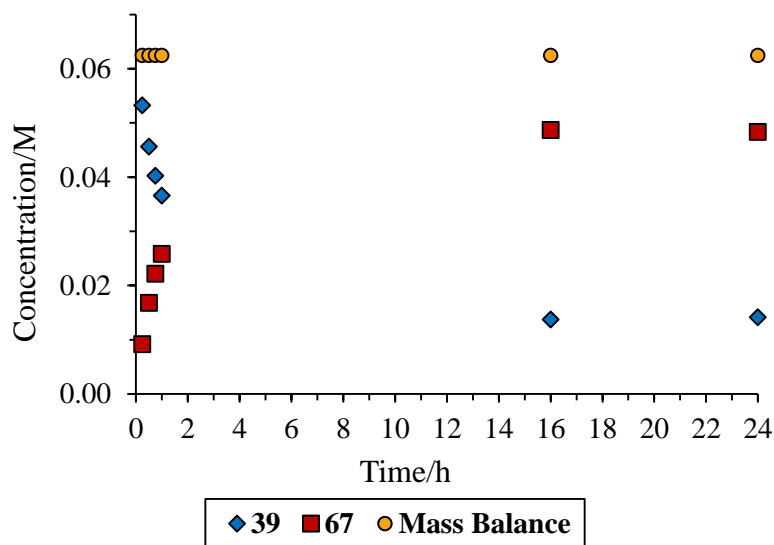
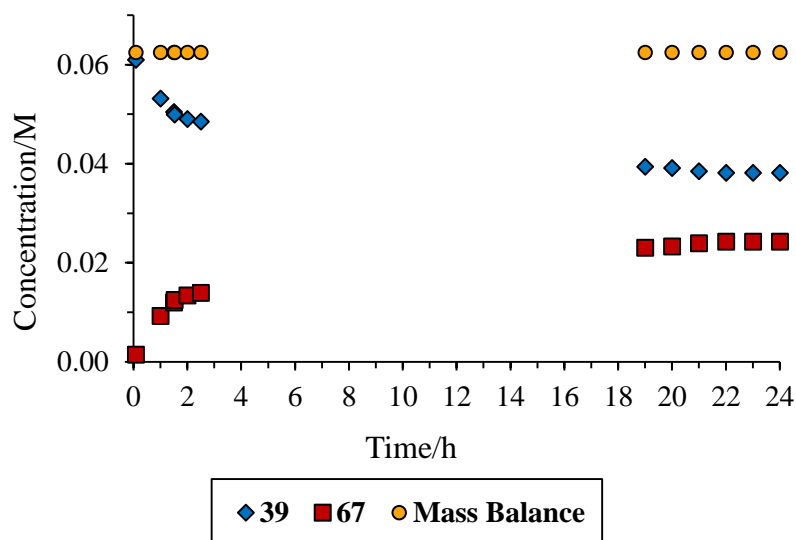


Figure 80 Catalyst control test with **36** with inert conditions.

### 5.6.22. Acetonitrile Addition Test

Triethylamine (35  $\mu\text{L}$ , 0.25 mmol, 1.00 eq) was added to a solution of **C.3** (11 mg, 12.5  $\mu\text{mol}$ , 5.0 mol%) and biphenyl (4 mg, 25.0  $\mu\text{mol}$ , 10 mol%) in acetone (4 mL) at 50  $^\circ\text{C}$  and stirred for 1 hour. **39** (27  $\mu\text{L}$ , 0.26 mmol, 1.00 eq) was added to the reaction and stirred for 24 hours. Acetonitrile (1 mL) was added to the reaction after 90 minutes. The pink homogeneous reaction was followed with GC; 41% conversion after 24 hours (Figure 81).

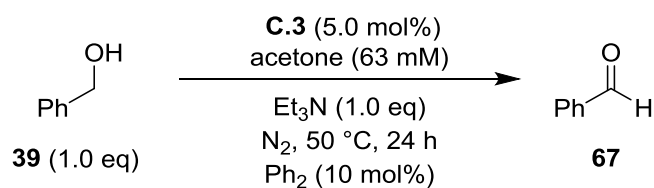


**Figure 81** Transfer dehydrogenation of **39** with the addition of MeCN at 1.5 hours.

### 5.6.23. <sup>1</sup>H NMR Monitored Experiment

Triethylamine (35  $\mu$ L, 0.25 mmol, 1.00 eq) was added to a solution of **C.3** (11 mg, 12.5  $\mu$ mol, 5.0 mol%) and biphenyl (4 mg, 25.0  $\mu$ mol, 10 mol%) in *d*<sub>6</sub>-acetone (4 mL) at 50 °C and stirred for 1 hour. **39** (27  $\mu$ L, 0.26 mmol, 1.00 eq) was added to the reaction and the solution transferred to an NMR tube under nitrogen. The pink homogeneous reaction was followed with <sup>1</sup>H NMR; 6% conversion after 24 hours (Figure 82).

**Table 38** Transfer dehydrogenation of **39**, followed using <sup>1</sup>H NMR in *d*<sub>6</sub>-acetone.



Spectrum	Time Stamp	Time (h)	39 CH <sub>2</sub> Integral <sup>a</sup>	Conversion (%) <sup>b</sup>
1	14:40	1.0	188.28	1.05
2	15:39	2.0	124.73	1.58
3	17:00	3.3	90.65	2.16
4	18:00	4.3	77.34	2.52
5	22:08	8.5	56.55	3.42
6	02:01	12.4	46.65	4.11
7	09:20	19.7	37.25	5.10
8	10:31	20.9	35.6	5.32
9	12:00	22.3	33.98	5.56
10	12:26	22.8	33.69	5.60
11	13:31	24.0	32.24	5.84

<sup>a</sup> Intergration of **39** CH<sub>2</sub> signal at 4.53 ppm with the **67** CHO signal at 9.96 ppm set to an integral of 1.00; spectra normalised using residual solvent peak for d<sub>6</sub>-acetone.

<sup>b</sup> Conversion calculated from:  $(1 / (1 + (i / 2))) \times 100$ , where *i* is the integral of **39** CH<sub>2</sub> signal at 4.53 ppm.

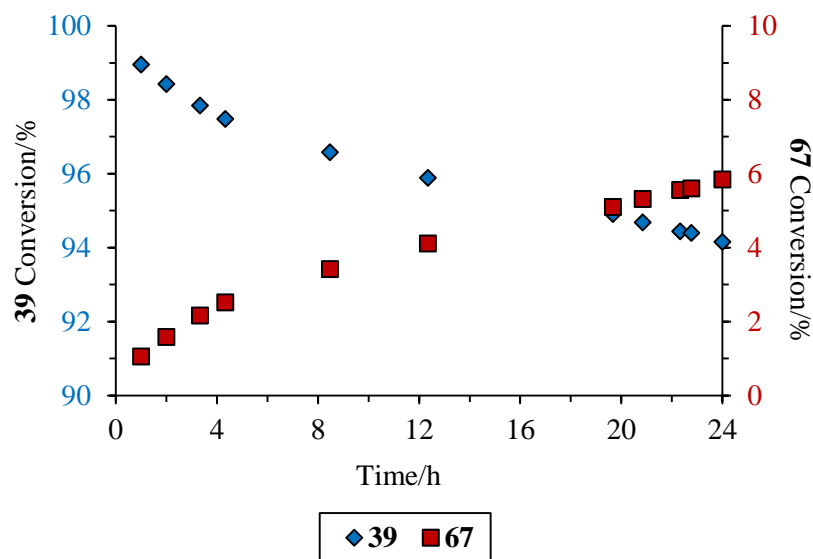
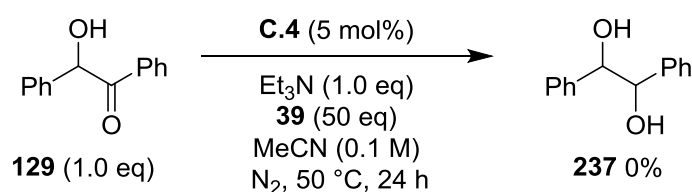


**Figure 82** Transfer dehydrogenation of **39** followed using <sup>1</sup>H NMR in d<sub>6</sub>-acetone.

## 5.7. Transfer Hydrogenation of Benzoin **129** with Benzyl Alcohol **39**



Triethylamine (35  $\mu\text{L}$ , 0.25 mmol, 1.00 eq) and **39** (1.3 mL, 12.5 mmol, 50.0 eq) were added to a stirred solution of **C.4** (9 mg, 12.5  $\mu\text{mol}$ , 5.0 mol%) and **129** (53 mg, 0.25 mmol, 1.00 eq) in acetonitrile (2.7 mL) under nitrogen and stirred at 50  $^{\circ}\text{C}$  for 24 hours. The reaction was analysed using  $^1\text{H}$  NMR with mesitylene (0.17 M) as an external standard. 0% conversion after 24 hours.

### 5.8. Control Test for Side Reactions using an IR Probe

A solution of  $\text{K}_2\text{CO}_3$  (3.45 mg, 25.0 mmol, 1.00 eq) in acetonitrile (25 mL) was monitored with an IR probe (resolution 4; scans 16; interval 60 s; Horizon MB) for 30 minutes at 50  $^{\circ}\text{C}$ . **67** (2.55 mL, 25.0 mmol, 1 eq) was added and the peak corresponding to the carbonyl stretch at  $1702\text{ cm}^{-1}$  was constant. After 30 minutes, **39** (2.60 mL, 25.0 mmol, 1.00 eq) was added and the mixture monitored for 3.5 hours at 50  $^{\circ}\text{C}$  (Figure 83). The peak areas remained constant.

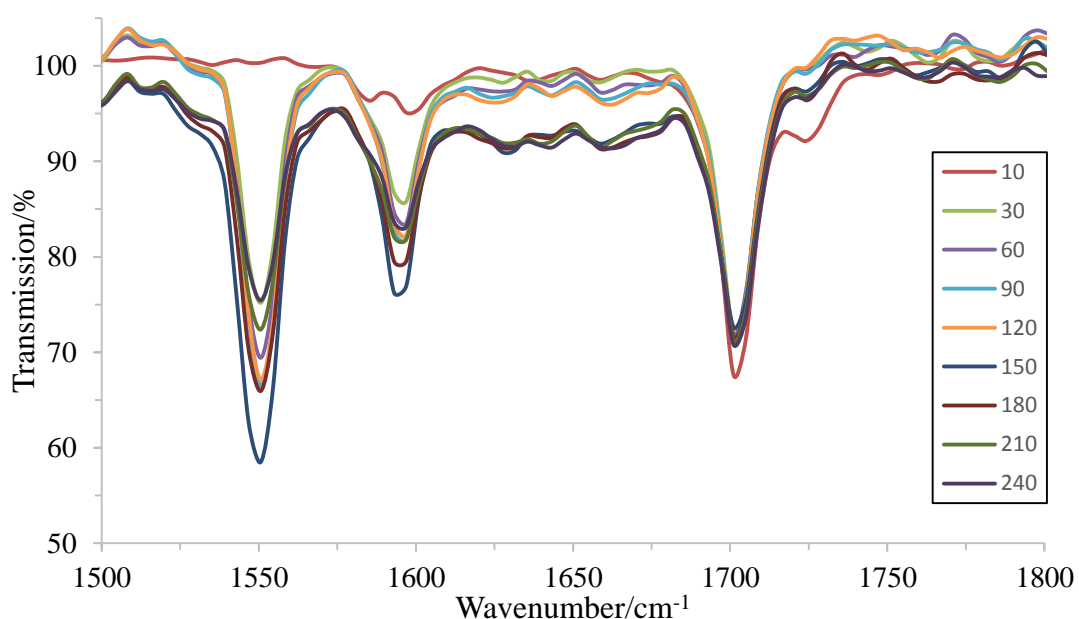
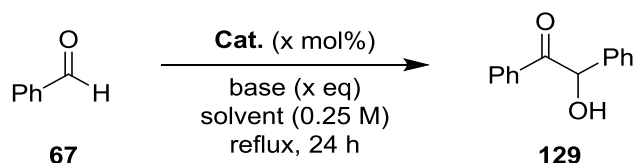


**Figure 83** Overlaid IR spectra (time in minutes) with separate additions of **67** and **39** at 0 and 30 minutes.

## 5.9. Benzoin Condensation with Benzaldehyde 67



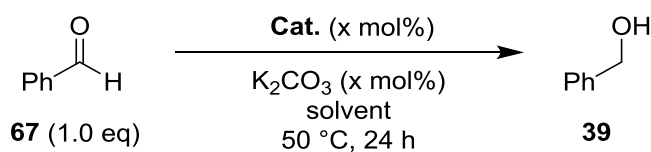
### 5.9.1. General Procedure

**67** (50 mL, 0.50 mmol, 1.00 eq) was added to a solution of catalyst (x mol%) and base (x eq) in solvent (0.25 M) and stirred at temperature for 24 hours. The reaction was cooled to room temperature and concentrated *in vacuo* and the organic layer was washed with DCM (2 x 20 mL) and extracted with brine (2 x 20 mL). The organics were combined and the solvent was removed *in vacuo* to give a crude oil. The oil was recrystallized from DCM and petrol to give the product as yellow needles (Table 39).

**Table 39** Catalyst tests for the benzoin condensation of **67** to **129**.

Entry	Catalyst	Catalyst Loading (mol%)	Base (eq)	Solvent	Temp (°C)	Yield (%)
1	C.4	1.0	K <sub>2</sub> CO <sub>3</sub> (0.1)	MeCN	40	0
2	C.1	5.0	Et <sub>3</sub> N (0.6)	EtOH	70	0
3	C.1	5.0	Et <sub>3</sub> N (0.6)	<sup>i</sup> PrOH	70	0
4	C.7.1	3.0	Et <sub>3</sub> N (5.0)	MeCN	50	0
5	L.7	5.0	Et <sub>3</sub> N (2.0)	MeCN	80	93

## 5.10. Transfer Hydrogenation





### 5.10.1.

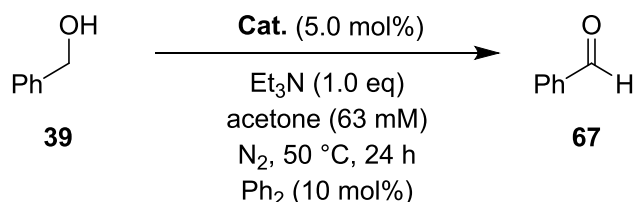
Complex **C.2** (21 mg, 25.0  $\mu\text{mol}$ , 1.0 mol%),  $\text{K}_2\text{CO}_3$  (35 mg, 0.25 mmol, 10 mol%) and biphenyl (GC standard, 39 mg, 0.25 mmol, 0.10 eq) were stirred in acetonitrile (2.5 mL) at 40 °C for 30 minutes. **67** (252  $\mu\text{L}$ , 2.50 mmol, 1.00 eq) was added and the reaction was stirred at 50 °C for 24 hours. The reaction was analysed using GC. 0% conversion after 24 hours.

### 5.10.2.

Catalyst **C.3** (11 mg, 12.5  $\mu\text{mol}$ , 5.0 mol%),  $\text{K}_2\text{CO}_3$  (36 mg, 0.26 mmol, 1.00 eq) and biphenyl (4 mg, 25.0  $\mu\text{mol}$ , 10 mol%) were stirred in acetonitrile (2 mL) at 40 °C for 30 minutes. *iso*-Propanol (750  $\mu\text{L}$ , 10.4 mmol, 40.0 eq) and **67** (27  $\mu\text{L}$ , 0.26 mmol, 1.00 eq) were added and the reaction was stirred at 50 °C for 24 hours. The reaction was followed using GC. 91% conversion after 24 hours.

## 5.11. Reactions using a Carousel Reactor

### 5.11.1. General Procedure for the Transfer Dehydrogenation of **39**



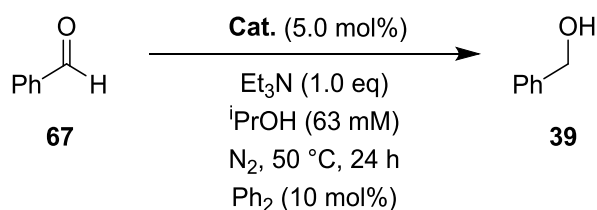
Catalyst (12.5  $\mu\text{mol}$ , 5.0 mol%) was added to a Radley's carousel tube and flushed with nitrogen for 30 minutes. A solution of biphenyl (4 mg, 25.0  $\mu\text{mol}$ , 10 mol%) in acetone (4 mL) was prepared under nitrogen, added to the catalyst and stirred at 50 °C for 30 minutes. Triethylamine (35  $\mu\text{L}$ , 0.25 mmol, 1.00 eq) was added to the reaction and stirred for 30 minutes. **39** (25  $\mu\text{L}$ , 0.25 mmol, 1.00 eq) was added to the reaction and stirred for 24 hours. The homogeneous reaction was sampled for GC. The solvent was removed *in vacuo* and analysed using  $^1\text{H}$  NMR (500  $\mu\text{L}$ , 0.17 M mesitylene in  $\text{CDCl}_3$ ) (Table 40).

**Table 40** The average conversions of the duplicate catalyst tests for the transfer dehydrogenation of **39**, analysed using GC (with biphenyl as an internal standard) and  $^1\text{H}$  NMR spectroscopy (with mesitylene as an external standard).

Entry	Catalyst	GC Conversion (%) <sup>a</sup>	s.d <sup>b</sup>	$^1\text{H}$ NMR Conversion (%) <sup>c</sup>	s.d <sup>b</sup>
1	None	0	0	0	0
2	<b>36</b>	81	0	78	1
3	<b>161</b>	29	1	22	1
4	<b>62</b>	51	8	49	1
5	<b>168</b>	29	5	27	6
6	<b>C.1</b>	7	2	3	0
7	<b>C.2</b>	16	0	11	0
8	<b>C.3</b>	23	2	16	2
9	<b>C.4</b>	78	2	73	4
10	<b>C.5</b>	11	3	7	3
11	<b>C.6</b>	69	6	65	12
12	<b>C.7.2</b>	1	0	0	0
13	<b>C.8</b>	27	2	22	2
14	<b>C.9</b>	3	1	1	0
15	<b>C.11</b>	60	0	56	0
16	<b>C.12</b>	13	1	8	1
17	<b>C.13</b>	66	1	62	2
18	<b>C.14</b>	0	0	2	0

<sup>a</sup> Conversion calculated from the average of two results with biphenyl (10 mol%) as an internal standard. <sup>b</sup> Standard deviation of the two results for both methods of analysis. <sup>c</sup> Conversion calculated from the average of two results with mesitylene (0.17 M) as an external standard.

### 5.11.2. General Procedure for the Transfer Hydrogenation of **67**



Catalyst (12.5  $\mu\text{mol}$ , 5.0 mol%) was added to a Radley's carousel tube and flushed with nitrogen for 30 minutes. A solution of biphenyl (4 mg, 25.0  $\mu\text{mol}$ ,

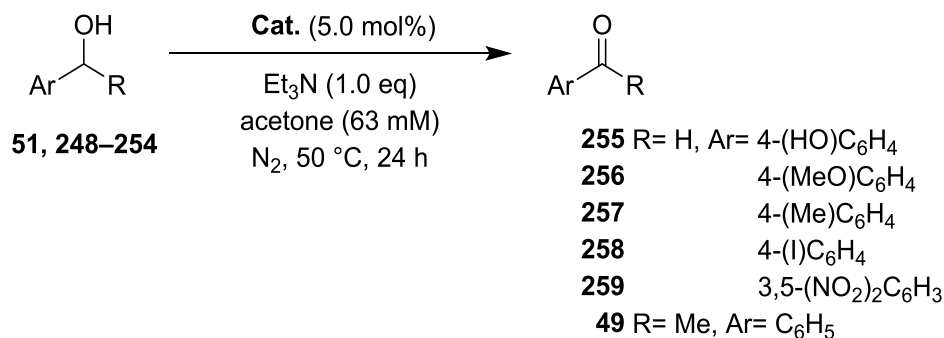
10 mol%) in *iso*-propanol (4 mL) was prepared under nitrogen, added to the catalyst and stirred at 50 °C for 30 minutes. Triethylamine (35  $\mu$ L, 0.25 mmol, 1.00 eq) was added to the reaction and stirred for 30 minutes. **67** (25  $\mu$ L, 0.25 mmol, 1.00 eq) was added to the reaction and stirred for 24 hours. The homogeneous reaction was sampled for GC. The solvent was removed *in vacuo* and analysed using  $^1\text{H}$  NMR (500  $\mu$ L, 0.17 M mesitylene in  $\text{CDCl}_3$ ) (Table 41).

**Table 41** The average conversions of the duplicate catalyst tests for the transfer hydrogenation of **67**, analysed using GC (with biphenyl as an internal standard) and  $^1\text{H}$  NMR spectroscopy (with mesitylene as an external standard).

Entry	Catalyst	GC Conversion (%) <sup>a</sup>	s.d. <sup>b</sup>	$^1\text{H}$ NMR Conversion (%) <sup>c</sup>	s.d. <sup>b</sup>
1	None	2	0	0	0
2	<b>36</b>	99	0	quant.	0
3	<b>161</b>	99	0	quant.	0
4	<b>62</b>	98	0	quant.	0
5	<b>168</b>	99	0	quant.	0
6	<b>C.1</b>	12	1	17	2
7	<b>C.2</b>	79	8	89	6
8	<b>C.3</b>	65	1	83	2
9	<b>C.4</b>	99	0	quant.	0
10	<b>C.5</b>	76	2	88	1
11	<b>C.6</b>	quant.	0	99	1
12	<b>C.7.2</b>	1	0	2	1
13	<b>C.8</b>	quant.	0	quant.	0
14	<b>C.9</b>	17	1	28	2
15	<b>C.11</b>	98	0	quant.	0
16	<b>C.12</b>	98	0	quant.	0
17	<b>C.13</b>	97	0	quant.	0
18	<b>C.14</b>	2	0	0	0

<sup>a</sup> Conversion calculated from the average of two results with biphenyl (10 mol%) as an internal standard. <sup>b</sup> Standard deviation of the two results for both methods of analysis. <sup>c</sup> Conversion calculated from the average of two results with mesitylene (0.17 M) as an external standard.

## 5.12. Scope



### 5.12.1. General Procedure

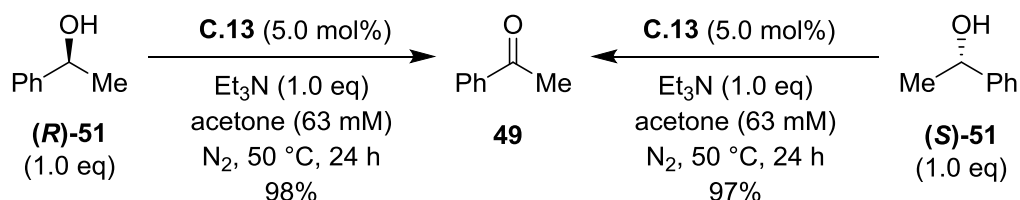
Catalyst (12.5 μmol, 5.0 mol%) was added to a Radley's carousel tube and flushed with nitrogen for 30 minutes. A solution of alcohol (0.25 mmol, 1.00 eq) in acetone (4 mL) was prepared under nitrogen, added to the catalyst and stirred at 50 °C for 30 minutes. Triethylamine (35 μL, 0.25 mmol, 1.00 eq) was added to the reaction and stirred for 24 hours. The homogeneous reaction was sampled for GC-MS. The solvent was removed *in vacuo* and analysed using <sup>1</sup>H NMR (500 μL, 0.17 M mesitylene in CDCl<sub>3</sub>) (Table 42).

**Table 42** Transfer dehydrogenation with catalysts **C.4**, **C.6** and **C.13**.

Substrate	Conversion (%) <sup>a</sup>		
	C.4	C.6	C.13
<b>248</b>	99	97	60
<b>249</b>	97	97	69
<b>250</b>	89	84	45
<b>39</b>	78	69	60
<b>251</b>	50	40	13
<b>252</b>	0	0	0
<b>51</b>	100	-	52
<b>253</b>	0	-	-
<b>254</b>	0	-	-

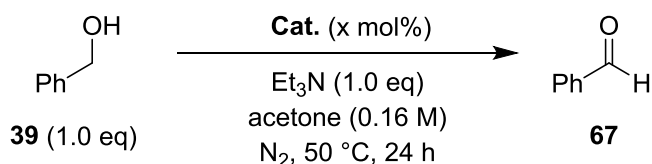
<sup>a</sup> Conversion calculated from the <sup>1</sup>H NMR spectra with 0.17 M mesitylene in CDCl<sub>3</sub> as an external standard. <sup>b</sup> 0.17 M mesitylene in d<sub>6</sub>-acetone used as an external standard for solubility. <sup>c</sup> Substrate condensed with acetone; no oxidation product observed.

### 5.13. Transfer Dehydrogenation of (*R*)- and (*S*)-1-Phenylethanol **51** with Complex **C.13**



Triethylamine (35  $\mu$ L, 0.25 mmol, 1.00 eq) and either (*R*)-**51** or (*S*)-**51** (30  $\mu$ L, 0.25 mmol, 1.00 eq) were added to a stirred solution of **C.13** (10 mg, 12.5  $\mu$ mol, 5.0 mol%) in acetone (4 mL) under nitrogen and stirred at 50 °C for 24 hours. The reaction was analysed using <sup>1</sup>H NMR with mesitylene (0.17 M in CDCl<sub>3</sub>) as an external standard. After 24 hours, (*R*)-**51** and (*S*)-**51** reached 98% and 97% conversion respectively.

### 5.14. Transfer Dehydrogenation of Benzyl Alcohol **39**: Catalyst Loading Tests



#### 5.14.1. General Procedure

Catalyst **C.4** (x mol%) was added to a Radley's carousel tube and flushed with nitrogen for 30 minutes. A solution of benzyl alcohol (169  $\mu$ L, 1.64 mmol, 1.00 eq) in acetone (10 mL) was prepared under nitrogen, added to the catalyst and stirred at 50 °C for 30 minutes. Triethylamine (226  $\mu$ L, 1.64 mmol, 1.00 eq) was added to the reaction and stirred for 24 hours. The homogeneous reaction was sampled for <sup>1</sup>H NMR (500  $\mu$ L sample with solvent removed *in vacuo* and 500  $\mu$ L of 0.17 M mesitylene in CDCl<sub>3</sub>). After 24 hours, the solvent was

removed *in vacuo* and followed using  $^1\text{H}$  NMR (500  $\mu\text{L}$ , 0.17 M mesitylene in  $\text{CDCl}_3$ ) (Table 43, Figure 84).

**Table 43** The catalyst tests with varied catalyst loadings.

Entry	Catalyst Loading (mol%)	Conversion (%) <sup>a</sup>
1	5.00	73 <sup>b</sup>
2	3.60	62
3	0.90	55
4	0.18	37

<sup>a</sup> Conversion calculated from the  $^1\text{H}$  NMR spectra with 0.17 M mesitylene in  $\text{CDCl}_3$  as an external standard. <sup>b</sup> Result taken from a previous reaction.

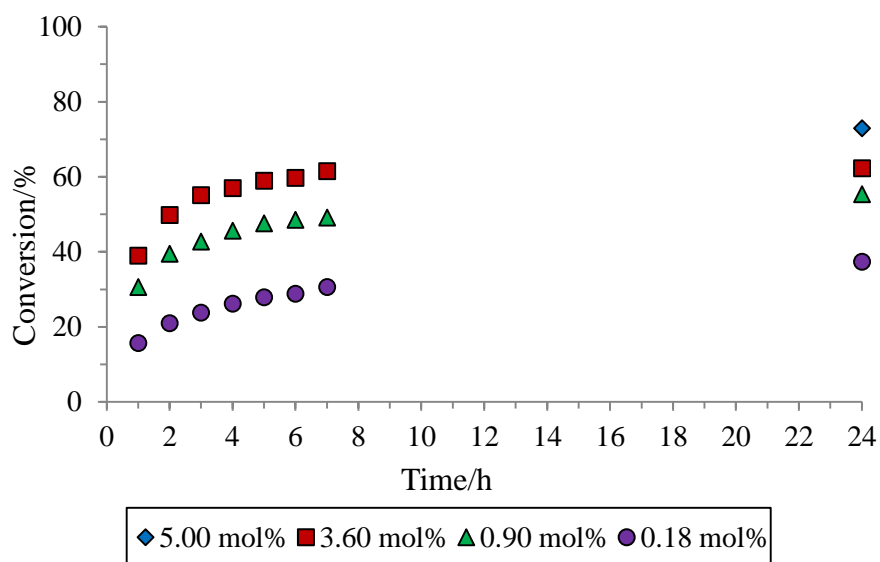
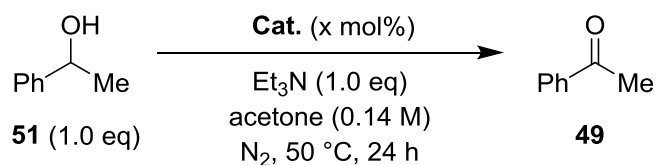


**Figure 84** The conversion calculated from  $^1\text{H}$  NMR spectroscopy with mesitylene as an external standard of **39** to **67** with varied catalyst loading (mol%). The 5.00 mol% result was taken from a previous experiment.

## 5.15. Transfer Dehydrogenation of 1-Phenylethanol **51**: Catalyst Loading Tests



### 5.15.1. General Procedure

Catalyst **C.4** (x mol%) was added to a Radley's carousel tube and flushed with nitrogen for 30 minutes. A solution of 1-phenylethanol (169  $\mu$ L, 1.40 mmol, 1.00 eq) in acetone (10 mL) was prepared under nitrogen, added to the catalyst and stirred at 50 °C for 30 minutes. Triethylamine (194  $\mu$ L, 1.40 mmol, 1.00 eq) was added to the reaction and stirred for 24 hours. The homogeneous reaction was sampled for GC-MS and <sup>1</sup>H NMR (1 mL sample with solvent removed *in vacuo* and 500  $\mu$ L of 0.17 M mesitylene in CDCl<sub>3</sub>). After 24 hours, the solvent was removed *in vacuo* and analysed using <sup>1</sup>H NMR (500  $\mu$ L, 0.17 M mesitylene in CDCl<sub>3</sub>). After 24 hours, the solvent was removed *in vacuo* and followed using <sup>1</sup>H NMR (500  $\mu$ L, 0.17 M mesitylene in CDCl<sub>3</sub>) (Table 44, Figure 85).

**Table 44** The transfer dehydrogenation of **51** with catalyst **C.4** with varied catalyst loadings.

Entry	Catalyst Loading (mol%)	Conversion (%) <sup>a</sup>
1	5.00	100
2	1.00	97 <sup>b</sup>
3	0.20	93

<sup>a</sup> Conversion calculated from the <sup>1</sup>H NMR spectra with 0.17 M mesitylene in CDCl<sub>3</sub> as an external standard. <sup>b</sup> The average conversion of two results.

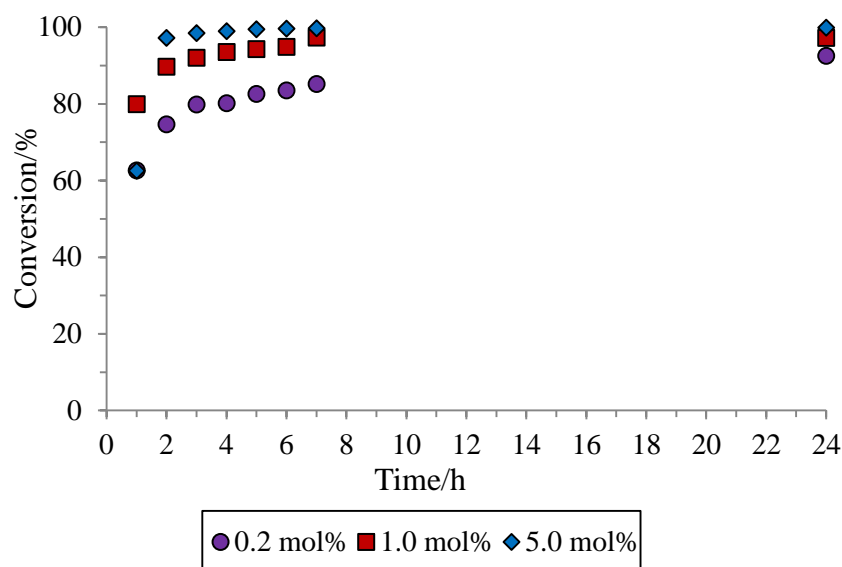
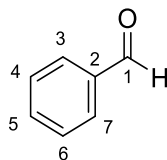


**Figure 85** The conversion calculated from  $^1\text{H}$  NMR spectroscopy with mesitylene as an external standard of **51** to **49** with varied catalyst loading (mol%).

## 5.16. Analytical Data for Catalysis Products

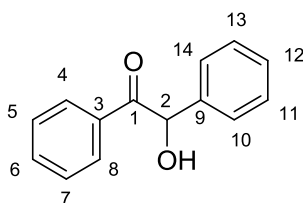
### 5.16.1. Benzaldehyde **67**



GCMS  $m/z = M^+$  106.0, Theoretical Mass = 106.0.  $^1\text{H}$  NMR (300 MHz,  $\text{CDCl}_3$ )  $\delta$ ; 10.05 (s, 1H,  $\text{CH-1}$ ), 7.91 (d,  $J = 7.7$  Hz, 2H,  $\text{CH-3/7}$ ), 7.73 – 7.61 (m, 1H,  $\text{CH-5}$ ), 7.56 (t,  $J = 7.7$  Hz, 2H,  $\text{CH-4/6}$ ).  $^{13}\text{C}$  NMR  $\{^1\text{H}\}$  (126 MHz,  $\text{CDCl}_3$ )  $\delta$ ; 192.45 (C-1), 136.42 (C-2), 134.49 (C-5), 129.79 (C-4/6), 129.02 (C-3/7). IR ( $\text{cm}^{-1}$ ); 3063, 2819, 2736, 1696, 1653, 1596, 1583. Spectral data is consistent with the literature.<sup>158</sup>

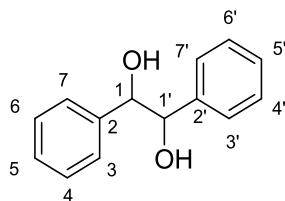


### 5.16.2. Benzoin 129



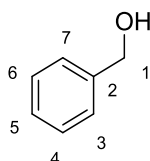
mp: 129.7–132.5 °C (Lit. 133–135 °C).<sup>159</sup> GCMS  $m/z = M^+$  212.0, Theoretical Mass = 212.1.  $^1\text{H}$  NMR (300 MHz,  $\text{CDCl}_3$ )  $\delta$ ; 7.92 (dd,  $J = 8.5, 1.3$  Hz, 2H,  $\text{CH-Ph}$ ), 7.66 – 7.47 (m, 1H,  $\text{CH-Ph}$ ), 7.45 – 7.14 (m, 7H,  $\text{CH-Ph}$ ), 5.96 (d,  $J = 6.1$  Hz, 1H,  $\text{CH-2}$ ), 4.58 (d,  $J = 6.1$  Hz, 1H,  $\text{OH}$ ).  $^{13}\text{C}$  NMR  $\{^1\text{H}\}$  (126 MHz,  $d_6$ -DMSO)  $\delta$ ; 199.14 (C-10), 139.71 (C-5), 134.71 (C-4), 133.18 (C-8), 128.80 (C-6), 128.55 (C-7), 128.43 (C-3), 127.66 (C-1), 127.23 (C-2), 75.65 (C-9). IR ( $\text{cm}^{-1}$ ); 3405, 3059, 3028, 2932, 1678, 1594, 1577, 1448. Spectral data is consistent with the literature.<sup>159</sup>

### 5.16.3. Hydrobenzoin 237



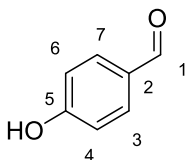
mp: 145.4–147.6 °C (Lit. 138 °C)<sup>160</sup>. GCMS:  $m/z = M^+ - \text{H}_2\text{O}$  196.2, Theoretical Mass = 196.2.  $^1\text{H}$  NMR (300 MHz,  $\text{CDCl}_3$ )  $\delta$ ; 7.92 (d,  $J = 7.4$  Hz, 4H,  $\text{CH-3/3'/7/7'}$ ), 7.52 (t,  $J = 7.4$  Hz, 2H,  $\text{CH-5/5'}$ ), 7.40 (t,  $J = 7.4$  Hz, 4H,  $\text{CH-4/4'/6/6'}$ ), 4.71 (s, 2H,  $\text{CH-1/1'}$ ), 4.57 (br s, 2H,  $\text{OH}$ ).  $^{13}\text{C}$  NMR  $\{^1\text{H}\}$  (126 MHz,  $d_6$ -DMSO)  $\delta$ ; 142.32 (C-5), 127.24 (C-4), 127.13 (C-3), 126.65 (C-2), 77.64 (C-7). IR ( $\text{cm}^{-1}$ ); 3496, 3386, 2893, 1491, 1451, 1383. Spectral data is consistent with the literature.<sup>160</sup>

### 5.16.4. Benzyl alcohol 39



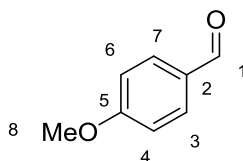
GCMS:  $m/z = M^+$  108.0, Theoretical Mass = 108.1.  $^1\text{H}$  NMR (500 MHz,  $\text{CDCl}_3$ )  $\delta$ ; 7.51 – 7.37 (m, 5H,  $\text{CH-Ph}$ ), 4.63 (d,  $J = 5.6$  Hz, 2H,  $\text{CH}_2\text{-1}$ ), 4.53 (t,  $J = 5.6$  Hz, 1H,  $\text{OH}$ ). Spectral data is consistent with the literature.<sup>161</sup>

#### 5.16.5. *p*-Hydroxybenzaldehyde 255



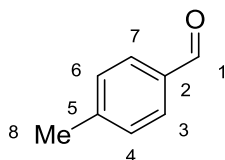
GCMS:  $m/z = M^+$  122.0, Theoretical Mass = 122.0.  $^1\text{H}$  NMR (500 MHz,  $d_6$ -acetone)  $\delta$ ; 9.85 (s, 1H,  $\text{CH-1}$ ), 8.34 (br s, 1H,  $\text{OH}$ ), 7.79 (d,  $J = 8.4$  Hz, 2H,  $\text{CH-3/7}$ ), 7.03 (d,  $J = 8.4$  Hz, 2H,  $\text{CH-4/6}$ ). Spectral data is consistent with the literature.<sup>162</sup>

#### 5.16.6. *p*-Methoxybenzaldehyde 256



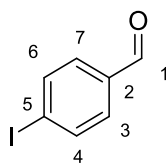
GCMS:  $m/z = M^+$  136.0, Theoretical Mass = 136.1.  $^1\text{H}$  NMR (500 MHz,  $\text{CDCl}_3$ )  $\delta$ ; 9.78 (s, 1H,  $\text{CH-1}$ ), 7.74 (d,  $J = 8.8$  Hz, 2H,  $\text{CH-3/7}$ ), 6.91 (d,  $J = 8.8$  Hz, 2H,  $\text{CH-4/6}$ ), 3.79 (s, 3H,  $\text{CH}_3\text{-8}$ ). Spectral data is consistent with the literature.<sup>163</sup>

#### 5.16.7. *p*-Methylbenzaldehyde 257



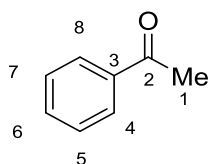
GCMS:  $m/z = M^+$  120.0, Theoretical Mass = 120.1.  $^1\text{H}$  NMR (500 MHz,  $\text{CDCl}_3$ )  $\delta$ ; 9.95 (s, 1H,  $\text{CH-1}$ ), 7.77 (d,  $J = 8.0$  Hz, 2H,  $\text{CH-3/7}$ ), 7.33 (d,  $J = 8.0$  Hz, 2H,  $\text{CH-4/6}$ ), 2.43 (s, 3H,  $\text{CH}_3\text{-8}$ ). Spectral data is consistent with the literature.<sup>164</sup>

#### 5.16.8. *p*-Iodobenzaldehyde 258



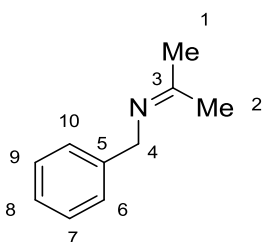
GCMS:  $m/z = M^+ 231.9$ , Theoretical Mass = 231.9.  $^1\text{H NMR}$  (500 MHz,  $\text{CDCl}_3$ )  $\delta$ ; 9.92 (s, 1H, *CH*-1), 7.88 (d,  $J = 8.4$  Hz, 2H, *CH*-3/7), 7.56 (d,  $J = 8.4$  Hz, 2H, *CH*-4/6). Spectral data is consistent with the literature.<sup>163</sup>

#### 5.16.9. Acetophenone 49



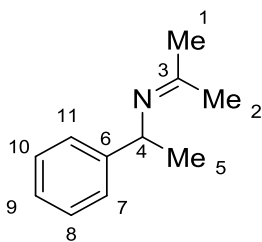
GCMS:  $m/z = M^+ 120.0$ , Theoretical Mass = 120.1.  $^1\text{H NMR}$  (500 MHz,  $\text{CDCl}_3$ )  $\delta$ ; 7.92 – 7.82 (m, 2H, *CH*-4/8), 7.53 – 7.44 (m, 1H, *CH*-6), 7.43 – 7.32 (m, 2H, *CH*-5/7), 2.52 (s, 3H, *CH*<sub>3</sub>-1). Spectral data is consistent with the literature.<sup>165</sup>

#### 5.16.10. *N*-(*iso*-Propylidene)benzylamine 260



GCMS:  $m/z = M^+ 147.1$ , Theoretical Mass = 147.1.  $^1\text{H NMR}$  (500 MHz,  $\text{CDCl}_3$ )  $\delta$ ; 7.32 – 7.26 (m, 1H, *CH*-6/7/9/10), 7.23 – 7.17 (m, 1H, *CH*-8), 4.43 (s, 2H, *CH*<sub>2</sub>-4), 2.07 (s, 3H, *CH*<sub>3</sub>-1), 1.91 (s, 3H, *CH*<sub>3</sub>-2). Spectral data is consistent with the literature.<sup>166, 167</sup>

### 5.16.11. *iso*-Propylidene-(1-phenylethyl)-amine 261



GCMS:  $m/z = M^+$  161.1, Theoretical Mass = 161.1.  $^1\text{H}$  NMR (500 MHz,  $\text{CDCl}_3$ )  $\delta$ ; 7.40 – 7.30 (m, 4H,  $\text{CH}$ -7/8/10/11), 7.24 – 7.20 (m, 1H,  $\text{CH}$ -9), 4.61 (q,  $J = 6.6$  Hz, 1H,  $\text{CH}$ -4), 2.07 (s, 3H,  $\text{CH}_3$ -1), 1.88 (s, 3H,  $\text{CH}_3$ -2), 1.49 (d,  $J = 6.6$  Hz, 3H,  $\text{CH}_3$ -5). Spectral data is consistent with the literature.<sup>168</sup>

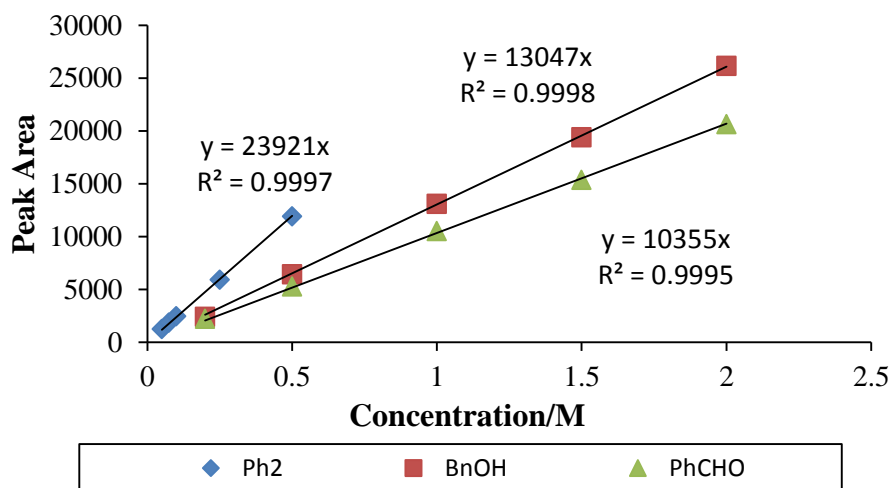
### 5.17. GC Calibration Data

GC method: oven temperature of 60 °C with a ramp of 15°C/min to 140°C and then 30 °C/min to 280 °C. Column: HP-5 column, length 30 m, internal diameter 320  $\mu\text{m}$ . GC samples were filtered through a plug of silica prior to loading. Solutions were made up with 50  $\mu\text{L}$  of sample in 1 mL MeCN or MeOH.

**Table 45** Retention times for compounds associated with the catalysis experiments.

Compound	$t_R$ (min)
Benzyl alcohol <b>39</b>	2.84
Benzaldehyde <b>67</b>	2.13
Benzoin <b>129</b>	8.75
4-Hydroxy-4-phenylbutan-2-one <b>242</b>	6.18 <sup>a</sup>
Benzylideneacetone <b>243</b>	5.99
Dibenzylideneacetone <b>244</b>	9.62
Biphenyl (standard)	6.10

<sup>a</sup> A sample was not available for calibration.



Compound	Ratio wrt S
Ph <sub>2</sub>	1.000
BnOH	0.545
PhCHO	0.433

**Figure 86** GC calibration plots for benzyl alcohol, benzaldehyde and biphenyl and the ratios of the gradients with respect to the internal standard which act as conversion factors.

## 6. References

1. L. M. Ambrosini and T. H. Lambert, *ChemCatChem*, 2010, **2**, 1373-1380.
2. A. A. Desai, E. J. Molitor and J. E. Anderson, *Org. Process Res. Dev.*, 2012, **16**, 160-165.
3. J. Lu, J. Dimroth and M. Weck, *J. Am. Chem. Soc.*, 2015, **137**, 12984-12989.
4. D. E. Fogg and E. N. dos Santos, *Coord. Chem. Rev.*, 2004, **248**, 2365-2379.
5. N. T. Patil, V. S. Shinde and B. Gajula, *Org. Biomol. Chem.*, 2012, **10**, 211-224.
6. G. J. Rowlands, *Tetrahedron*, 2001, **57**, 1865-1882.
7. D. Enders, A. Greb, K. Deckers, P. Selig and C. Merckens, *Chem. Eur. J.*, 2012, **18**, 10226-10229.
8. K. Sonogashira, Y. Tohda and N. Hagihara, *Tetrahedron Lett.*, 1975, **16**, 4467-4470.
9. C. G. Overberger, T. S. Pierre, C. Yaroslavsky and S. Yaroslavsky, *J. Am. Chem. Soc.*, 1966, **88**, 1184-1188.
10. N. Takeda, M. Irisawa and M. Komiyama, *J. Chem. Soc., Chem. Commun.*, 1994, 2773-2774.
11. M. Shibasaki and N. Yoshikawa, *Chem. Rev.*, 2002, **102**, 2187-2210.
12. H. Wang, Q. Deng, Z. Zhou, S. Hu, Z. Liu and L.-Y. Zhou, *Org. Lett.*, 2016, **18**, 404-407.
13. J.-L. Hsu, C.-T. Chen and J.-M. Fang, *Org. Lett.*, 1999, **1**, 1989-1991.
14. B. A. Anderson, E. C. Bell, F. O. Ginah, N. K. Harn, L. M. Pagh and J. P. Wepsiec, *J. Org. Chem.*, 1998, **63**, 8224-8228.
15. S. Ko, B. Kang and S. Chang, *Angew. Chem. Int. Ed.*, 2005, **44**, 455-457.
16. F. Bihelovic, R. Matovic, B. Vulovic and R. N. Saicic, *Org. Lett.*, 2007, **9**, 5063-5066.
17. S. Beligny, S. Eibauer, S. Maechling and S. Blechert, *Angew. Chem. Int. Ed.*, 2006, **45**, 1900-1903.
18. X.-P. Yin, X.-P. Zeng, Y.-L. Liu, F.-M. Liao, J.-S. Yu, F. Zhou and J. Zhou, *Angew. Chem. Int. Ed.*, 2014, **53**, 13740-13745.
19. B. Simmons, A. M. Walji and D. W. C. MacMillan, *Angew. Chem. Int. Ed.*, 2009, **48**, 4349-4353.
20. D.-F. Chen, F. Zhao, Y. Hu and L.-Z. Gong, *Angew. Chem. Int. Ed.*, 2014, **53**, 10763-10767.
21. C. Xu, F.-C. Jia, Z.-W. Zhou, S.-J. Zheng, H. Li and A.-X. Wu, *J. Org. Chem.*, 2016, **81**, 3000-3006.
22. J. Louie, C. W. Bielawski and R. H. Grubbs, *J. Am. Chem. Soc.*, 2001, **123**, 11312-11313.
23. S. Fustero, J. Miró, M. Sánchez-Roselló and C. del Pozo, *Chem. Eur. J.*, 2014, **20**, 14126-14131.
24. M. J. Campbell and F. D. Toste, *Chem. Sci.*, 2011, **2**, 1369-1378.
25. S. P. Lathrop and T. Rovis, *J. Am. Chem. Soc.*, 2009, **131**, 13628-13630.
26. S.-S. Zhang, J.-Q. Wu, X. Liu and H. Wang, *ACS Catal.*, 2015, **5**, 210-214.
27. S. W. Youn, H. S. Song and J. H. Park, *Org. Lett.*, 2014, **16**, 1028-1031.

28. S. Wang, C. Miao, W. Wang, Z. Lei and W. Sun, *ChemCatChem*, 2014, **6**, 1612-1616.
29. M. Rueping, J. Dufour and L. Bui, *ACS Catal.*, 2014, **4**, 1021-1025.
30. J. Zhou, *Multicatalyst System in Asymmetric Catalysis*, John Wiley and Sons, New York, 1st edn., 2014, **1**, 2, 103.
31. S. Jenni, M. Leibundgut, T. Maier and N. Ban, *Science*, 2006, **311**, 1263-1267.
32. L. Stryer, *Biochemistry*, 4th edn., W. H. Freeman, New York, 1995.
33. C. E. Müller, R. Hrdina, R. C. Wende and P. R. Schreiner, *Chem. Eur. J.*, 2011, **17**, 6309-6314.
34. C. E. Müller, D. Zell and P. R. Schreiner, *Chem. Eur. J.*, 2009, **15**, 9647-9650.
35. A. Zanardi, R. Corberán, J. A. Mata and E. Peris, *Organometallics*, 2008, **27**, 3570-3576.
36. J. A. Mata, F. E. Hahn and E. Peris, *Chem. Sci.*, 2014, **5**, 1723-1732.
37. A. Zanardi, J. A. Mata and E. Peris, *J. Am. Chem. Soc.*, 2009, **131**, 14531-14537.
38. S. Gonell, M. Poyatos, J. A. Mata and E. Peris, *Organometallics*, 2012, **31**, 5606-5614.
39. A. Zanardi, J. A. Mata and E. Peris, *Chem. Eur. J.*, 2010, **16**, 10502-10506.
40. A. Zanardi, J. A. Mata and E. Peris, *Chem. Eur. J.*, 2010, **16**, 13109-13115.
41. J. S. M. Samec, J.-E. Backvall, P. G. Andersson and P. Brandt, *Chem. Soc. Rev.*, 2006, **35**, 237-248.
42. G. Zassinovich, G. Mestroni and S. Gladiali, *Chem. Rev.*, 1992, **92**, 1051-1069.
43. Y. Sasson and J. Blum, *J. Org. Chem.*, 1975, **40**, 1887-1896.
44. R. L. Chowdhury and J.-E. Backvall, *J. Chem. Soc., Chem. Commun.*, 1991, 1063-1064.
45. T. Ikariya and A. J. Blacker, *Acc. Chem. Res.*, 2007, **40**, 1300-1308.
46. S. Hashiguchi, A. Fujii, J. Takehara, T. Ikariya and R. Noyori, *J. Am. Chem. Soc.*, 1995, **117**, 7562-7563.
47. A. J. Blacker and B. J. Mellor, *International Pat.*, University of Leeds, WO 98/42643, 1998.
48. X. Li, J. Blacker, I. Houson, X. Wu and J. Xiao, *Synlett*, 2006, 1155-1160.
49. R. J. Lundgren, M. A. Rankin, R. McDonald, G. Schatte and M. Stradiotto, *Angew. Chem. Int. Ed.*, 2007, **46**, 4732-4735.
50. C. Thoumazet, M. Melaimi, L. Ricard, F. Mathey and P. Le Floch, *Organometallics*, 2003, **22**, 1580-1581.
51. T. Touge, T. Hakamata, H. Nara, T. Kobayashi, N. Sayo, T. Saito, Y. Kayaki and T. Ikariya, *J. Am. Chem. Soc.*, 2011, **133**, 14960-14963.
52. N. Uematsu, A. Fujii, S. Hashiguchi, T. Ikariya and R. Noyori, *J. Am. Chem. Soc.*, 1996, **118**, 4916-4917.
53. G. E. Dobereiner and R. H. Crabtree, *Chem. Rev.*, 2009, **110**, 681-703.
54. K.-i. Fujita, S. Furukawa and R. Yamaguchi, *J. Organomet. Chem.*, 2002, **649**, 289-292.
55. A. J. Blacker, M. M. Farah, M. I. Hall, S. P. Marsden, O. Saidi and J. M. J. Williams, *Org. Lett.*, 2009, **11**, 2039-2042.

56. M. G. Mura, L. De Luca, M. Taddei, J. M. J. Williams and A. Porcheddu, *Org. Lett.*, 2014, **16**, 2586-2589.
57. K.-i. Fujita, T. Yoshida, Y. Imori and R. Yamaguchi, *Org. Lett.*, 2011, **13**, 2278-2281.
58. M. H. S. A. Hamid, P. A. Slatford and J. M. J. Williams, *Adv. Synth. Catal.*, 2007, **349**, 1555-1575.
59. J. M. Ketcham, I. Shin, T. P. Montgomery and M. J. Krische, *Angew. Chem. Int. Ed.*, 2014, **53**, 9142-9150.
60. Y. Tsuji, K. T. Huh, Y. Ohsugi and Y. Watanabe, *J. Org. Chem.*, 1985, **50**, 1365-1370.
61. M. G. Edwards, R. F. R. Jazzar, B. M. Paine, D. J. Shermer, M. K. Whittlesey, J. M. J. Williams and D. D. Edney, *Chem. Commun.*, 2004, 90-91.
62. M. H. S. A. Hamid, C. L. Allen, G. W. Lamb, A. C. Maxwell, H. C. Maytum, A. J. A. Watson and J. M. J. Williams, *J. Am. Chem. Soc.*, 2009, **131**, 1766-1774.
63. Y. Zhang, C.-S. Lim, D. S. B. Sim, H.-J. Pan and Y. Zhao, *Angew. Chem. Int. Ed.*, 2014, **53**, 1399-1403.
64. V. R. Jumde, L. Gonsalvi, A. Guerriero, M. Peruzzini and M. Taddei, *Eur. J. Org. Chem.*, 2015, 1829-1833.
65. J. Leonard, A. J. Blacker, S. P. Marsden, M. F. Jones, K. R. Mulholland and R. Newton, *Org. Process Res. Dev.*, 2015, **19**, 1400-1410.
66. EMEA/CHMP/SWP/4446/2000, Guideline on the Specification Limits for Residues of Metal Catalysts or Metal Reagents., Committee for Medicinal Products for Human Use (CHMP), London, 2008
67. G. Stork, R. Terrell and J. Szmuszkovicz, *J. Am. Chem. Soc.*, 1954, **76**, 2029-2030.
68. Y. Hayashi, T. Itoh, N. Nagae, M. Ohkubo and H. Ishikawa, *Synlett*, 2008, 1565-1570.
69. L. Cheng, X. Wu and Y. Lu, *Org. Biomol. Chem.*, 2007, **5**, 1018-1020.
70. M. P. Lalonde, Y. Chen and E. N. Jacobsen, *Angew. Chem. Int. Ed.*, 2006, **45**, 6366-6370.
71. A. T. Biju, N. Kuhl and F. Glorius, *Acc. Chem. Res.*, 2011, **44**, 1182-1195.
72. D. M. Flanigan, F. Romanov-Michailidis, N. A. White and T. Rovis, *Chem. Rev.*, 2015, **115**, 9307-9387.
73. R. S. Massey, C. J. Collett, A. G. Lindsay, A. D. Smith and A. C. O'Donoghue, *J. Am. Chem. Soc.*, 2012, **134**, 20421-20432.
74. M. W. Washabaugh and W. P. Jencks, *J. Am. Chem. Soc.*, 1989, **111**, 674-683.
75. J. S. Buck and W. S. Ide, *J. Am. Chem. Soc.*, 1931, **53**, 2350-2353.
76. T. Ugai, R. Tanaka and T. Dokawa, *J. Pharm. Soc. Jpn*, 1943, **63**, 293-300.
77. R. Breslow, *J. Am. Chem. Soc.*, 1958, **80**, 3719-3726.
78. Y. Hachisu, J. W. Bode and K. Suzuki, *J. Am. Chem. Soc.*, 2003, **125**, 8432-8433.
79. J. R. Struble, J. Kaeobamrung and J. W. Bode, *Org. Lett.*, 2008, **10**, 957-960.
80. C. J. Collett, R. S. Massey, J. E. Taylor, O. R. Maguire, A. C. O'Donoghue and A. D. Smith, *Angew. Chem. Int. Ed.*, 2015, **54**, 6887-6892.



81. S. E. O'Toole, C. A. Rose, S. Gundala, K. Zeitler and S. J. Connon, *J. Org. Chem.*, 2010, **76**, 347-357.
82. D. Enders and U. Kallfass, *Angew. Chem. Int. Ed.*, 2002, **41**, 1743-1745.
83. T. Jousseume, N. E. Wurz and F. Glorius, *Angew. Chem. Int. Ed.*, 2011, **50**, 1410-1414.
84. C. Kaiser, D. F. Colella, M. S. Schwartz, E. Garvey and J. R. Wardell, *J. Med. Chem.*, 1974, **17**, 49-57.
85. R. Hett, Q. K. Fang, Y. Gao, S. A. Wald and C. H. Senanayake, *Org. Process Res. Dev.*, 1998, **2**, 96-99.
86. H. J. Yoon, Y.-W. Kim, B. K. Lee, W. K. Lee, Y. Kim and H.-J. Ha, *Chem. Commun.*, 2007, 79-81.
87. V. Kumar and S. Dev, *Tetrahedron*, 1987, **43**, 5933-5948.
88. D. Enders, A. Henseler and S. Lowins, *Synthesis*, 2009, 4125-4128.
89. Y. Zhu, L. Fan, C.-H. Chen, S. R. Finnell, B. M. Foxman and O. V. Ozerov, *Organometallics*, 2007, **26**, 6701-6703.
90. C. Pifferi and R. Cini, *J. Chem. Soc., Dalton Trans.*, 1998, 2679-2688.
91. R. Cini, S. Defazio, G. Tamasi, M. Casolaro, L. Messori, A. Casini, M. Morpurgo and M. Hursthouse, *Inorg. Chem.*, 2007, **46**, 79-92.
92. A. Neveling, G. R. Julius, S. Cronje, C. Esterhuysen and H. G. Raubenheimer, *Dalton Trans.*, 2005, 181-192.
93. E. Reisner, V. B. Arion, A. Eichinger, N. Kandler, G. Giester, A. J. L. Pombeiro and B. K. Keppler, *Inorg. Chem.*, 2005, **44**, 6704-6716.
94. J. G. Vos, J. G. Haasnoot and G. Vos, *Inorg. Chim. Acta*, 1983, **71**, 155-162.
95. Z.-S. Hu, Y.-H. Lin, S.-C. Jin and J. G. Vos, *Acta Crystallogr., Sect. C: Cryst. Struct. Commun.*, 1989, **45**, 1490-1493.
96. F. G. Gelalcha, B. Bitterlich, G. Anilkumar, M. K. Tse and M. Beller, *Angew. Chem. Int. Ed.*, 2007, **46**, 7293-7296.
97. J. E. D. Martins and M. Wills, *Tetrahedron: Asymmetry*, 2008, **19**, 1250-1255.
98. J. E. D. Martins, G. J. Clarkson and M. Wills, *Org. Lett.*, 2009, **11**, 847-850.
99. S. F. Zhu, J. B. Xie, Y. Z. Zhang, S. Li and Q. L. Zhou, *J. Am. Chem. Soc.*, 2006, **128**, 12886-12891.
100. G. W. Kabalka and A. R. Mereddy, *Tetrahedron Lett.*, 2006, **47**, 5171-5172.
101. N. Ahangar, A. Ayati, E. Alipour, A. Pashapour, A. Foroumadi and S. Emami, *Chemical Biology & Drug Design*, 2011, **78**, 844-852.
102. B. Narayana, K. K. Vijaya Raj, B. V. Ashalatha, N. S. Kumari and B. K. Sarojini, *Eur. J. Med. Chem.*, 2004, **39**, 867-872.
103. W. T. Caldwell and S. M. Fox, *J. Am. Chem. Soc.*, 1951, **73**, 2935-2936.
104. D. Webb and T. F. Jamison, *Org. Lett.*, 2012, **14**, 568-571.
105. H. Makio, A. V. Prasad, H. Terao, J. Saito and T. Fujita, *Dalton Trans.*, 2013, **42**, 9112-9119.
106. A. Dondoni, G. Fantin, M. Fogagnolo, A. Medici and P. Pedrini, *Synthesis*, 1987, 998-1001.
107. G. T. Giuffredi, S. Purser, M. Sawicki, A. L. Thompson and V. Gouverneur, *Tetrahedron: Asymmetry*, 2009, **20**, 910-920.
108. D. Enders, O. Niemeier and T. Balensiefer, *Angew. Chem. Int. Ed.*, 2006, **45**, 1463-1467.

109. R. Braslau, H. Kuhn, L. C. Burrill li, K. Lanham and C. J. Stenland, *Tetrahedron Lett.*, 1996, **37**, 7933-7936.
110. A. J. Blacker, *The Handbook of Homogeneous Hydrogenation*, Wiley-VCH Verlag GmbH, 1st edn., 2008, **1**, 35, 1219.
111. M. R. Churchill and S. A. Julis, *Inorg. Chem.*, 1977, **16**, 1488-1494.
112. I. B. Lundina and I. Y. Postovskii, *Chem. Heterocycl. Compd.*, 1967, **3**, 201-204.
113. W. Fan, Y. Wu, X.-K. Li, N. Yao, X. Li, Y.-G. Yu and L. Hai, *Eur. J. Med. Chem.*, 2011, **46**, 3651-3661.
114. J. D. Blakemore, N. D. Schley, D. Balcells, J. F. Hull, G. W. Olack, C. D. Incarvito, O. Eisenstein, G. W. Brudvig and R. H. Crabtree, *J. Am. Chem. Soc.*, 2010, **132**, 16017-16029.
115. C. Pettinari, R. Pettinari, F. Marchetti, A. Macchioni, D. Zuccaccia, B. W. Skelton and A. H. White, *Inorg. Chem.*, 2007, **46**, 896-906.
116. A. E. Roa, J. Campos, M. Paneque, V. Salazar, A. Otero, A. Lara-Sanchez, A. M. Rodriguez, I. Lopez-Solera and M. V. Gomez, *Dalton Trans.*, 2015, **44**, 6987-6998.
117. D. F. Kennedy, B. A. Messerle and M. K. Smith, *Eur. J. Inorg. Chem.*, 2007, 80-89.
118. X.-Q. Xiao and G.-X. Jin, *J. Organomet. Chem.*, 2008, **693**, 3363-3368.
119. M. E. G. Mosquera, P. Gomez-Sal, I. Diaz, L. M. Aguirre, A. Ienco, G. Manca and C. Mealli, *Inorg. Chem.*, 2016, **55**, 283-291.
120. C. Janiak, *J. Chem. Soc., Dalton Trans.*, 2000, 3885-3896.
121. A. Schumacher, M. Bernasconi and A. Pfaltz, *Angew. Chem. Int. Ed.*, 2013, **52**, 7422-7425.
122. J. A. Molina de la Torre, P. Espinet and A. C. Albéniz, *Organometallics*, 2013, **32**, 5428-5434.
123. *H. J. Hagemeyer Jr, United States Pat.*, US2656360 (A), 1953.
124. K. R. Kopecky and T. Gillan, *Can. J. Chem.*, 1969, **47**, 2371-2386.
125. J. T. Klein, L. Davis, G. E. Olsen, G. S. Wong, F. P. Huger, C. P. Smith, W. W. Petko, M. Cornfeldt, J. C. Wilker, R. D. Blitzler, E. Landau, V. Haroutunian, L. L. Martin and R. C. Efland, *J. Med. Chem.*, 1996, **39**, 570-581.
126. E. Hofer and R. Keuper, *Synthesis*, 1983, 466-467.
127. S. K. U. Riederer, P. Gigler, M. P. Högerl, E. Herdtweck, B. Bechlars, W. A. Herrmann and F. E. Kühn, *Organometallics*, 2010, **29**, 5681-5692.
128. S. K. U. Riederer, B. Bechlars, W. A. Herrmann and F. E. Kuhn, *Dalton Trans.*, 2011, **40**, 41-43.
129. S. K. U. Riederer, B. Bechlars, W. A. Herrmann and F. E. Kühn, *Eur. J. Inorg. Chem.*, 2011, 249-254.
130. K. Fujita, S. Furukawa and R. Yamaguchi, *J. Organomet. Chem.*, 2002, **649**, 289-292.
131. H. Stetter and H. Kuhlmann, *Org. Synth.*, 1984, **62**, 170.
132. E. C. Carmichael, V. D. Geldart, R. S. McDonald, D. B. Moore, S. Rose, L. D. Colebrook, G. D. Spiropoulos and O. S. Tee, *J. Chem. Soc., Perkin Trans. 2*, 1997, 2609-2620.
133. K. Murata, K. Okano, M. Miyagi, H. Iwane, R. Noyori and T. Ikariya, *Org. Lett.*, 1999, **1**, 1119-1121.
134. H. Wren, *J. Chem. Soc., Trans.*, 1909, **95**, 1593-1602.

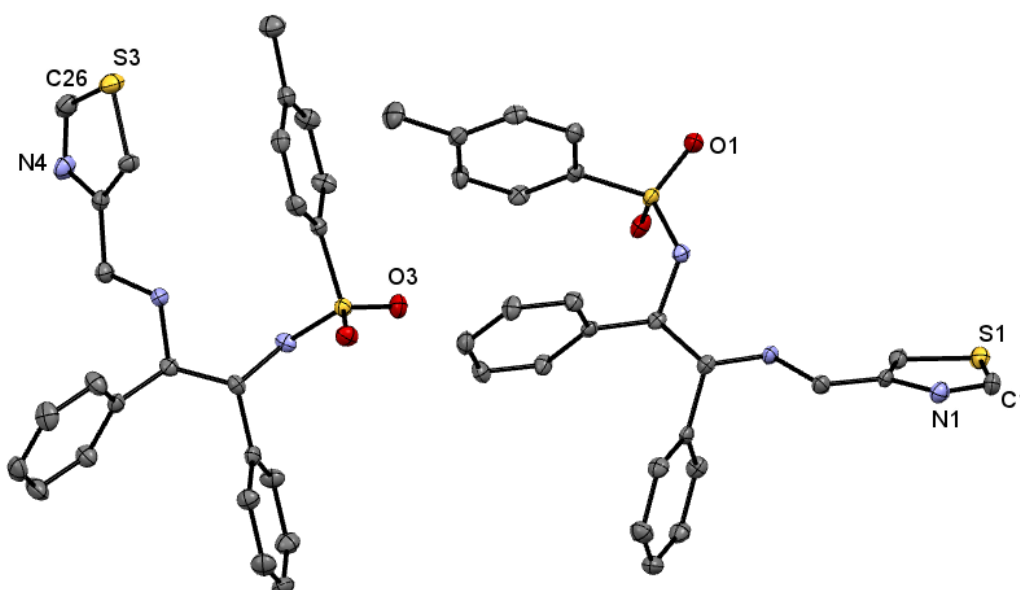
135. I. Piel, M. D. Pawelczyk, K. Hirano, R. Fröhlich and F. Glorius, *Eur. J. Org. Chem.*, 2011, 5475-5484.
136. T. C. Johnson, W. G. Totty and M. Wills, *Org. Lett.*, 2012, **14**, 5230-5233.
137. J. R. Miecznikowski and R. H. Crabtree, *Organometallics*, 2004, **23**, 629-631.
138. D. C. Gerbino, D. Augner, N. Slavov and H.-G. Schmalz, *Org. Lett.*, 2012, **14**, 2338-2341.
139. S. Cannizzaro, *Liebigs Ann. Chem.*, 1853, **88**, 129-130.
140. N. A. Owston, A. J. Parker and J. M. J. Williams, *Chem. Commun.*, 2008, 624-625.
141. N. A. Owston, T. D. Nixon, A. J. Parker, M. K. Whittlesey and J. M. J. Williams, *Synthesis-Stuttgart*, 2009, 1578-1581.
142. N. A. Owston, A. J. Parker and J. M. J. Williams, *Org. Lett.*, 2007, **9**, 73-75.
143. D. A. DiRocco, E. L. Noey, K. N. Houk and T. Rovis, *Angew. Chem. Int. Ed.*, 2012, **51**, 2391-2394.
144. S. A. Buntin and R. F. Heck, *Org. Synth.*, 1983, **61**, 82-84.
145. A. J. Blacker, *The Handbook of Homogeneous Hydrogenation*, Wiley-VCH Verlag GmbH, 1st edn., 2008, **1**, 35, 1236-1237.
146. M. Zafir, X. Sun and A. Gavriilidis, *Ind. Eng. Chem. Res.*, 2008, **47**, 8995-9005.
147. H. Adkins, R. M. Eloffson, A. G. Rossow and C. C. Robinson, *J. Am. Chem. Soc.*, 1949, **71**, 3622-3629.
148. M. Kazushi, A. Tomoyuki and T. Kazuhide, *Chem. Lett.*, 1998, **27**, 1199-1200.
149. T. Matsumoto, H. Yamamoto and S. Inoue, *J. Am. Chem. Soc.*, 1984, **106**, 4829-4832.
150. D. S. Noyce and S. A. Fike, *J. Org. Chem.*, 1973, **38**, 3316-3318.
151. F. A. Davis, J. C. Towson, M. C. Weismiller, S. Lal and P. J. Carroll, *J. Am. Chem. Soc.*, 1988, **110**, 8477-8482.
152. J.-L. Hsu and J.-M. Fang, *J. Org. Chem.*, 2001, **66**, 8573-8584.
153. D. G. I. Petra, P. C. J. Kamer, A. L. Spek, H. E. Schoemaker and P. W. N. M. van Leeuwen, *J. Org. Chem.*, 2000, **65**, 3010-3017.
154. J. L. Belletire, R. A. Bills and S. A. Shackelford, *Synth. Commun.*, 2008, **38**, 738-745.
155. J. Averdung, C. Wolff and J. Mattay, *Tetrahedron Lett.*, 1996, **37**, 4683-4684.
156. A. Weißberger and H. Bach, *Ber. Dtsch. Chem. Ges.*, 1931, **64**, 1095-1108.
157. C. Martínez and K. Muñoz, *Adv. Synth. Catal.*, 2014, **356**, 205-211.
158. A. Wang and H. Jiang, *J. Org. Chem.*, 2010, **75**, 2321-2326.
159. T. J. Donohoe, A. Jahanshahi, M. J. Tucker, F. L. Bhatti, I. A. Roslan, M. Kabeshov and G. Wrigley, *Chem. Commun.*, 2011, **47**, 5849-5851.
160. K. S. Anju, S. Ramakrishnan, A. P. Thomas, E. Suresh and A. Srinivasan, *Org. Lett.*, 2008, **10**, 5545-5548.
161. S. Kumar, F. Saleem and A. K. Singh, *Dalton Trans.*, 2016, **45**, 11445-11458.
162. J. Kwon, N. T. Hiep, D.-W. Kim, S. Hong, Y. Guo, B. Y. Hwang, H. J. Lee, W. Mar and D. Lee, *J. Nat. Prod.*, 2016, **79**, 1938-1951.

163. M. Tabata, K. Moriyama and H. Togo, *Eur. J. Org. Chem.*, 2014, 3402-3410.
164. R. Kawahara, K.-i. Fujita and R. Yamaguchi, *J. Am. Chem. Soc.*, 2012, **134**, 3643-3646.
165. A. Gonzalez-de-Castro and J. Xiao, *J. Am. Chem. Soc.*, 2015, **137**, 8206-8218.
166. B. Paul, K. Chakrabarti and S. Kundu, *Dalton Trans.*, 2016, **45**, 11162-11171.
167. F. Texierboullet, *Synthesis-Stuttgart*, 1985, 679-681.
168. J. S. Johnson and R. G. Bergman, *J. Am. Chem. Soc.*, 2001, **123**, 2923-2924.

## 7. Appendix

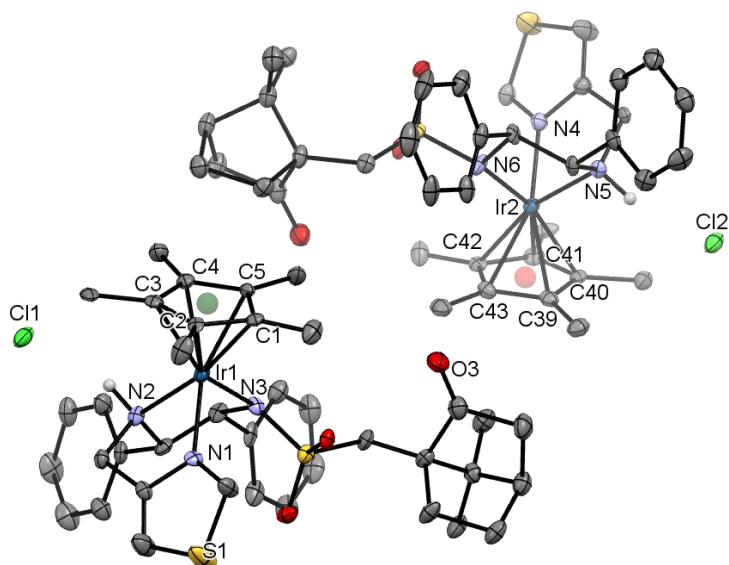
### X-Ray Crystal Structure Data

#### L.1



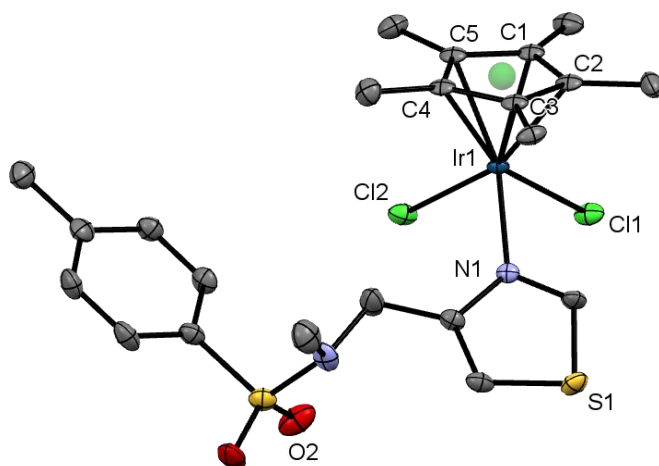
Identification code	exp_1564
Empirical formula	C <sub>25</sub> H <sub>25</sub> N <sub>3</sub> O <sub>2</sub> S <sub>2</sub>
Formula weight	463.60
Temperature/K	120.02(10)
Crystal system	orthorhombic
Space group	P2 <sub>1</sub> 2 <sub>1</sub> 2 <sub>1</sub>
a/Å	5.46792(10)
b/Å	18.8677(3)
c/Å	44.1959(8)
α/°	90
β/°	90
γ/°	90
Volume/Å <sup>3</sup>	4559.56(14)
Z	8
ρ <sub>calc</sub> /cm <sup>3</sup>	1.351
μ/mm <sup>-1</sup>	2.339
F(000)	1952.0
Crystal size/mm <sup>3</sup>	0.29 × 0.14 × 0.09
Radiation	CuKα (λ = 1.54184)
2θ range for data collection/°	6.16 to 147.774
Index ranges	-6 ≤ h ≤ 6, -21 ≤ k ≤ 23, -45 ≤ l ≤ 54
Reflections collected	17185
Independent reflections	8967 [R <sub>int</sub> = 0.0417, R <sub>sigma</sub> = 0.0571]
Data/restraints/parameters	8967/0/595
Goodness-of-fit on F <sup>2</sup>	1.053
Final R indexes [I ≥ 2σ (I)]	R <sub>1</sub> = 0.0417, wR <sub>2</sub> = 0.0965
Final R indexes [all data]	R <sub>1</sub> = 0.0465, wR <sub>2</sub> = 0.0990
Largest diff. peak/hole / e Å <sup>-3</sup>	0.30/-0.37
Flack parameter	-0.011(11)

### C.3



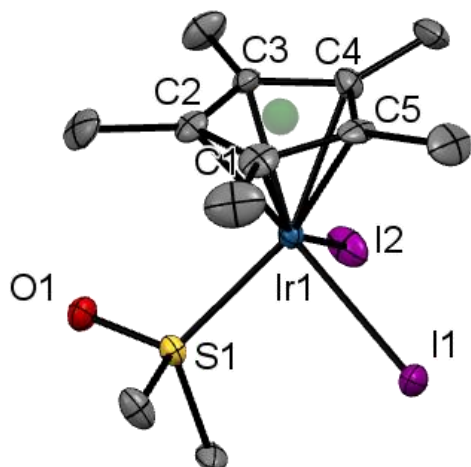
Identification code	picl
Empirical formula	$C_{38}H_{47}ClIrN_3O_3S_2$
Formula weight	885.55
Temperature/K	119.97(13)
Crystal system	monoclinic
Space group	$P2_1$
$a/\text{\AA}$	17.2721(6)
$b/\text{\AA}$	12.4309(3)
$c/\text{\AA}$	17.9981(8)
$\alpha/^\circ$	90
$\beta/^\circ$	105.818(4)
$\gamma/^\circ$	90
Volume/ $\text{\AA}^3$	3718.0(2)
Z	4
$\rho_{\text{calc}}/\text{g cm}^{-3}$	1.582
$\mu/\text{mm}^{-1}$	3.815
F(000)	1784.0
Crystal size/ $\text{mm}^3$	$0.24 \times 0.07 \times 0.05$
Radiation	MoK $\alpha$ ( $\lambda = 0.71073$ )
$2\theta$ range for data collection/ $^\circ$	5.868 to 59.58
Index ranges	$-20 \leq h \leq 24, -17 \leq k \leq 16, -23 \leq l \leq 23$
Reflections collected	48320
Independent reflections	18059 [ $R_{\text{int}} = 0.0609, R_{\text{sigma}} = 0.0846$ ]
Data/restraints/parameters	18059/973/879
Goodness-of-fit on $F^2$	1.030
Final R indexes [ $I \geq 2\sigma(I)$ ]	$R_1 = 0.0466, wR_2 = 0.0788$
Final R indexes [all data]	$R_1 = 0.0714, wR_2 = 0.0878$
Largest diff. peak/hole / $e \text{\AA}^{-3}$	1.39/-1.93
Flack parameter	-0.017(7)

### C.4



Identification code	JM124_Mo
Empirical formula	C <sub>22</sub> H <sub>29</sub> N <sub>2</sub> O <sub>2</sub> S <sub>2</sub> Cl <sub>2</sub> Ir
Formula weight	680.69
Temperature/K	120.01(17)
Crystal system	monoclinic
Space group	P2 <sub>1</sub> /c
a/Å	21.2275(18)
b/Å	7.2138(4)
c/Å	16.0785(10)
α/°	90.00
β/°	101.968(7)
γ/°	90.00
Volume/Å <sup>3</sup>	2408.6(3)
Z	4
ρ <sub>calc</sub> /cm <sup>3</sup>	1.877
μ/mm <sup>-1</sup>	5.961
F(000)	1336.0
Crystal size/mm <sup>3</sup>	0.16 × 0.09 × 0.03
Radiation	MoKα (λ = 0.71073)
2θ range for data collection/°	5.98 to 56.58
Index ranges	-22 ≤ h ≤ 28, -9 ≤ k ≤ 7, -21 ≤ l ≤ 13
Reflections collected	15540
Independent reflections	5970 [R <sub>int</sub> = 0.0501, R <sub>sigma</sub> = 0.0641]
Data/restraints/parameters	5970/0/263
Goodness-of-fit on F <sup>2</sup>	1.088
Final R indexes [I ≥ 2σ (I)]	R <sub>1</sub> = 0.0466, wR <sub>2</sub> = 0.0768
Final R indexes [all data]	R <sub>1</sub> = 0.0603, wR <sub>2</sub> = 0.0817
Largest diff. peak/hole / e Å <sup>-3</sup>	2.24/-2.09

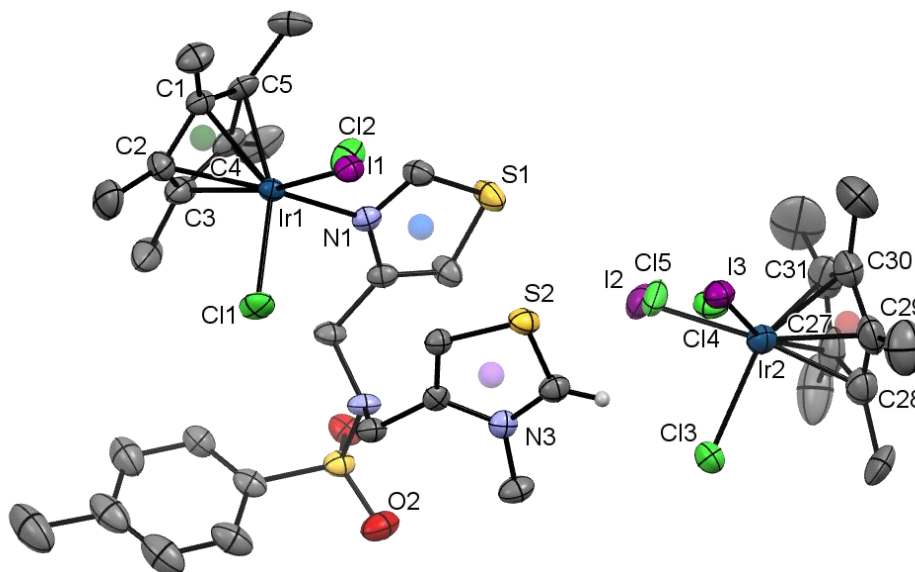
[Cp\*IrI<sub>2</sub>(DMSO)]



Identification code	JAM170_Mo
Empirical formula	C <sub>12</sub> H <sub>21</sub> I <sub>2</sub> IrOS
Formula weight	659.35
Temperature/K	120.00(10)
Crystal system	monoclinic
Space group	P2 <sub>1</sub> /c
a/Å	13.6118(4)
b/Å	12.8985(3)
c/Å	19.2732(5)
α/°	90.00
β/°	96.212(3)
γ/°	90.00
Volume/Å <sup>3</sup>	3363.95(15)
Z	8
ρ <sub>calc</sub> /cm <sup>3</sup>	2.604
μ/mm <sup>-1</sup>	11.719
F(000)	2400.0
Crystal size/mm <sup>3</sup>	0.22 × 0.11 × 0.08
Radiation	MoKα (λ = 0.71073)
2θ range for data collection/°	6.02 to 62.72
Index ranges	-19 ≤ h ≤ 19, -18 ≤ k ≤ 15, -27 ≤ l ≤ 28
Reflections collected	28601
Independent reflections	9767 [R <sub>int</sub> = 0.0610, R <sub>sigma</sub> = 0.0771]
Data/restraints/parameters	9767/0/321
Goodness-of-fit on F <sup>2</sup>	1.045
Final R indexes [I ≥ 2σ (I)]	R <sub>1</sub> = 0.0442, wR <sub>2</sub> = 0.0671
Final R indexes [all data]	R <sub>1</sub> = 0.0692, wR <sub>2</sub> = 0.0795
Largest diff. peak/hole / e Å <sup>-3</sup>	1.69/-1.80

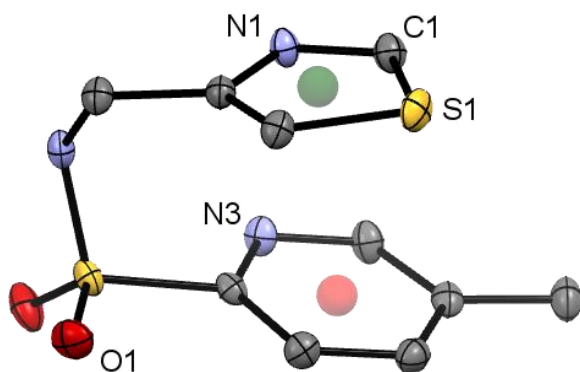


### C.7.1



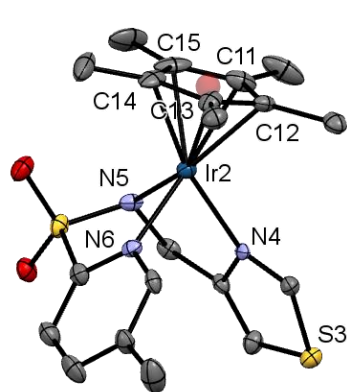
Identification code	JAM170_2_Mo
Empirical formula	$C_{40}H_{52}Cl_{15.55}I_{1.45}Ir_2N_3O_2S_3$
Formula weight	1822.68
Temperature/K	120.03(10)
Crystal system	triclinic
Space group	P-1
a/Å	12.8968(2)
b/Å	13.1630(2)
c/Å	21.0772(6)
$\alpha$ /°	92.2184(19)
$\beta$ /°	98.7805(19)
$\gamma$ /°	106.1231(16)
Volume/Å <sup>3</sup>	3384.65(14)
Z	2
$\rho_{\text{calc}}/\text{cm}^3$	1.788
$\mu/\text{mm}^{-1}$	5.328
F(000)	1744.0
Crystal size/mm <sup>3</sup>	0.32 × 0.21 × 0.09
Radiation	MoK $\alpha$ ( $\lambda = 0.71073$ )
2 $\theta$ range for data collection/°	5.888 to 62.452
Index ranges	$-18 \leq h \leq 17, -19 \leq k \leq 19, -30 \leq l \leq 30$
Reflections collected	56431
Independent reflections	19383 [ $R_{\text{int}} = 0.0683, R_{\text{sigma}} = 0.0917$ ]
Data/restraints/parameters	19383/118/679
Goodness-of-fit on $F^2$	1.033
Final R indexes [ $I \geq 2\sigma(I)$ ]	$R_1 = 0.0667, wR_2 = 0.1632$
Final R indexes [all data]	$R_1 = 0.1040, wR_2 = 0.1880$
Largest diff. peak/hole / e Å <sup>-3</sup>	2.30/-2.24

## L.8

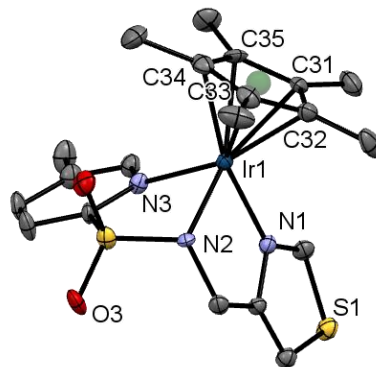


Identification code	JAM2_251_Mo_a_twin1_hklf4
Empirical formula	C <sub>10</sub> H <sub>11</sub> N <sub>3</sub> O <sub>2</sub> S <sub>2</sub>
Formula weight	269.34
Temperature/K	119.97(13)
Crystal system	triclinic
Space group	P-1
a/Å	7.9036(6)
b/Å	7.9397(5)
c/Å	11.3310(9)
α/°	70.084(7)
β/°	82.973(7)
γ/°	62.293(7)
Volume/Å <sup>3</sup>	591.31(9)
Z	2
ρ <sub>calc</sub> /g/cm <sup>3</sup>	1.513
μ/mm <sup>-1</sup>	0.443
F(000)	280.0
Crystal size/mm <sup>3</sup>	0.32 × 0.19 × 0.15
Radiation	MoKα (λ = 0.71073)
2θ range for data collection/°	5.828 to 62.658
Index ranges	-11 ≤ h ≤ 11, -11 ≤ k ≤ 11, -16 ≤ l ≤ 16
Reflections collected	7823
Independent reflections	7823 [R <sub>int</sub> = ?, R <sub>sigma</sub> = 0.0494]
Data/restraints/parameters	7823/0/160
Goodness-of-fit on F <sup>2</sup>	1.007
Final R indexes [I ≥ 2σ (I)]	R <sub>1</sub> = 0.0743, wR <sub>2</sub> = 0.2102
Final R indexes [all data]	R <sub>1</sub> = 0.1036, wR <sub>2</sub> = 0.2306
Largest diff. peak/hole / e Å <sup>-3</sup>	1.38/-0.58

**C.10**



I2

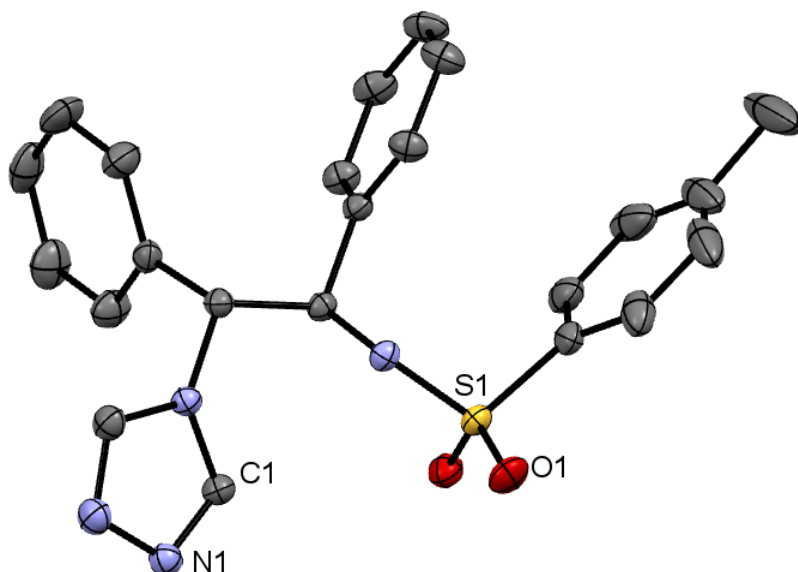


I1



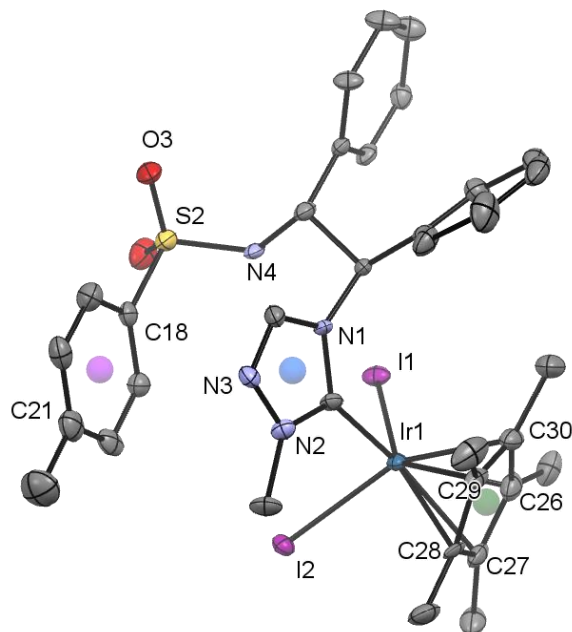
Identification code	JAM3_316_Mo_b
Empirical formula	C <sub>21</sub> H <sub>27</sub> Cl <sub>2</sub> IrN <sub>3</sub> O <sub>2</sub> S <sub>2</sub>
Formula weight	807.57
Temperature/K	120.00(16)
Crystal system	monoclinic
Space group	P2 <sub>1</sub>
a/Å	15.8194(4)
b/Å	9.79020(18)
c/Å	17.4568(3)
α/°	90
β/°	95.879(2)
γ/°	90
Volume/Å <sup>3</sup>	2689.41(10)
Z	4
ρ <sub>calc</sub> /cm <sup>3</sup>	1.995
μ/mm <sup>-1</sup>	6.489
F(000)	1544.0
Crystal size/mm <sup>3</sup>	0.29 × 0.05 × 0.03
Radiation	MoKα (λ = 0.71073)
2θ range for data collection/°	6.272 to 62.908
Index ranges	-23 ≤ h ≤ 22, -14 ≤ k ≤ 14, -25 ≤ l ≤ 25
Reflections collected	72851
Independent reflections	16246 [R <sub>int</sub> = 0.0655, R <sub>sigma</sub> = 0.0659]
Data/restraints/parameters	16246/1/589
Goodness-of-fit on F <sup>2</sup>	1.048
Final R indexes [I ≥ 2σ (I)]	R <sub>1</sub> = 0.0414, wR <sub>2</sub> = 0.0669
Final R indexes [all data]	R <sub>1</sub> = 0.0546, wR <sub>2</sub> = 0.0720
Largest diff. peak/hole / e Å <sup>-3</sup>	2.05/-1.95
Flack parameter	0.5

## L.13



Identification code	JAM2_277_4_Cu
Empirical formula	C <sub>23</sub> H <sub>22</sub> N <sub>4</sub> O <sub>2</sub> S
Formula weight	418.50
Temperature/K	119.99(15)
Crystal system	orthorhombic
Space group	P2 <sub>1</sub> 2 <sub>1</sub> 2 <sub>1</sub>
a/Å	9.26295(12)
b/Å	10.76616(15)
c/Å	21.8237(3)
α/°	90
β/°	90
γ/°	90
Volume/Å <sup>3</sup>	2176.40(5)
Z	4
ρ <sub>calc</sub> /cm <sup>3</sup>	1.277
μ/mm <sup>-1</sup>	1.535
F(000)	880.0
Crystal size/mm <sup>3</sup>	0.17 × 0.09 × 0.08
Radiation	CuKα (λ = 1.54184)
2θ range for data collection/°	8.102 to 148.608
Index ranges	-11 ≤ h ≤ 11, -12 ≤ k ≤ 13, -27 ≤ l ≤ 26
Reflections collected	22649
Independent reflections	4442 [R <sub>int</sub> = 0.0444, R <sub>sigma</sub> = 0.0301]
Data/restraints/parameters	4442/0/276
Goodness-of-fit on F <sup>2</sup>	1.019
Final R indexes [I >= 2σ (I)]	R <sub>1</sub> = 0.0282, wR <sub>2</sub> = 0.0696
Final R indexes [all data]	R <sub>1</sub> = 0.0303, wR <sub>2</sub> = 0.0712
Largest diff. peak/hole / e Å <sup>-3</sup>	0.24/-0.28
Flack parameter	-0.007(7)

## C.14



Identification code	JAM2_285_Mo_a
Empirical formula	C <sub>35.3</sub> H <sub>42.3</sub> Cl <sub>2.6</sub> I <sub>2</sub> Ir <sub>4</sub> O <sub>2.35</sub> S
Formula weight	1130.46
Temperature/K	119.98(18)
Crystal system	monoclinic
Space group	P2 <sub>1</sub>
a/Å	10.0659(5)
b/Å	21.3806(11)
c/Å	19.0488(9)
α/°	90
β/°	90.185(5)
γ/°	90
Volume/Å <sup>3</sup>	4099.6(4)
Z	4
ρ <sub>calc</sub> /cm <sup>3</sup>	1.832
μ/mm <sup>-1</sup>	5.019
F(000)	2176.0
Crystal size/mm <sup>3</sup>	0.19 × 0.04 × 0.02
Radiation	MoKα (λ = 0.71073)
2θ range for data collection/°	5.952 to 56.564
Index ranges	-13 ≤ h ≤ 9, -28 ≤ k ≤ 28, -25 ≤ l ≤ 25
Reflections collected	54860
Independent reflections	20325 [R <sub>int</sub> = 0.0737, R <sub>sigma</sub> = 0.1003]
Data/restraints/parameters	20325/865/878
Goodness-of-fit on F <sup>2</sup>	1.030
Final R indexes [I ≥ 2σ (I)]	R <sub>1</sub> = 0.0544, wR <sub>2</sub> = 0.1085
Final R indexes [all data]	R <sub>1</sub> = 0.0727, wR <sub>2</sub> = 0.1184
Largest diff. peak/hole / e Å <sup>-3</sup>	4.85/-1.26
Flack parameter	-0.027(4)